

Towards the Development of Flexible Substrate Materials for Label-free Surface Enhanced Raman Spectroscopy (SERS) and Photo-induced Enhanced Raman Spectroscopy (PIERS)

Doctor of Philosophy

Zahra Khan

Department of Chemistry, UCL

2022

A thesis presented to University College London in partial fulfilment for the
requirements of the Degree of Doctor of Philosophy

Supervised by Ivan P. Parkin



Declarations

I, Zahra Khan, confirm that the work presented in this thesis is my own. Where information has been derived from other sources, I confirm that this has been indicated in the thesis where applicable.

Abstract

This thesis is concerned with the label-free detection of small molecules and macromolecules using enhanced Raman spectroscopic techniques: Surface-enhanced Raman Spectroscopy (SERS) and photo-induced enhanced Raman spectroscopy (PIERS). The work focuses on the development of reproducible and stable plasmonic nanoparticles (NPs) incorporated into flexible substrates to realise their SERS potential. The materials have been designed to fulfil the criteria of flexible and sensitive substrates in many applications with an emphasis in the biomedical field, especially within wound healing. A number of measurements on varying molecules were conducted to assess the SERS efficacy of the substrates. Most of the novel research presented in this thesis is proof-of-concept, laying the framework for further work.

Chapter I highlights the importance of SERS and potential of PIERS with a thorough evaluation of the literature. Motivations behind the research as well as the aims of this work are addressed. Theoretical concepts are introduced with a touch on the mathematical background. Key principles and parameters influencing SERS and considerations are all covered to give a complete outline of the topic.

The next few chapters focus on the results of this thesis. Chapter II provides synthetic routes for gold nanoparticles and includes a comparative study on the influence on nanoparticle shape on their subsequent SERS function. The effects of capping agents on the shape, size and stability of the NPs are examined. These are fully characterised and functional SERS testing is carried out using a range of molecules to fully evaluate their SERS ability. Surface modification is also attempted in this work with great concern given to overpowering solvent effects. Several biomarkers are introduced with qualitative SERS analysis. Duplex testing was performed to determine the specificity and sensitivity of the gold NPs.

Chapter III starts investigating flexible materials as SERS substrates. These are readily available, low cost and biocompatible materials with gold NPs incorporated into them to become SERS active. Simple methods for synthesis

and data collection are presented as well as their SERS results. Paper and PDMS, whilst having some advantages lack clear Raman enhancement with inherent material signals dominating the spectra. Gelatine based hydrogels are chosen as an ideal candidate for SERS substrates. Many gelatine/polymer blends are synthesised and characterised to find the optimum gel regarding both mechanical and chemical permanence as well as SERS capability. Studies looking into cross-linking agents to establish the best synthetic protocol are executed. There is always a trade-off between highest functional efficiency and a more 'green' and sustainable approach. The PVA/hydrogel nanocomposite material exhibits valuable SERS whilst maintaining a facile methodology for synthesis and data acquisition.

Chapter IV extends the SERS studies to biological macromolecules such as proteins and wound biomarkers. Both colloidal NPs and hydrogels are used as substrates. Concentration studies are conducted and attempts at correlating intensity with concentration are made, to limited realization. Real samples from patients are probed with patterns and trends hypothesised. These are corroborated against photographic evidence of the wound. Preliminary machine learning is employed to help classify the data with suggestive, positive results.

Chapter V inspects PIERS on biomolecules with varying degrees of enhancements, but low concentration detection of glucose is reported. Different TiO_2 substrates are investigated for their influence in the PIERS effect and are characterised appropriately. The preparation method, film thickness and wetting behaviour of the property are likely parameters that can impact the PIERS property of the substrate. Comparisons between SERS and PIERS reveal complex mechanistic considerations between the two phenomena. As a novel technique the possibilities to fully realise the potential of PIERS is yet to be explored, but there is a lot more research to be done to fully understand the effect.

This thesis concludes with a summary of the key findings from the experimental work and presents possible avenues for further research to consolidate and advance the current work.

Impact Statement

The work conducted in this doctorate focuses on the label-free detection of molecules using SERS and PIERS. The results presented in this thesis can benefit research groups looking into the detection of biomarkers without the need for external Raman tags. The analytes that can be detected using the gold nanoparticles synthesised here are not limited to the biological field. The method of fabricating the citrate capped gold nanoparticles is facile with the seeds having a long shelf-life and the protocol creates reproducible gold NPs with good stability. These have demonstrated to have some duplex functionality showing that with greater optimisation, these properties can be exploited in a vast range of applications.

The flexible, transparent hydrogels fabricated in this work provide an alternative to conventional SERS substrates. Gold nanoparticles have successfully been embedded into the hydrogel matrix in a rapid and easy approach with long shelf life and high SERS output. The hydrogels are formed using a 'green' cross-linker making them more environmentally friendly. The hydrogels have demonstrated SERS efficacy with a range of biomolecules as well as wound samples, paving the way for additional research. Employing SERS to look at wound samples is novel and the work in this thesis offers proof of concept and thus, can be the start of implementing a new tool to assess wound biomarkers in a point of care (POC) setting.

The research into SERS and PIERS have given rise to several considerations that are paramount in conducting these experiments. The effect of the solvent and how this can obscure the data is important as these molecules have shown to dominate the SERS spectra. The results can be useful in providing an insight into the interactions the analyte might have at a molecular level, especially when evaluating proteins. The PIERS data reveals that many parameters can affect the final PIERS effect such as doping, wetting behaviour and thickness of the TiO₂ thin films. Analysing biomolecules using PIERS determined that it is a versatile technology. Research groups will be able to extend the work carried out in this thesis for greater impact outside the lab as preliminary data suggests that the substrates presented here offer great SERS and PIERS capacity.

Acknowledgements

Firstly, I must acknowledge the work of others presented in this thesis. The seed mediated growth method was derived from the gold nanoparticle synthesis carried out by Luca Panariello, and these were used for some of the PIERS measurements in Chapter V. Mabel Cornwell also provided some gold NPs for the PIERS chapter for initial data collection. One of the PIERS substrates in Chapter V investigated was prepared by Alina Negrea, using APCVD, under the supervision of Professor Ivan Parkin. Meltem Yilmaz supported the work by performing the IR data presented in Chapter III. A huge thank you for the staff at NUS for assisting with the TEM, and Dr Jayakumar Perumal for providing the PDMS substrates studied in Chapter III as well as guiding me and sharing knowledge of SERS in the biological field throughout my time in Singapore. Big thanks to Steve Firth for Raman and SEM training and offering solutions for technical issues and Martin Vickers for training and assistance with XRD. I should express my gratitude to Kevin To for assistance with EF calculations and Sultan Ben-Jaber for helpful discussions of SERS and its mechanisms. Thanks to Sanjay Sathasivam and Joanna Borowiec for help with film thickness and XPS measurements, respectively. Daniel Glass shared very insightful information about PIERS for which I am very grateful. Thanks to Kris Page for general lab enquiries and water contact angle measurement training.

I must extend my appreciation to my primary supervisor Professor Ivan Parkin for always showing support and encouragement throughout my entire PhD, even when in Singapore. The ongoing support for all academic and personal matters has been appreciated. Professor Malini Olivo for supervising me at A*STAR, in Singapore and the lab group for welcoming me and helping me with my research. Dr Zhimei Du helped a lot with the organisation and always a good communicator with events and deadlines.

Finally, a huge thank you to my friends and family who have provided me with continued support and love. Throughout the highs and lows, it has always been a blessing to have such great friends for encouragement and reassurance.

Table of Contents

Declarations	2
Abstract	3
Impact Statement	5
Acknowledgements	6
List of Figures	10
List of Tables	19
List of abbreviations	20
Chapter One	24
Chapter I: Introduction and Literature Review	25
1.1 Motivations	25
1.2 Surface Enhanced Raman Spectroscopy (SERS)	27
1.2.1 Mechanisms	28
1.2.2 Hotspots	32
1.2.3 Substrates	33
1.2.4 Novel materials	37
1.2.5 Surface modification	39
1.2.6 Considerations	41
1.2.7 Advantages of SERS	42
1.2.8 Enhancement factors (EFs)	43
1.2.9 Flexible substrates	46
1.3 Biomedical applications	50
1.3.1 Wound healing	54
1.4 Challenges and drawbacks	56
1.5 Data processing for Raman spectroscopy	57
1.6 PIERS	59
1.6.1 Introduction	59
1.6.2 Mechanisms	60
1.6.3 Materials	61
1.6.4 Applications	62
1.7 Aims and Objectives	63
1.7.1 Research problem	63
1.7.2 Research Aim	63
Chapter Two	65

Chapter II: Investigating Colloidal Gold Nanoparticles for SERS Substrates	66
2.1 Introduction	66
2.2 Materials and Reagents	67
2.3 Experimental	68
2.3.1 Synthesis	68
2.3.2 Self-assembled monolayers (SAMs)	69
2.3.4 Target analytes	70
2.3.4 Characterisation	71
2.3 Results and discussion	74
2.3.1 Preliminary SERS	74
2.3.2 Capping agents	87
2.3.3 Self-assembled monolayers (SAMs)	104
2.4 Conclusions	114
Chapter Three	116
Chapter III: Developing Flexible Sensor Materials for Label Free SERS	117
3.1 Introduction and Aims	117
3.2 Experimental	118
3.2.1 Materials and reagents	118
3.2.3 Characterisation	122
3.3 Results and Discussion	124
3.3.1 Filter Paper	124
3.3.2 Polydimethylsiloxane (PDMS)	128
3.3.3 Hydrogels	135
3.4 Conclusions	159
Chapter Four	162
Chapter IV: Label-free SERS on Biological Samples	163
4.1 Introduction and Aims	163
4.2 Experimental	165
4.2.1 Reagents and Materials	166
4.2.2 Methods	166
4.3 Results and Discussion	168
4.3.1 Proteins	168
4.3.2 Wound Samples	186
4.4 Conclusions	202

Chapter Five	205
Chapter V: PIERS	206
5.1 Introduction and aims	206
5.2 Experimental	208
5.2.1 Reagents and Materials	208
5.2.2 Synthesis	208
5.2.3 Characterisation	209
5.3 Results and discussion.....	210
5.3.1 PIERS measurements	212
5.3.2 Concentration studies.....	213
5.3.3 Different TiO₂ thin films	216
5.4 Considerations.....	224
5.5 Conclusions	225
Chapter Six	227
Chapter VI: Conclusions and Future Work.....	228
6.1 Results overview	229
6.1.1Chapter II.....	229
6.1.2 Chapter III.....	229
6.1.3 Chapter IV	229
6.1.4 Chapter V	230
6.2 Summary	231
6.3 Future areas of research.....	231
References.....	234

List of Figures

<i>Figure 1 Jablonski diagram of energy states for Rayleigh, stokes and anti-stokes scattering. Reproduced with permission from reference [13].</i>	28
<i>Figure 2 Schematic of plasmon oscillation for a sphere, showing the displacement of the conduction electron charge cloud relative to the nuclei. Reproduced with permission from reference [17].</i>	30
<i>Figure 3 Schematic diagram of relative energies of excited electron-hole pairs generated in the metal nanoparticle relative to the HOMO and LUMO of the chemisorbed adsorbate. Reproduced with permission from reference [22].</i>	31
<i>Figure 4 Schematic of a hotspot. The local electromagnetic field in the interparticle nanogaps have significantly strong electromagnetic enhancements. Reproduced with permission from reference [27].</i>	32
<i>Figure 5 Schematic showing (A) when the analyte is in the hotspot region and (B) when the analyte is on the metal nanoparticle and not in the hotspot. These will experience different enhancements, even on the same substrate. Reproduced with permission from reference [30].</i>	33
<i>Figure 6 Schematic describing the Fren's method of forming gold nanoparticles using high heat and citrate reduction on gold (III) chloride trihydrate as the starting material. Adapted from reference [44].</i>	35
<i>Figure 7 Various shapes of gold nanoparticles. Reproduced with permission from reference [50].</i>	36
<i>Figure 8 Schematic of various semiconductor-based SERS applications. Reproduced with permission from reference [56].</i>	37
<i>Figure 9 Representation of a SAM structure showing the head group, tail and functional group The head group is attached to the substrate.</i>	39
<i>Figure 10 Schematic showing a flexible tape decorated with nanoparticles for SERS. The adhesive can make quick contact with any shaped object for SERS analysis. Reproduced with permission from reference [106].</i>	47
<i>Figure 11 Schematic showing the SERS detection of different biomolecules. Reproduced with permission from reference [38].</i>	50
<i>Figure 12 Schematic demonstrating the differences between the label-free SERS detection and the SERS approach using dye labels as reporter molecules. The Raman signals from the indirect method are produced from the tags employed whereas the Raman signals come directly from the analyte itself in the label-free method. Reproduced with permission from reference [133].</i>	53

<i>Figure 13 Photocatalytic mechanism of semiconductor materials. Reproduced with permission from reference [158].....</i>	<i>59</i>
<i>Figure 14 (a) UV-C light creates oxygen vacancies V_o in the TiO_2 conduction band. (b) The sample is deposited and the laser light photoexcited the TiO_2, leading to increase in charge on the nanoparticles. (c) The charged nanoparticles lead to the PIERS enhancement. (d) The PIERS effect gradually diminishes as the V_o are completely replenished over time. Reproduced with permission from reference [159]</i>	<i>61</i>
<i>Figure 15 Diagram showing the seed mediated growth method for gold nanoparticles. This protocol was used for the synthetic experiments for all type of gold colloidal nanospheres</i>	<i>68</i>
<i>Figure 16 Molecular structure of the different SAMs employed in this study: A) 1- Octanethiol, B) 1- Dodecanethiol, C) 1,4 Benzenedimethanethiol and D) 11-Mercaptobenzoic acid.....</i>	<i>70</i>
<i>Figure 17 Schematic illustrations of A) the Raman instrumentation and B) the SERS acquisition</i>	<i>72</i>
<i>Figure 18 SERS spectra of 1 mM RB on the different kinds of gold nano shapes. The background was removed and the baseline was offset for clarity.</i>	<i>74</i>
<i>Figure 19 TEM images of A) gold nano-spheres B) gold nano- shapes and C) gold nano-stars</i>	<i>75</i>
<i>Figure 20 Average DLS measurement of the different colloidal gold structures</i>	<i>76</i>
<i>Figure 21 (Left) UV-Vis spectra for the different gold nanostructures and (right) UV-Vis spectra for the gold nano-spheres at different time intervals</i>	<i>77</i>
<i>Figure 22 (Left) Zeta potential for the different gold nanostructures and (right) image showing stable and aggregated gold nanoparticles. Reproduced with permission from reference [72].</i>	<i>77</i>
<i>Figure 23 (Left) Diagram showing the different stabilisation effects on gold nanoparticles and (right) TEM image of the gold nano-spheres showing some aggregation.....</i>	<i>80</i>
<i>Figure 24 SERS spectra of the different gold nanostructures with 1 μL RB. The background was removed and the baseline was offset for clarity.....</i>	<i>81</i>
<i>Figure 25 Diagram to show aggregation of gold NPs over time.....</i>	<i>83</i>
<i>Figure 26 Schematic to show data collection for the wet and dry samples</i>	<i>84</i>

<i>Figure 27 SERS spectra of 10 mM PABA with gold nanoparticles acquired in both wet and dry conditions. The background was removed and the baseline was offset for clarity</i>	<i>85</i>
<i>Figure 28 Molecular structures for A) TRIS-base B) sodium citrate and C) CTAB</i>	<i>87</i>
<i>Figure 29 UV-Vis spectra of the different capped gold NPs</i>	<i>89</i>
<i>Figure 30 Average DLS measurement of the different capped gold NPs.....</i>	<i>89</i>
<i>Figure 31 Zeta potential of the different capped gold NPs</i>	<i>90</i>
<i>Figure 32 Diagram showing the difference between aggregation and agglomeration. Reproduced with permission from reference [201].....</i>	<i>90</i>
<i>Figure 33 Image showing the different capped gold NPs. (From left to right) CTAB, citrate and TRIS</i>	<i>91</i>
<i>Figure 34 SERS spectra of the different capped gold NPs with 1 mM RB at laser power 1%.....</i>	<i>91</i>
<i>Figure 35 Molecular structure of 4-ATP</i>	<i>93</i>
<i>Figure 36 SERS spectra of the different capped gold NPs with 10 mM ATP ...</i>	<i>93</i>
<i>Figure 37 Diagram illustrating the favourable S-Au bond.....</i>	<i>94</i>
<i>Figure 38 Schematic showing the increasing solvent molecules (circles) and fewer solute molecules (triangles) in a SERS system.....</i>	<i>94</i>
<i>Figure 39 Diagram showing the gold NP capped with CTAB and the surrounded by the analyte</i>	<i>95</i>
<i>Figure 40 Raman spectrum of CTAB-capped gold NPs by themselves with highlighted (*) peaks attributed to CTAB.....</i>	<i>95</i>
<i>Figure 41 Molecular structure of tryptophan</i>	<i>96</i>
<i>Figure 42 SERS spectra of different capped gold NPs with 10 mM tryptophan</i>	<i>96</i>
<i>Figure 43 Raman spectrum of solid glutamate and SERS spectrum of CTAB capped gold NPs with 50 mM glutamate with the Raman spectrum of CTAB substrated from it to correct for signals coming from CTAB. Te background was removed and the baselin was offset for clairty</i>	<i>98</i>
<i>Figure 44 Raman spectrum of solid GABA and SERS spectrum of CTAB capped gold NPs with 50 mM GABA with the Raman spectrum of CTAB substrated from it to correct for signals coming from CTAB. The background was removed and the baseline was offset for clarity.....</i>	<i>98</i>

<i>Figure 45 Schematic showing the method for duplexing. Briefly, 1:1 ratio of gold: analyte were mixed well. Then 1:1 ratio of two samples were mixed together before data acquisition.....</i>	<i>99</i>
<i>Figure 46 Normal Raman spectra of solid tryptophan and PABA with SERS spectrum of citrate capped gold NPs with 10 mM tryptophan and 10 mM PABA with highlighted bands. The red stars show signals from PABA and the blue stars show signals from tryptophan. The spectra were normalised for clarity .</i>	<i>100</i>
<i>Figure 47 Normal Raman of solid SA and tryptophan with the SERS spectrum of citrate capped gold NPs with 1 mM SA and 10 mM tryptophan with highlighted bands. The red stars show signals from tryptophan and the blue stars show signals from SA. The spectra were normalised for clarity</i>	<i>101</i>
<i>Figure 48 Normal Raman of solid GABA and glutamate with SERS spectrum of citrate capped gold NPs with 50 mM GABA and 50 mM glutamate with highlighted bands. The red stars show signals from GABA and the blue stars show signals from glutamate (Glu). The spectra were normalised for clarity ..</i>	<i>103</i>
<i>Figure 49 (Left) Diagram showing how a SAM is formed on the gold surface via S-Au bonds. Reproduced with permission from reference [219], and (right) schematic of the ways that SAMs can be arranged around a spherical gold NP.</i>	<i>104</i>
<i>Figure 50 Average DLS size measurement of gold NP and gold NP with DDT</i>	<i>106</i>
<i>Figure 51 UV-Vis spectra of gold NP and the gold NP with DDT</i>	<i>106</i>
<i>Figure 52 A) Molecular structure of Arg and B) Molecular structure of the protonated form of Arg</i>	<i>107</i>
<i>Figure 53 Normal Raman spectra of solid Arg, 2 mM DDT solution, and the SERS spectra of the gold/DDT with 10 mM Arg and the gold NPs alone. The highlighted bands come from the Arg (green stars) and the DDT (blue stars). The spectra were normalised for clarity</i>	<i>107</i>
<i>Figure 54 UV-Vis spectra of gold NPs and gold NPs with BDT.....</i>	<i>1099</i>
<i>Figure 55 Normal Raman of Arg and 2 mM BDT solution and SERS spectra of gold NPs and BDT with 10 mM Arg and, the Raman spectrum of gold NPs by themselves. The spectra were normalised for clarity</i>	<i>110</i>
<i>Figure 56 Diagram showing how the SAM could be positioned on the gold surface. (right) A disulphide bond between two BDT molecules. Reproduced with permission from reference [226].</i>	<i>111</i>
<i>Figure 57 Normal Raman of solid ornithine and SERS spectra of gold NPs with BDT and DDT with 10 mM ornithine. The spectra were normalised for clarity</i>	<i>112</i>

<i>Figure 58 Raman spectrum of EtOH.....</i>	<i>112</i>
<i>Figure 59 Normal Raman of solid SA and SERS Spectra of gold NPs with 1 mM SA and commercially available BBI gold with 1 mM SA. The blue stars show signals from SA. The spectra were normalised for clarity.</i>	<i>114</i>
<i>Figure 60 SERS spectra of synthesised citrate capped gold NPs and BBI commercially available gold NPs with 1 mM RB. The background was removed and the baseline was offset for clarity</i>	<i>114</i>
<i>Figure 61 (Left) The different polymers used for hydrogel synthesis to be mixed with gelatine and (right) the different cross linkers used for the synthesis of the hydrogels, based on literature recommendations</i>	<i>120</i>
<i>Figure 62 Schematic showing the hydrogel synthesis protocol.....</i>	<i>120</i>
<i>Figure 63 Schematics to show the different method of SERS acquisition on hydrogels. (Left) Immersing the gel in the analyte solution and (right) drop casting gold & analyte onto the gel</i>	<i>121</i>
<i>Figure 64 SERS spectra of 1 mM RB on FP and glass slide with gold NPs. The background was removed and the baseline was offset for clarity</i>	<i>125</i>
<i>Figure 65(Left) Raman spectrum of solid SA, SERS spectrum of gold NPs with NaCl and 1 mM SA on FP and gold NPs with 1 mM SA on FP, and (right) Raman spectrum of FP and solid Cys, and the SERS spectra of gold NPs with 10 mM Cys on FP with and without NaCl. The spectra were normalised for clarity</i>	<i>126</i>
<i>Figure 66 Diagram showing how Cys can interact with the gold NPs</i>	<i>127</i>
<i>Figure 67 SEM image of untreated PDMS. Reproduced with permission from Dr Jayakumar.....</i>	<i>129</i>
<i>Figure 68 (Left) Photograph of PDMS with gold, and (right) Raman spectrum of PDMS alone and SERS spectra of 1 mM and 1 μM RB on gold/PDMS. The spectra were normalised for clarity</i>	<i>130</i>
<i>Figure 69 Diagram showing the surface modification of PDMS. The polymers were layered on step-by-step before the gold layer. Gold NPs were mixed with the analyte and drop cast onto the surface before Raman acquisition.....</i>	<i>131</i>
<i>Figure 70 Normal Raman of solid SA and the SERS spectra of 1 mM SA on the modified and unmodified PDMS. The spectra were normalised for clarity</i>	<i>132</i>
<i>Figure 71 (Left) Diagram showing the modification of PDMS with the SAM and (right) the normal Raman spectra of solid SA and EtOH, and the SERS spectra of 1 mM and 1 nM SA on the PDMS modified with BDT SAM. The spectra were normalised for clarity.....</i>	<i>133</i>

<i>Figure 72 Schematic of integrating gold NPs during the curing stage of PDMS fabrication. Reproduced with permission from reference [103]</i>	<i>134</i>
<i>Figure 73 Image depicting the gelation process. Reproduced with permission from reference [108].....</i>	<i>135</i>
<i>Figure 74 Photographs of the different polymer/gelatine hydrogel blends synthesised; A) PVA, B) PVP and C) PEG</i>	<i>136</i>
<i>Figure 75 (Left) UV-Vis spectra of the gold NP solution and the gold incorporated gelatine hydrogel, and (right) the optical transmission graph of the hydrogel. These are typical data from the PVA/gelatine blend.</i>	<i>137</i>
<i>Figure 76 The IR spectra of the different polymer/gelatine hydrogel blends and the gelatine gel by itself with a zoom in into the fingerprint region of the spectra.</i>	<i>138</i>
<i>Figure 77 Schematic showing a hydrogel in its swollen and shrunken stages. Reproduced with permission from reference [238].....</i>	<i>142</i>
<i>Figure 78 Normal Raman of a typical hydrogel and the SERS spectrum of the gold NPs incorporated into the hydrogel and the SERS spectra of 1 mM tryptophan, SA and PABA on the nanocomposite hydrogels</i>	<i>144</i>
<i>Figure 79 Schematic to show the data collection of the hydrogels. The gel was immersed into the analyte solution for a few hours before it was taken out and SERS was acquired.</i>	<i>145</i>
<i>Figure 80 Normal Raman of powder NAT and SERS spectra of the different hydrogels with 10 mM NAT. The spectra were normalised for clarity.</i>	<i>146</i>
<i>Figure 81 Normal Raman of solid tryptophan and SERS spectra of different hydrogels with 10 mM tryptophan. The spectra were normalised for clarity....</i>	<i>147</i>
<i>Figure 82 Photographs of PVA/gelatine hydrogel cross-linked with A) glutaraldehyde, B) genipin and C) citric acid.....</i>	<i>148</i>
<i>Figure 83 UV-Vis spectra of the PVA/gelatine nanocomposite hydrogel with the different cross-linking agents</i>	<i>149</i>
<i>Figure 84 (Left) Normal Raman of solid SA and SERS of the PVA/gelatine nanocomposite gel with 1 mM SA with the different cross linking agents, and (right) the same, with 10 mM Cys. The spectra were normalised for clarity....</i>	<i>150</i>
<i>Figure 85 Schematic showing the method for incorporating more gold into the SERS system by immersing the gel into a solution containing 1:1 ratio of gold NPs and analyte before Raman acquisition</i>	<i>152</i>

Figure 86 Normal Raman of solid SA and SERS spectra of 1 mM SA on the PVA/gelatine hydrogels with the different cross-linking agents using new protocol as demonstrated in Figure 89. The spectra were normalised for clarity.	153
Figure 87 Normal Raman of solid Arg and SERS spectra of PVA/gelatine hydrogels with 10 mM Arg with different cross linking agents; citric acid (CA), and glutraldehyde (GA) The spectra were normalised for clarity	154
Figure 88 (Left) Normal Raman of solid tryptophan (Trp) and dopamine (DA) and the SERS spectrum of PVA/gelatine nanocomposite gel with 10 mM tryptophan and 10 mM DA combined, and (right) normal Raman of solid SA and PABA and the SERS spectrum of the hydrogel with 1 mM SA and 10 mM PABA combined. The spectra were normalised for clarity.....	156
Figure 89 (Left) Normal Raman of solid tryptophan and the SERS spectra of just gold NPs and the hydrogel with 10 mM tryptophan and (right) normal Raman of solid tryptophan and the SERS spectra of the hydrogel with 1 mM and 10 mM concentration of tryptophan. The spectra were normalised for clarity.....	157
Figure 90 Image showing the direct and label approach for SERS of proteins. Reproduced with permission from reference [224].....	164
Figure 91 Molecular diagrams of the different protein biomarkers	169
Figure 92 (Left) Normal Raman of aq. BSA and (right) Normal Raman of aq. 5 mg/mL IL-1 α and the SERS spectra of 1 mg/mL IL-1 α on the gold NPs and the hydrogel. The background was removed and the baseline was offset for clairty	170
Figure 93 Normal Raman of 10 mg/mL aq. solution of (Left) IL-6 and (right) IL-18, followed by the SERS spectra of the hydrogels and the gold NPs with 1mg/mL of the respective proteins. The background was removd and the baseline was offset for clarity	171
Figure 94 diagram showing how molecules can be weakly and strongly adsorbed onto the gold NPs. Reproduced with permission from reference [210]	172
Figure 95 Repeated measurements of SERS spectra with 1mg/ mL of IL-6 on (Left) Gold NPs and (right) hydrogel. The background was removed and the baseline was offset for clarity.....	174
Figure 96 (Left) Normal Raman of 5 mg/mL TNF- α and SERS spectra of 0.1 mg/mL TNF- α on bre gold NPs and the hydrogel, and (right) the Normal Raman of 5 mg/mL MMP9 and the SERS spectra of 0.1 mg/mL MMP9 on bare gold NPs and the hydrogel. The background was removed and the baseline was offset for clarity.....	175

<i>Figure 97 Diagram showing the different structures of a protein. Reproduced with permission from reference [348].</i>	176
<i>Figure 98 (Left) The SERS spectra of different concentration of IL-18 on gold NPs and (right) the SERS spectra of different concentrations of IL-6 on gold NPs. The background was removed and the baseline was offset for clarity</i>	177
<i>Figure 99 SERS spectra of different concentration of IL-18 on hydrogel. The background was removed and the baseline was offset for clarity</i>	178
<i>Figure 100 Diagram to show gold NP-protein complexes. Adapted from reference [248].</i>	179
<i>Figure 101 Graphs showing intensity vs concentration for two different peak positions for A) IL-6 and B) IL-18. The data was averaged over 10 spectra collected for each concentration at different positions of the laser on the same sample</i>	180
<i>Figure 102 Peak intensity for two different concentrations at several peak positions for A) IL-18 and B) IL-6</i>	181
<i>Figure 103 Normal Raman of the proteins IL-18 and IL-6 and the SERS spectrum of 1 mg/mL IL-6 and 1 mg/mL IL-18 on (Left) gold NPs and (right) hydrogel</i>	183
<i>Figure 104 Normal Raman of MMP9 and TNF-α and the SERS spectrum of 1 mg/mL of MMP9 and 1 mg/mL of TNF-α on (Left) gold NPs and (right) hydrogel</i>	186
<i>Figure 105 SERS spectra of wound samples for patient 1 (top) and patient 2 (bottom) over 4 weeks on gold NPs. The background was removed and the baseline was offset for clarity. (Right) Graphs showing the intensity of certain peaks over the 4 weeks. These are averaged over 20 spectra taken from different laser spot position of the same sample.</i>	188
<i>Figure 106 SERS spectra for (top) patient 1 and (bottom) patient 2 over 4 weeks on hydrogels. The background was removed and the baseline was offset for clarity. (Right) peak intensities changing over time for each patient. These are averaged over 20 spectra taken from different laser spot positions of the same sample.</i>	190
<i>Figure 107 Schematic illustrating the different methods for hydrogel data collection when A) the hydrogel is left overnight and B) the hydrogel is quickly dip coated in the wound samples.</i>	191
<i>Figure 108 SERS spectra for patient 3 on hydrogels after different contact time with the samples A) overnight and B) few seconds. The background was removed and the baseline was offset for clarity</i>	192

Figure 109 (Left) Loading plot and (right) Score plot with a 95% confidence ellipses for (top) patient 1 and (bottom) patient 2.....	196
Figure 110 The score plot for the spectral data for both patients and the proteins with a 95% confidence ellipse	199
Figure 111 PC1 and PC2 loadings for the spectral data from both patients and proteins	201
Figure 112 Diagram showing how a hydrogel can be multi-functional. Reproduced with permission from reference [122].....	204
Figure 113 Diagram illustrating the PIERS effect. The addition of the UV irradiation improves the signals greatly over the SERS spectrum. Reproduced with permission from reference [164].	206
Figure 114 SEM images of (Left) TiO_2 surface and (right) backscatter to show the gold NP distribution on the surface of the TiO_2 thin film.....	211
Figure 115 PIERS and SERS spectra of 1 mM 4-MBA on gold NPs. The background was removed and the baseline was offset for clarity	212
Figure 116 PIERS and SERS spectra of 1 mM glutamatec on gold NPs. The background was removed and the baseline was offset for clarity	213
Figure 117 XRD patterns for the different TiO_2 thin films	216
Figure 118 XPS data for (Left) Ti 2p, typical for all films and (right) Sn 3d found in the APCVD thin film	217
Figure 119 Hall effect measurements on the different titania thin films.....	218
Figure 120 The PIERS spectra of 1 mM glucose (left) and tryptophan (right) on different TiO_2 thin films	220
Figure 121 Water contact angle images for A) Pilkington Activ™ B) APCVD and C) AACVD TiO_2 thin films displaying the non centro-symmetric droplets on the surface	222
Figure 122 (Left) PIERS AND SERS spectra of 1 mM Arg on gold NPs and AACVD TiO_2 thin film and (right) the same set of spectra for 1 mM Ala. The background was removed and the baseline was offset for clarity	224
Figure 128 Diagram illustrating how Raman spectra can be converted to a plot used for the classification of complex molecules using PCA. Reproduced with permission from reference [155]	232

List of Tables

<i>Table 1 The potential biomarkers and their effect on wound healing. Reproduced with permission from reference [146].....</i>	<i>56</i>
<i>Table 2 Table showing the measured pH of the different capped gold NPs</i>	<i>90</i>
<i>Table 3 Table describing the characteristics of the different hydrogel blends.</i>	<i>140</i>
<i>Table 4 Table showing the swelling measurements of the different hydrogel blends both in water and EtOH</i>	<i>141</i>
<i>Table 5 Table showing the normalised relative intensities of different bands in the SERS spectra of the hydrogels with 10 mM tryptophan.....</i>	<i>147</i>
<i>Table 6 Table showing the EF calculations for the different proteins at specified concentrations.....</i>	<i>183</i>
<i>Table 7 Table showing the photographs and the measurements of the wound over 4 weeks for patient 1</i>	<i>193</i>
<i>Table 8 Table showing the photographs and the measurements of the wound over 4 weeks for patient 2</i>	<i>194</i>
<i>Table 9 Table showing the peak intensities of two significant 4-MBA peaks in their SERS and PIERS spectra.....</i>	<i>213</i>
<i>Table 10 Table showing the average calculated film thickness of the different films</i>	<i>218</i>

List of abbreviations

4-ATP – 4-Aminothiophenol

4- MBA- 4- Mercaptobenzoic acid

AA – Ascorbic acid

AACVD – Aerosol-assisted chemical vapour deposition

AEF – the Analytical Chemistry (point of view) Enhancement Factor

APCVD – Atmospheric pressure chemical vapour deposition

AgNP(s)- Silver nanoparticle(s)

Ala – Alanine

Arg – Arginine

Aq. – Aqueous

Au- Gold

AuNPs- Gold nanoparticles

BSA – Bovine serum albumin

CA – Citric acid

CM – Chemical enhancement

CRE – Coffee ring effect

CT – Charge transfer

CTAB - Cetyltrimethyl ammonium bromide

Cys - Cysteine

DA – Dopamine hydrochloride

DDT – 1 Dodecanethiol

EF- Enhancement factor

ELISA- The enzyme-linked immunosorbent assay

EM – Electromagnetic

EtOH- Ethanol

FT-IR- Fourier transform infrared radiation

FP- Filter paper

GA - Glutaraldehyde

GABA – Gamma-aminobutyric acid

GERS – Graphene enhanced Raman Scattering

Glutamate – Glutamic acid

Gluc - Glucose

PABA – Para-amino benzoic acid

Phe- Phenylalanine

PCA – Principal component analysis

POC- Point of care

IL- Interleukin

LC-MS – Liquid chromatography mass spectrometry

LOD- Limit of detection

mM – Millimolar

MMP9 – Matrix metalloproteinase 9

Nm- Nanometre

nM – Nanomolar

NP(s) – Nanoparticle(s)

Oct – Octanethiol

Orn – Ornithine

PAA – Poly(acrylic) acid

PAH - Poly(allylamine hydrochloride)

P4VP-co-MMA - Poly(4-vinyl pyridine-b-methyl methacrylate)

PAM – Polyacrylamide

PC – Principal component

PCA – Principal component analysis

PD – Parkinson's disease

PDMS – Polydimethylsiloxane

PEG- Polyethylene glycol

Pg – Picogram

Ph – Phenyl

Phe – Phenylalanine

PIERS – Photo-induced enhanced Raman spectroscopy/scattering

PVA- Poly(vinyl alcohol)

PVP- Polyvinylpyrrolidone

SA – Salicylic acid

SAM/(s)- Self-assembled monolayer(s)

SEM- Scanning electron microscopy

SERS – Surface-enhanced Raman spectroscopy/ scattering

SH- Thiol

SMEF – Single molecule enhancement factor

SnO₂- Tin oxide

SP- Surface plasmon

SPR – Surface plasmon resonance

TEM- Transmission electron microscopy

TiO₂ - Titanium dioxide

TNF- α - Tumour necrosis factor α

TRIS – Tris base (Trisaminomethane)

Trp – Tryptophan

Tyr – Tyrosine

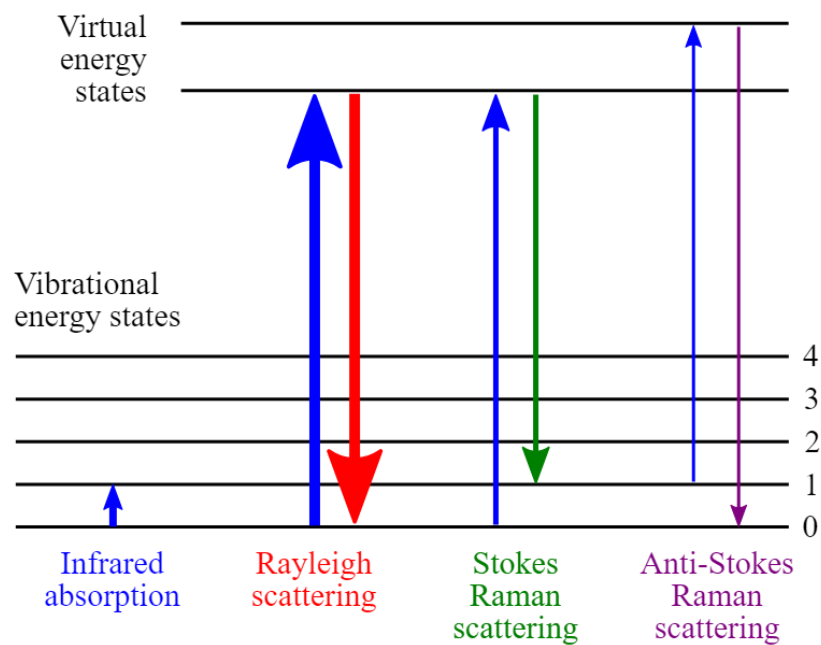
RB – Rhodamine B

XPS - X-ray photoelectron spectroscopy

XRD- X-ray diffraction

Chapter One

Introduction and Literature Review



Chapter I: Introduction and Literature Review

This chapter will provide the motivations behind the research and the current developments of the topics of interest in the field. A critical evaluation of published material will be given in relation to the relevant, current area of study followed by the main objectives at the latter part of the chapter.

1.1 Motivations

This section will briefly describe the motivations behind the research followed by a further detailed introduction to the key words and phrases used here.

The detection of low concentration analytes in a variety of diverse fields including biomedicine, food safety, explosives etc^{1–3}. has driven the need for more sophisticated and rapid analytical tools with high sensing capabilities. The identification of biomarkers in biological fluids allow for better prognosis and diagnosis for clinicians to use in many different applications from cancer to wound healing. A biomarker is a biological molecule that can provide health information of an individual based on its concentration in the body⁴. The monitoring of a biomarker can indicate a persons' health status and whether an unhealthy subject is improving.

Diabetes mellitus is an ongoing public health concern in several countries and chronic wounds are a common symptom that some patients develop. There are several methods that are used by clinicians but for the specific purpose of wound healing there is a lack in quantitative and chemical understanding of the wound status. Currently, wound management is stretching the limits of health systems globally, and non-healing wounds constitute a major portion of the healthcare spending in developed nations⁵. Often doctors are relying solely on observation of the wound to dictate whether it is healing or non-healing without knowing the biological composition of the wound which would give a better idea of the overall condition of the wound. Visual inspection and manual measurement of the wound size is subjective, often inaccurate and inconsistent^{6,7}.

Several biomarkers exist that have been found to have implications for the wound. An optical method that has been established but has yet to have real clinic use is surface-enhanced Raman spectroscopy (SERS). By developing a SERS based on-site diagnostic tool to monitor and detect non healing wounds clinicians would be able to provide correct interventions to prevent the wound from becoming chronic. To the knowledge of the author, at this present time there are no early diagnostic technologies being used to manage wounds hence this approach is desirable.

Two methodologies exist for the acquisition of SERS spectra: label and label-free⁸. The former involves the use of external tags to indirectly identify the analyte of interest whereas the latter is simply the acquisition of the analyte directly. In the biomedical field SERS has widely been used in a labelled manner to assess the concentration of biomarkers. Label-free SERS, however, is a simpler and more rapid method that could save time in a point-of-care (POC) setting. With a richer understanding of the SERS effect and mechanisms as well as advanced progress in nanofabrication techniques, SERS is on the edge of going out of the laboratory and into the real world as a sophisticated analytical tool.

The key hypotheses that this thesis wants to address are:

- Reproducible method for developing plasmonic nanoparticles with high stability and SERS efficacy.
- Effect of modifying the nanoparticles (with a self-assembled monolayer or capping agent) on the SERS ability of the nanoparticles, especially with biological targets.
- Detection of various biologically relevant analytes via label-free SERS, both individually and in a duplex system.
- Developing and characterising flexible materials as SERS substrates.
- Studying wound samples using label free SERS and identifying trends in the data.
- Investigating PIERS as an extension of SERS with different materials and analytes.

Ensuring the methodologies are as green as possible, keeping the processes low cost and utilising easily available reagents are all important considerations for this work to ensure repeatability and applicability beyond the lab bench.

The rest of the chapter outlines the fundamental reason for the scientific interest in SERS including but not limited to the theoretical mechanisms, materials currently used, and applications. The key aspects of SERS as well as intuitive explanations have been provided. Highly technical language and mathematical jargon have been avoided to make this work suitable for scientists with different degrees of specialisation in this field and for better communication of the more relevant qualities concerning the thesis research. Towards the latter part of the chapter, PIERS is introduced and relevant information pertaining to the technology with reference to literature is summarised.

1.2 Surface Enhanced Raman Spectroscopy (SERS)

SERS is a well-established analytical method and has grown exponentially since its discovery in the 1970s. The number of papers published, and the ongoing research shows its importance in the scientific community⁹. SERS is a highly sensitive and specific tool for detection and analysis with applications extending a wide range, with particular interest in monitoring environmental contamination, detection of chemical warfare agents and biological sensing.

Raman spectroscopy is a technique used to identify molecules using their vibrational modes much like Infra-red (IR) spectroscopy, yet Raman spectra results from the scattering of light by vibrating molecules where IR spectra arises from the absorption of light by vibrating molecules. Raman can be described by the change in wavelength that is observed where a photon undergoes Raman scattering, that is, the inelastic scattering of a photon off a molecular bond¹⁰. Photons can lose energy in favour of a molecule that gets promoted from the ground state to its first excited vibrational state or conversely, gain energy from a molecule that undergoes the opposite process, named Stokes and anti-stokes Raman scattering, respectively (see Figure 1). Raman spectra normally report Stokes bands, due to their stronger intensity compared to anti-Stokes bands.

Raman spectroscopy is an optical method well suited for the identification and characterisation of both known and unknown targets. It possesses many advantageous properties such as high recognition capabilities, non-destructive analysis, minimum sample preparation requirements, multiplexing and potential on-site performance with portable instrumentation¹¹. However, it has remained a marginalised technique for trace detection due to the low scattering cross-sections of many molecules and hence is deemed a weak effect, approximately six to ten orders of magnitude less efficient than fluorescence. SERS overcomes this shortcoming by amplifying the Raman signals.

In 1978, an unexpectedly large Raman signal was observed from pyridine adsorbed on a roughened silver electrode¹². Before long, several researchers confirmed the earliest findings and speculations on its origin were hypothesised. SERS combines the intrinsic advantages of Raman with high sensitivity that, in some cases, can even allow for single molecule detection^{13,14}. The generation of enhanced intensity comes from placing the molecules near the surface of suitable nanostructured, plasmonic substrate.

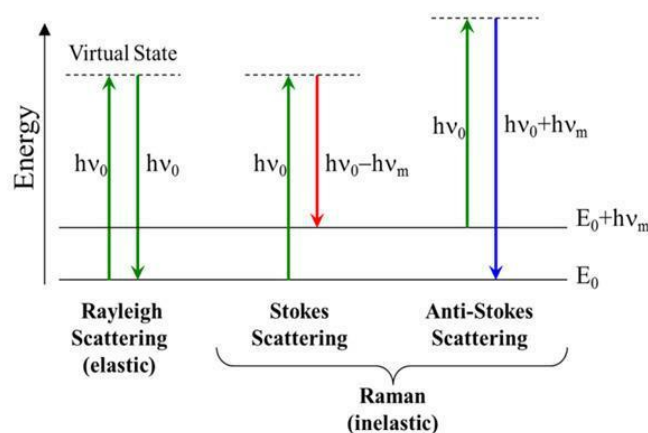


Figure 1 Jablonski diagram of energy states for Rayleigh, stokes and anti-stokes scattering. Reproduced with permission from reference [13].

1.2.1 Mechanisms

Much of the early work regarding SERS was carried out to achieve an understanding of the origin of the effect with the conclusion that SERS was primarily due to the electronic enhancement associated with the excitation of intense local surface plasmons^{15,16}. Studies in its early years confirmed that the

SERS enhancement is two-fold and is related to an electromagnetic and chemical effect.

The exact mechanistic details of SERS have been a topic of great conversation and controversy within the SERS community. However, it has been agreed that the phenomenon arises due to two different mechanisms that work simultaneously and will be discussed here: the electromagnetic enhancement (EM) and the chemical enhancement (CM). The definitions of these terms have not always been used consistently which is why they are yet to be fully understood. Full physical details will not be discussed as that is beyond the scope of this study.

Electromagnetic enhancement (EM)

This mechanism has played an important role in understanding SERS since its inception, having been the subject of many reviews.

The dominant mechanism of SERS is the electromagnetic enhancement which arises from the metal itself and is therefore present in each SERS case and is sometimes referred to as a ‘first-layer effect’¹⁷. When an electromagnetic wave interacts with a metal surface, the fields at the surface are different than those observed in the far field. Essentially, the light from the laser excites the surface plasmons, which are the coherent, collective oscillations of conduction (valence band) electrons, Figure 2^{16,18}. Surface plasmons can either be propagating or localized. Excitation of the surface plasmons generates large electromagnetic fields at the surface of the rough metal¹⁹. When the electron cloud is displaced relative to the nuclei, a restoring force arises from the attraction between the electrons and the nuclei that results in oscillation of the electron cloud relative to the nuclear framework. The interaction of the electric field with the dipolar field leads to a redistribution of electric-field intensities in areas around the metal clusters²⁰. A molecule nearby or adsorbed onto the metal surface feels an enhanced excitation intensity. This is a feature typical of the substrate and is independent of the type of molecule.

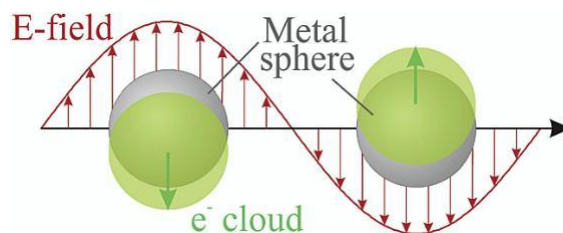


Figure 2 Schematic of plasmon oscillation for a sphere, showing the displacement of the conduction electron charge cloud relative to the nuclei. Reproduced with permission from reference [17].

The electric field at the molecule position is strongly affected by the plasmonic response of the structure and can be much larger in magnitude than the incident field, especially when exciting at a wavelength close to the optical resonances of the structures (the localised surface plasmon resonances (LSPRs)). However, in order to reach its maximum effectiveness, EM enhancements requires the molecule to be placed not too far from the substrate surface.

Chemical enhancement

It is widely recognised that there is a second mechanism that operates independently of the EM enhancement. The importance of the chemical enhancement has been of much discussion. Although its contribution to the overall SERS effect is less so than the EM enhancement, it still plays a vital role. This enhancement comes from chemical interactions between the analyte and the gold itself making it a mechanism that varies greatly depending on the analyte being studied. Many studies classify this enhancement as any effect that might result from a change of the Raman polarizability in SERS conditions with respect to that of a bare molecule.

The chemical enhancement is typically explained by the charge transfer (CT) mechanism. When a molecule is adsorbed onto a metal surface, new electronic states are formed due to chemisorption^{21,22}. The magnitude of the polarizability depends explicitly on the available optical transitions. The new indirect transitions provided by the overlap of molecular orbitals provide a channel for

the polarizability to be modified. It is not uncommon for the highest occupied molecular orbital (HOMO) and lowest unoccupied molecular orbital (LUMO) of the adsorbate to be symmetrically disposed in energy with respect to the Fermi level of the metal, Figure 3. A photo-driven charge transfer mechanism between the HOMO and unoccupied states of the Fermi level can be triggered²³. Charge transfer excitations may likely occur at lower energy than intrinsic intramolecular excitations of the adsorbate. The magnitude of the effect rarely exceeds a factor of ~ 10 . This enhancement is molecule dependent and requires direct contact or very small separation between the molecule and the substrate so is considered a short-range effect.

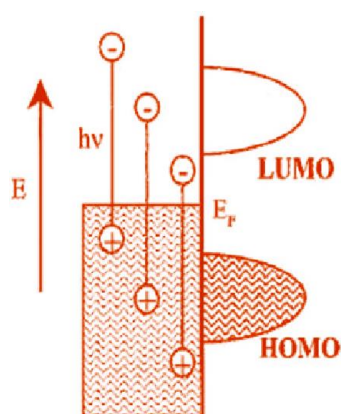


Figure 3 Schematic diagram of relative energies of excited electron-hole pairs generated in the metal nanoparticle relative to the HOMO and LUMO of the chemisorbed adsorbate. Reproduced with permission from reference [22].

It is important to note that such chemical effects may lead to quenching as well as enhancements. There are many ways in which the Raman polarizability can be modified in the presence of metallic substrates. Several possible mechanisms exist to explain the chemical effects, but they are all dependent on the molecule under consideration, as they reflect the physiochemical interaction of the molecule with the substrate²⁴. Thus, the chemical enhancement is analyte specific and cannot, in general, be invoked to describe the general properties of SERS.

The separation between the two mechanisms may not be so clear cut because the relative orientation of the molecule with respect to the local field may cause the Raman bands to be enhanced differently depending on their Raman polarizability tensor²⁵. Therefore, it can be said that SERS is electromagnetic in origin but also depends on the type of molecule being probed and its interaction

with the surface. Although, these are often treated as separate phenomena, scientists are attempting to create a unified theory of SERS.

1.2.2 Hotspots

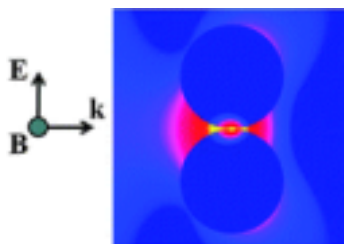


Figure 4 Schematic of a hotspot. The local electromagnetic field in the interparticle nanogaps have significantly strong electromagnetic enhancements. Reproduced with permission from reference [27].

Approximately 10 years after the discovery of SERS, single molecule detection was reported which made the technique the first vibrational spectroscopy to achieve single molecule for chemical systems^{26,27}. Evidence suggests that this phenomenon arises from nanoparticle aggregates. The area of high EM intensity in the nanoparticle junction is referred to in SERS as hotspots. Hotspots can be defined as highly localised regions of intense local field enhancement caused by surface plasmon resonances, usually occurring within interstitial crevices in metal structures, Figure 4²⁸.

It has been found that these contribute a high percentage to the overall SERS intensity of a sample, and therefore need to be addressed. The size of the hotspots from coupled nanostructures is extremely small (1-5 nm) but the Raman signals of probe molecules at these locations contribute significantly to the total Raman signal²⁷. First generation hotspots are made from single nanostructures, such as nanospheres, nano cubes or nanorods freely suspended in a homogenous medium. These hotspots exhibit moderate SERS activity. The second generation of hotspots are generated by the coupling of nanostructures with controllable interparticle nanogaps²⁹. These hotspots exhibit excellent SERS activity. This strong electromagnetic enhancement is crucial in the detection of trace number of molecules³⁰. The order of magnitude of enhancement may decay quickly with increasing distance from the hotspot.

Therefore, very different Raman intensities are seen for molecules adsorbed inside and outside of the hotspot region as illustrated in Figure 5.

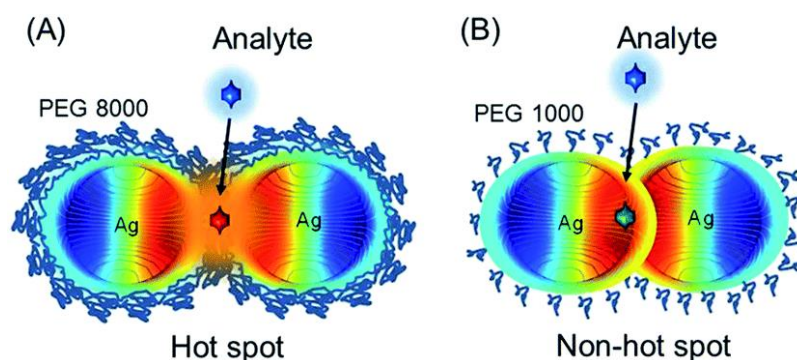


Figure 5 Schematic showing (A) when the analyte is in the hotspot region and (B) when the analyte is on the metal nanoparticle and not in the hotspot. These will result in different enhancements, even on the same substrate. Reproduced with permission from reference [30].

Plasmonic hotspots have been proved to decisively contribute to SERS where the EM field is greatly concentrated. Unfortunately, these hotspots are randomly generated and display considerable uncertainties which is one of the reasons for the poor reproducibility of SERS signals of metallic substrates³¹. This makes quantitative detection very difficult as hotspots are randomly distributed in their intensity, shape and density; all hotspots for a given surface are intrinsically different in their optical properties. In other words, quantification is sacrificed in order to gain sensitivity³².

1.2.3 Substrates

A SERS substrate is a general denomination for any plasmon-resonance supporting structure that will produce suitable Raman amplification. Arguably, the best substrates are ones that support the strongest plasmon resonances giving the largest enhancements¹¹. 2D substrates are commonly employed and refer to the metal subject supported onto a single macroscopically flat surface such as a glass slide³³.

Nanoparticles, whilst exhibiting strong near-field electromagnetic amplifications, suffer from poor stability, thus widening the search for alternate SERS substrate materials³⁴. Factors to consider when designing a SERS substrate are surface area, cost of fabrication and sample preparation.

Plasmonic materials

SERS was first performed using substrates fabricated by electrochemical roughening, however these are ill-defined resulting in poor reproducibility. Since its inception numerous research groups have been devoted to the optimisation of SERS substrates for high enhancement and for greater ease of use^{35–37}.

As stated, SERS is an effect that comes from the presence of metallic nanoparticles in proximity of a target analyte. The success of SERS is highly dependent on the interaction between adsorbed molecules and the surface of plasmonic nanostructures. It has always been exclusively associated with three metals: silver, gold and copper. Noble metal gold and silver nanoparticles are particularly well suited to design optical probes for SERS and are the most popular choice due to their high electromagnetic enhancement and simple preparation. While copper and silver have both shown SERS capabilities, gold is the metal of choice when considering biomedical applications due to its non-toxicity and biocompatibility^{38,39}. All three metals have LSPRs that cover most of the visible and near infrared wavelength range where most Raman measurements occur, making them convenient and ideal substrates.

Most analytes are first prepared in solution and then transferred to a surface⁴⁰. The adsorption efficiency is a critical factor when measuring SERS. If the probe does not attach to the metallic surface no SERS signal is observed. SERS can yield information on how molecules interact with the surfaces, and allows for the detection of very low concentrations of analytes.

2D substrates are a popular choice, referring to the SERS substrate supported onto a flat surface like a glass slide or silicon wafer. Drop casting, spin coating and dip coating are examples of how the solution can be transferred onto the flat surface⁴¹. In all these approaches, a precise estimate of how many molecules are transferred is extremely difficult. The molecule density tends to be non-uniform and affected by surface tension⁴².

Colloidal gold, whilst having its disadvantages is still the most common and standard preference for SERS due to its simplicity in production. It is normally

used as suspensions and their plasmonic properties can easily be modified altering their sizes and shapes in order to improve the SERS activities.

Frens method involving the one-step reduction of gold using sodium citrate is widely used but suffers from irreproducibility⁴³. This aqueous synthesis reduces metal salts to form the metallic nanoparticles, relying on dilute conditions and charge stabilisation by adsorbed ionic species to suppress aggregation and thereby produce a stable colloid, Figure 6. The nucleation and growth stages during chemical reduction determines the size distribution of the nanoparticles⁴⁴. Scalability can be limiting but toxicity is generally not a significant issue. The size impact on the colour of NPs can be directly observed by the naked eye. The origin of the colour is attributed to the collective oscillation of the free conduction electrons induced by an interacting electromagnetic field⁴⁵. This phenomenon is known as surface plasmon resonance (SPR).

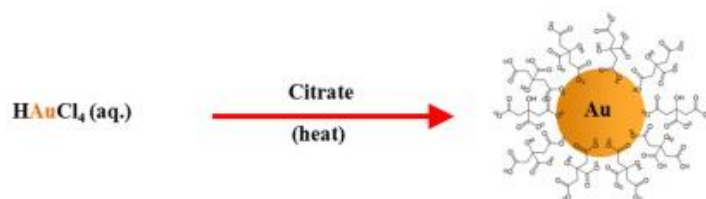


Figure 6 Schematic describing the Frens method of forming gold nanoparticles using high heat and citrate reduction on gold (III) chloride trihydrate as the starting material. Adapted from reference [44].

A wide range of research has been dedicated to the synthesis of gold nanoparticles focusing on its shape and size control. Several methods exist for the synthesis of gold nanoparticles: often categorized into top-down or bottom-up protocols. They can also be divided into physical, chemical and biological methods. Chemical routes are the most common and require reducing agents to initiate the process and promote nanoparticle nucleation. A seed mediated method may be applied to develop gold nanoparticles with tuneable diameters, according to the proportion between the precursor and the seeds^{46–48}. This method is used to add some control to the resulting nanoparticles. Hydroxylamine and ascorbic acid are common reducing agents used in the seed mediated growth of gold NPs. Room temperature syntheses of noble

metal nanoparticles involving synthetic surfactants and bio-based reductants and capping agents have been reported⁴⁹.

The nanoscale properties of gold NPs are size and shape dependent and thus, there has been extensive effort to control size, shape and surface composition of the nanoparticles, Figure 7. For spherical nanoparticles, aggregation has been used to improve the SERS signals due to the formation of hotspots. Since colloidal suspensions are thermodynamically instable and tend to flocculate, the control of the aggregation of AuNPs is of great importance to determine their practical applications. Aggregation gives rise to local field hotspots which greatly enhances the Raman intensity due to an increase in local field. NP aggregation is a dynamic process in which the NP size distribution changed over time making this method difficult to control resulting in low reproducibility⁵⁰. To overcome this, many groups have utilised anisotropic metal NPs with shapes comprising sharp tips that derive extremely strong hotspots without requiring aggregation methods⁵¹.

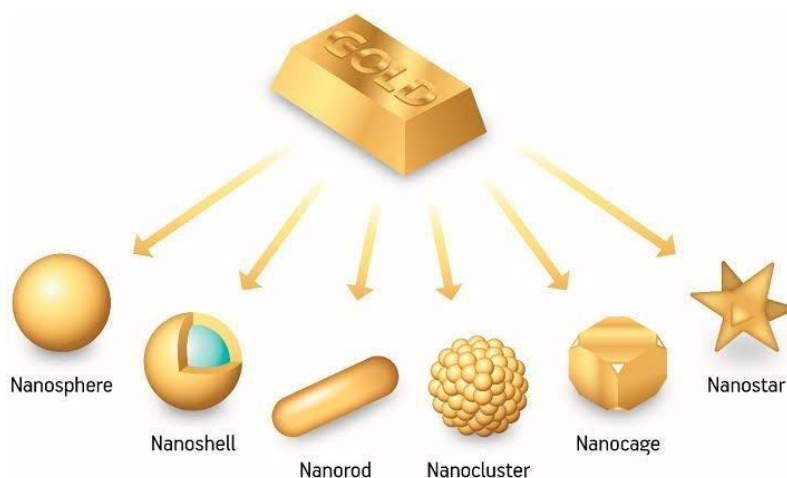


Figure 7 Various shapes of gold nanoparticles. Reproduced with permission from reference [50].

Gold NPs with different geometries, such as spheres, rods, triangles, prisms, urchins, wires and stars have been explored in specific biomedical applications in dispersed forms^{52–54}. In recent years, nanoparticles with different components and dimensions have been widely applied to detect biological molecules. At present, there exists a plethora of work which has been undertaken to demonstrate the SERS effects of different molecules with different shaped nanoparticles, so much so that is not easy to establish the principal parameters

which need to be optimised for effective and reproducible SERS. When comparing the SERS efficacy of gold nanoparticles of different shapes but similar dimensions it was found that the SERS response was equivalent for all nanoparticle types, indicating that the optimisation can be achieved by enhancing the absorbance of the nanoparticle at the Raman source wavelength^{53,55}.

1.2.4 Novel materials

Many new materials have been researched that have been reported to show SERS, although they do not fit the traditional definitions of SERS substrates because they do not support surface plasmons that contribute to the electromagnetic enhancement^{56,57}. These substrates involve only the chemical enhancements, attributed to charge transfer bands, resonances with inter-band transitions and π - π stacking interactions⁵⁸. These allow for a better understanding of the SERS mechanisms. Determining methods to study the enhancements of SERS will enable further improvement for the family of SERS substrates.

Graphene has been explored as a material for SERS with progress being made in establishing graphene as a plasmonic material in the infrared (IR) region. Graphene is a monolayer of sp^2 bonded carbon atoms packed into a honeycomb, crystalline structure with unique physical and chemical properties. It has a large surface area, superior molecule adsorption ability and can effectively quench the photoluminescence of fluorescent dyes and drastically reduce the fluorescence background^{59–61}. Additionally, as it only serves as a charge transfer SERS substrate it allows for studies of the chemical mechanism



Figure 8 Schematic of various semiconductor-based SERS applications. Reproduced with permission from reference [56].

without the interference of EM. To date, many attempts have been made to fabricate graphene-based SERS materials, both as hybrid materials, integrating typical noble metal nanoparticles for high-performing SERS substrates as well as standalone graphene-only substrates, termed graphene enhanced Raman spectroscopy (GERS).

Semiconductors such as ZnO, ZnS, CuO and TiO₂ have received much attention for their functionality as pictured in Figure 8, and can act as SERS substrates through charge transfer to the target analyte molecule, and aid reusability via photocatalytic photodegradation of adsorbed molecules upon exposure to UV light^{62,63}. However, these surfaces have not achieved comparable SERS enhancement than their metallic nanoparticle-based counterparts. The charge transfer at the semiconductor-analyte interface plays a major role in Raman scattering enhancement⁶⁴. Semiconductors have an energy gap between the full valence band and the empty conduction band, thus, the charge transfer between semiconductors and molecules depends on their energy levels. While the theory is still evolving, semiconductor-based SERS media have already been recognized as promising with several applications that rely on the diverse physical and chemical properties of the material. Advantages include molecular specificity and *in situ* analysis capability. They exhibit novel surface properties that enable better surface bonds to capture analytes, extending the possible systems and functionalities that can be studied.

Yet, the limitation with metal-free-SERS active substrates is that enhancement factors (EFs) are typically low, in the range of 10-10². Hybrid structures combining noble metals and semiconductors with varying morphologies have also been reported and used for SERS for multi analyte detection. Significant enhancements can be obtained by using these composites which combine the electromagnetic enhancement of the metal NPs with the chemical enhancement effects of the semiconductor and adsorbates^{3,65,66}. Further exploration of novel, non-conventional substrates will open new avenues of research for SERS.

1.2.5 Surface modification

Unfortunately, one disadvantage of the use of metallic nanoparticles is their low affinity to certain molecules especially those of biological importance. As mentioned earlier, most analytes are first prepared in solution and then transferred onto a surface. Bare metal substrates lack the selectivity that will allow their use in complex samples. The adsorption efficiency is a critical factor when measuring SERS; if the probe does not attach to the metallic surface no SERS is observed. A way to overcome this hinderance is modifying the surface of the gold to allow for better analyte attachment and thus, higher SERS signal intensities.

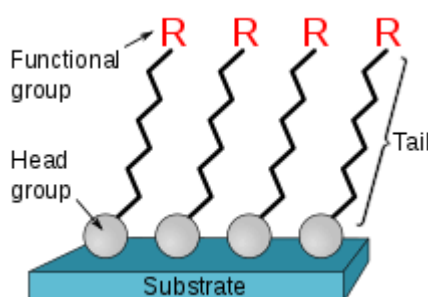


Figure 9 Representation of a SAM structure showing the head group, tail, and functional group. The head group is attached to the substrate.

Surface functionalisation have been previously used by several researchers to expand the range of applications of these materials. There are two approaches for this: performing the surface modification of colloidal gold by chemisorbing thiols or the synthesis of colloidal metals with an organic monolayer in a one-step process^{67,68}. The modification of these SERS active substrates improves selectivity, long term stability, reproducibility and substrate functionalisation.

A general approach to enhance the capturing of the analyte is by altering the surface chemistry by functionalising the substrate. Self-assembled monolayers (SAMs) are utilised by forming a thin layer over the surface of the gold improving the interaction between the gold and the molecule of interest⁶⁹. The metal surfaces are highly active in the chemisorption of organosulfur compounds. Organic molecules containing a thiol group (-SH) can be spontaneously adsorbed on gold surfaces to form well organised SAMs (see Figure 9). SAMs are derived from the adsorption of organic molecules onto

surfaces of metals to form a thin layer^{67,70}. They can affect the interface properties in many ways. To create a SAM, either the gold or silver surface is reacted with a molecule that has a functional group, such as a thiol or amine, that will chemisorb on the surface. There are many commercially available thiols and amines that can be used to prepare SAMs. The thiol chosen to form a SAM has chemical moieties that has an affinity for the desired analyte^{71,72}.

A typical example of a molecule used for SAM formation is made up of a thiol group which attaches to the substrate, and the hydrocarbon tail can be varied in order to alter the thickness of the SAM. The terminal group is important as it can be changed in order to confer a specific surface chemistry to suit the intended application of the monolayer⁷³. By increasing the number of carbons making up the alkanethiols, the distance of the adsorbed analyte from the plasmonic nanostructure is increased. Molecules that are close to the surface experience a greater local electric field enhancement than those that are further away. Short chain thiols have proved the most useful in that they enable analytes to couple with the large local electric field⁷⁴. However, NPs functionalised with longer alkanethiols are more stable and easier to handle than those with shorter ones making them the more practical option.

Besides aliphatic thiols and alcohols, assemblies can also be prepared with monomers containing polarizable functional groups such as aromatic rings and multiple terminal functional groups. The molecular self-assembly of long chain alkanethiols on gold has drawn considerable attention over the past decade^{70,75,76}. The monolayers formed are stable to physical manipulation and washing with polar solvents. Both gold and silver metal surfaces are highly responsive towards adsorption of molecular probes by both physisorption and chemisorption mechanisms which facilitate surface functionalisation. SAMs of alkanethiols on the gold surface Au (1 1 1) are the most studied because of their well-packed structure, stability and flexibility in adjusting the chain length.

There are several interesting applications of functionalised gold colloids that might benefit from their ability to tailor their surface properties using SAMs. Biomolecules bound to carboxyl-terminated SAMs could be applied for

biological probes. A charged surface can be created by the adsorption of a SAM of molecules that are terminated with an ionizable functional group.

SAM systems are of varying stability and conformation regardless of solvent effects, ambient condition and excitation sources. Solvent effects have been addressed to show how they influence SERS sensitivity and monolayer conformational changes and stability⁷⁷.

1.2.6 Considerations

Although SERS may offer extraordinary sensitivity and can compete with other spectroscopic techniques like IR, mass spectroscopy and fluorescence, it is a fact that several parameters must be carefully considered for optimal enhancement and spectral reproducibility. The two main parameters that need to be discussed when considering SERS are the substrate and the instrumentation as these have the biggest affect in the final SERS result⁷⁸. The molecule under study is also an important factor but is very specific to the experiment itself. Careful design of the system and deliberation of these parameters is important to exploit the use of SERS in a number of applications.

The instrument and more specifically the laser wavelength may lead to discrepancies in SERS datasets. The selection of laser excitation wavelength has a significant impact on experimental capabilities. And whilst typically visible excitation is used (532 and 633 nm), SERS has been reported from the near UV, the near IR and even longer wavelengths such as 1280 and 1550 nm^{79,80}. This process is often determined by a need to compromise between minimising sample fluorescence and maximising scattering efficiencies. Most biological samples are fluorescent in nature, therefore higher frequency lasers are deemed more appropriate, although there is evidence that the metallic nanoparticles can reduce the level of fluorescence. Furthermore, a drift in the optical alignment and subtle changes in either the sample position or laser power density can cause spectral intensity variations not related to the concentration of the analyte^{81–83}. Therefore, it is very important to routinely calibrate the instrument to standardise the conditions.

The substrates usually chosen for SERS are coinage metals which have been commented on in length already. These are available in two forms: solid state or in a colloidal suspension. Solid state SERS involves a flat surface with a roughened metal layer on top whereas colloids involve metal nanoparticles suspended in solution and are generally the most favoured due to their low cost and ease of preparation. The SERS measurements in colloidal solutions tend to show a better reproducibility than that on a two-dimensional solid substrate due to the average effect of millions of hotspots in the 3-D detection volume compared to the surface area of the 2-D substrate.

A SERS spectrum is a sum of analyte signals and background noises that arise from substrate photoluminescence, fluorescence and Raman signals from the solvent or impurities. Noise may dominate the SERS signals of interest at low concentration or if the analyte has generally weak Raman bands. Whilst changing the excitation wavelength may alleviate some of the problems, a better solution is to directly improve the signal^{20,84}. This can be done by comprehensive substrate design with a high number of hot spots, setting acquisition time as short as possible and improving the binding affinity between the analyte and the surface.

It should be noted that when optimising parameters within a SERS experiment, it is not necessarily true that the conditions ideal for signal enhancement are optimal to reproducibility and so a compromise between the two objectives must be established³².

1.2.7 Advantages of SERS

SERS is a great alternative to other bio-optical methods and spectroscopic techniques because not only is it highly specific and sensitive, going down to single molecule detection, it also benefits from being non-destructive^{32,85}. One attractive aspect of SERS is its high specificity, providing a unique fingerprint of the molecule under study. This makes it easy to distinguish the SERS signature from any other background signals and allows for the possibility of simultaneous monitoring of many different probes, termed multiplexing.

Furthermore, SERS can yield information on how molecules interact with the surface. It has been employed in studies evaluating the underlying behaviour of molecules in different chemical systems, providing deeper theoretical insights.

The abrupt decay of the electromagnetic fields ensures that only the integrator molecule on or near the substrate surface are probed⁸⁶. This makes SERS particularly useful for surface studies, trace analyses and biomolecular interactions. Another distinct advantage is that SERS can be conducted in aqueous environments as water exhibits very weak Raman signals and therefore does not interfere with the system.

Raman requires virtually no sample preparation which significantly saves costs. In other techniques, the preparation procedures can be time consuming, labour intensive and destructive. These issues are eliminated when performing Raman spectroscopy. Raman spectra can be acquired in a matter of seconds demonstrating its high throughput capability encouraging rapid analysis of multiple spectra at a time. Furthermore, Raman spectra can be obtained non-invasively, which means the final product can be tested in their packaging if needed⁸⁷.

SERS-based platforms offer distinct advantages especially for biomedical imaging and detection. Comparing to fluorescence, Raman scattering is almost instantaneous meaning the signals are much more stable against photodegradation and photobleaching⁸⁸. Additionally, Raman signals have a peak width of 1-2 nm, almost 10-100 times narrower than that of fluorescence emission⁸⁹, making the analysis of more complex spectra less complicated.

1.2.8 Enhancement factors (EFs)

There is a requirement to quantify the effectiveness of a SERS substrate and the most useful way is by calculating the enhancement factor (EF) which is a measurement of the magnitude of the enhancement^{90,91}. The amplification of the signal is measured compared to the Raman signal under normal conditions: the ratio of SERS signal to the Raman signal that would be obtained for the same molecule in the absence of the SERS substrate, with all other conditions

being equal. EFs allow for the comparison of SERS substrates in literature and provide a way to categorise them⁹². The number can be large enough to allow for the observation of single molecule.

Enhancement Factors are still a topic of debate, with several definitions existing, a few of which will be discussed here. The enhancement is not as straightforward to calculate and has been a subject of intense controversy, resulting in the criticism of SERS for not living up to its original expectations⁹³. The inability to characterise the signals properly links to difficulty in measuring the EFs adequately with quoted values differing by several orders of magnitude for similar experimental conditions.

It is now generally accepted that there are different definitions of the SERS EF depending on experimental conditions. Three important ones will be discussed here, although there are many more that can be read upon in literature^{94,95}.

1. The Single Molecule Enhancement Factor (SMEF)

- This is the SERS enhancement felt by a given molecule at a specific point. The development of the field of single-molecule SERS contributes significantly to understanding the magnitude of the SERS EF. The maximum SERS EF typically occurs at specific positions on the surface (so-called hot spots) and only those molecules adsorbed there can benefit from it⁹⁶. The SMEF is not unique and is only related to the individual molecule and depends on many parameters including the exact position of the molecule and the orientation of the substrate. This is not relevant to this report and is therefore not included.

2. The SERS Substrate point of view

- When dealing with average SERS signals it is important to define one or more SERS substrate EFs which can be used to compare the average SERS enhancements across different substrates⁹⁷. In most SERS studies, this EF is commonly used. Accurate determination of number of molecules measured (N) within the laser excitation volume is required.

$$EF = \frac{\frac{I_{SERS}}{N_{SERS}}}{\frac{I_{NRS}}{N_{NRS}}}$$

I_{SERS} and I_{NRS} represent the band intensity of the SERS and normal Raman respectively and N_{SERS} and N_{NRS} are the number of adsorbed target molecules with and without gold nanoparticles within the laser spot, respectively.

3. The Analytical Chemistry Point of View (AEF)

- This EF represents a simple model for the SERS EF, whose measurements can be easily reproduced and is useful when it is hard to estimate the number of analyte molecules present. This is intuitive and relevant for analytical chemistry applications. It is useful for practical applications but depends on many factors, in particular, adsorption properties and surface coverage of the probe. It is also heavily dependent on the sample preparation⁹⁸. Most SERS experiments will start with the analyte in solution at a known concentration, so the SERS EF can be naturally defined by normalising with respect to concentrations:

$$AEF = \frac{\frac{I_{SERS}}{C_{SERS}}}{\frac{I_{NRS}}{C_{NRS}}}$$

I_{SERS} and I_{NRS} represent the band intensity of the SERS and normal Raman respectively and C_{SERS} and C_{NRS} represent the concentration of the analyte in the SERS and normal Raman measurements. The AEF is relatively straightforward to define and measure and therefore can be used for benchmarking²⁴. It is also well suited to characterise SERS performance for analytical application and for SERS in colloidal solutions. However, it may strongly depend on the sample preparation procedures for example, the AEF on the same SERS substrate following preparation by either drop casting or spin coating could cause differences of several orders of magnitude.

All enhancement factors are defined with respect to the non-SERS of the same molecule in the same conditions as the SERS experiments. It is important to note that the EFs are highly non-uniform on a substrate even on a nanoscale⁹⁹. Dramatic improvements of the SERS EFs can be achieved by developing new methods of targeted adsorption of the analytes on the SERS substrates with attempting to position them preferentially at hotspots only.

Overall, SERS EFs are well understood at present with the EM model of SERS having been verified experimentally. The broad class of chemical effects as well as surface selection rules still pose challenges and more work needs to be done to elucidate these effects⁹³. The excitement surrounding very large SERS EFs has slowly died down, and most overestimations of the EFs can be tracked to improper definitions and other subtle sources of error. SERS EFs should be used as tool to infer other important physical properties of SERS, and not relied on solely for determining the quality of a substrate, with EFs of 10^6 and 10^8 being perfectly respectable figures for a good SERS substrate⁹⁷.

1.2.9 Flexible substrates

Traditional SERS substrates that have been habitually reviewed suffer from rigidity and stiffness that impede their use in certain applications. Whilst metallic nanoparticles especially gold are of value, the media in which they are employed is of importance. Nanoparticle systems all suffer from the same limitations for use in sensor devices: they are 'free-floating' colloidal suspensions that must be physically immobilised on a surface of supporting material to be used in continuous monitoring¹⁰⁰. Glass and silicon are common scaffolds that are used for SERS with the most universal method for performing SERS measurements being to deposit a liquid sample onto a rigid silicon or glass substrate that acts as a nanostructures noble metal surface. When the sample dries, analyte molecules within the sample adsorb onto the nanostructured metal surface where they will experience the electromagnetic and chemical enhancements associated with SERS. Rigid SERS substrates are restrained to a certain application in the real world and are not suitable for direct analysis of surface analytes, especially on uneven or not easily accessible surfaces⁸⁷. These rigid substrates can only be used once making

them cost-inefficient. The abovementioned inflexible substrates usually only serve as support and do not contribute to the SERS enhancement. When considering use for living organisms, more stringent biocompatibility requirements hold: materials must be soft to match the surrounding tissue, non-immunogenic and must be designed with sufficient optical properties to allow for tissue penetration⁹⁴.

There is a need for flexible substrates to present SERS the upper hand it needs for widespread applications, especially in biomedical fields. The integration of plasmonic nanostructures onto flexible substrates offer advantages such as transparency, deformability, anti-static properties, biocompatibility and non-destructive measuring¹⁰¹. Several flexible substrates have already been investigated for SERS having gained a lot of traction in recent years from research groups, exemplified in Figure 10. Different materials such as filter paper, tapes, cotton swabs and polymers have been reported for the fabrication of flexible SERS substrates^{102–105}.

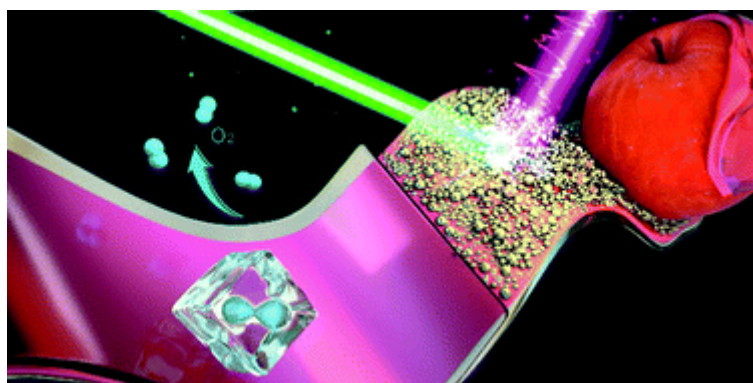


Figure 10 Schematic showing a flexible tape decorated with nanoparticles for SERS. The adhesive can make quick contact with any shaped object for SERS analysis. Reproduced with permission from reference [106].

Flexible and adhesive SERS substrates in the form of a tape for rapid detection of pesticide residues in fruit and vegetables was recently demonstrated¹⁰⁶. The tape was fabricated by decorating the commercial tape with gold nanoparticles via the conventional drop-dry method. The SERS active tape can retain its chemical properties and remain sticky providing the feasibility for easy sampling of complex surfaces. These were reported to show rapid and sensitive detection as well as stability and low cost¹⁰⁵.

There are many publications and patents describing methods of attachment/binding of nanoparticles onto paper^{102,107,108}. With excellent features such as low cost, ease-of-use, flexibility, robustness and long-term stability, paper offers a promising platform as a SERS substrate for bioassays. Paper-based microfluidics and sensing represents a new approach to extremely low cost devices for molecular analysis because cellulose is biodegradable, renewable and abundant in nature; thus cellulose based products can be inexpensively produced and even recycled^{109,110}. The soft texture of paper allows for conformal contact with the surface of analytes by swabbing. Studies illustrate colloidal gold being added drop wise onto filter paper as highly active SERS substrates¹¹¹. Gold are the NPs of choice for analysing the SERS potential of paper since they are more stable and less susceptible to oxidation than other SERS active nanoparticles. However, this method does not produce uniform distribution due to the drying process meaning more aggregation will be formed at the edge of the droplet.

Gold-nanoparticle treated paper turns to red purple, visually depicting the concentration of the NP solution being used. The SERS intensity has been found to increase linearly with the concentration of the gold nanoparticles solution applied to the paper due to the packing density increasing. Limits of detection (LODs) have been reported in some publications to be lower than 1 nm as samples with low concentration still exhibited good signal to noise ratio with the main peaks still observable¹¹¹. The SERS substrates on cellulose paper demonstrate an EF of about 10^5 to 10^7 which is on par with many of the self-assembly and direct assembly techniques^{107,111}. However, sample delivery needs to be controlled and variation in measured signal intensity across various locations has always been a concern for SERS, especially when the substrate has randomised features. Paper is not transparent, limiting its application in fields like *in situ* detection. Moreover, it is not reusable as it is difficult to remove the molecules adsorbed into the pores of paper.

For flexible and transparent SERS-active films, many polymer films such as polydimethylsiloxane (PDMS), polymethylmethacrylate (PMMA), polyethylene terephthalate (PET) and polyethylene (PE) have been used as supporting materials for plasmonic nanostructures¹¹². PDMS is a widely used polymer

material for fabricating microfluidic chips due to its favourable qualities, like transparency, outstanding elasticity, good thermal stability and ease of fabrication^{103,113}. The use of PDMS in combination with gold nano stars has resulted in fabrication of macroscale highly sensitive SERS substrates with controllable thickness and good adhesion to fruit surfaces. These composites have been reported to show excellent time stability and resistance to harsh conditions. PDMS embedded with silver nanoparticles (AgNPs) can act as a platform for direct analysis on arbitrary surfaces as well as providing SERS enhancements due to the electromagnetic mechanism. It has been reported that these AgNPs-PDMS substrates act as a flexible and efficient tool for highly sensitive Raman detection with the SERS performance remaining excellent withstanding high tensile and bending strain^{114,115}.

The free-standing hydrogel is also an excellent candidate as a 3D support for metal NPs. Hydrogels offer convenience for SERS observations, especially with portable instruments for *in situ* or field detection¹¹⁶. Hydrogels are a kind of polymer or macromolecule with a chemical or physical cross-linking structure which can absorb a lot of water but are insoluble in water. They have good biocompatibility and low friction as a soft humid material as well as offering excellent mechanical properties¹¹⁷. Functional materials combined with nanostructures introduced into polymers has received widespread research interest. Hydrogels showcase several technical features such as stability and consistency in a swelling environment and during storage and high absorption ability. They are odourless and nontoxic with maximum biodegradability without the formation of toxic groups.

When hydrogels and nanoparticles are combined in a composite material, new properties can be harnessed for different applications. The hydrogel offers stability to the nanoparticles, allows the particles to be held down and could also render new functionalities to the hydrogel. Directly embedding inorganic metal nanostructures into a hydrogel matrix would show potential as SERS substrates as it could make measurements more reliable for many analytical applications. Several hydrogels have been reported demonstrating SERS capabilities including Agrose gels, poly acryl(amide) (PAA) hydrogels, gelatine, collagen and polyvinyl alcohol (PVA) based hydrogels^{118–120}. Utilising gold encapsulated

hydrogels makes for consistent and reproducible SERS substrates. Recent studies have focused on composite hydrogels combining different polymers with tailored chemistries in order to create bioactive systems with customised functional properties^{121,122}.

Therefore, although nanoparticles have the strongest SERS enhancement, the SERS signals they provide are often irreproducible. Nanoparticle suspensions are an unstable system and the interparticle structure changes over time. Biocompatible, nanocomposite, flexible materials provide an effective alternative to rigid substrates and embedding plasmonic nanoparticles in the matrix spatially confines the colloidal solutions enabling for better SERS functionality.

1.3 Biomedical applications

As expressed earlier, the motivation behind this research stems from the need to help clinicians with the detection and identification of biomarkers. SERS has found several uses in the biomedical field extending from diagnostics to biosensing, depicted in Figure 11.

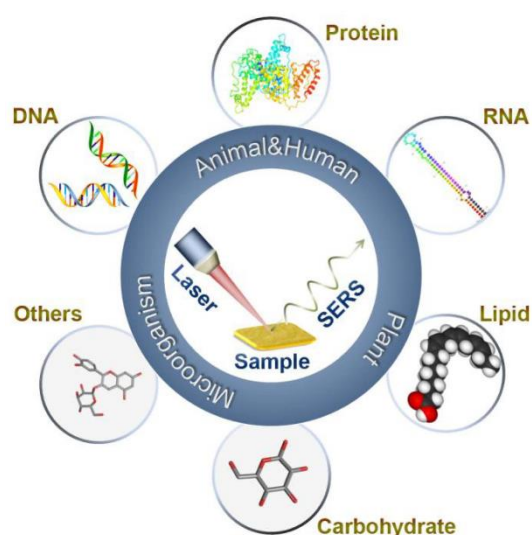


Figure 11 Schematic showing the SERS detection of different biomolecules. Reproduced with permission from reference [38].

There is great interest in the development of sensitive and selective biosensing techniques for various chemical and biological applications. The high selectivity

of SERS makes it an ideal tool to screen reaction processes at the molecular level and the analysis of biomolecules is essential for disease diagnostics, food safety inspection and environmental monitoring^{38,123}. SERS offers an excellent platform for the development of diagnostic assays as well as optical imaging tools. SERS fingerprinting of individual molecules permits excellent multiplexing capabilities because of the narrow spectral width of Raman peaks. Thus, the number of research articles on SERS in the biomedical field has grown exponentially.

A biological marker (biomarker) is a substance used as an indication of biological state. It is either produced by the diseased organ or by the body in response to disease. The detection and identification of biomarkers is of high importance for the early detection of diseases^{4,124}. Furthermore, by means of SERS, the structure and orientation towards the metallic surface and the chemical environments of the proteins and their interactions can also be monitored. Biomarkers can be categorised based on the type of information they provide as predicative, diagnostic and indicative¹²⁵. Predictive biomarkers can be used to predict outcomes or provide likelihood of benefit from treatment. Diagnostic biomarkers can identify the presence of a single biomolecule or multiple factors that have the potential to influence the clinical outcome. An indicative biomarker monitors disease progression and can be utilised to measure the response to therapy in real time. Detecting biomarkers in body fluids is cheaper and potentially more effective than other standard imaging processes that are routinely used for diagnostics, especially for cancer¹²⁶.

Delivering molecular structural information from the target analyte in aqueous solution is the most important advantage of SERS, which has not been possible by any other technique and therefore, SERS has become a useful spectroscopic method in the detection and analysis of biomolecules. Generally, the SERS detection of biomolecules is very straightforward. Two approaches are utilised for the SERS detection of biological targets: direct and indirect, described in Figure 12.

The direct method is based on vibrational information of target proteins themselves, whereas the indirect method detects target proteins by SERS

signals of Raman reporter molecules that are linked to the target analyte^{2,127,128}. While direct detection may seem straightforward, reliable and convenient, complications have been attributed to low Raman cross-sections of certain analytes as well as interference from other molecules in the sample. Label-free detection can be difficult to implement in some cases due to its limited sensitivity. The intrinsic SERS spectra of biomolecules at relatively low concentration are difficult to detect and poor selectivity in some complex mixtures because of overlapping band signals make sample identification difficult^{129,130}.

The indirect approach uses Raman reporters, attached to the nanoparticles, commonly known as SERS tags. SERS applications for nucleic acids mostly involve the indirect method to detect and quantify target strands. The most common method is to prepare nanoparticles functionalised with specific molecules that give distinct Raman spectra and can be used with affinity reagents to 'tag' specific molecules^{81,123,131}. SERS tags provide the SERS signals when the analyte interacts by means of molecular recognition chemistry e.g., antibodies with the reporter molecule. Indirect detection is then based on the signals of these 'tags' attached to the target analyte instead of the analyte itself. When the target molecule is introduced to the SERS substrate the Raman signal intensity and spectral profile of the Raman reporter changes due to the recognition of the target analyte. This approach provides highly reproducible

SERS measurements and low detection limits of the target analyte due to the sensitivity of the Raman reporter¹³².

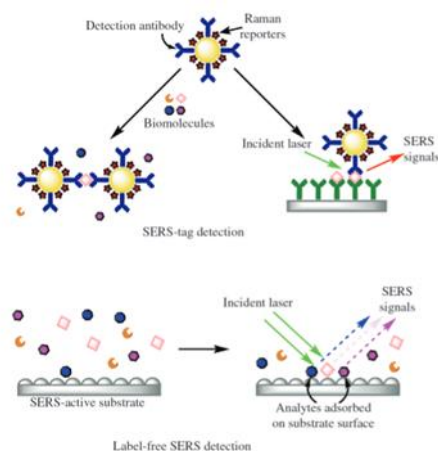


Figure 12 Schematic demonstrating the differences between the label-free SERS detection and the SERS approach using dye labels as reporter molecules. The Raman signals from the indirect method are produced from the tags employed whereas the Raman signals come directly from the analyte itself in the label-free method. Reproduced with permission from reference [133].

Whilst the most direct approach simply requires attaching the analytes to bare SERS-active substrates enabling the SERS fingerprints of the targets to be acquired, it is difficult to obtain reproducible SERS spectra of one target protein under different experimental conditions due to the changes of protein conformation and orientation. Some small biomolecules can be detected directly by commonly used SERS substrates, but the sensitivity is rather low, especially for those that have a weak affinity to the metal surface. However, promising studies regarding the molecular detection in simple systems as well as the investigation of biological fluids show the potential of label-free SERS for the detection of both therapeutic and illicit drugs.

When using label-free SERS approaches, all biomolecules present in the system could contribute to the recorded SERS spectra^{133,134}. The chemical affinity of these molecular species to the employed SERS active substrate plays a decisive role on the appearance of the spectra. Most of the published studies compare the SERS spectra from two classes of individuals: patient and healthy controls. Substantial progress has been achieved in label-free SERS, aiming at discriminating cancer patients from healthy individuals by identifying biomarkers at early stages of the disease for example, direct SERS analysis of nucleic

acids have been performed using traditional colloidal suspensions of silver and gold nanoparticles.

Compared to other technologies or SERS sensors that require auxiliary labelling modification, label-free SERS has the competitive characteristics of rapidity, simplicity and being cost effective⁷⁵. However, further investigations are required to allow for detailed band assignments of SERS spectra of body fluids.

The interest in SERS for ultrasensitive detection of biomolecules such as haemoglobin, glucose, cancer, pathogens and viruses has increased over the past few years^{11,135–137}. The SERS detection of various biomolecules has been reported, such as proteins, enzymes, viruses, bacteria, cancer markers etc. Several SERS-based sensing platforms have been developed, ranging from nanoparticles to nano-post arrays to nanowires and nanochips. These detection mechanisms are based on Raman labels in close proximity to the metal surface and multiplex DNA detection in a homogenous solution have been reported¹³⁸. Functional SERS nanotags are needed for highly selective SERS images of biomarkers on cells. PEGylated Ag-Au hollow nanospheres have been developed with excellent stability under various salt, pH and temperature conditions. These SERS substrates were able to detect two different phenotypes of breast cancer. Pancreatic cancer biomarkers have also been successfully detected using a SERS-based immunoassay platform^{132,139,140}.

To this end, several groups have published findings that validate SERS as a sensing technology for various biomedical applications. The current literature indicates the great promise of using SERS as a low-cost, highly sensitive, and high through-put methodology for emerging liquid biopsy diagnostics.

1.3.1 Wound healing

Diabetes causes impairment in the body's production of, or sensitivity to insulin, a hormone that allows the cells to take and use glucose from the bloodstream for energy⁶. This disruption to insulin makes it difficult for the body to manage blood glucose levels. When blood glucose remains high, it destroys the function of white blood cells.

Diabetic wounds are the most common type of chronic wound. There is a big difference between wound healing in healthy and diabetic patients. A major problem with diabetic wounds is that they do not follow the normal process of wound healing. When a person has diabetes, wounds can take longer to heal which can increase the risk of infections and further complications⁷. There is a great need in the medical fields to investigate a real-time expression of biological markers to better understand their roles in disease progression. A sensor that can monitor the biomarkers necessary for disease diagnosis or prognosis would add valuable information for patient treatments as well as fostering a better understanding of the roles the proteins play in disease evolution¹⁴¹.

Minor wounds, cuts and burns can lead to serious health issues for people with diabetes. Chronic wounds can hinder the quality of life for many diabetic patients as they are slow to heal, do not heal well or never heal¹⁴². According to some reports, foot ulcers will develop in about 1 in 4 people with diabetes and can ultimately lead to foot amputation. Wound healing is a multifaceted process governed by sequential, yet overlapping phases including haemostasis, inflammation, proliferation and remodelling. A wound's chemical composition involves a variety of proteins, and cytokines are of great interest for the treatment of chronic wound healing and the development of anti-inflammatory pharmaceuticals^{143,144}. Cytokines are a group of proteins and glycoproteins that act as regulators. The cytokines group includes interleukins (ILs), tumour necrosis factors (TNFs), interferons and chemokines.

Biologically relevant levels of cytokines IL-1, IL-6 and TNF- α are detectable and studies have shown that these levels change when comparing healing wounds to non-healing^{5,145}. These proteins were reported to be significantly higher in non-healing wounds, Table 1. Metalloproteinase enzymes (MMPs) and their regulators, tissue inhibitor of matrix metalloproteinase (TIMPs) play an important role in wound healing. MMPs mediate critical steps in almost every phase of the wound healing. Therefore, levels of MMPs and elastase also prove to be good prognosticators of wound behaviour. The lower the levels of MMP and the ratio of MMP-9/TIMP the greater the chance of wound healing

improving, serving as convenient and suitable biomarkers for estimating the outcome of wound recuperation¹⁴⁶.

Serum and effluent are both considered ideal biological samples for measuring host proteins because they are illustrative of the current state of recovery and severity of bacterial colonisation¹⁴⁷. To depict a patient's current state of healing, wound effluent is considered highly revealing on the grounds that it directly reflects the wound site's microenvironment which displays the damaged tissue's current mechanisms of repair. Wound swabs provide biomaterial that can be used for semi-quantitative and qualitative microbiology^{147,148}. Soon, it is hoped that changes and/or presence of an associated biomarker will be used as one of the endpoints in clinical trials.

Molecules	Effect on wound healing
MMP levels	Raised in non-healing wounds
MMP/TIMP ratios	Raised in non-healing wounds
Gene expression analysis	Increased expression of bacterial housekeeping genes, decreased expression of host housekeeping genes
Cytokine levels	Raised in non-healing wounds
Procalcitonin levels	Raised in non-healing wounds
Myeloperoxidase levels in wound fluid	Raised in non-healing wounds
Reactive oxygen species	Raised in non-healing wounds

MMP–matrixmetalloprotease;TIMP–tissue inhibitors of metalloproteases

Table 1 The potential biomarkers and their effect on wound healing. Reproduced with permission from reference [146].

1.4 Challenges and drawbacks

All in all, Raman and SERS measurements can be carried out easily, rapidly and with good reproducibility. SERS has solidified its place in science with the vast research database providing testimony to its impact in the fields of chemistry, physics, material science, nanoscience and the life sciences. Despite its advances in these areas, there are limitations that should be addressed.

Quantitative SERS has been notoriously difficult, with challenges attributed to subtle differences in nanostructures that affect the observed Raman enhancements¹⁴⁹. This is particularly true for SERS detection and identification of biomolecules. The SERS fingerprints of simple proteins are not always specific which can obscure the results. The translation of the analytical potential of SERS beyond purely academic levels is hindered by the complex matrix in which biological samples come in, where other molecular entities with good affinity for the metallic surface can compete with, or prevent, the adsorption of the target analyte onto the plasmonic nanomaterial¹⁵⁰. Another well-known challenge that is common for most biomolecules is their susceptibility to degrade when exposed to non-natural conditions such as intense laser lights.

SERS signals contain both molecular contributions and a large continuum background that is associated with the plasmonic nanostructures¹³⁰. The origin of the continuum background is not fully understood but is generally attributed to some form of plasmonic emission which can vary with solvents, ionic strength and changes in nanoparticle structure¹⁵¹. The background can sometimes overpower the analyte signals and cannot be removed as easily.

1.5 Data processing for Raman spectroscopy

Despite the great recent developments of SERS in life sciences and healthcare, its evolution towards becoming a routine tool in clinical settings and routine biomedical research has fallen behind. A main cause of this delay is due to the absence of well-established standardised methods for a consistent analysis of spectral data providing useful information for accurate interpretation¹⁵².

The identification and quantification of components in biological samples by spectroscopic methods is hindered because of the biological media's diverse nature. The spectra from heterogenous biological systems consisting of many biomolecules are complex: data from samples in their native matrices contain interfering substances. In addition to that, the differences from one sample to another in different pathological conditions are very small and difficult to observe in raw spectra¹⁵³. To obtain meaningful information and deeper insight into the data, processing and analysing the data is of paramount significance. To utilise the complete information of the complex spectra, multivariate analysis

is needed. This refers to data analytical methods that deal with more than one variable at a time with the aim of perceiving relationships between the variables¹⁵⁴.

Once the SERS spectra are obtained, they should be conveniently analysed and deconvoluted to extract the chemical and even structural information. The application of multivariate analysis in biology and chemistry is termed chemometrics. These statistical methods help identify patterns in the data allowing for the models to predict new data of a similar type. Various data mining methods are used in conjunction with SERS, such as principal component analysis (PCA), linear discriminant analysis (LDA) and partial-least squares (PLS)^{153,155,156}. PCA has already been proposed in combination with SERS for label-free diagnosis and pathological classification. It has become a popular technique for differentiating analyte components and identifying patterns without reference to prior knowledge. PLS has been used in combination with discriminant analysis for the classification of different tumour stages¹⁵⁷.

Data processing is a crucial step in Raman analysis to extract the accurate information, but it is still an active research area as optimisation of the steps according to the sample and its matrix are needed¹⁵⁶. Depending on the objective of the study, one or more of the data analysis methods can be applied for effective interpretation of data.

1.6 PIERS

1.6.1 Introduction

In more recent years there have been more discoveries involving Raman spectroscopy; an additional Raman scattering enhancement exceeding SERS. It was found that when a semiconductor (TiO_2 , ZnO , CdTe) is irradiated with UV light followed by the collection of the Raman spectrum, a substantial increase in the EF is observed, beyond the normal SERS effect¹⁵⁸. This phenomenon has been termed photo-induced enhanced Raman scattering (PIERS), Figure 13. These substrates are typically photo-active metal oxides, most notably titanium dioxide which has been extensively researched for its numerous properties. The chemical enhancement is thought to contribute majorly to the observed large enhancement signals in this effect^{159,160}. This effect can be used to improve the magnitude of Raman signals. Semiconductor materials also hold several advantages including superior biocompatibility, environmental friendliness, high chemical stability, low cost, and abundant sources which make them competitive candidates for PIERS substrates.

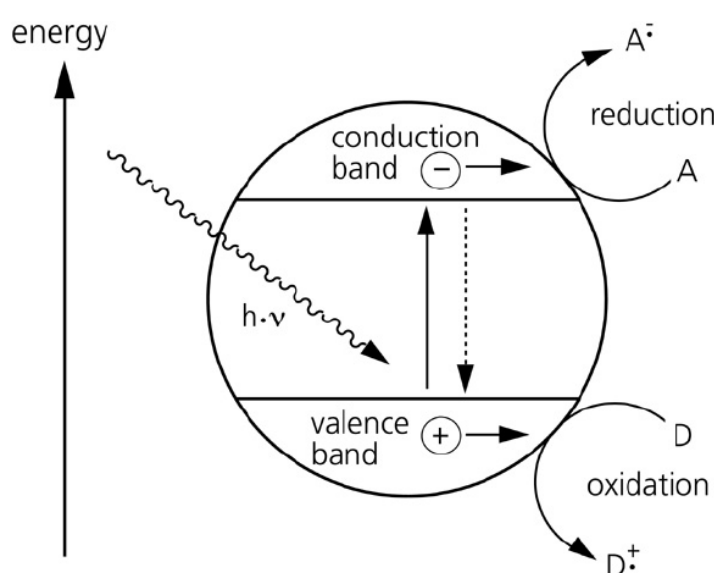


Figure 13 Photocatalytic mechanism of semiconductor materials. Reproduced with permission from reference [158].

1.6.2 Mechanisms

Despite the impressive PIERS enhancement factors and explosion in recent demonstrations of its utility, the mechanistic details remained undetermined. It has been proposed that pre-irradiation of a semiconductor gives rise to this PIERS enhancement. It was first proposed that the PIERS effect comes from the ultra-violet (UV) light induced charge migration from the semiconductor to the metallic nanoparticle^{159,161}. UV treatment produces oxygen vacancy defects in the conduction band of the semiconductor e.g., the absorption of light by defect states in TiO₂. Once in the conduction band, mobile electrons migrate to the plasmonic nanoparticle, and a charge transfer (CT) occurs from the metal to the adsorbed molecules. A mechanism for the CT of photoexcited electrons in TiO₂ to metal nanoparticles has been established as depicted in Figure 14, but there remain other possibilities for the additional Raman signal enhancement of PIERS over SERS.

One hypothesis to explain this is the increased electron density on the silver or gold nanoparticles which increase the electromagnetic enhancement¹⁶². As more electrons are transferred to the metallic nanostructure, the electromagnetic field around the particles will be enhanced creating stronger Raman signals. However, this theory can be discounted as theoretical predictions estimate that a purely electromagnetic contribution to the PIERS enhancement will only increase the enhancement factor by no more than 13%¹⁶³.

Metal to ligand CT resonant enhancement has been favoured by current studies whereby additional ligand-to-metal charge transfer or metal-to-ligand charge transfer bands form between the analyte and the metallic nanoparticle which adds a further resonance Raman enhancement in addition to the plasmonic field enhancement¹⁶⁴.

Another explanation is the photo-induced electron transfer from the nanoparticle to the analyte increasing the intrinsic Raman polarizability, leading to a change in the intrinsic Raman cross-section of the chemisorbed molecule on the metallic nanoparticle surface as opposed to the cross section of a non-

chemisorbed molecules^{165,166}. This would depend on the binding energies of the different adsorption geometries, where some may be more favourable than others. This highlights the importance of the binding geometries between the analyte and the metal as molecules will prefer to coordinate with the nanoparticle via certain functional groups to account for steric factors¹⁵⁹.

Moreover, surface plasmons on heterogeneous surfaces can induce hot electron migration among the semiconductor and metallic nanoparticles upon UV irradiation. Thus, higher SERS enhancements and improved sensitivity can be achieved by incorporating nanostructures into semiconductor materials¹⁶⁷.

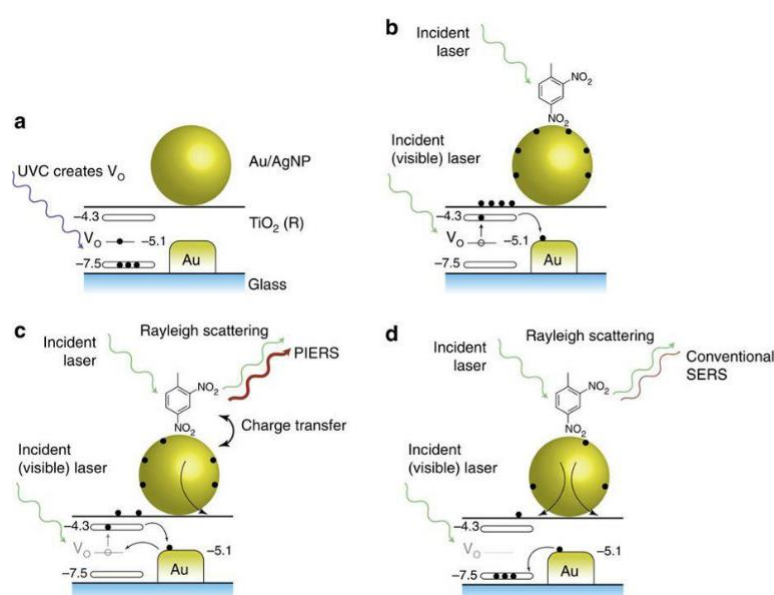


Figure 14 (a) UV-C light creates oxygen vacancies V_O in the TiO_2 conduction band. (b) The sample is deposited and the laser light photoexcites the TiO_2 , leading to increase in charge on the nanoparticles. (c) The charged nanoparticles lead to the PIERS enhancement. (d) The PIERS effect gradually diminishes as the V_O are completely replenished over time. Reproduced with permission from reference [159]

1.6.3 Materials

Among the various semiconductor materials, TiO_2 has attracted considerable attention as both a SERS-active substrate and a photocatalyst enjoying high stability, high activity and low toxicity¹⁶³.

Semiconductor materials have been frequently proposed as a prospective interface for the immobilization of biomolecules¹⁶⁸. They can form coordination

bonds with the amine and carboxyl groups of biomolecules, allowing their bioactivity to be maintained. Thin metal oxide films are employed as substrates in a broad range of fields including the active surface for SERS. These work well for PIERS suggesting that these substrates can be applied to broader applications. Although other rough substrates are available and provide SERS and PIERS enhancement, vapour-deposited thin films are widely used because of their stability and ease of preparation and characterization^{158,169}.

1.6.4 Applications

As it is still a new technology in its infancy, the extent of the applications of PIERS have not been fully investigated but early research shows that this could be useful in the detection of explosive materials as well as very trace levels of toxins in other research areas. It has the potential to enhance the Raman scattering 10-fold over established SERS methods. For practical SERS detection, a recyclable SERS substrate is highly desirable in performing multiple experiments and reducing costs¹⁷⁰. The advancement of SERS is still limited by using expensive and large Raman instruments hampering their application in rapid field analysis. However, the integration of the PIERS technique with a portable Raman device would make it possible for practical applications¹⁶⁴. Currently, there is inadequate research on the preparation of PIERS substrates and the practical detection applications.

Recently, design rules for fabricating an ideal PIERS substrate were concluded after studying the PIERS effect of TiO_2 ¹⁵⁹. These requirements include a crystalline semiconductor capable of absorbing the visible Raman excitation laser, a semiconductor conduction band energy greater than the Fermi level of plasmonic nanoparticles, a probe molecule capable of undergoing charge transfer and whose Raman polarizability is enhanced and not suppressed upon charge transfer¹⁷¹. These detailed conditions set limits on the range of semiconductor and molecular system that can exploit the PIERS effect and raises the question whether PIERS can be as broadly applied as SERS.

Nonetheless, work is still needed to investigate the influence of morphology, crystallinity, phase, crystal size and composition of the semiconductor materials in relation to its PIERS effect.

1.7 Aims and Objectives

1.7.1 Research problem

The monitoring of biomarkers holds great promise as clinical diagnostics to facilitate the successful treatment of disease and improve the patients' survivability. Most approaches in clinical diagnostics are accomplished using lab-based sandwich-type immunoassays which are tedious, time consuming and require experienced personnel making them unsuitable as a rapid, high throughput clinical diagnostic method. Similarly, SPR and fluorescence also face challenges.

There is an urgent need to address the problems preventing SERS from a promising technique to a practical one. Further efforts are required to improve the data reproducibility, substrate stability and substrate-analyte interactions.

1.7.2 Research Aim

SERS is promising technology offering enhanced sensitivity, simplified instrumentation and increased analytical throughput. With its many desirable attributes, SERS offers a potential POC technology with the ability to detect and quantify low concentrations of molecules. Raman scattering does not require external labels and has been widely used in the biological and pharmaceutical fields¹⁷². Furthermore, it provides a promising tool to reveal structural differences between different biological components. These differences are subtle so more sensitive and reliable analysis such as principal component analysis (PCA) is required.

However, firstly it is necessary to prove the concept of flexible materials as plasmonic substrates for label-free SERS, especially for this application. The biosensing capabilities of these SERS substrates to detect complex biomolecular targets is investigated with several additional parameters considered. The design of a substrate should not only give high SERS output but fulfil extensive criteria from its mechanical properties to the reproducibility of

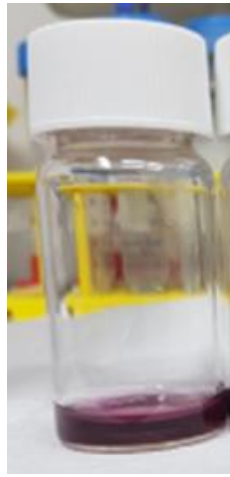
the signal. Only after careful characterisation can these substrates be thought of for use in a biomedical context.

The following chapters will explore the topics covered in Chapter I in more depth with an emphasis on the results obtained in the studies. Initial examination is conducted on developing effective SERS colloidal substrates, looking at, and comparing gold nanoparticles and applying them to analytes for SERS detection. Following this, flexible substrate materials are developed for SERS analysis. Initially small molecules are chosen as target analytes, but this progresses to macromolecules like proteins and biological samples. Finally, PIERS is investigated as a phenomenon as an extension to this field, with a focus on detection of biologically relevant molecules and the influence different parameters have on the observed effect.

The aim of this thesis is to develop stable colloidal gold nanoparticles with longevity and high SERS ability that can be incorporated into flexible materials to introduce SERS activity into the newly functionalised materials. These materials should be able to detect and identify a host of different molecules by producing unique, reproducible, fingerprint Raman spectra without the use of any tags or labels. This should set a precedent to research into label free SERS for the successful detection of biomarkers for disease prognosis, providing clinicians with an alternative, complimentary technique for biosensing. The work conducted in this thesis is novel with very little literature on the particulars concerned so any results provide a better scientific understanding to applying SERS utilising these methodologies.

Chapter Two

Investigating Colloidal Gold Nanoparticles for SERS Substrates



Chapter II: Investigating Colloidal Gold Nanoparticles for SERS Substrates

2.1 Introduction

The basis of SERS relies on the electromagnetic enhancement mechanism of nanoparticles (NPs) as discussed in chapter I and thus, producing good quality NPs is fundamental for performing SERS measurements. Bare gold NPs are unstable and will undergo aggregation gradually precipitating as metallic powder. Nanoparticles can be stabilised using protective or capping agents that cover and prevent aggregation by keeping the particles away from each other⁴⁹. The most common mechanism for the stabilisation of NPs is charge stabilisation and steric stabilisation. By acquiring a charge on the surface, they repel each other from becoming aggregates. Coating the NP with large molecules prevents them from touching each other by steric effects¹⁷³. NP size can be controlled by the strength and concentration of the reducing agent. The shapes of the gold NPs can be controlled by adding surfactants during synthesis¹⁷⁴. These will cause a change in surface energy and control particle aggregation. The choice of suitable capping moieties is crucial in stabilising colloidal solutions and their uptake into living cells and the environment.

Gold nanoparticles are promising candidates as SERS substrates as they are easy to prepare, more stable than silver and copper and are biocompatible¹⁷⁵. Gold NPs present in suspensions are called colloids. Colloids are attractive in research due to their intrinsic properties, such as high surface to volume ratio^{176,177}. The synthesis of gold NPs by trisodium citrate mediated reduction of aqueous chloroauric acid is one of the most popular synthesis strategies for gold NPs¹⁷⁸. This synthesis approach involves the rapid addition of citrate into a hot aqueous solution of chloroauric acid where the citrate acts as a reducing agent, capping agent and pH mediator simultaneously. This method has been modified and optimised over many years.

A common approach for controlling the morphology of NPs is the seed-mediated growth method. It has been established that this method produces particles of an improved mono-dispersion relative to the Turkevich methods and

works by allowing smaller particles to grow into larger particles of a pre-determined size. The seed mediated growth of gold nanoparticles is categorically divided into two steps⁴⁷. The first step involves the formation of spherical gold seeds by rapid reduction of gold ions using a strong reducing agent in the presence of a stabilising agent. The second step involves the addition of the seeds to a growth solution containing chloroauric acid, capping agents and reducing agents¹⁷⁹. The synthesis of the seeds is done at elevated temperature as it is the best way to control the monodispersity of the seeds.

This chapter will outline several strategies employed to produce gold nanoparticles of different shapes and sizes, and how these may correlate to their SERS functionality. This chapter focuses more on the experimental side of obtaining gold nanoparticles as well as their ability to enhance Raman signals from a range of different analytes. The reproducibility, ease of preparation and stability will all play an important role in determining the suitability of the gold NPs for biomedical applications. This chapter also demonstrates the role of capping agents on the final SERS performance of the gold nanoparticles. Optimum reaction conditions will be investigated, and a protocol is established that will be used for the remainder of the chapters. Modification of the gold NPs as well as researching their multiplex ability will be discussed in this chapter to yield the highest functioning gold NPs.

This comparative study investigates which gold nanoparticle substrate is the most effective for research into label-free SERS of biomolecules, while considering all parameters that dictate the suitability of the gold NP for its practical applications.

2.2 Materials and Reagents

Tetrachloroauric acid (III), 99% ($\text{HAuCl}_4 \cdot 3\text{H}_2\text{O}$), sodium borohydride, $\geq 98.0\%$ (NaBH_4), L- ascorbic acid (AA), 99%, trisodium citrate, anhydrous, $\geq 99.0\%$, citric acid, $\geq 99.5\%$, cetyl-trimethylammonium bromide, $\geq 99\%$ (CTAB), Tris base, Trizma® base, $\geq 99\%$ (Tris), Rhodamine B, $\geq 95\%$ (RB), 2-naphthalenethiol 99% (NAT), 4-aminothiophenol, $\geq 97.0\%$ (ATP), para-aminobenzoic acid, ReagentPlus®, $\geq 99\%$ (PABA), gamma – aminobutyric acid, $\geq 99\%$, (GABA), L- glutamic acid, $\geq 99\%$ (Glu), L-tryptophan, $\geq 98\%$ (Trp), Dopamine hydrochloride

(DA), L-cysteine, 97%, (Cys), salicylic acid 99% (SA), D-glucose, $\geq 99.5\%$, 1-octanethiol, 98% (Oct), 1-dodecanthiol, 98%, (DDT) and 1,4-benzenedimethanethiol, 98%, (BDT) were all purchased from Sigma Aldrich Ltd. Ultrapure deionised water and absolute ethanol 99.9%, extra pure, used as supplied from Sigma Aldrich Ltd, was used for solution preparation and experiments. All chemicals were used as received without any further purification.

2.3 Experimental

Several methods were utilised to produce both silver and gold nanoparticles as well as composites. However, gold nanoparticles showed higher stability and therefore were the plasmonic material of choice.

2.3.1 Synthesis

A protocol was established for the synthesis of reproducible gold nanoparticles with high SERS functionality with various capping agents, Figure 15. This method is simple, facile and scalable. Highly stable and long living gold seeds are synthesised by the reduction of gold ions using sodium citrate. 1 volume% $\text{HAuCl}_4 \cdot \text{H}_2\text{O}$ was mixed in 100 mL of distilled water at 100°C on a hotplate and magnetically stirred. 1 mL of 1 wt% sodium citrate was added followed by 2 mL of 0.075 wt% sodium borohydride in 1 wt.% citrate. Stirring was maintained at boiling temperature for an hour then allowed to cool to room temperature after a pale dark purple colour had been attained.

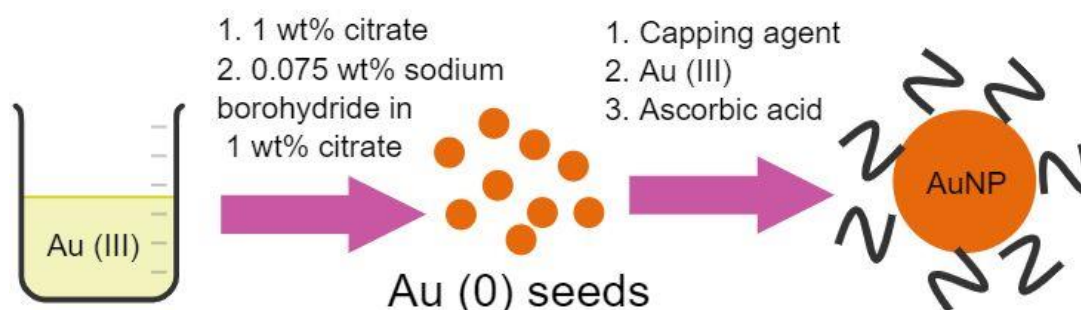


Figure 15 Diagram showing the seed mediated growth method for gold nanoparticles. This protocol was used for the synthetic experiments for all type of gold colloidal nanospheres.

1 wt. % sodium citrate, 100 mM TRIS base and 1 wt. % CTAB were all dissolved in distilled water and used as prepared as capping agents for the gold nanoparticles.

The seeds can be kept at room temperature and have a long shelf life. These can be used each time synthesis is required. For the growth stage, 2 mL seeds were added to 20 mL distilled water, 500 μ L of the capping agent, 500 μ L of 25 mM HAuCl_4 and these were magnetically stirred at room temperature. One minute after the addition of the gold, 500 μ L of 100 mM Ascorbic acid with 10 μ L of 10 mM sodium hydroxide was added and colour change from a light yellow to purple-red was instant. The best result was achieved by making the reagents required for the growth step fresh. This ratio of reagents was found to produce the most reproducible and stable gold NPs (spheres).

To further expand the catalogue of SERS substrates, gold nano shapes featuring a range of different shapes from spheres, triangles and hexagons were synthesised. 0.75 mL of 25 mM HAuCl_4 was added to 1 mL of 5 mM aqueous solution of PVP. After letting it stir magnetically for 1 minute. 0.2 mL of 100 mM ascorbic acid was added and left for 5 minutes. A deep purple colour was observed indicating the formation of gold nanostructures.

The synthesis protocol followed here was designed to obtain gold nano stars. 100 μ L of 10 mM silver nitrate and 150 μ L of 25 mM HAuCl_4 were added to 3 mL of 2 mM CTAB in a beaker with constant magnetic stirring. 24 μ L of Au seeds was added followed by the dropwise addition of 120 μ L of 100 mM ascorbic acid. The colour change was seen after constant stirring for 15 minutes. A blue colour was observed.

2.3.2 Self-assembled monolayers (SAMs)

Alkanethiols are the most commonly prepared reagents for the surface modification of gold nanoparticles. The molecular self-assembly of long chain alkanethiols on gold has drawn considerable attention over the past decade.

Different molecules were chosen to modify the surface of the gold nanoparticles. 2 mM solution of the alkanethiols: 1- octanethiol (OCT), 1- dodecanethiol (DT), 1,4 benzenedimethanethiol (BDT) and 11-

mercaptoundecanoic acid (MUA) were synthesised in 99% ethanol. All these reagents contain a sulphur group allowing for the easy chemisorption to colloidal gold particles. The hydrocarbon chain is varied as well as the terminal group to see the effect this would have in the resulting SERS spectra. The actual fabrication of the SAM is done by immersing the SERS substrate in a nonaqueous solution of the thiol. The SAM protects the SERS active surface from degradation thereby extending its lifetime.

1 volume% of the SAM was mixed with the gold nanoparticles in a vortex:10 μ L of the SAM in 1 mL gold NP. A 1:1 ratio of this mixture with the analyte was then drop cast onto a glass slide for Raman acquisition.

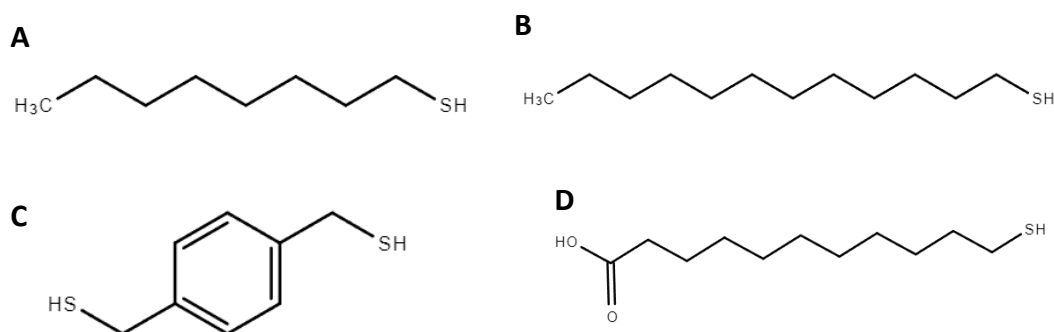


Figure 16 Molecular structure of the different SAMs employed in this study: A) 1-Octanethiol, B) 1-Dodecanethiol, C) 1,4 Benzenedimethanethiol and D) 11-Mercaptoundecanoic acid.

2.3.4 Target analytes

A range of different probe molecules were chosen to assess the SERS activity of the substrates synthesised. 1 mM and 1 μ M Rhodamine B (RB) were prepared in aqueous solution using deionised water. Several probe molecules were investigated, and 100 mM stock solutions were prepared in suitable solvents, DI water or ethanol, depending on solubility. Probe molecules included tryptophan, 4- aminothiophenol (ATP), cysteine (Cys), glucose (Gluc), salicylic acid (SA), glutamate, γ -Aminobutyric Acid (GABA) and para-aminobenzoic acid (PABA). These were diluted as required for concentration studies using the most suitable solvent.

2.3.4 Characterisation

UV-VIS

UV-Vis measurement is done using Model S-200 Vis Spectrophotometer from Boeco system, Germany with a single beam tungsten halogen lamp for the light source. Disposable cuvettes were used, and water was used to serve as the blank for background measurement. 0.5 mL to 1 mL of sample volume was used measured at a wavelength range of 320 to 800 nm at a wavelength scan speed of 2400 nm/min with absorbance ranging from -0.3 to 3.00. The data was stored on a SD card and transferred to PC using the software MasterReport, for further processing of data.

Dynamic light scattering (DLS)

The hydrodynamic particle size and surface ζ -potential of the AuNPs were measured using a zetasizer (Malvern Zetasizer Nano ZS). Briefly, samples were diluted in solvent of choice and injected into a Malvern capillary cell and placed in the zetasizer. The hydrodynamic radius of the particle was then measured using DLS. The same sample was subjected to Laser Doppler Micro-electrophoresis which measures the velocity of the particles across the electrodes and enables the calculation of the zeta potential. The back scattered light collection was set at 90 degrees. Each sample was analysed in a triplicate and each measurement was an average of three 30 second runs. Data was collected and analysed using MAS OPTION particle size software. Hydrodynamic diameters were referred to as the effective diameter cumulant analysis.

TEM

TEM studies were made by using JEOL JEM-2010F at an acceleration voltage of 200 kV. A drop of the dispersion was placed on carbon-coated copper grid purchased from Sigma Aldrich Ltd followed by drying at room temperature overnight.

Raman

Two different Raman instrumentations were utilised since over the course of this PhD, the work was carried out in two institutions, A*STAR, Singapore and UCL, UK.

A Renishaw 1000 spectrometer equipped with a 633 nm laser was used for Raman spectroscopy studies. The diameter of the light spot area was 1 μm and the spectral resolution and the incident power were 1 cm^{-1} and 9 mW respectively. The spectra were recorded with an accumulation time of 10 s.

SERS measurements of samples were performed using a Renishaw InVia Raman upright microscope (Renishaw InVia, UK) with a 633 nm laser. This Raman system was integrated with a Leica microscope and the laser light was coupled through an objective lens (20 x, 0.75 numerical aperture), which was used to excite the sample and to collect the scattered Raman signal. The prominent Rayleigh scattering was blocked using a notch filter and the beam spot on the sample was $\sim 1 \mu\text{m}$. 10 spectra per sample were acquired over 10 different spot areas. Each spectrum was integrated 10 sec, in the range of 400-1800 cm^{-1} . After collecting the SERS spectra, post-processing was done using wire 3.4 software associated with the instrument. The background subtraction was done by a cubic spine interpolation. The instrument was calibrated with signal from standard silicon at 520 cm^{-1} . The laser power was kept at 100% unless it lead to saturation, in which case the laser power went down to 1%, as was often with the Rhodamine B samples.

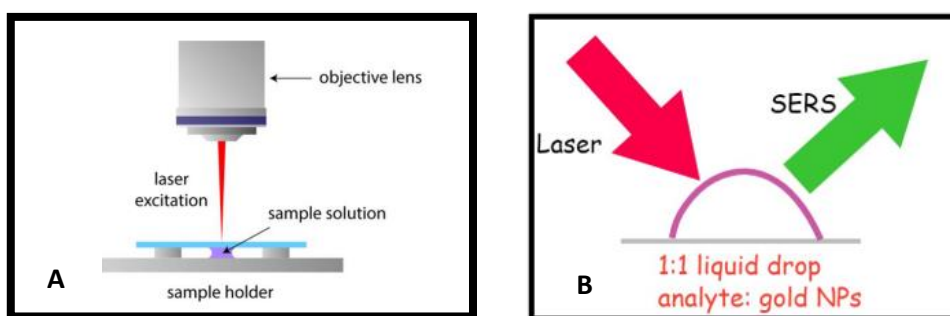


Figure 17 Schematic illustrations of A) the Raman instrumentation and B) the SERS acquisition.

A 1:1 volumetric ratio of gold NPs: analytes were mixed, vortexed for 30 seconds, before drop casting on a glass slide for Raman acquisition. This means equal quantity of both the gold NPs and analyte were mixed, and 10 μ L was deposited on the glass slide. The concentration of gold NPs was difficult to evaluate due to the seed growth method employed. The concentration of gold seeds was kept constant in each experiment and can be estimated that the final concentrations did not vary greatly but these are difficult to approximate. Studies using BBI, commercially available gold NP solution, confirmed that a 1:1 volumetric ratio was the optimal ratio, giving the highest SERS result.

Baseline correction is performed before the normalisation of the Raman spectra to avoid bias. Normalising the spectra allows for further chemometric analysis to be conducted. The intensity is not displayed for all the Raman spectral graphs as the purpose of this study is to compare which gold nanostructure gives a good SERS result, hence the focus is on the qualitative analysis rather than the quantitative values of the intensities. Rhodamine B samples were done at low laser power (LP = 1%) which can be seen in their low intensities. The Raman intensities are shown for discerning and comparing the different gold NPs with the same analyte, and whether it is relevant in demonstrating the results. The intensities are not displayed for the duplexing or SAM testing as the current study is more interested in whether the peaks can be detected in the sample and for the analysis of multiple spectra at one time .

Once the gold nanoparticles were produced, they were fully characterised.

2.3 Results and discussion

2.3.1 Preliminary SERS

Initial SERS studies were performed on each of the gold nanoparticles with 1 mM Rhodamine B (RB). RB is a synthetic dye and has been labelled as an illegal additive in food by European Food Safety Authority¹⁸⁰ (EFSA). It was selected as a probe molecule to assess the SERS ability of the different nanoparticles due to its easily identifiable spectral peaks as well as practical applications.

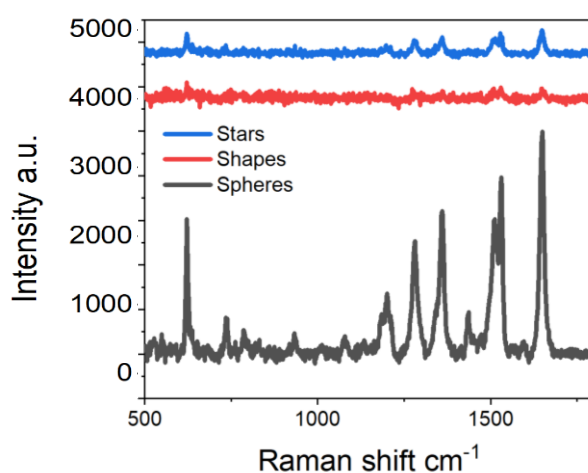


Figure 18 SERS spectra of 1 mM RB on the different kinds of gold nano shapes. The background was removed and the baseline was offset for clarity.

All of the gold nanostructures showed characteristic peaks of RB at 1193 cm^{-1} , 1354 cm^{-1} , 1504 cm^{-1} and 1644 cm^{-1} attributed to the different aromatic C-C bending, C-H bending and C=C stretching¹⁸¹. These can be seen very obviously at 1 mM concentration. The different shapes were compared with the spherical gold colloids and these peaks are easily identifiable. It can be observed that the SERS spectra exhibited well-defined and high-resolution Raman spectral lines in the absence of any background fluorescence. RB molecules can be adsorbed on the surface of citrate-stabilised gold NPs due to electrostatic interaction.

Characterisation of gold nanoparticles

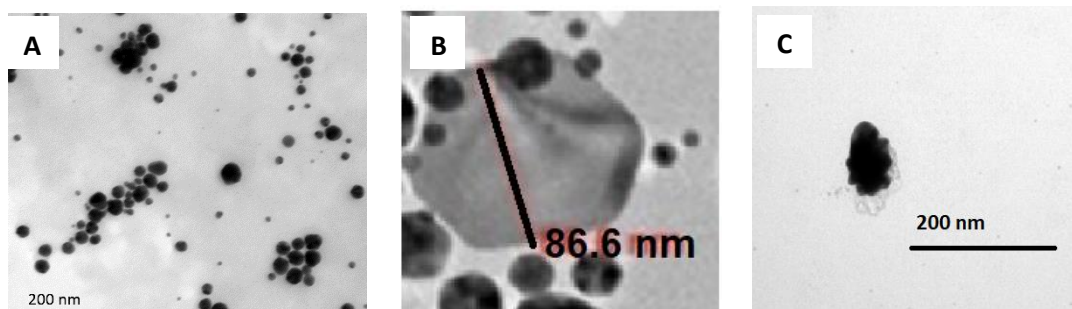


Figure 19 TEM images of A) gold nano-spheres B) gold nano- shapes and C) gold nano-stars with some indication of their sizes.

The size of the different gold nanostructures is an important parameter to consider when addressing the resulting SERS function of the plasmonic nanomaterials. The sizes quoted are only an average and both the stars and the shapes had very broad bands in their DLS data indicating a wide size distribution. There are several definitions of various parameters for characterising a gold nano star which may lead to discrepancies within the data and why the UV-Vis is very red shifted but the DLS quantifies the stars to be smaller than the shapes. Even though the recipe was followed to produce stars it was not successful. They are ill defined and non-uniform but can be referred to as multi-faceted gold nanoparticle. For NPs that are not spherical the DLS provides the radius of a hypothetical hard sphere moving at the same speed to that of the aspherical NP within dispersion. The detection limit of DLS varies from instrument to instrument, because the detected scattering light intensity is related to the wavelength and power of the incident light, the type of detector, and the detection angle¹⁸². High concentration of NPs results in multi-scattering where the scattered light from one particle interacts with other particles before reaching the detector and loses intensity. As a result, the obtained size is artificially smaller. NPs also tend to agglomerate, thus making it difficult to

produce high quality DLS data from dispersions with agglomerated NPs as the bigger lumps scatter too much light causing damage to the laser¹⁸³.

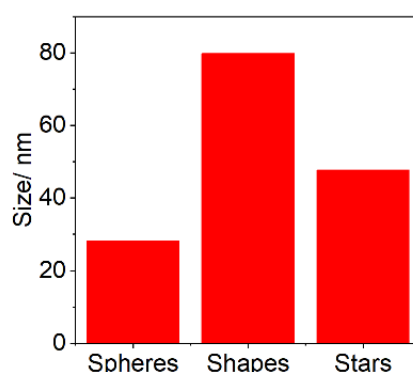


Figure 20 Average DLS measurement of the different colloidal gold structures.

The nano shapes have the largest size distribution, which is corroborated with the TEM images, Figure 19 and 20. The morphology of the shapes can be seen with a variety of particles formed. Many different shapes were synthesised including triangles, rods and hexagons. There appears to be no control in the type of shape forming. This is corroborated by other reports of PVP stabilised nanoparticles producing a wide variety of different geometrical shapes. The TEM shows the size, degree of aggregation, and dispersion as well as the heterogeneity of the nanomaterial. The PVP molecular weight affects the rate of nucleation leading to the formation of different sized polyhedral shapes. TEM images reveal the distribution of particles in small monodisperse groups, but the stars are seen to be in aggregates. For the colloidal spheres, there is more uniformity in the NP size and shape, with a smaller size distribution. Although there are some overlaps among parts of the globular gold NPs, they are not agglomerated; instead, the morphology of each particle is still maintained. The anisotropic multi-faceted gold NPs show several small nanoscale branches protruding from the centre bulk particle, but these are ill-defined. CTAB is used to direct the growth of the stars, allowing preferential lengthening of the gold crystal whilst silver ions are used for creating active sites¹⁸⁴. For nano stars, the twin defects on the surface of the seed are postulated to weaken the binding of the positively- charged CTAB surfactant, allowing for the growth of branches at

these sites. It has been reported that the morphology and particle size can be controlled by changing the amount of gold seed precursor and CTAB.

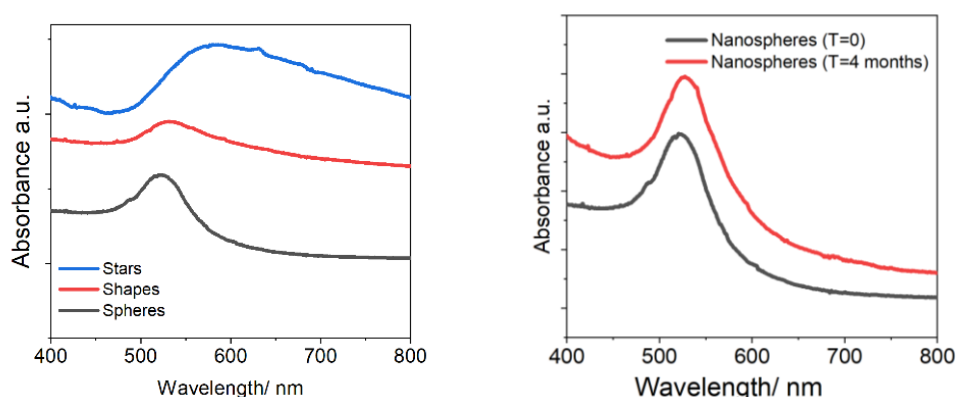


Figure 21 (Left) UV-Vis spectra for the different gold nanostructures and (right) UV-Vis spectra for the gold nano-spheres at different time intervals.

Gold NPs interaction with light is strongly dictated by their structural properties. Due to the collective oscillation of free electrons in the conduction band, nanoparticles demonstrate a characteristic surface plasmon resonance (SPR) band which ranges from 515 to 570 nm in the visible region¹⁷⁸. For small monodisperse gold NPs, the SPR causes an absorption in the blue-green portion of the spectrum while red light is reflected, yielding a rich red colour. As particle size increases, the wavelength of the SPR band shifts to longer, redder wavelengths. This can be observed with change in colour to pale blue or purple. The colour of the gold nanospheres show the fingerprint colour, a red wine, corresponding to its characteristic surface plasmon (SP) absorption peak at 522 nm, Figure 21.

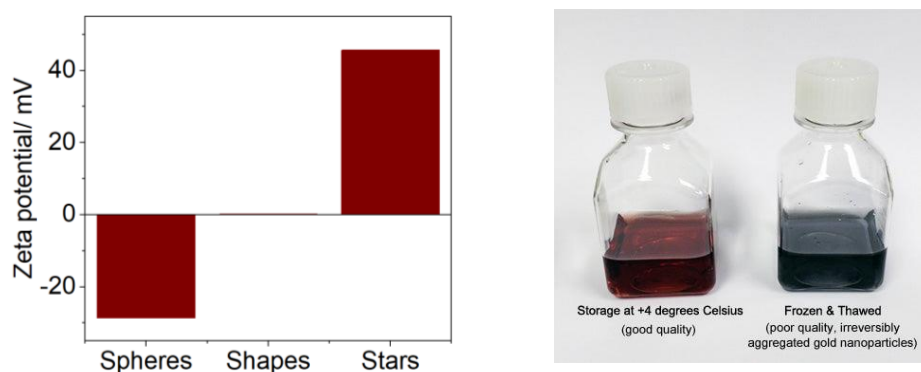


Figure 22 (Left) Zeta potential for the different gold nanostructures and (right) image showing stable and aggregated gold nanoparticles. Reproduced with permission from reference [72].

The UV-Vis spectra confirm the data from the DLS with the spheres being the most blue-shifted with the SPR band at 522 nm. The stars have a spiky uneven surface causing a red shift in the SP peak, around 561 nm. The UV-Vis band shape indicates the dispersity of the nanostructures; both the shapes and spheres seem to be monodispersed but the broad band for the stars indicate the stars have formed aggregates which can be verified by the TEM. It is to be noted that whilst UV-Vis spectra can reveal data about the concentration of the gold NPs the data presented cannot be directly correlated with the concentration as some samples were diluted for the data to be within the parameters of the instrument. The peak profile, width and position is of the biggest relevance to the current study. The size distribution can be refined by controlling the nucleation and growth stages during chemical reduction. The narrow size distribution of the gold spherical colloids can be attributed back to the synthetic route; the seed-mediated growth. Consistent gold seeds are vital to control subsequent shape and size.

UV-Vis spectroscopy is a simple and reliable method to monitor the stability of the nanoparticles. The optical properties of gold nanoparticles change when particles aggregate and the conduction electrons near each particle surface become delocalised and are shared amongst neighbouring particles. When this happens, the SPR shifts to lower energies, causing the absorption peak to red-shift to longer wavelengths. As particles destabilise the peak will broaden, or secondary peaks may become present due to the formation of aggregates. Flocculation may lead to sediment or phase separation to occur⁷². These are accompanied with visual changes in the colour of the solution, Figure 22. The gold spheres showed a similar SPR peak even after a significant amount of time had passed. The peak has only slightly been red shifted but the band width remains the same implying the absence of any aggregation.

The zeta potential provides useful information about the charge carried by the gold NPs and therefore its stability and ability to interact with analyte molecules. If the particles have a sufficiently high repulsion, the dispersion will resist to flocculation and the gold NP system will be stable¹⁸⁵. Most of the gold NP dispersions carry an electric charge which is strongly linked to the pH of the system. Surface ions that are adsorbed onto the surface of the gold NP can

lead to a positively charged surface or a negatively charged surface depending on the nature of the surfactant. The magnitude of the zeta potential gives an indication of the potential stability of the system. A large positive or negative value describes a repulsion of the particles, having no tendency for them to come together. However, if the particles have low zeta potential values, then there will be no force preventing the particles coming together and flocculating³⁷. Generally, organic molecules bound to the NP core impart stability through electrostatic repulsion, steric stabilisation or a combination of both mechanisms. The gold spheres had a large negative zeta potential at -29 mV which is typical for citrate-stabilised nanoparticles. The citrate ion is anionic and therefore negative on the surface of gold nanoparticles, but it is important to note that the zeta potential is a property of the whole system including pH, ionic strength and composition and not just the particles themselves. It was found that, by increasing the pH of the ascorbic acid by the addition of sodium hydroxide, the system became more stable. The addition of the alkali to the system makes it acquire more charge. The stabilizing effect of protective surface layers has been well documented. Citrate is one of the most common of these and provides a highly negatively charged surface with good stability in water and weakly-buffered solutions.

CTAB is a positively charged surfactant and the zeta potential value depends on the CTAB concentration. CTAB is known to form bilayer structures on the surface of metals. Hence, the gold nano stars demonstrated a high positive zeta potential. Empirically, it is considered that absolute zeta potential values higher than ± 30 mV are indicative of stable dispersions¹⁸⁶. The shapes exhibited zero zeta potential implying minimum stability. The L-ascorbic acid was used as a reducing agent whilst the PVP acted as a stabilizing agent. In previous studies, surface charge has been manipulated by changing the polarity index of the reaction medium, adding ethanol to water in various volume ratios. PVP provides steric stabilisation, but the final NPs are neutrally charged which agrees with literature confirming the absence of significant charge on the particles. Steric stabilisation is simple, only requiring the addition of a polymer. Results in literature show very different behaviour of charge stabilised NPs to steric stabilised NPs. It has been hypothesized that PVP stabilised NPs are

more stable and widely dispersed at low concentration, but these need further testing¹⁸⁷. The zeta potential values are typical of the synthetic routes described here. By observation, the gold spheres possessed a strong shelf life, maintaining their colour over a few months, validated by the UV Vis spectrum (Figure 21) whereas the gold nano shapes and multi-faceted gold NPs underwent flocculation and sedimented out of the solution. These were evident by the dark sediment at the bottom of the sample in a colourless solution.

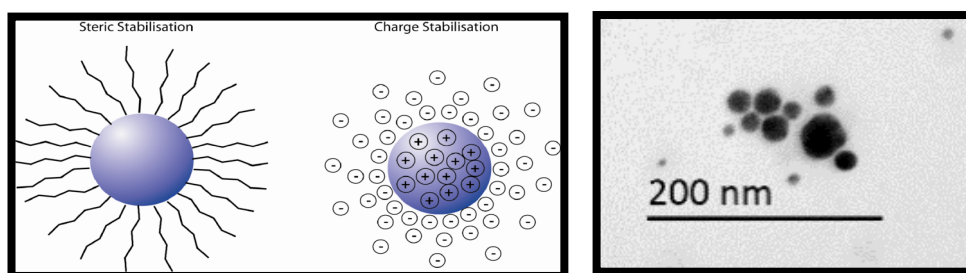


Figure 23 (Left) Diagram showing the different stabilisation effects on gold nanoparticles and (right) TEM image of the gold nano-spheres showing some aggregation.

The SERS function was tested at a lower concentration of RB, 1 μM . Distinct peaks belonging to the RB molecule can still be detected at this concentration, Figure 23. The spectra do become noisier, and the Raman peaks gradually drop as the concentration decreases which is to be expected. The peak at 620 cm^{-1} can be easily identifiable with all three nanostructures attributing to the xanthene ring puckering. It is also important to note that in SERS not all peaks are equally enhanced. The SERS profile follow the same pattern for both concentrations studied, with the gold spheres demonstrating the highest SERS efficacy. This can be explained by the cationic nature of the dye meaning that it is highly adsorbed on to citrate stabilised gold NPs. The homogeneity of the SERS signal is a significant parameter in evaluating the practicality of the SERS substrate. Repeat measurements were taken at arbitrary locations of the sample droplet and the Raman signals remained largely consistent at different points of acquisition.

Size effect of gold NPs

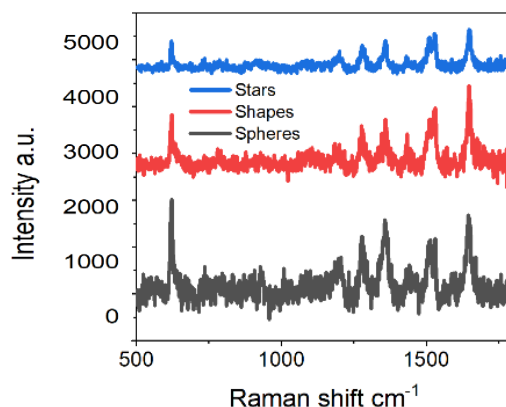


Figure 24 SERS spectra of the different gold nanostructures with 1 μ L RB. The background was removed and the baseline was offset for clarity.

A vast amount of research in SERS has been focused on correlating NP size with its SERS ability. Various groups have studied and reported the relationship between the enhancement and the shape and size of the gold NPs^{101,188,189}.

The results indicate that the SERS enhancement is highly dependent on many factors including the size, however, with controversial conclusions.

Nevertheless, there is agreement that it could be analyte dependent. The surface area of the SERS substrates is directly related to the enhancement achieved for a SERS measurement and can explain why all the nanostructures showed SERS intensity for RB. But because there is a large distribution in the sizes of the stars and the shapes it is difficult to accurately determine whether the size played a significant role in the overall SERS performance. There are other factors involved in the determination of the magnitude of enhancement. It is known that the local electromagnetic enhancement increases with increasing particle size.

As NP size increases, the convex shape of the surface becomes flatter, and the particles absorb less light, resulting in less inelastic scattering on the surface, leading to a weakening of the EM field on the surface and the overall SERS enhancement¹⁹⁰. Both the nano shapes and the multi-faceted gold NPs were bigger in size than the spheres and this may explain why the SERS intensity was highest for the spheres with average size 30 nm. As mentioned earlier,

increasing the size correlated to a red shift in SPR band. Largest SERS intensities have been reported for gold NPs with an SPR maximum between the wavelengths for laser excitation and for the vibrational band under study. Here, the 633 nm laser was chosen as it is closest to the SPR band of the NPs. The SERS signals were highly reproducible, suggesting that the hot spots are evenly distributed over the droplet sample. The advantages of faceted particles have been discussed but there has not been many findings on the experimental effects of the particle size and shape on the resulting SERS effect¹⁹¹. There has been reports of a class of star-shaped gold nanoparticle with sharp edges and tips that show a very high sensitivity to local changes in the dielectric environment, as well as larger enhancements of the electric field around the nanoparticle. Similar results have been found for gold NPs with sharp features. Gold nano shapes in the form of triangles have been studied with the conclusion that the concentration and size of triangles leads to optimal SERS conditions¹⁹¹. The local electric field enhancement in metallic nanostructures is strongly dependent on the shape of the metal protrusion.

Nanotriangles contain three sharp vertices that can contribute significantly to their optical and electronic properties. However, the shapes produced in this study covered a wide array, making it impossible to come to similar conclusions. In other studies where PVP has been used as a stabilising agent and a mild reducing agent, the resulting gold nanoparticles have been of different shapes¹⁸⁷. Having a mix of geometries may have resulted in a reduced SERS signal as well as affecting the aggregation state. Aggregation is not a well-controlled phenomenon and adds uncertainty and variability to the SERS system. This prompts further investigation into the isolation of different nano shapes to define their SERS ability. This contrasts with other studies in which nano stars showed to exhibit the highest SERS enhancement¹⁹². Nano stars contain a higher number of sharp corners and edges and have a more complex anisotropic shape. Due to their shape, different plasmon resonances have been observed and the Raman modes oscillate at markedly different frequencies in gold materials. These modes originate from the degree and direction of polarisation of the electron cloud relative to the incident electric field. Since nano stars contain more tips there should be a higher local field enhancement

but the particles synthesised here were pseudo-star shapes with no real defined protrusions, explaining why the SERS spectra for RB was not the highest. This also highlights the challenges in reproducing reported synthetic routes with accuracy. If the NPs cannot be reproduced uniformly then the SERS will also suffer. It is well known that the optical properties of metal nanostructures are more sensitive to shape and less so to size⁵⁵. By having a heterogeneous solution containing gold NPs of varying geometries its SERS efficacy may be reduced.

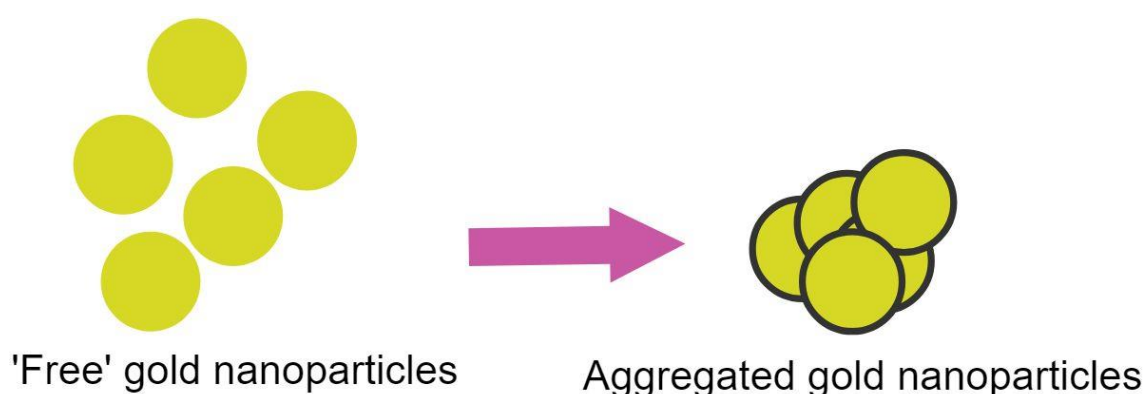


Figure 25 Diagram to show aggregation of gold NPs over time.

As a result of colloidal preparation, a fraction of the particles is aggregated into clusters. Molecules on the gold nano spheres' clusters scatter more strongly, thus enhancing their Raman intensity. Among each cluster size, hotspots are present in the gaps. The colloidal solution did show some particle dimers and a four-particle, nonlinear cluster can be seen in the TEM. These exhibit particularly high SERS, although SERS is highly variable among clusters as cluster shape and particle gap width are not controlled. Research groups have experimented on cluster size but have reached no conclusive results. In one study, colloidal dimers were found to enhance SERS more efficiently than clusters with a few more particles¹⁹³. SERS intensity is more strongly determined by the width of interparticle gaps. Precise measurement of gap width is difficult and goes beyond the scope of this study. The colloidal gold nano spheres, whilst being monodisperse, can form dimers, trimers and quadrimers that have resonances that span a broad range of wavelengths including the wavelength of the laser. Therefore, among each cluster size, hotspots are presents in the gaps. From nanoparticle clusters, large

electromagnetic enhancements are generated by gap plasmons within the nanojunctions. With the gold nano spheres prepared, there was a large ensemble of nanoclusters which could account for the high SERS for both concentrations of RB studied.

Wet vs dry droplets



Figure 26 Schematic to show the data collection for the wet and dry samples.

The Raman acquisition in this present study was performed on a wet droplet for each sample. Both wet and dry samples were tested to determine their influence on the SERS effect. This approach for sample collection may affect the resulting SERS capabilities of the gold nanostructures, and the observed SERS spectra. This was tested on probe molecule para-aminobenzoic acid (PABA) instead of RB. Generally, observation of resonance Raman scattering of RB is difficult because of the overwhelming amount of fluorescent produce with resonant excitation. When the sample spot dries, the intensity is too saturated for any effective Raman detection. The successful detection of RB Raman peaks for wet droplet acquisition demonstrates that collecting the sample in its liquid phase quenched some fluorescence.

PABA is a non-toxic B-complex vitamin and is an accepted measure to assess the completeness of 24 hours urine collection¹⁹⁴. It is considered a nutritional biomarker that is generally defined as an indicator of nutritional status with respect to intake or metabolism of dietary constituents. At 10 mM concentration, aqueous solutions of PABA were mixed with the colloidal gold NPs before drop casting on a glass slide. Raman was acquired immediately on the wet droplet while the droplet was allowed to dry for a few hours before Raman acquisition for the dried sample. At 10 mM concentration, the PABA does not exhibit its own Raman spectrum, so the SERS peaks are compared to the Raman spectrum taken from its solid powder form, Figure 27. For the peaks in the

spectral region of 1100-1800 cm^{-1} , there is one-to-one correspondence between the normal Raman and the SERS spectra. There is a strong peak, clearly

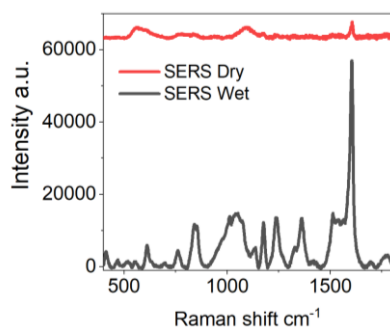


Figure 27 SERS spectra of 10 mM PABA with gold nanoparticles acquired in both wet and dry conditions. The background was removed and the baseline was offset for clarity.

identifiable at 1605 cm^{-1} which can be attributed to the in-plane ring breathing mode which dominates the spectra. The SERS spectra of the dried sample shows the carboxyl stretch at 1376 cm^{-1} which is absent in the dry sample. The appearance of different peaks in the SERS can be explained by the anionic form of PABA being present in solution and it is not uncommon to see shifts in the SERS peaks when comparing the spectrum to the normal Raman, imputable to the SERS selection rules and changes in orientation of the PABA molecule on the gold NPs. The peak at 1185 cm^{-1} can be identified in all three spectra which can be attributed to the in-plane benzene ring stretching vibration¹⁹⁵. Here, the wet spectrum of PABA is more defined, less noisy and reveals more peaks than the dried sample. While many studies dry the analytes before Raman acquisition, it has been reported that the SERS enhancement is stronger when the analyte is still wet. In point of care (POC) detection, it is imperative that a reading can be obtained as soon as the sample is applied to minimise waiting time. When the droplet remains a 'drop' it forms a small lens at the surface. This serves to further focus the laser, increasing the laser intensity.

The wet drop has a higher index refraction than the air, so the electric fields of the laser are further enhanced, producing a greater enhancement in the SERS signal. When the water is allowed to evaporate for dry collection, a so called 'coffee-ring' phenomenon occurs because of the radial outward flow that is compensating for solvent loss due to evaporation of the peripheries, which

results in an uneven distribution of the molecules and the nanoparticles within the dried droplet area¹⁹⁶. This could explain why the gold spheres gave the best SERS signals when compared to the other nanostructures as during wet sample collection the distribution is random and the sample is dynamic, so on average the SERS intensity is highest with the spheres as these appeared to be the most monodispersed. The aim of gaining reproducible spectra is governed by the interaction between the nanoparticle and analyte. Due to the outward solvent flow during evaporation, there is an uneven distribution of aggregates in a dry sample hindering the quality and reproducibility of the spectra by piling up of the nanoparticles and the analytes at the edges¹⁹⁷. Thus, even if the stars and shapes formed a high number of aggregates, in the wet sample, these are more difficult to locate, and a wet sample gives a better overall indication of the total SERS effect of the nanostructure being studied.

Summary

The effect of the gold spherical nanoparticle size on SERS enhancement has been studied experimentally. 50 nm diameter size has been reported to show the maximum SERS EF, where others research groups have reported the optimal size of particles to be in the range from 30 nm to 100 nm¹⁸⁹. Regardless of the exact size, there is an optimal range for effective SERS enhancement. When particles are too small, the effective light scattering properties diminish and when the particle size approaches the scale of the excitation wavelength, they become preferentially excited in nonradiative modes, leading to a decline in SERS efficacy.

Colloidal gold is more biocompatible than silver, its chemistry is well known, and its preparation is easier at desirable sizes. Much research has been conducted on its safe use in biological specimens. It will not create adverse or toxic reactions when encountering the skin, tissue, or internal organs. However, the concentration and the size of the gold NP does affect its toxicity with gold NPs above 30 nm being biocompatible at a limit of 5 mg/ mL¹⁹⁸. Along with it demonstrating high stability and reliable SERS measurements, these gold nanospheres were chosen as the nanoparticle of choice for the progression of

the studies. Measurements were conducted without any centrifugation or cleaning steps following synthesis representing a facile approach directly after the synthesis stage. The method for the preparation of the size and morphology- controlled gold nanoparticles was facile and practical. The enhancement factor (EF) was not calculated for the different gold nanostructures for rhodamine B as the fluorescent compound makes it hard to precisely estimate the enhancement factor of the Raman signals. The normal Raman intensities cannot be established due to the vibrational bands being very weak compared to the signals arising from the fluorescence, even at the lowest laser power intensity.

2.3.2 Capping agents

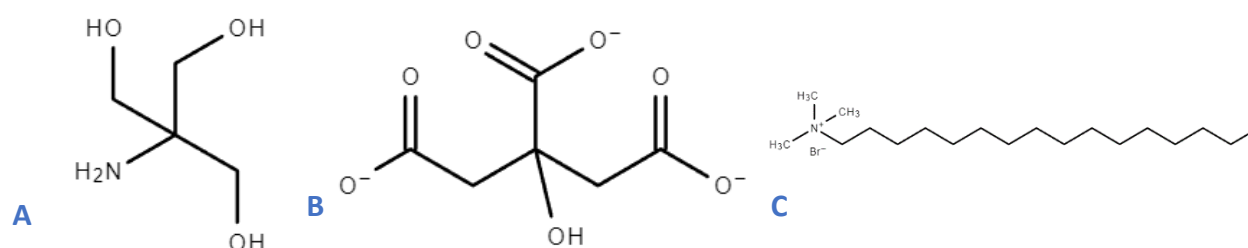


Figure 28 Molecular structures for A) TRIS-base B) sodium citrate and C) CTAB.

Gold colloids were easily synthesised with different capping agents to determine the most stable, reproducible and optimal SERS substrate for the detection of the analytes of interest. The seed mediated growth protocol used for the synthesis for the gold nano spheres was applied for the different capped gold nanoparticles. Citrate, Tris and CTAB were used as capping agents. Reducing agents or stabilisers under non-toxic chemicals are important for biomedical applications. TRIS is one of the most widely used buffers of nucleic acids and proteins in biochemistry and is active in reduction reactions in various conditions due to its specific structure¹⁹⁹. Citrate reduction is one of the most common methods for gold NP synthesis with a vast amount of literature dedicated to it. CTAB, a cationic surfactant is widely used in the synthesis of variously shaped gold nanocrystals. Positively charged gold nanoparticles have been developed for drug and gene delivery and have been used in biomedical applications. CTAB specifically has been applied to the SERS detection of biomolecules. Capping agents bind to the surface of the nanoparticle and prevents aggregation by repulsive or steric forces. They can also be used to

functionalise nanoparticles in extrinsic SERS application by providing a link to the bind the nanoparticle to the probe molecule²⁰⁰.

Characterisation

The colour of the final solution using citrate is blood red whereas the TRIS-capped NPs are more purple/red wine in colour and this is confirmed by the red-shift in the UV-Vis spectra. The CTAB-capped NPs produced a darker purple colour which is consistent with the SPR band being red shifted. These indicate the size and shape of the resulting nanoparticles to increase in the order citrate>TRIS>CTAB. The concentration of all the gold nanoparticles was estimated to be the same. The diameters of the NPs produced was estimated using DLS. The sizes strongly corroborate with the UV-Vis data, with the CTAB-capped NPs having the biggest size and most broad size distribution. The size and shape of gold NPs determine the spectral position of the SPR band and its width. The TRIS-capped NPs show a slight redshift in the SPR band towards a slightly longer wavelength highlighting the size increase. As demonstrated in Figure 29, citrate capped AuNPs show the well-known plasmon peak at 522 nm. All three gold NPs have a diameter greater than 30 nm which have shown to be more stable and essential for many diagnostic applications. The CTAB-capped NPs show a great redshift in the SPR band which is expected for the synthetic route employed. The broad band reveals a range of shapes and sizes were produced as well as larger aggregates. While not fully defined, the appearance of a second peak for the CTAB-capped NPs is attributed to the change of interspacing distance between the NPs.

The size of nanoparticles may change with time due to aggregation during storage conditions. Colloidal citrate capped gold NPs do not aggregate significantly over time as the spectrum revealed a single absorption peak. The absolute value of the zeta potential confers the stability of the gold NPs. The surface charge of the three capping agents covered a range of values as evidenced by their zeta potential values. These represent both positive and negative charges on the surfaces which can influence the gold NP behaviour and resulting SERS effect. Both TRIS and citrate demonstrate a negative zeta potential whilst CTAB is positive. Small changes in the metal particles surface charge can have serious implications in terms of stability, sensitivity to the environment as well as electro-kinetic properties. The nanoparticles surface charge is of utmost importance as the interaction between the analyte and the colloidal particles is a primary requisite for obtaining strong Raman enhancement. The zeta potential magnitudes are quite high demonstrating a moderate level of stability for the colloidal nanoparticles. While CTAB has a zeta potential of + 44 mV, making it highly stable under guidelines classifying NP dispersions, the reality is more complex.

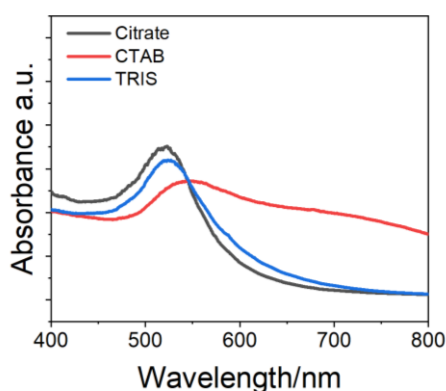


Figure 29 UV-Vis spectra of the different capped gold NPs.

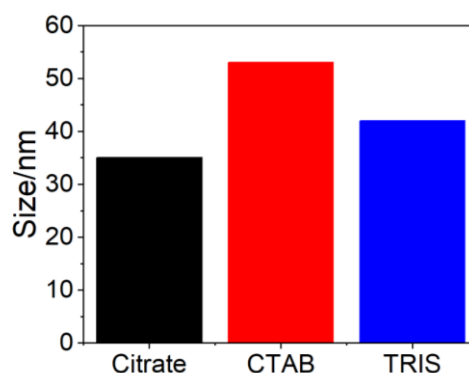


Figure 30 Average DLS measurement of the different capped gold NPs.

Although the zeta potential does provide an indication on colloidal stability it does not reflect the entire picture. Therefore, it is not uncommon to come across unstable colloids with high zeta potential values. CTAB capped NPs did not have a long shelf-life with changes in its stability visually recognisable by the naked eye after a few days. The formation of large aggregates usually results in agglomeration and flocculation of the nanoparticles exemplified in Figure 32.

Nanoparticle	pH
Citrate capped	3.77
TRIS capped	3.69
CTAB capped	3.03

Table 2 Table showing the measured pH of the different capped gold NPs.

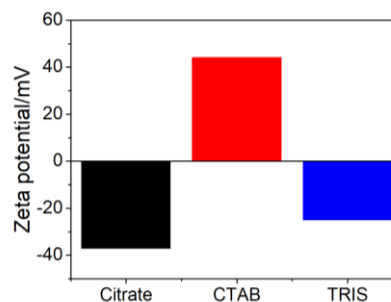


Figure 31 Zeta potential of the different capped gold NPs.

Aggregation is observed when dispersed molecules collide to form aggregates, an assembly of particles exhibiting an identifiable collective behaviour and the rate is dependent on the number of collision and the probability of cohesion²⁰¹. The phenomenon poses significant challenges for the translation of nanoparticles technology from the lab to a clinical product⁷². Aggregation and clustering allow for higher SERS to be obtained from hot spots but also results in larger particle size distribution and a lower reproducibility of the signal. CTAB-capped NPs had to be freshly synthesised many times before SERS could be conducted; this is heavily time consuming in practical applications.

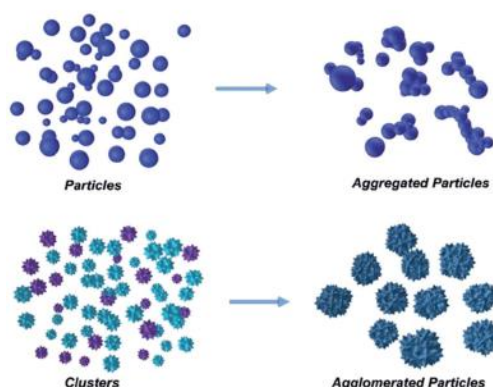


Figure 32 Diagram showing the difference between aggregation and agglomeration. Reproduced with permission from reference [201].

The pH plays a vital role in control of the size, shape, nucleation and growth of gold NPs. The pH can affect the overall stability but also how the analyte molecule interacts with the gold NPs and therefore its SERS magnitude²⁰². The pH increased in the order CTAB>TRIS>citrate as indicated in Table 2, all comprising a low pH, anticipated with the starting materials employed in this study. Most of the reagents required to produce the seed solution were acidic.

Even though TRIS and CTAB possess a higher pH value in aqueous solution once they were added to the seed reaction mixture, the pH dropped significantly along with the addition of further acidic reagents. While the electromagnetic enhancement is the dominant mechanism for SERS, chemical enhancement also plays a role because of its dependence on the electron density of the molecules. The pH can induce electron density variations in the molecules and allows for the separation of both enhancement effects on the SERS signal. It has been reported that pH can influence the observed SERS signals of small molecules and is important to note when interpreting SERS spectral data¹⁷⁸. The analytes may undergo protonation in acidic conditions affecting the adsorption of the target species on the gold substrate. For the citrate reduction method, it has been reported that when the pH of the reacting mixture is lower than 3.8 the resulting gold nanoparticles no longer stay dispersed after the reaction is complete. The mean diameter of the NPs decreases as the pH is increases, which agrees with the results reported here. However, there has been no studies conducted for the seed-mediated growth approach. At low pH, the preparation tends to produce a larger yield of faceted particles which may be useful for tuning the field enhancement of the Raman scattering.

SERS



Figure 33 Image showing the different capped gold NPs. (From left to right) CTAB, citrate and TRIS.

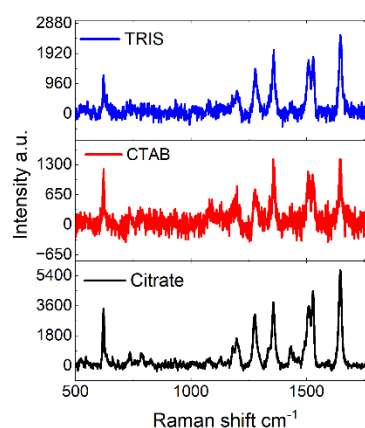


Figure 34 SERS spectra of the different capped gold NPs with 1 mM RB at laser power 1%.

SERS was first performed using 1 mM RB and all peaks can be clearly identified, and the spectra match each other indicating that all three moieties can detect RB, and there are no residual signals appearing from the capping agents used. The dominant peaks at 1649 cm^{-1} , 1509 cm^{-1} , 1360 cm^{-1} , 1217

cm^{-1} and 622 cm^{-1} are observed. The peaks can be assigned to xanthene ring stretch, the C-N stretch and the xanthene ring bending modes²⁰³. The citrate-capped gold NPs showed the highest enhancement. RB has been shown to be well adsorbed on the surface of citrate capped NPs. In neutral solution RB is a zwitterion due to the deprotonation of the carboxylic group and the benzene ring and therefore would tend to interact with the negatively charge gold NPs. Both the TRIS and citrate show negative zeta potential and therefore would show higher SERS. To further evaluate the SERS for each of the different capped NPs, other analytes were analysed.

4-aminothiophenol (ATP) was investigated as an analyte for the detection ability for the different capped gold NPs. Bifunctional ATP has a thiol (SH) group that is easily cleaved to form a metal-S bond and the protonated amino group can be adsorbed onto the negatively charged gold surface through electrostatic forces. The spectral bands observed in both the Raman and SERS of ATP have been classified into 4 different modes: A1, A2, B1 and B2²⁰⁴. Figure 40 shows the SERS for 10 mM ATP in ethanol and the ordinary Raman of the ATP solid powder. The predominant bands are located at 1594 and 1087 cm^{-1} , which can be assigned to the A1 (in plane, in-phase) modes of the ATP molecules; the C-S stretching vibration, which is in good agreement with previously reported data. The band visible at 1491 cm^{-1} is attributed to C-C (benzene ring) stretching mode²⁰⁵.

The SERS spectra for the different capped gold NPs share the same profile to the powder Raman except for slight variations in the relative intensities for some peaks as well as the addition of further peaks. The band at 464 cm^{-1} which is dominant in the Raman and becomes weaker in the SERS spectra can be explained based on the surface structure of the gold nanoparticles. This suggests a preferential binding of the ATP molecules on the surface of the gold NPs through the sulphur atom. There may be changes in the charge transfer conditions which may result in different enhancement behaviours. Changes in the charge transfer effect is supported by the corresponding intensity increases of the B2, in plane, ring stretching vibrational mode at 1433 cm^{-1} . The enhancement of this mode suggests the perpendicular orientation of the molecules on the gold surface. Different modes are enhanced by the two

mechanisms of SERS. The appearance of additional bands is not uncommon, and it is important to note that no ordinary Raman could be seen at 1 mM concentration without the presence of gold. The parallel spectral profile for all the capped NPs highlights that both positive and negative charged NPs can successfully detect 4-ATP in a non-aqueous solvent. The enhancement of the Raman mode at 1360 cm^{-1} is observed for CTAB and citrate capped NPs implying that the gold atoms make additional covalent bonds with 4-ATP molecules through the nitrogen atoms. There does not seem to be a correlation between the size of the particles and the resulting SERS for this current probe molecule. Some of the vibrational bands of 4-ATP can be enhanced due to the metal-to-molecule charge transfer (CT) mechanism which largely depends on the energy of excitation and the metal surface potential, hence why the different capped gold NP substrates cause a large increase in the intensity of the overall spectra.

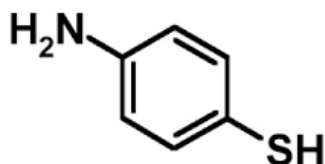


Figure 35 Molecular structure of 4-ATP.

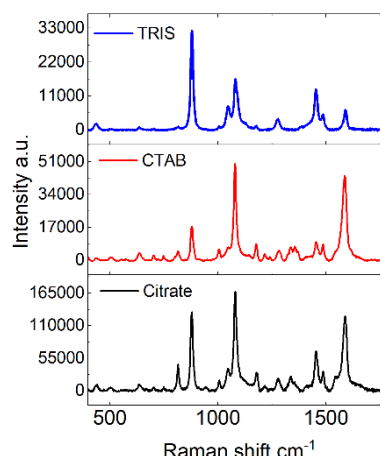


Figure 36 SERS spectra of the different capped gold NPs with 10 mM ATP.

Solvent effect

The peak at 882 cm^{-1} is an expected Raman peak associated with ethanol, which is identifiable in the SERS and not the Raman. It has been reported that the chemical nature of solvents plays a decisive role in the SERS of species adsorbed²⁰⁶. Ethanol can act as a competing agent in the system taking up sites on the substrate. Despite the prominence of ethanol in the SERS spectra, the bands of 4-ATP still dominate the SERS response, owing to the formation of the S-Au bonds (Figure 37). At lower concentration of the probe molecule the

solvent is present in higher concentration meaning that statistically the solvent molecules are more likely to be probed than the analyte molecules, Figure 35. Ethanol has its own inherent Raman spectrum and could interfere with the consequent SERS result of the substrates. SERS is rarely performed in non-aqueous solvent; hence, these results demonstrate the high SERS efficacy of the gold NPs which have a strong affinity for the ATP molecules.

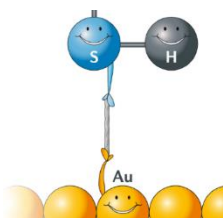


Figure 37 Diagram illustrating the favourable S-Au bond.

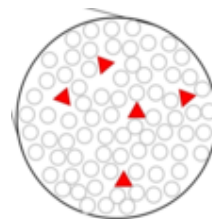


Figure 38 Schematic showing the increasing solvent molecules (circles) and fewer solute molecules (triangles) in a SERS system.

SERS of biomarkers

To further extend the applicability of the gold substrates, biological relevant molecules were prepared to determine if label-free detection of these target analytes could be established. Tryptophan is an extremely important amino acid for a variety of biological functions in living organisms²⁰⁷. Changes in the concentration of this amino acid can point to identification of cancerous tissues or even confirm symptoms of depression in patients. Therefore, there is a need to identify and quantify the concentration of tryptophan (Trp) in human blood. A 10 mM concentration of aqueous tryptophan was produced for SERS analysis. To interpret the resulting spectra, it is necessary to have a fundamental understanding of the interactions of individual amino acids and peptides with metal substrates²⁰⁸. The spectra reflect the mechanisms involved, both the EM and CM as well as the organisation and orientation of the analyte on the metal surface. Figure 42 shows the SERS of tryptophan and it can be seen that the spectra are much noisier than with other small molecules. The band assignment is performed based on published data. All three gold NPs have noise in the spectra, hindering the quality of the data. However, the most relevant indole band can be observed at 1007 cm^{-1} , ascribed to the benzene breathing vibration. The band at 758 and 1358 cm^{-1} is attributed to the symmetric

breathing mode and stretching COO^- mode, respectively¹⁷⁵. In general, a reduced number of bands are observed in the series of SERS spectra compared with that of the solid form. This is most likely due to conformers and specific orientation of the amino acid. The aliphatic bending CH_2 mode around 1361 cm^{-1} displays a random spectral behaviour, observed for CTAB and citrate capped NPs but very weak in the solid powder Raman. These confirm the hypothesis of different confirmations of tryptophan on the various gold substrates. The fact that all three spectra are dissimilar compared to the other probed analytes suggests the nature of the gold-tryptophan interaction is drastically modified. The high signal to noise (SNR) ratio emphasises the challenge of label free SERS on biological targets.

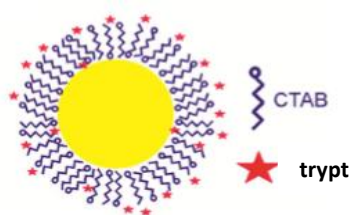


Figure 39 Diagram showing the gold NP capped with CTAB and the surrounded by the analyte.

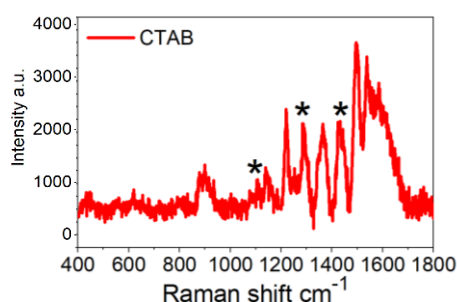


Figure 40 Raman spectrum of CTAB-capped gold NPs by themselves with highlighted (*) peaks attributed to CTAB.

The size, surface charge, and the presence of functional groups on the biomarker's surface play a defining role in the interaction between the gold and amino acid. TRIS-capped NPs shows a very weak spectrum whereas the CTAB-capped NPs, whilst showing more defined, narrower spectral bands, contains a lot of additional peaks that are not attributed to the amino acid, obstructing effective SERS for low concentration biomolecules. The CTAB gold NPs display the highest intensity, but these extra signals are characteristic of CTAB. The bands at 1127 , 1295 and 1460 cm^{-1} are assigned the C-C stretch, CH_2 twist and the CH_3 deformation of the CTAB molecules²⁰⁹. This arises due to the excess CTAB left in the solution which can be removed by centrifugation. However, the CTAB bilayer is physisorbed onto the gold NP surface and

constitutes a dynamic structure. Even if it were possible to remove all the unbound CTAB from the solution, some CTAB would eventually still enter the sample from the gold surface. The spectrum of the CTAB-capped gold NPs displayed its own detailed peaks as shown in Figure 40. The difficulty in obtaining a reasonable and rich spectrum is not surprising in the field of label-free SERS detection, especially for biomolecules due to their low affinity to the metallic surfaces and low sensitivity. If the gold NPs show their own inherent Raman this further increases the limitations in effective detection due to signal overlapping and reduced sensitivity.

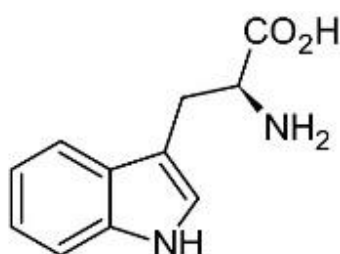


Figure 41 Molecular structure of tryptophan.

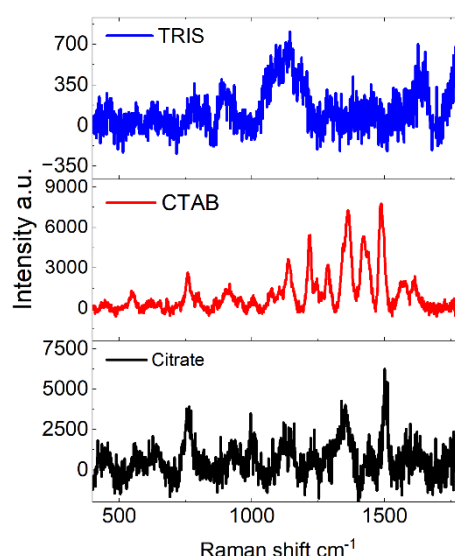


Figure 42 SERS spectra of different capped gold NPs with 10 mM tryptophan.

Neurotransmitter studies

Since CTAB- capped gold NPs are positively charged and have been reported to bind better with biomolecules, further studies were conducting using brain biomarkers to further evaluate their SERS function. γ -Aminobutyric acid (GABA) and glutamate (Glu) are major neurotransmitters in the brain. Changes in each of these metabolites have been implicated in the pathophysiology of a number of neurological disorders, such as but not limited to schizophrenia, autism, epilepsy and addiction²¹⁰. These biomarkers are useful in understanding brain function as well as treatment monitoring. Therefore, accurate and reliable estimation of glutamate and GABA is of significant interest. 50 mM aqueous

solutions of GABA and glutamate were prepared, and the SERS was collected, shown in Figures 43 and 44. As the gold substrates already exhibited their own Raman signals, the spectra acquired from the sample was subtracted from the CTAB gold NPs own inherent spectra to give an indication of whether the target analyte was being probed. The initial raw spectra were dominated by the CTAB peaks, but after data manipulation, the subsequent spectra displayed some Raman bands. These were normalised for ease of comparison and the normal Raman of both GABA and glutamate were taken from the solid powder form. The experimental results indicate GABA signals at 1235, 1332 and 1441 cm^{-1} attributed to the NH_2 and CH_2 bands²¹¹. The spectrum is only providing information between 1200 and 1600 cm^{-1} and the rest of it is too noisy to make out any distinct peaks. The bands appear wider in the SERS, making it more challenging for precise assignment. This can be due to the analysis performed on the raw data but also, the vibrational modes observed in SERS are not solely those of the molecule being probed, but the sample as adsorbed on the substrate. It is quite common that the full width half maximum (FWHM) of a SERS peak is broader than that of the ordinary Raman peak due to the more heterogenous state of molecules on the surface²¹¹. Glutamate signals are seen at 907, 1114 and 1356 cm^{-1} attributed to the C-C-N band and CH_2 band. There is good correspondence between the SERS bands of GABA and glutamate in water in the 50 mM range with their regular Raman. Both SERS spectra are unique confirming that the peaks are from the biomarkers themselves with no interference from the substrate. The appearance of band at 1386 cm^{-1} corresponding to the symmetrical stretching of the COO^- group is common for both GABA and glutamate²¹². The glutamate spectrum appears to be more resolved due to the formation of its fully ionised form. In contrast with GABA, glutamate has two $-\text{COOH}$ groups that can be deprotonated to form an overall negatively charged ion. This net charge may mean that there is a higher affinity to the positively charged CTAB-capped NPs enhancing its SERS effect, but there is no evidence to substantiate this theory in the current study. Yet, it can be stated that the effective surface charge impacts interactions of nanoparticles with the analyte directly influencing the mobility of the nanoparticles,

rationalising why glutamate may have a stronger affinity to the CTAB gold NPs than GABA.

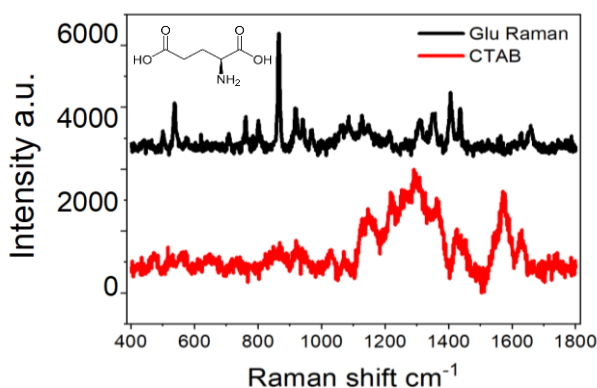


Figure 43 Raman spectrum of solid glutamate and SERS spectrum of CTAB-capped gold NPs with 50 mM glutamate with the Raman spectrum of CTAB subtracted from it to correct for signals coming from CTAB. The background was removed and the baseline was offset for clarity.

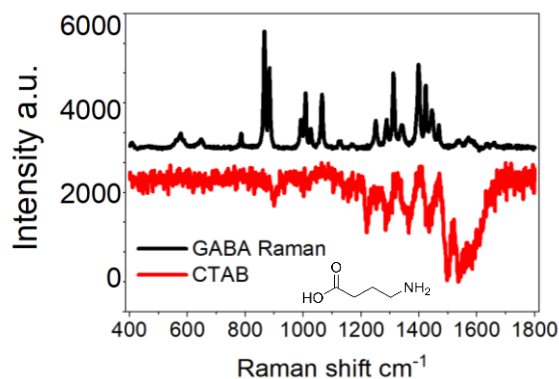


Figure 44 Raman spectrum of solid GABA and SERS spectrum of CTAB-capped gold NPs with 50 mM GABA with the Raman spectrum of CTAB subtracted from it to correct for signals coming from CTAB. The background was removed and the baseline was offset for clarity.

Even though these results are promising, positively charged Au nanoparticles produced from CTAB have been reported to show a high level of biological toxicity. However, one study specifies that, although the precursor of nanoparticles may be toxic, CTAB-capped gold nanoparticles themselves are not necessarily detrimental to cellular function, but the long-term effects of the nanoparticles need to be examined.

Neither CTAB nor TRIS-capped gold nanoparticles demonstrated high stability impacting their SERS capability. This was evident in their aggregation state and visual precipitation out of solution. Several biological species were studied with all synthesised NPs. TRIS-capped NPs did not demonstrate a high SERS behaviour and the tightly packed CTAB bilayer resulting in its own Raman signals is not conducive for biological functionalisation. The size and shape of the citrate-capped gold NPs synthesised in this manner were monodisperse with no signs of agglomeration. As the citrate capped once again demonstrated the best SERS efficacy, demonstrating excellent characteristics for the detection of both fluorescent and non-fluorescent targets with reasonable sensitivity, the citrate capped gold colloidal spheres were tested with multiple

analytes simultaneously to showcase their versatility and competence in more complex duplex systems.

Multiplexing

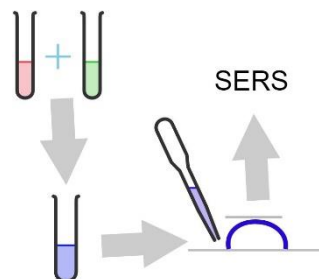


Figure 45 Schematic showing the method for duplexing. Briefly, 1:1 ratio of gold: analyte was mixed well. Then 1:1 ratio of two samples were mixed before data acquisition.

SERS fingerprinting of individual molecules permits excellent multiplexing capabilities because of the narrow spectral width of Raman peaks. The simultaneous detection of more than one analyte from a single sample without the need for separation and using a single sample readout is an attractive goal in a number of analytical situations, especially for the detection of biomolecules²¹³. The multiplexing capability of SERS is often stated by researchers; however, this is not substantiated by practical experiments. A schematic of the sample preparation is shown in Figure 45. Firstly, 10 mM of PABA and tryptophan (Trp) were investigated together. Both are molecules of biological significance. The label-free Raman acquisition was carried out and the spectrum displayed is an average. The normal Raman and the SERS has been normalised for ease of comparison. The normal Raman is from the powder, solid phase. The SERS spectrum illustrates peaks from both analytes. Although some peaks are of low intensity, they are still easily distinguishable from the background and can be assigned to one of the analytes. The bands at 812, 1250 and 1575 cm^{-1} are attributed to the tryptophan and the bands at 636, 1177 and 1602 cm^{-1} correspond to the PABA in the sample. At the same concentration, the SERS response from the mixture is not dominated by one analyte over the other showing that there is no preferred adsorption of the analytes on the gold NPs even though PABA has a thiol group so would be expected to form strong Au-S bonds. The presence of both molecules, even for

tryptophan (absence of thiol group) demonstrate a positive outcome for duplex testing.

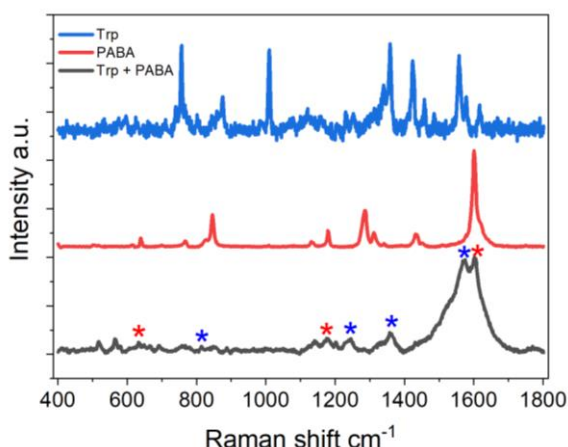


Figure 46 Normal Raman spectra of solid tryptophan and PABA with SERS spectrum of citrate capped gold NPs with 10 mM tryptophan and 10 mM PABA with highlighted bands. The red stars show signals from PABA and the blue stars show signals from tryptophan. The spectra were normalised for clarity.

Salicylic acid (SA), a phytochemical, is present in various plants where it has a vital role in protection against pathogenic agents. It also has beneficial effects on human health and is commonly used in cosmetics, however, some products containing SA may not be safe to use during pregnancy so identifying the molecule is useful²¹⁴. It can act as a model molecule for SERS enhancement and consists of a benzene ring and carboxyl group, which have been reported to be involved in the adsorption of SA on SERS substrates. It is known to be SERS active with gold and silver nanoparticles but does not exhibit electronic absorption in the visible spectral range. Since water is common medium in SERS experiments, most SERS studied compounds are water soluble. SA is not water soluble so was dissolved in ethanol, whilst the tryptophan is water-soluble.

The multiplex detection of these two molecules was carried out at different concentrations: 1 mM SA and 10 mM tryptophan. The SERS spectrum demonstrates good quality bands from both analytes. There may be some overlap where bands are observed at similar wavelengths, but certain parts of the spectrum can be used to differentiate the signals and attribute these to each of the analytes in the sample. The band at 1336 cm^{-1} represents the COO^-

symmetric vibrations while 1225 cm^{-1} is attributed to the C-O stretching mode. Tryptophan shows identifiable, distinct bands at 879 cm^{-1} attributed to the symmetric breathing mode, 1448 cm^{-1} from the C-H stretching and 1612 cm^{-1} , due to the C=C stretching mode¹²⁹. The duplex spectrum seems to be well resolved and SA bands are still apparent despite being at a lower concentration. The presence of ethanol in the sample does not hinder the performance of the SERS substrate as the Raman spectra can exhibit several miscellaneous peaks attributed to the solvent when using ethanol. Alcohols have very low affinity to metal surfaces, making the observation of functional groups in the spectrum difficult. The SERS response may become weaker as the fraction of organic solvent in the matrix increases due to the increased solubility as well as increased competition by the ethanol molecules, which can occupy sites on the substrate. In this system, there were three competing analytes, including the organic solvent, however, the resulting SERS spectrum still exhibited unique signals from the analytes of interest without too much interference from the solvent. This validates the SERS ability of the colloidal citrate-capped gold NPs for label-free duplex detection of low concentrations of biomolecules.

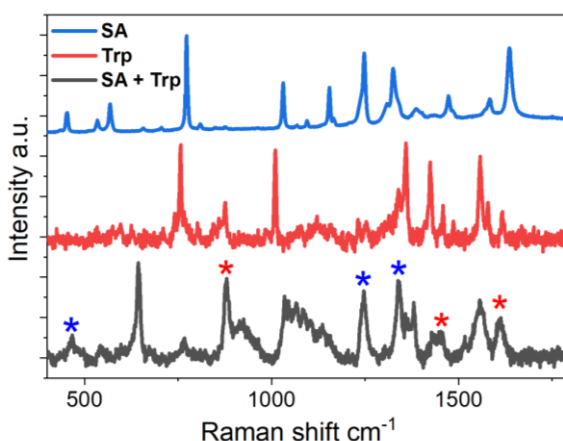


Figure 47 Normal Raman of solid SA and tryptophan with the SERS spectrum of citrate capped gold NPs with 1 mM SA and 10 mM tryptophan with highlighted bands. The red stars show signals from tryptophan and the blue stars show signals from SA. The spectra were normalised for clarity.

To further evaluate the practicality of the SERS substrates, the neurotransmitters were tested at 50mM concentration. The spectrum acquired, Figure 48, has low intensity, broad bands making assignment of the spectral features more challenging. Yet, certain bands can be identified from the

analytes. Simultaneous measurement of glutamate and GABA are crucial for accurate diagnosis of neurological disorders, and potentially for developing novel neuropharmacological agents. There have been no reports of using SERS for duplex testing of glutamate and GABA largely due to the difficulty in resolving the Raman spectrum and the overlapped bands, an obvious consequence of the similarity in their molecular structure.

As the citrate-capped gold NPs displayed no inherent Raman signature bands, the spectrum collected is purely from the analytes measured. These were dissolved in aqueous solution meaning there was no interference from the solvent. The 907 cm^{-1} (C-C-N band) and 1114 cm^{-1} (CH_2 band) are attributed to glutamate. The band present at 1441 cm^{-1} (CH_2 band) and 1235 cm^{-1} (NH_2 band) can be assigned to the GABA, as well as the small band at 1537 cm^{-1} which has been enhanced in the SERS compared to the normal Raman which may be assigned to the CH_2 bending mode.

It is important to note that while the Raman spectrum of 'free' molecules such as the powder reference molecules can be simply predicted by applying symmetry and point group theory. For SERS, the prediction and interpretation are not as straightforward. For a vibrational mode to achieve a high SERS enhancement, it requires the mode to have a polarizability change along the direction of the local EM field. This is the basis for the concept known as surface selection rules which determine the peaks that are enhanced in SERS experiments²¹⁵. Therefore, it is not uncommon that the resultant SERS spectra profiles vary from that of the Raman of the solid form. Researchers have found that molecules in different solvents present significant Raman shifts up to 9 cm^{-1} for some vibrational modes, compared to the solid sample²¹⁶. Although the spectrum is not very well defined, individual bands from both analytes can be differentiated without the need for labels or multivariate tools for analysis demonstrating the specificity and sensitivity of the gold NPs. In this case the citrate capped gold NPs are acidic so they can protonate the analytes, and this would have improved the substrate-analyte adsorption process, since the analytes and the nanoparticles carry opposite charges, which should encourage better adsorption.

These neurotransmitter analytes are very tough to ascertain using label-free SERS so the experiments had to be conducted at higher concentrations than other analytes. The glutamate concentration in the blood of healthy adults ranges from 40 to 60 μM where plasma GABA levels are reported to be in the range 100-130 $\mu\text{mol/mL}$ ^{210,217}. These levels are much lower than the concentrations studied in this report, however, this does prompt further investigation into the optimisation of the SERS substrates for use in multiplex detection. Only SERS with Ag NPs have been reported for the detection of GABA and glutamate to date.

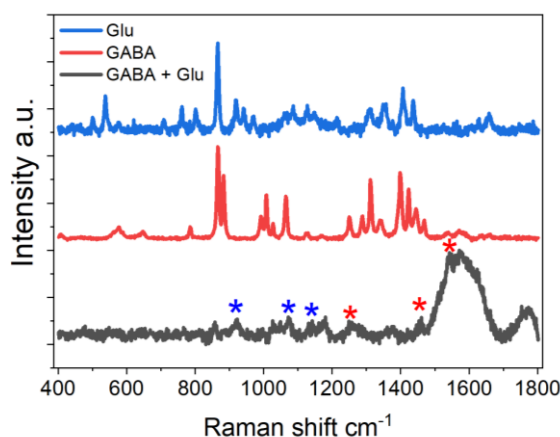


Figure 48 Normal Raman of solid GABA and glutamate with SERS spectrum of citrate capped gold NPs with 50 mM GABA and 50 mM glutamate with highlighted bands. The red stars show signals from GABA and the blue stars show signals from glutamate (Glu). The spectra were normalised for clarity.

Considerations

Designing substrates for the entrapment of analytes is common because the process is analyte dependent, with different chemical species having different hydrophobicity, charges, sizes as well as functional groups, so there is no uniform optimisation protocol to follow. From literature, there exists several approaches towards the optimisation of SERS experiments. In this study, the high performing citrate capped gold nanospheres have proven their flexibility in detecting a variety of target analytes (that have been categorised as complicated for SERS detection), at different concentrations, in both aqueous and non-aqueous solvents without the use of external labels.

Spread spectrum SERS and dynamic SERS have both been utilised for label-free detection of neurotransmitters but the results from the current study

suggests a more simple, facile and rapid label-free approach could be effective for the detection of a number of biomarkers, promoting further investigation into the full optimisation of gold substrates²¹⁸.

2.3.3 Self-assembled monolayers (SAMs)

There have been many accounts in literature stating the SERS spectra of proteins and DNA are difficult to reproduce and interpret. Vibrational assignments of organic molecules adsorbed on metal nanostructures are considered difficult since the SERS spectra strongly depend on the specific functional groups for the surface adsorption and the surface orientation of adsorbates. SAMs have the potential to address these problems as they form readily on gold. They are thin enough to allow significant local-field enhancement, and their compositions, structural orders and interfacial properties can be tailored for molecular retention²¹⁹. The controlled adsorption of biomolecules onto a metal surface from aqueous solutions is a crucial step in the fabrication of biochemical sensors. SAMs have been previously utilised by a number of researchers^{73,220–222}.

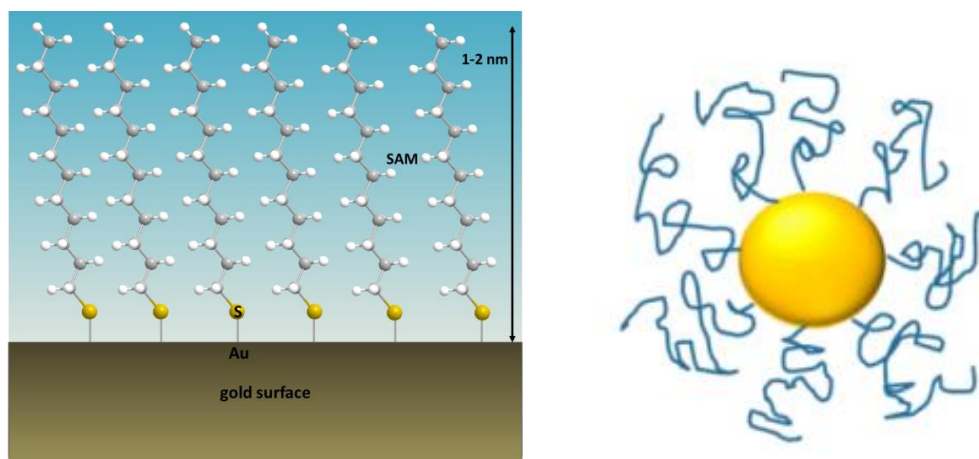


Figure 49 (Left) Diagram showing how a SAM is formed on the gold surface via S-Au bonds. Reproduced with permission from reference [219], and (right) schematic of the ways that SAMs can be arranged around a spherical gold NP.

Gold NPs have strong binding affinities for thiols and amines, where modification of the surface can lead to improved stability of gold NPs dispersions. Alkanethiols are the preferred organic compounds for the construction of monolayers on gold because sulphur, in its reduced form, presents high affinity towards the gold surface. This affinity also favours the

displacement of unintended organic materials whose absorption usually fulfils the requirement for lowering the free energy of the metal-monolayer interface. The exact mechanism of this interaction (thiol – Au) is still not fully understood with many theories postulated about the underlying chemistry.

A total of 4 SAM reagents were prepared. These were dissolved in ethanol and mixed with the gold NP colloidal solution in a one pot, easy, quick synthesis. Self-assembled monolayers are formed by simply immersing a substrate into a solution of the active material. The assembly process is governed by energetically favourable interactions such as van der Waals forces, electrostatic forces and hydrogen bonding. The UV-Vis was taken to ensure the successful formation of the SAM on the surface of the gold. During a typical self-assembly process, several competing forces exist simultaneously, and the final state of assembly depends on the balance between all the forces.

Dodecanethiol (DDT) was the first SAM to be examined. When it encounters the gold surface at room temperature, the S-H bond breaks and the resulting thiolate forms chemical bonds at the gold surface. Figure 51 reveals that the SPR band of the functionalised gold NPs has been redshifted which is in agreement with the DLS measurement where the size of the gold NPs has increased after the addition of the DDT, demonstrating effective attachment onto the gold surface. The presence of ligands anchored onto the surface can be indirectly probed by a shift in the SPR band. However, the actual structure and organisation of the SAM at the gold NP surface is challenging to assess and to date remains poorly characterised, even in literature.

The DLS data shows that the size of the NPs significantly increase upon the addition of the SAM which contradicts a monolayer of DDT, which is only a few nm, being formed at the surface. This implies that there is a relatively large layer formed determined by the number of DDT on the gold NP surface. Small changes in the hydrodynamic diameter cannot be detected by DLS. This affects the compactness and thickness of the SAM, but also depends on the conformation and on the amount of solvent present. If any NP aggregates were present, these would dominate the analysis hindering the quality of the DLS measurements. The 'perfect' self-assembled monolayer that is often sketched

in literature, Figure 49, is far from reality, and different types of defects exist in the SAMs which is important to consider²²³. In fact, there are several types of defects typically found for alkanethiols and can either be a small number of missing molecules or regions where the molecules have a certain degree of disorder. Moreover, the sulphur moieties on the gold defines the free space available for the molecules, which will organise themselves to optimise the intermolecular interactions within their geometric constraints. The final structure of the SAM is highly dependent on the structure of the molecular constituent, the gold substrate and the self-assembly process. This goes beyond the scope of this study so will not be covered in any more depth here.

The self-assembly of thiols involving lying down and standing up transitions is governed by the balance between intermolecular and molecule-substrate interactions and the gold surface response to the chemisorption process⁷⁴. The SAM ordered structure is determined by competing forces; the interaction between the headgroup and the substrate and the interchain van der Waals forces. Although van der Waals forces are weak, they can influence the self-assembly of organic molecules with long hydrocarbon chains. DDT, a long chain alkanethiol with only a hydrocarbon backbone and tail group of CH₃ can take up a lot of conformations due to the nature of its spatial arrangement. For methyl terminated molecules, the tailgroup-tailgroup interaction is not very strong so should not play a significant role for the final structure of the SAM. However, the intermolecular interactions decided by the van der Waals forces between the C-H backbones play a crucial role in the packing of the surface.

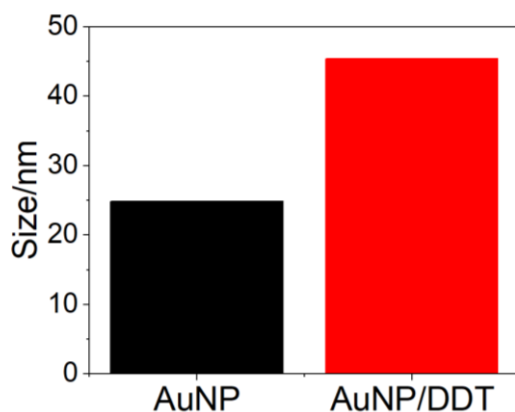


Figure 50 Average DLS size measurement of gold NP and gold NP with DDT.

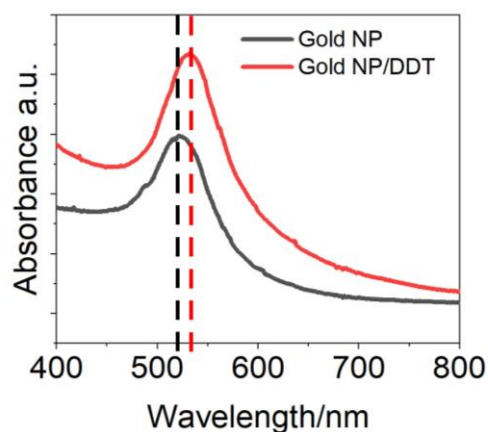


Figure 51 UV-Vis spectra of gold NP and the gold NP with DDT.

The data shown here corresponds with different DDT conformations and the large diameter may be attributed to the DDT assuming a conformation of chains back folding on the gold NPs, and these may be in uniform formation. The SPR band is narrow representing monodisperse gold NPs where if large aggregates had formed, a broader, less defined band would be expected. As a result of the very strong S-Au interaction, the molecules try to occupy every available site on the surface, pushing together molecules that are already bound but it is difficult to say how saturated the surface coverage is. Despite the lack of accurate characterisation of the DDT on the gold, the data does suggest that the SAM has been adopted onto the gold surface, but some disorder in the system may be present.

SERS

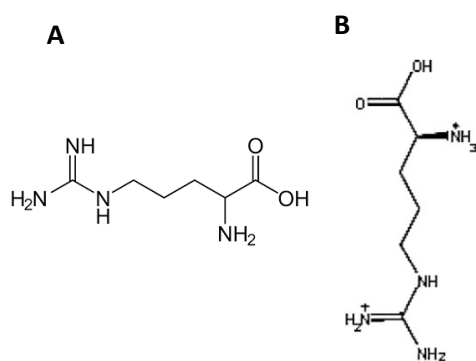


Figure 52 A) Molecular structure of Arg and B) Molecular structure of the protonated form of Arg.

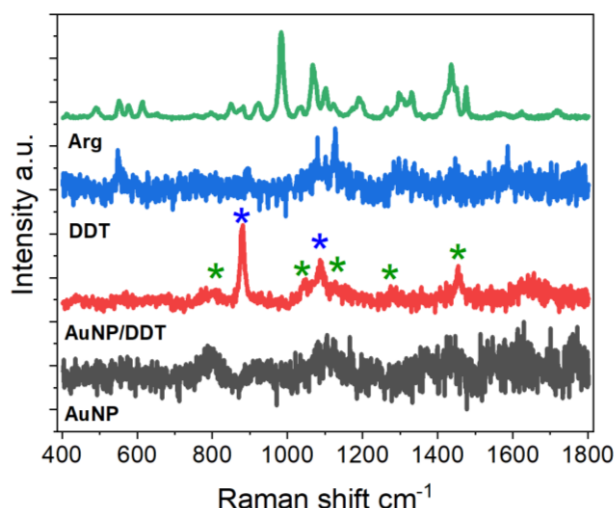


Figure 53 Normal Raman spectra of solid Arg, 2 mM DDT solution, and the SERS spectra of the gold/DDT with 10 mM Arg and the gold NPs alone. The highlighted bands come from the Arg (green stars) and the DDT (blue stars). The spectra were normalised for clarity.

SERS was acquired following the same sample preparation protocol. L- arginine (Arg) is an amino acid that can be metabolised to form several bioactive molecules that serve important physiological functions. It has also been reported to be a biomarker for Alzheimer's disease²²⁴. Different structures for arginine predominate at specific pH ranges as displayed in Figure 52. Alkanethiols are typically of low pH, combined with the acidic gold NPs, the α -amino and α -carboxyl groups are protonated and the positively charged guanidium group is in its protonated form. Arg does not bind well with gold

NPs, resulting in no SERS activity when mixed with just gold which can be seen with its very weak SERS spectrum even though the gold NPs carry a negative charge. Chemisorption of alkanethiols to colloidal gold NPs can eliminate the negative charges that normally stabilise the against aggregation. The exposed methyl groups of the DDT confer with the gold NPs with a hydrophobic character, promoting their aggregation, and hence, their stability.

The SERS efficacy of the functionalised gold NPs was tested to see if DDT can assist with the detection of Arg. The SAM exhibits its own characteristic SERS spectrum that can be used for calibration purposes. The resulting spectrum indicates that signals from both the DDT and the Arg are observed. The weak bands present at 793, 1046 and 1287 cm^{-1} are assigned to the deformation of the $(\text{NH}_2/\text{NH}_2)^+$ guanidinium moiety and the vibrations of the aliphatic chain²²⁵. The medium intensity band at 1444 cm^{-1} suggests this vibration is close to the metal surface and could be ascribed to a NH vibration of the guanidinium group. The strong band at 875 cm^{-1} is attributed to the CH_2 rocking vibrations and the medium band at 1084 cm^{-1} is assigned to the C-C stretching of the DDT. These assignments are based on values reported in the relevant literature.

The DDT SERS spectra is not very comprehensive as the Raman of the bulk liquid has a very rich spectrum. When combining the DDT and the gold with no analyte, some signals can be observed but these are not overpowering the spectrum. The intensity of the 875 cm^{-1} peak indicates that the signal may be overlapping from both the SAM and the Arg. Arg has a small band at 873 cm^{-1} from the stretching C-C vibration as well as the twisting NH bond. The result is that the signal at the corresponding wavenumber intensifies and is slightly broader. The SERS spectrum consists mainly of signals coming from the guanidinium group, suggesting that the amino acid interacts with the DDT through that group. The appearance of the band at $\sim 550 \text{ cm}^{-1}$ could be the Raman active S-S bending mode suggesting the formation of disulphides which occurs when alkanethiols are oxidised. However, this seems very unlikely in this case. The absence of a band at 941 cm^{-1} (SH bend) which would indicate a thiol group confirms that the gold-S bond had been formed. It is important to note that the Au-S bond vibrations are in the region 200-300 cm^{-1} , thus were not measured here. Based on theoretical and experimental results, interfacial SERS

EM enhancement decreases exponentially with increasing chain lengths for alkyl groups chemically bound to Au surfaces. Molecules close to the surface experience a greater local electric field enhancement than those that are further away. The Arg may not have been able to come into close enough contact for the EM enhancement to work effectively, as judging by the DLS measurements, the analyte would be far from the gold NP core.

The terminal functional group of the SAM determines the properties of the interface between the SAM and the analyte. The methyl group of the DDT shows not to have interacted significantly to the Arg resulting in lower quality SERS output. To expand the range of SAMs studied, 1,4 benzenedimethanethiol (BDT), an aromatic alkanethiol with two thiol groups, was examined. The UV-Vis SPR band shows a red-shift confirming the attachment of the BDT on the gold NPs. The spectral profile does not change indicating that the size distribution has not changed and that all the gold NPs in the solution successfully bound to the BDT with good surface coverage and high packing density. The orientation of the BDT on the gold surface is assumed to be in an arranged fashion, the attachment from either of the two thiol groups present (symmetrical molecule) with the benzene ring providing spatial rigidity and steric hinderance to assist with a more ordered monolayer forming, as represented in Figure 56. This agrees with literature that the adsorption geometry is perpendicular to the surface with one S-H projecting at the surface. However, the exact fate of the thiol hydrogen atom upon adsorption also remains an issue of continued conjecture.

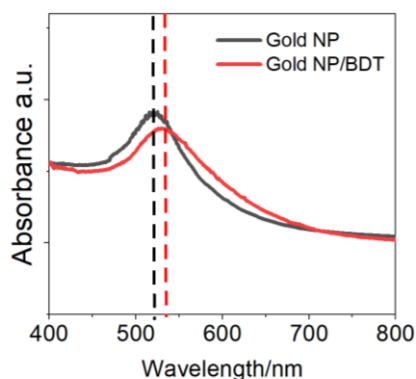


Figure 54 UV-Vis spectra of gold NPs and gold NPs with BDT.

The SERS spectrum was collected, and the results are displayed in Figure 55. The broadening of some of the peaks supports the chemisorption of the BDT on the gold. A shoulder at 676 cm^{-1} is evident, corresponding to the C-S stretching of the free thiol. Along with this, a small broad peak at 780 cm^{-1} attributed to the C-S-H bending, lending support to the proposed geometry. Unfortunately, the results do not indicate that BDT is a better SAM for the detection of Arg. The SERS spectrum is showing identical peaks to just the BDT alone meaning that the SAM is the only molecule being detected by SERS. The similarity between the spectra for both the DT and BDT suggests that the peaks may also be due to the solvent – ethanol rather than the SAM itself, or a combination of both. There are peaks present in the spectrum that may be attributed to the Arg but these overlap with its own signals complicating the band assignment process. The terminal end group, the thiol, does not bind to the Arg molecules and even if it did, the SERS response is not intense enough to overpower the dominant peaks of the SAM itself. It could also be that the terminal thiol reacts with another BDT molecule to form a disulphide bond, and thus extending the distance between the gold surface and the analyte molecules. In this structure, lateral van der Waals interactions are strong, leading to an organised monolayer and the energetics prefer this to a face-on structure²²⁶. The S-S stretching frequency in disulphides of this kind occurs in the range $470\text{--}500\text{ cm}^{-1}$. Whilst examining this range, there is a feature of the BDT spectrum at round 480 cm^{-1} , a very weak band which can be attributed to the S-S stretching

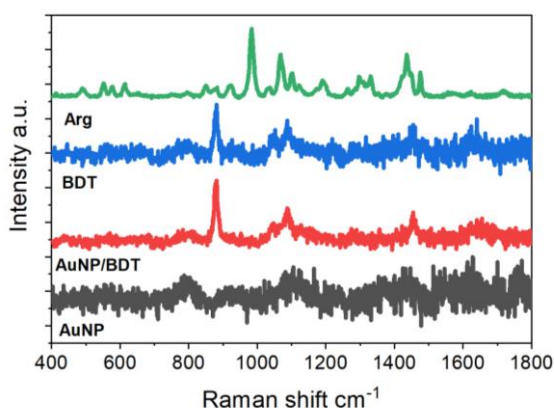


Figure 55 Normal Raman of Arg and 2 mM BDT solution and SERS spectrum of gold NPs/ BDT with 10 mM Arg and, Raman spectrum of the gold NPs by themselves. The spectra were normalised for clarity.

vibration. This could mean that a bilayer, or even multilayers are formed but there is not enough data to fully characterise this. This would explain the lack of analyte signals from the SERS measurements as changes in the nanoparticle-substrate distance directly affects the Raman intensity. It has been reported than even a minor change in gap distance can significantly affect the intensity observed. Based on theoretical and experimental results, interfacial SERS electromagnetic enhancements decrease exponentially with increasing chain length for alkyl groups chemically bound to Au and Ag surfaces²²⁷. Molecules further away from the surface will experience a lesser local field enhancement.

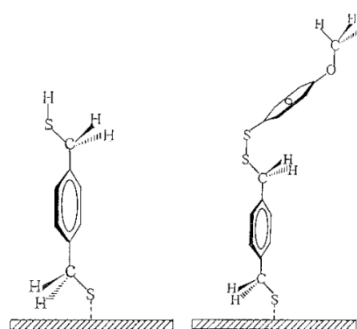


Figure 56 Diagram showing how the SAM could be positioned on the gold surface. (Right) A disulphide bond between two BDT molecules. Reproduced with permission from reference [226].

To compare both SAMs, the SERS spectra of ornithine (Orn), an amino acid related to the urea cycle and the risk of type 2 Diabetes, was studied. Several functional groups are present in ornithine, so it is a good biomolecule to test the different SAMs for their attachment capabilities. Figure 57 confirms that the dominating signals must be due to the solvent used as both SERS spectra reveal almost identical profiles. This agrees with literature whereby the sensitivity of SERS is greatly reduced by the presence of organic solvents, such as methanol or ethanol. This interferes with the study of the effectiveness of the SAM, if in all cases the ethanol dominates the SERS response. Despite this, the BDT SAM does show some low intensity bands that can be ascribed to ornithine. The CH deformation can be seen at 1490 and 1462 cm^{-1} and the 1231 cm^{-1} is due to the CH_3 twisting vibration²²⁸. This may indicate a better affinity for the ornithine molecule to the BDT layer, but it is very difficult to say anything with conviction based on the data acquired here. However, there is no systematic explanation for the influence of different solvent environments on

Raman detection of biomolecules. Dielectric constant is an important property of a solvent, which characterizes solvation ability, namely the electrostatic interaction between dipole distance of polar solvent and dipole moment of solute molecule. The polar solvent effect on the solute molecules is generated by electrostatic charge distribution, which can influence electron distribution and molecular configuration of solute molecules, resulting in poor Raman performance²²⁹. The SAMs were not water-soluble and that meant that the Raman spectra exhibits these miscellaneous peaks attributed to the ethanol present in the system. Neither the methyl nor the thiol group seem to be optimum end groups for the SAM. SAM substrates having CH₃ terminal groups have been reported to show the highest SERS intensity on metal films attributed to the more uniform SAM formed between the SERS active metal films thereby reducing the metal layer to metal layer direct contact sites. The SAM is kept stable and uniformity is reinforced by the van der Waals forces between the hydrocarbon chains.

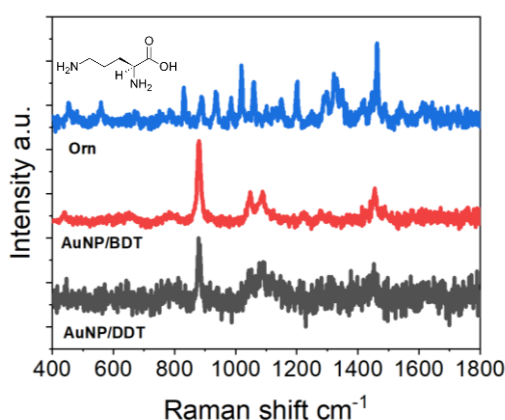


Figure 57 Normal Raman of solid ornithine and SERS spectra of gold NPs with BDT and DDT with 10 mM ornithine. The spectra were normalised for clarity.

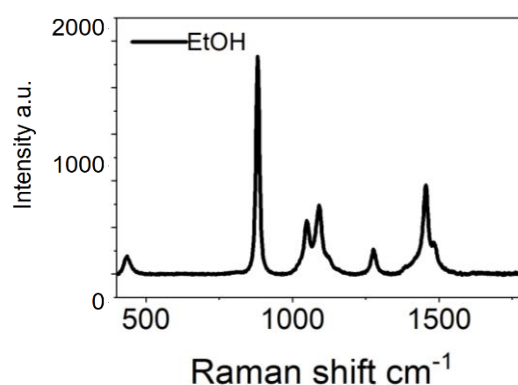


Figure 58 Raman spectrum of EtOH.

Octanethiol (Oct) and mercaptoundecanoic acid (MUA) were also analysed for the formation of SAMs at the gold surface. The typical SERS spectra would match that of Figure 58, the Raman measurement of liquid ethanol. The same problem with the solvent was observed in all cases. The dominating signals in the spectra was due to the ethanol with a high intensity band at 879 cm⁻¹ attributed to the C-C-O stretching vibration. Therefore, it was not possible to

determine if the SAMs facilitated in the SERS activity but highlighted the importance of the solvent effect when considering SERS experiments and measurements. However, considering the concentration of EtOH is equal in all cases, the spectrum of the BDT/ gold NPs shows the most activity which may be related to the ornithine in the system. Two sets of peaks at $\sim 1300\text{ cm}^{-1}$ as well as a small shoulder band to the left of the 1454 cm^{-1} peak from ethanol, can be assigned to the CH_2 vibrational modes, wagging and deformations.

The adsorption of the molecule at the surface may be influenced by solvent-analyte interactions. The solvent may interact with the plasmonic substrate, leading to competition for the available SERS binding sites. The solvent can strongly interact with the analyte, potentially holding back the analyte molecules from interacting with substrate sites. Despite the lack of emphasis on solubility in SERS literature, there are a few reports on the subject. The possibility that the solvent itself may adsorb and get trapped with other analytes on the SERS substrate has been considered. The molecular factors that may influence the solvation process include differences in polarity, localised dipole moments of the solute and solvent and the abilities of the solute and solvent of forming hydrogen bonds. The occupation of electrophilic sites with ethanol species results in fewer sites available for binding of the biomolecules that are neutrally charged²³⁰. Ethanol is weakly acidic and with ethanol in the SERS system, the concentration of protons in the solution increases. With this increase, more analyte molecules will get protonated, and this may affect the gold-analyte binding process. The chemical environment of the molecule is important as the behaviour observed is intriguing since the Raman bands appear shifted for different solvents²¹⁶. Certain vibrational modes can be more susceptible to the molecular interaction with the solvent modifying its SERS response thus making band assignment more difficult than in purely aqueous solutions. By lowering the concentration of ethanol in the sample, a more resolved spectrum may have been achievable with BDT as a potential SAM. 1,4-Benzenedimethanethiol is a relatively unstudied SAM and this is the first time it has been applied to the detection of biomolecules.

2.4 Conclusions

The overall theme of this chapter was founded on the development of SERS-active substrates with high reproducibility and the ability to detect a multitude of different analytes.

The citrate capped gold spheres were found to be the best in terms of detection ability with good sensitivity and specificity as well as reproducing similar spectral data. The gold NPs synthesised in this study had a long shelf life and a protocol to synthesise these was established by way of a facile, rapid, seed mediated growth method. The seed solution could be re-used for several months, and the resulting gold nano-spheres were proven to have the same size and shape verified by UV-Vis, DLS and TEM measurements.

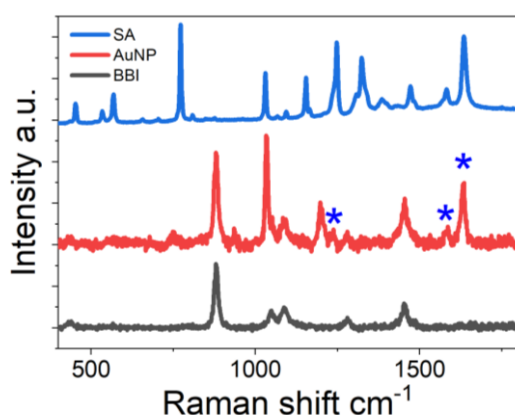


Figure 59 Normal Raman of solid SA and SERS Spectra of gold NPs with 1 mM SA and commercially available BBI gold with 1 mM SA. The blue stars show signals from SA. The spectra were normalised for clarity.

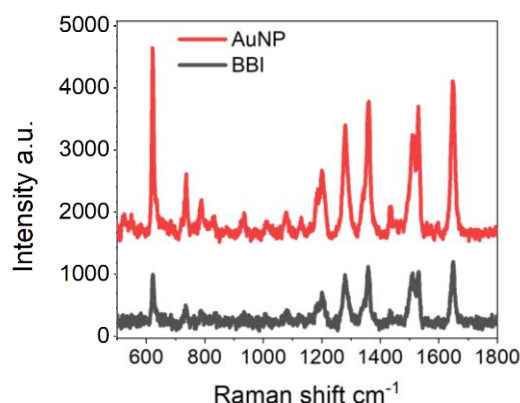


Figure 60 SERS spectra of synthesised citrate capped gold NPs and BBI commercially available gold NPs with 1 mM RB. The background was removed and the baseline was offset for clarity.

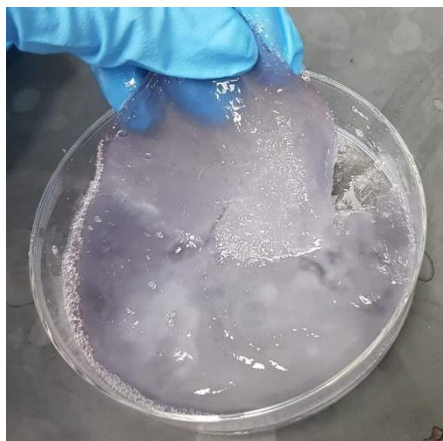
The citrate capped gold NPs were compared with commercially available BBI gold NP solutions and the SERS revealed that the ones synthesised here demonstrated higher SERS efficacy, especially with the biomolecules, Figure 59 and 60. Even in a non-aqueous solvent, the AuNPs exhibited distinct signals attributed to SA molecules, where the BBI SERS response was dominated by the solvent signals as depicted in Figure 59.

Experimenting with different capping agents revealed that citrate capped gold NPs gave good SERS signals with a variety of probe molecules as well as duplex detection. The gold NPs were used to acquire SERS spectra with a methodology in a label-free manner which has not been reported before. The actual nominal enhancement was not the overall defining characteristic, but more the ability of the gold NPs to detect challenging probe molecules without the need of external tags thus simplifying the preparation and data collection steps. There is an apparent gap between the high-quality performance shown in numerous publications and the relatively low practical performance in the detection of real samples. EFs were not calculated in this chapter as the EF may vary when different analytes are used, due to the different strength of interaction between the analyte and the SERS substrate. And for this practical application, the lowest detectable concentration is more meaningful. Greater optimisation to fully recognise the enhancement capacity should be studied. It is now not only crucial to demonstrate the high SERS enhancement while neglecting matters such as low signal fluctuation, high uniformity and stability, high affinity to the analyte and less photo-induced reaction or desorption. These are all vital issues to consider when contemplating the practical application of SERS.

Functionalising the gold NPs was attempted but unfortunately the SERS spectra were overshadowed by the ethanol bands. This validates concerns regarding the solvent influence involving SERS experiments. The SAMs did not intensify or detect any analyte signals even though with the gold alone, peaks other than ethanol could still be observed (see Figure 60). Queries relating to the SAMs orientations on the gold surface were discussed and interesting questions pertaining to the order of the SAM and substrate-analyte distance and how these can impact the SERS response are routes for further investigation. Changing the backbone and terminal group of the SAM did not result in much difference when trying to determine biomarkers. Reports have shown that solubility has an important effect on SERS due to a suppression in adsorption in cases where the analyte is highly soluble in the solvent. This research highlights the importance of careful consideration of the solvent applied when designing SERS experiments.

Chapter Three

Developing Flexible Sensor Materials for Label Free SERS



Chapter III: Developing Flexible Sensor Materials for Label Free SERS

3.1 Introduction and Aims

Conventional rigid and planar supports such as glass and silicon wafers are impractical in several applications which hinders the use of SERS technology in certain fields for example, *in situ* food contaminants. Therefore, there is a need for developing SERS active flexible substrates with high sensitivity and reproducible outputs¹⁰¹. They can make full contact with the sample and are easy to prepare. Today, the most common approach for performing SERS measurements is to deposit a droplet of a liquid sample onto a rigid silicon or silicon substrate which require pre-treatments for detecting solid samples with a non-planar surface, thus non-invasive detection is not possible. In contrast, flexible materials including paper, polymer films, adhesive tapes to name a few have received great interest as SERS substrates, which can attach well to curved surfaces, providing portability²³¹. Flexible SERS substrates offer many advantages; they can be cut into any desired shape and size for on-demand use, they can be easily swabbed or wrapped on sample surfaces, they are non-destructive and *in situ* detection can be recognised. Moreover, wearable and lightweight flexible SERS substrates can be combined with portable Raman devices to provide on field detection, serving as a powerful analytical tool in real word applications for biomarker analysis. Robust and reproducible SERS substrates is still under development, and the property needs to be improved and adapted to a wide range of analytes and biological samples.

The work presented in this chapter comprises of investigating three different flexible materials: filter paper, PDMS and hydrogels, with biomedical applications in mind. These materials were chosen due to their low cost, rapid synthesis and preparation processes and biocompatibility. The aim of this work is to provide insight into alternative materials that can become SERS active by incorporating gold NPs into them. The gold NPs mentioned in this chapter refer to the ones synthesised in Chapter II. Several methods were used for synthesis and characterisation and are discussed in further detail in this chapter. For the

substrates to be suitable for the specific purpose of designing a flexible sensory material, several parameters need to be considered in addition to its SERS efficacy. These are all reviewed in this chapter.

The criteria required for flexible substrates besides their ability to easily bend without breaking, includes adhesive properties for easy conormal attachment and detachment to surfaces introducing no destruction to the sampled surface, relatively high transparency enables Raman collection from both sides of the material, cost efficiency, easy fabrication, reusability and/ or recyclability, reproducibility, scalability, high capability for chemical analysis and vast applicability. The SERS functionality should result in uniform enhancements, high throughput, multiplex potential, specificity, and sensitivity. Fulfilling all these parameters is extremely challenging so there always needs to be priority given to a few of the most significance. Label free detection of biomolecules on flexible substrates has not been researched so this chapter provides novel, proof-of-concept results in determining which substrates offer the biggest potential in satisfying the above criteria.

3.2 Experimental

3.2.1 Materials and reagents

Polyvinyl alcohol, (Mw approx.200,000) for synthesis (PVA), polyethylene glycol 10,000 (PEG), polyvinylpyrrolidone, average mol wt 40,000 (PVP), Poly(N-isopropyl acrylamide), amine terminated, average mol wt 5,000 (PAM), poly(4-vinylpyridine-co-butyl methacrylate) 90% (P4VP-co-MMA), N-hydroxy succinimide, 98%, (NHS), 1-Ethyl-3-[3-dimethylaminopropyl] carbodiimide hydrochloride, ≥98.0% (EDC), carbodiimide, 99%, (DCC), acetic acid, ReagentPlus®, ≥99%, sodium bicarbonate, glutaraldehyde solution, 50 wt.% in H₂O, genipin ≥98% (HPLC), powder, citric acid, gelatine from bovine skin (type B) and laboratory filter paper were all purchased from Sigma Aldrich Ltd and used as supplied. Ultrapure deionised water was used for all solution preparation and experiments. All glassware was cleaned with acetone and isopropyl alcohol (IPA) then washed with Milli-Q water before use.

SERS experiments were conducted on the same analyte molecules prepared in chapter II.

Filter paper

Laboratory standard filter paper was used as supplied. The paper was submerged in a solution of Au NP solution for a few hours, then was removed and allowed to dry. The citrate reduced gold NPs synthesised in Chapter II are employed for these studies.

2 μ L of analyte was drop cast onto the paper substrate and allowed to dry before SERS analysis.

Polydimethylsiloxane (PDMS)

PDMS monomer and curing agent was mixed in a container in 10:1 ratio. Mixture was spread uniformly in a 75 mm diameter Petri dish and allowed to settle. The PDMS in the petri dishes were subjected to alternating vacuum and room pressure to remove any trapped air bubbles. The PDMS was cured for 3 hours at 65°C, cooled to room temperature and stored. A rectangular sheet of PDMS was cut out and immersed in 100% ethanol, sonicated for 30 minutes and dried.

The untreated PDMS was cut into shapes arbitrarily and submerged into a solution of gold for even coating of gold onto the surface. Gold NPs were also drop cast onto the PDMS sheet as well as spin coated to get the best uniform distribution of gold on the surface.

Hydrogels

A range of different hydrogels were prepared using gelatine as the core material. Figure 61 describes the different polymers and cross-linking agents utilised for the synthesis of hydrogels. These polymers were readily available and have been reported to form hydrogels in literature. The cross-linking agents were researched to ensure the best hydrogel was formed in terms of mechanical strengths.

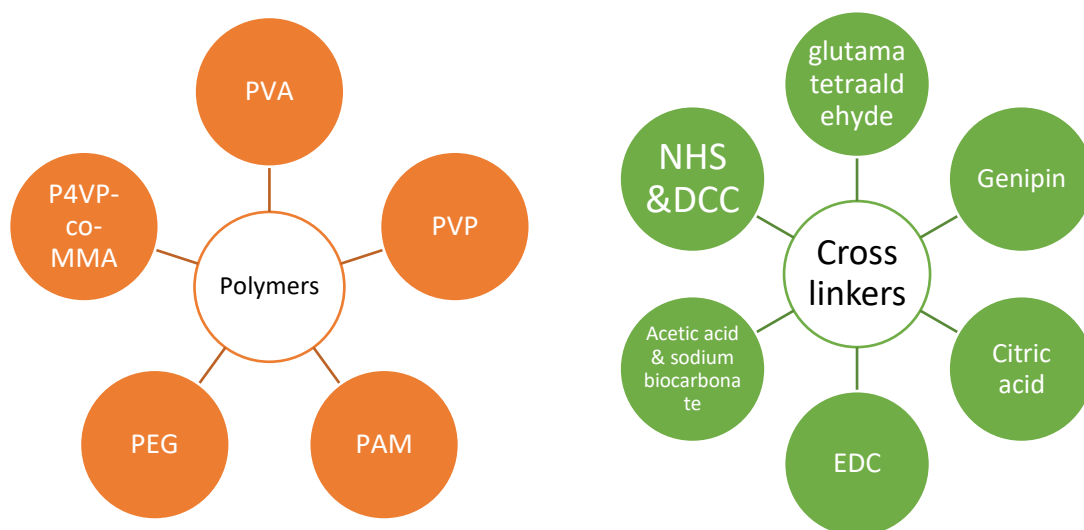


Figure 61 (Left) The different polymers used for hydrogel synthesis to be mixed with gelatine and **(right)** the different cross linkers used for the synthesis of the hydrogels, based on published synthetic routes.

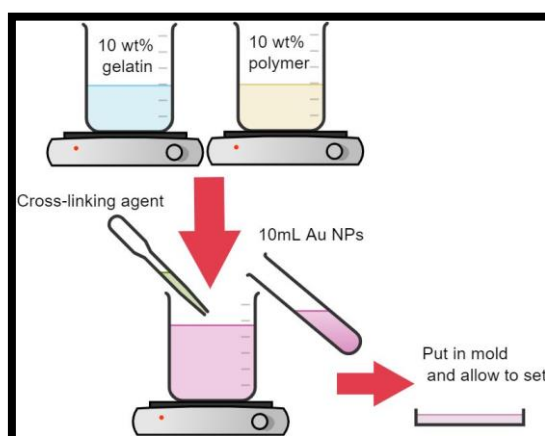


Figure 62 Schematic showing the hydrogel synthesis protocol.

Figure 62 briefly describes the method of gel formation. Optimum concentrations and volumes were found through trial and error. Briefly, 10 wt.% gelatine was mixed with distilled water at 70°C and 10 wt.% of the polymer was mixed with distilled water at 70°C in separate beakers on magnetic hotplates. As the polymers needed a bit longer to dissolve (approx. 1 hour). Once the solutions were thoroughly dissolved, the gelatine was then poured into the polymer solution slowly under constant stirring. Then, an appropriate amount of cross-linking agent was added (2 mL of 0.125% glutaraldehyde (aq), 0.2 mg of genipin in 500 µL EtOH, 1 mL 50 mM citric acid) along with 10 mL of citrate-capped gold NPs (synthesis discussed in Chapter II). The whole mixture was stirred magnetically on heat for a few more minutes before pouring it into a petri dish that was used as a mould and left for a couple of hours for gelation to occur. Gelation occurred at both room temperature and 4 °C. The hydrogels were stored in the refrigerator at 4°C and taken out when needed. Several methodologies for achieving the best SERS results were tested. Examples are given in Figure 63.

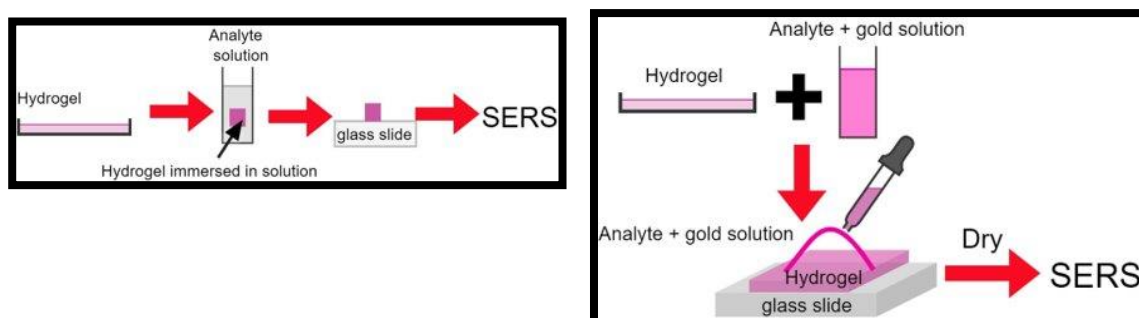


Figure 63 Schematics to show the different method of SERS acquisition on hydrogels. (Left) Immersing the gel in the analyte solution and (right) drop casting gold & analyte onto the gel.

EF calculations

The EF calculations presented in this chapter are from the analytical chemistry point of view.

$$AEF = \frac{\frac{I_{SERS}}{C_{SERS}}}{\frac{I_{NRS}}{C_{bulk}}}$$

Where I_{SERS} and N_{SERS} is the intensity of the band in the SERS spectrum and normal Raman spectrum, respectively, and C_{SERS} and C_{bulk} refer to the estimations of the concentration of the analyte in the SERS and normal Raman spectra. This equation, although useful for practical applications strongly depends on many factors and it is worthwhile to note that C_{SERS} is estimated and does not fully characterise the number of adsorbed molecules. This equation was chosen as it is well suited for colloidal solutions and gives a good comparison of substrates with different analytes, providing the experimental conditions are the same. The EF calculations were performed on Excel using a spreadsheet.

3.2.3 Characterisation

UV-VIS

UV-Vis measurement was done using Model S-200 Vis Spectrophotometer from Boeco system, Germany with a single beam tungsten halogen lamp for the light source. Disposable cuvettes were used, and water was served as the blank for background measurement. 0.5 mL to 1 mL of sample volume was measured at a wavelength range of 320 to 800 nm, at a wavelength scan speed of 2400 nm/min with absorbance ranging from -0.3 to 3.00. The data was stored on a SD card and transferred to a PC using the software MasterReport, for further processing of data.

Fourier Transform Infrared Spectroscopy (FT-IR)

A PerkinElmer Spectrum 2000 FTIR spectrophotometer with an ATR attachment, using 16 scans and a resolution of 4 cm^{-1} was used for the IR experiments. The measurement range was $4000\text{-}400\text{ cm}^{-1}$. The ATR crystal was ZnSe. The data was converted to XY files and analysis was performed on Origin. The IR spectra were used to characterise the functional groups and chemical vibrational frequencies of the polymers in the polymer gelatine composite hydrogels.

Raman

SERS measurements of samples were performed using a Renishaw InVia Raman upright microscope (Renishaw InVia, UK) with a 633nm laser. This Raman system was integrated with a Leica microscope and the laser light was coupled through an objective lens (20 x, 0.75 N.A), which was used to excite the sample and also to collect the scattered Raman signal. The prominent Rayleigh scattering was blocked using a notch filter and the beam spot on the sample was ~1 µm. 10 spectra per sample were acquired over 10 different spot areas. Each spectrum was integrated for 10 seconds, in the range of 400-1800 cm⁻¹. After collecting the SERS spectra, post-processing was done using wire 3.4 software associated with the instrument. The background subtraction was done by a cubic spline interpolation. The instrument was calibrated with signal from standard silicon at 520 cm⁻¹.

Background correction was performed before normalisation of spectra. Normalisation was performed on spectra for ease of comparison and thus, the intensity is not shown on the Raman graph i.e., when multiple spectra are shown at once to indicate significant Raman bands relevant to the current study. Non normalised spectra are displayed when the experiments are related to the spectrum of an individual substrate with a single biomarker, and their Raman intensities are shown.

Swelling

Swelling measurements were performed in both water and ethanol solvents. Small bits of hydrogels were cut into random shapes- small enough to fit into a small 2 mL capillary tube. The original weight was recorded on a scale. The hydrogels were all then left into the solution for an amount of time before being taken out of the solution and weighed immediately. To ensure accuracy and consistency, the measurements were allowed to plateau before recording their final weight. This was then repeated until however long the study lasted. The degree of swelling was calculated using the equation below.

$$\text{Swelling (\%)} = \frac{\text{New weight of gel}}{\text{Initial weight of hydrogel}} \times 100$$

Scanning electron microscopy (SEM)

Field emission scanning electron microscope (FE-SEM) from Hitachi was used to image the PDMS substrates, FE-SEM imaging were performed on the samples with Accelerating voltage of 1 kV and at magnifications of 150 k.

3.3 Results and Discussion

3.3.1 Filter Paper

Paper based sensing represents a new and outstanding approach to extremely low-cost devices for molecular analysis. Cellulose is biodegradable, renewable, and abundant in nature thus cellulose-based products can be inexpensively produced or recycled. Filter paper is one of the most common substrates and it can be combined with nanostructures for many applications.

Several methodologies were tested to optimise the sample preparation and collection. The paper was left in a solution of gold then a solution of analyte consequentially, the paper was submerged into a solution of the gold and analyte, or the gold and analyte was drop cast onto the paper. Previous studies have reported SERS intensity increasing with increasing time of immersion of paper in the AuNP solution. The optimum time being at 30 minutes, as beyond this time the SERS intensity begins to decline due to the large amount of AuNP attached to the surface of filter paper causing aggregation. The high absorption of AuNPs onto paper was realised by van der Waals binding without any retention aid.

The paper had visibly turned the same colour as the AuNP solution demonstrating the embedment of the NPs onto the paper, Figure 67. Due to the high concentration of NPs on the paper UV-Vis could not be used to determine the SPR band. The colour indicated the high absorption of the gold NPs. The longer the paper was submerged in the gold NP solution the darker the colour observed to demonstrate the high density of gold NPs attached to the paper surface.

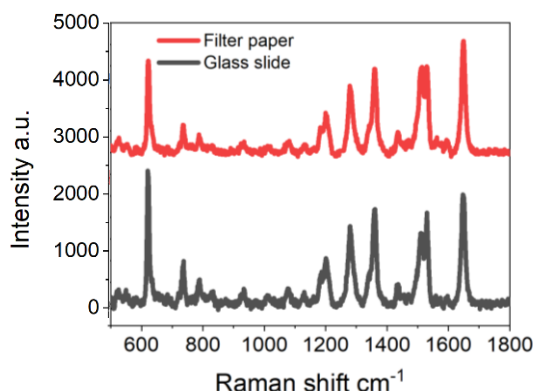


Figure 64 SERS spectra of 1 mM RB on filter paper and glass slide with gold NPs. The background was removed and the baseline was offset for clarity.

SERS was preliminarily performed with 1 mM of RB. Immobilising the gold NPs on the paper as well as the RB dye molecules resulted in a highly coloured material. This increased the fluorescence and hindered the successful detection of the RB molecules at any lower concentration. Figure 64 exhibits the SERS spectra on the paper and the glass slide for comparison. Distinct Raman bands belonging to RB can be seen with the paper substrate as well as for the glass. The intensities are similar to each other highlighting the efficacy of paper as a SERS platform. High intensity peaks at 618, 1183, 1362 and 1649 cm^{-1} attributed to the C-C-C bend and C-C stretching modes are clearly identifiable in both spectra which are distinguishable and specific for RB. Most biological

molecules are transparent so the issue of concentrating the signals would be removed.

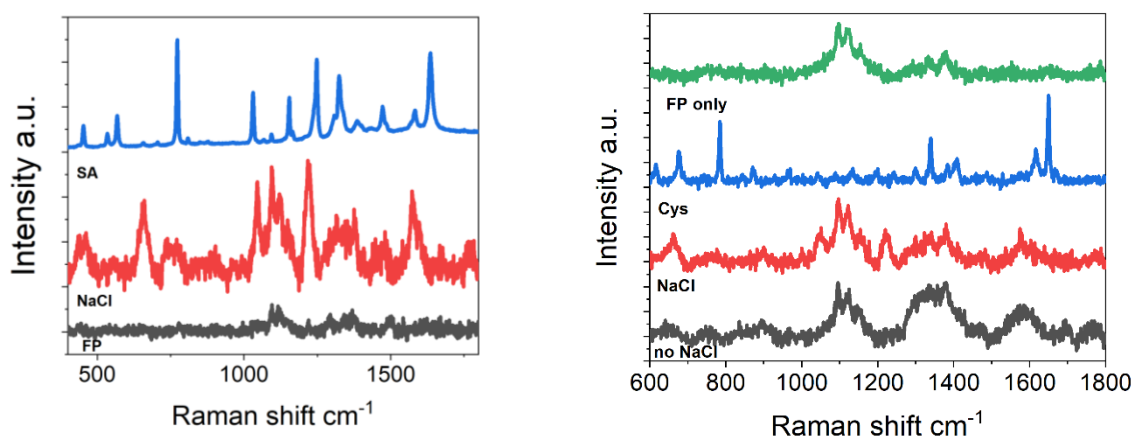


Figure 65 (Left) Raman spectrum of solid SA, SERS spectrum of gold NPs with NaCl and 1 mM SA on FP and gold NPs with 1 mM SA on FP, and **(right)** Raman spectrum of FP and solid Cys, and the SERS spectra of gold NPs with 10 mM Cys on FP with and without NaCl. The spectra were normalise for clarity.

The addition of NaCl to the gold colloids induces aggregation, which should greatly increase the electromagnetic enhancement. Chloride ions change the adsorption sites, orientation, aggregation, and the interaction strength of gold surfaces. The SERS spectrum of 1 mM salicylic acid (SA) was acquired with and without the presence of gold using SA and is depicted in Figure 65. It is very evident that the NaCl greatly increases the SERS ability of the filter paper substrates. The peaks at 1248 and 1034 cm⁻¹ corresponds to the C-H bending vibration modes. The most efficiently enhanced spectral bands are those that are related to the vibrations of chemical groups being near the surface of nanoparticles and having a vibrational transition moment perpendicular to the NP's surface. However, the Raman spectrum of bare filter paper exhibited its own bands, contradicting certain literature where no background interference was observed. Yet, in other studies, the filter paper had an inherent Raman spectrum which agrees with the results here. This highlights the issue of discrepancies present in a lot of SERS literature with contradictory results causing uncertainty when comparing experimental values with published work. Each SERS experiment should be analysed as a standalone to minimise doubt when reporting results.

10 mM cysteine (Cys) was probed, and the SERS spectra are displayed in Figure 65. Cysteine is a sulphur containing amino acid and is a biomarker for various types of diseases such as cardiovascular disease, diabetes and certain cancers²³². Low levels of cysteine can be indicative of these health conditions and so detection is important. Filter paper shows its own peaks at 1095, 1123 and 1376 cm^{-1} which can be ascribed to C-O stretching ring modes and C-H deformation of cellulose, the primary key component of filter paper. These filter paper bands appear to dominate both SERS spectra for Cys but signals can be seen belonging to the analyte in the NaCl spectrum. Cysteine has a rotatable torsional angle and so, three conformers of cysteine may exist. It is known that there is strong chemisorption between cysteine and metal nanoparticle through the thiol group, Figure 66. The weak band at about 980 cm^{-1} on the ordinary Raman of the powder cysteine is from the bending vibrations of the thiol group. In the SERS spectra of the Au-Cys complexes, this band disappears due to the formation of S-Au bonds instead. There is a shift in the bands in the region of 600 to 1000 cm^{-1} when cysteine interacts with gold, but some characteristic peaks are still identifiable. Peaks at 673, 1050 and 1232 cm^{-1} can be attributed to COO^- scissoring vibration, C-N stretch and CH_2 twist respectively²³³. The small shoulder at around 1599 cm^{-1} represents the COO^- asymmetric stretch.

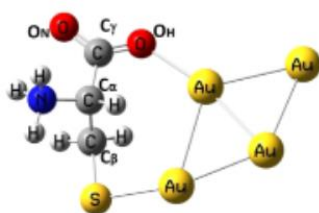


Figure 66 Diagram showing how Cys can interact with the gold NPs.

Summary

These results indicate that whilst filter paper can detect certain biomolecules, with other analytes, the paper signals dominated the SERS response and so it was not a suitable flexible substrate for this study. Nevertheless, the addition of sodium chloride seemed to help with the aggregation of the gold NPs, thus improving the SERS ability. The main limitations of paper substrates for SERS

sensors are their high porosity, inherent hygroscopic nature, and hydrophilic surface properties reducing their sensitivity and reproducibility. Since the nanoparticles are exposed to air, the shelf life is shortened ranging from hours to days. This means that the substrates must typically be freshly prepared prior to performing SERS analysis. Due to the high porosity of the filter paper, the gold NPs absorb all the way through, and it is difficult to assess the number of NPs available on the surface to participate in SERS. But if the NPs and analyte are mixed together before deposition, then they are immobilised on the surface together and the locations of hotspots are already predetermined and therefore, providing challenges in obtaining high SERS enhancements. The spatial inhomogeneity of the NP morphology and the hotspot distribution are the main reasons for the fluctuations in SERS intensity. Despite the ease of preparation and low cost, filter paper did not meet the criteria for this study but paves the way for future work where it can be used as an effective SERS substrate outside of biomedical applications with further optimisation.

3.3.2 Polydimethylsiloxane (PDMS)

SERS substrates characterised by plasmonic NPs synthesised on polymers have been the subject of previous studies. PDMS belongs to a group of polymeric organosilicon compounds. Due to its versatility and rheological properties, it is the most widely used silicon-based organic polymer with several advantages including deformability, non-toxicity and is non-flammable. PDMS has already been reported as an ultrasensitive SERS platform. PDMS films were untreated and used as given. Two methods were tested for optimal SERS effect: one being the gold was first coated on the substrate before the analytes were drop cast, and the second where both the analyte and gold were mixed before these were drop cast on the PDMS and allowed to dry. Acquisition was taken immediately after.

Figure 67 presents the SEM image of a typical PDMS film. The morphology of the PDMS films shows a rough surface caused by the ductile material fracture. The surface roughness agrees with the hydrophobic nature of PDMS. The untreated PDMS has a cracked surface. This cracked or rough topology correlates with the amount of curing agent added. It has been reported that

contact angle is dependent on the curing time and temperature¹⁰³. The rougher the surface is, the lower the wettability of hydrophobic PDMS.

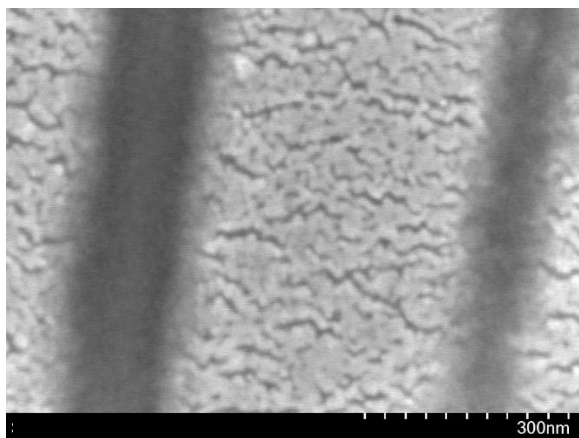


Figure 67 SEM image of untreated PDMS. Reproduced with permission from Dr Jayakumar.

PDMS is a visibly transparent material, ideal for use in several biological related applications. Upon the addition of gold, there was a slight purple/red hue on the surface as shown in Figure 69. The ease of cutting the PDMS film into smaller shapes is one of its many pros as a flexible substrate. The gold does not appear to be uniformly distributed on the surface and the adhesion of the gold on the PDMS film is not very effective, and this can be due to the drop cast method of deposition which may ensue in some challenges. A drop of liquid containing a suspension of the gold NPs is literally drop casted on the surface. The evaporation of sessile droplets containing suspended particles under ambient conditions often forms a ring like pattern, where the periphery of the ring is concentrated with the solute, in this case, gold nanoparticles: termed the 'coffee ring effect' (CRE). Here the ring pattern is not visible by eye but the different in the colour on the PDMS surface indicates the variation of the gold concentration with a build up towards the edge of the PDMS substrate. Furthermore, the surface hydrophobicity can influence the formation of the ring pattern. The distribution of the non-volatile gold NPs is governed by various factors and so it is difficult to suppress the CRE to obtain a more uniform distribution. Another consideration is the adhesion of the AuNPs to the PDMS substrate, making the transfer process more challenging. The film of gold on the PDMS surface is very thin and easy to peel off and be scratched. Protecting the AuNPs can be done simply by coating the surface with colourless nail polish due to its rapid drying

time and scratch resistant properties which has been applied to silver nanowires on electrodes²³⁴. However, this would be ineffectual for this study as SERS is a surface technique and the gold and analyte must be available on the surface for successful analyte probing.

SERS

Preliminary SERS analysis with RB showed that even at micromolar concentrations that signature RB peaks at 1354, 1504, 1523 and 1642 cm^{-1} are observed. However, the PDMS has its own peaks that can be seen in the SERS with high intensity. The strong bands at 616 and 689 cm^{-1} are attributed to the Si-CH₃ symmetric rocking vibration. The medium intensity bands at 1266 and 1412 cm^{-1} are ascribed to the CH₃ symmetric and asymmetric bending vibrations, respectively. As the PDMS has a signature Raman spectrum all other peaks appearing in the SERS can be assigned to the analyte of interest. Even at micromolar concentration the RB can be successfully detected with a well resolved spectrum.

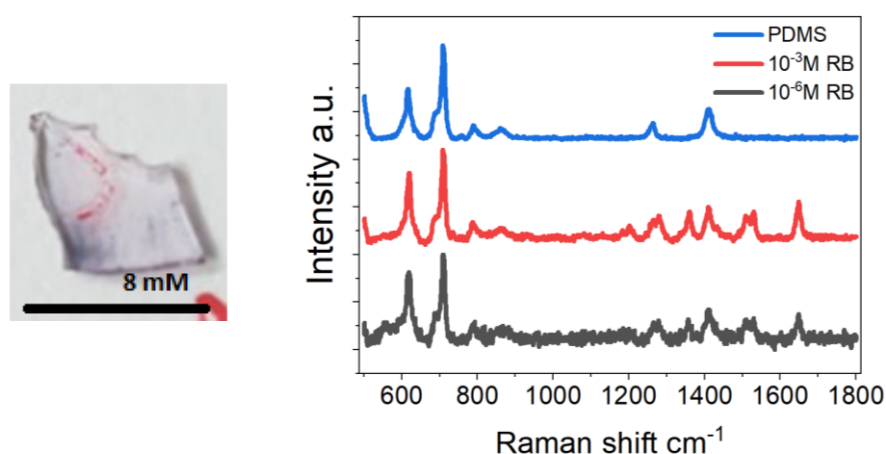


Figure 68 (Left) Photograph of PDMS with gold, and (right) Raman spectrum of PDMS alone and SERS spectra of 1 mM and 1 μM RB on gold/PDMS. The spectra were normalised for clarity.

Modification

To encourage the attachment of the biological analytes on to the PDMS surface, different methods were devised to modify the PDMS and the gold for greater adhesion and better SERS. PDMS is hydrophobic by nature and the way to render it hydrophilic is challenging because of the elastomeric property of PDMS which induces its surface recovery and thus, its hydrophobicity. One

attempt to create hydrophilic PDMS for better uniformity of the gold coating is to build a layer-by-layer assemble through consecutive adsorption of polyanions and polycations. First, a series of reagents were added to the PDMS, following reported procedures in literature, illustrated in Figure 69. The last step was the addition of gold. The use of water-based solvent for dopamine, PAA and PAH ensures its stability and removes solvent interference during SERS. When the analyte was added onto the surface of the modified substrate, no signals could be detected so mixing the analyte of interest with gold before drop casting is an essential step to observe any kind of SERS.

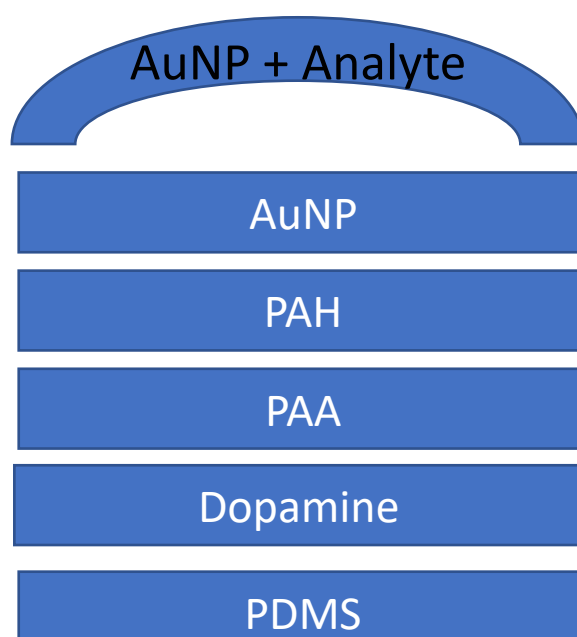


Figure 69 Diagram showing the surface modification of PDMS. The polymers were layered on step-by-step before the gold layer. Gold NPs were mixed with the analyte and drop cast onto the surface before Raman acquisition.

With the modification, the dominating PDMS peaks appear to diminish and distinct peaks belonging to salicylic acid (SA) are noted, Figure 70. Due to the extra layers of several additional materials over the PDMS the distance between the surface and the PDMS substrate may be too large for the EM enhancement to take effect. The unmodified PDMS demonstrates a SA peak at 1632 cm^{-1} due to the C=O stretching vibration. The modified PDMS, whilst having a more vibrant spectrum still has many miscellaneous peaks. However, peaks present at 1030 , 1241 , 1465 cm^{-1} attributed to the C-O stretching vibrations can be observed from the SA. The additional peaks that appear can be from any of the polymers used for the modification as these have their own Raman spectra and are likely to be probed as much as the target analyte if they are close to the surface. Whilst these steps were designed to increase the hydrophilicity and the gold coating on the PDMS surface, it was not evident that it was successful. Any gaps in the layer of gold would leave the polymers exposed for SERS and the more polymers that are employed, the more convoluted the consequent SERS might be, making it difficult for band assignment²³⁵.

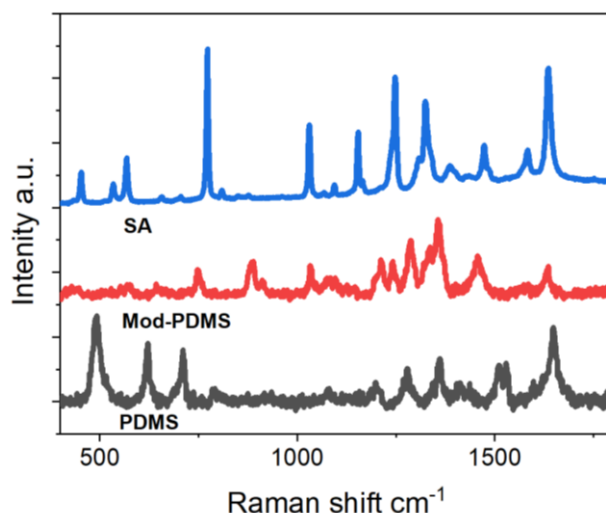


Figure 70 Normal Raman of solid SA and the SERS spectra of 1 mM SA on the modified and unmodified PDMS. The spectra were normalised for clarity.

Treatment of the PDMS this way did not greatly improve the SERS function. The gold was not resistant to cleaning with water and other solvents showing that it was still very weakly adsorbed on the surface. However, this would mean that the PDMS itself is recyclable and for each experiment, the gold and analyte layer could be removed from the surface easily and a new analyte could be

deposited for SERS on the same film. This, in theory, implies that a single piece of PDMS substrate can be used multiple times. Nonetheless, the SERS activity is not high enough to trade off for the weak adsorption of gold on the surface.

To further assess the utility of the PDMS as a flexible SERS substrate, the SAMs that were previously investigated in chapter II were studied to determine whether they would enhance the biomolecules' peaks. The sample preparation differs from earlier due to the addition of gold with the analyte before spectra acquisition. This was to ensure that enough gold was present to interact with the SAM as well as the analyte and to not saturate the surface with solvent molecules which dominated the spectra in previous experiments. The SERS spectra in Figure 71 shows the results where SA was probed to a concentration all the way to the nanomolar range with BDT. Ethanol peaks can be seen at 883, 1050 and 1093 cm^{-1} which are the most prominent peaks in the spectra. The lack of PDMS peaks shows that the surface has been covered as only the surface signals can be picked up. A weak band in the millimolar spectrum at 706 cm^{-1} can be attributed to the SA, but other than that there are no defining bands present that can be conclusively assigned to the analyte, once again highlighting the solvent effect issues arising in SERS. As the concentration decreases, the number of solvent molecules increases, and the SERS spectrum would be expected to be dominated by the ethanol. The modification process complicates the SERS with the additional components in the matrix giving rise

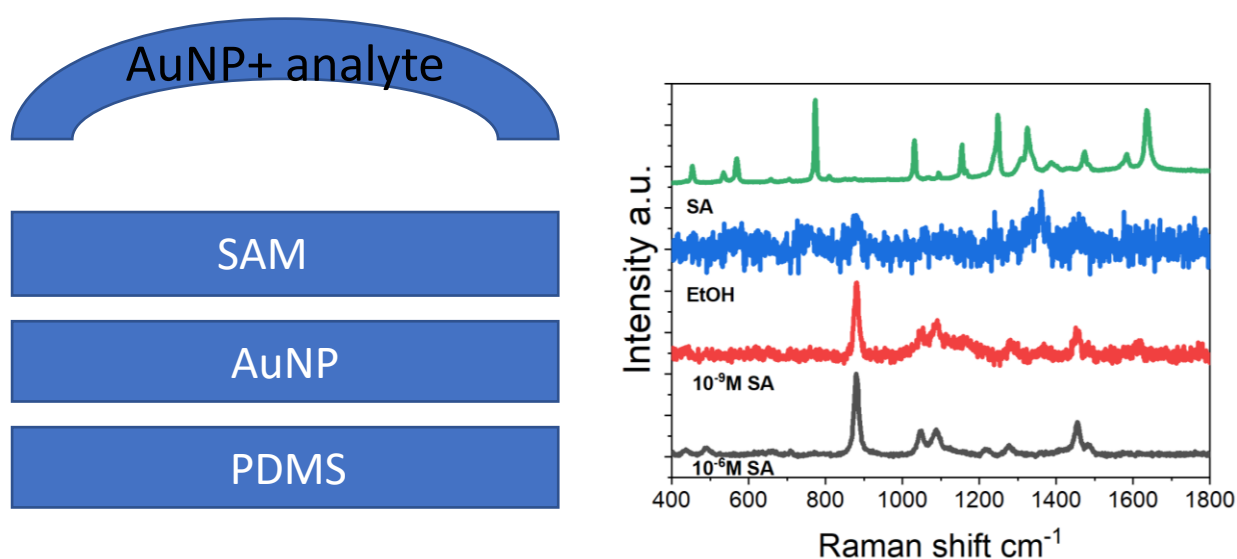


Figure 71 (Left) Diagram showing the modification of PDMS with the SAM and (right) the normal Raman spectra of solid SA and EtOH, and the SERS spectra of 1 mM and 1 nM SA on the PDMS modified with BDT SAM. The spectra were normalised for clarity.

to miscellaneous signals that can be attributed to multiple molecules present in the sample of interest. This signifies the importance of keeping the number of components in the sample as low as possible, especially in this label-free manner. Dodecanethiol was also studied and whilst some peaks may be owing to the SA, it cannot be reported with confidence.

Summary

PDMS has a range of properties that has contributed to its established reputation as a flexible material in the biomedical field. The fabrication of PDMS is facile and whilst some literature is available on SERS-active PDMS films, the majority focuses on silver NPs rather than gold. There has been suggestions that the method of incorporating the gold on the PDMS surface could be improved to directly embed the gold NPs into the PDMS mixture before curing, Figure 72. However, this has shown to interfere with the chemistry preventing successful PDMS formation. Also, this may not help with the issue of overpowering substrate signals in the SERS spectra. Modification of the material does appear to alleviate the problem slightly, but not to great effect. With the addition of the SAMs, solvent bands mask any analyte peaks that may be present. Therefore, whilst it showed strong initial promise, it was not investigated further.

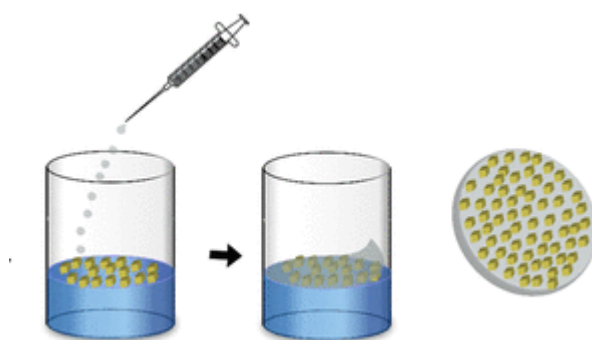


Figure 72 Schematic of integrating gold NPs during the curing stage of PDMS fabrication. Reproduced with permission from reference [103].

3.3.3 Hydrogels

Background

Gelatin was selected as the basis of the hydrogels because it possesses excellent biocompatibility, biodegradability and non-immunogenicity. It is abundantly available from nature, easily processed into various shapes and forms and is inexpensive. Gelatin is one of the most commonly used precursors for the preparation of a range of bio-hydrogels, either alone or in combination with other polymers¹⁰⁴. These properties make gelatin an appealing macromolecule in the design and development of new functional materials. However, some drawbacks of pure gelatin gels hinder their applications; poor mechanical properties and water sensitivity have been recognised as the most limiting ones. Hence, a number of hydrogels were prepared using different weight % of gelatin and polymer as well as cross linking agents until the most ideal one was found. The citrate capped gold NPs were freshly prepared using the protocol described in chapter II and were mixed into the matrix before gelation occurred.

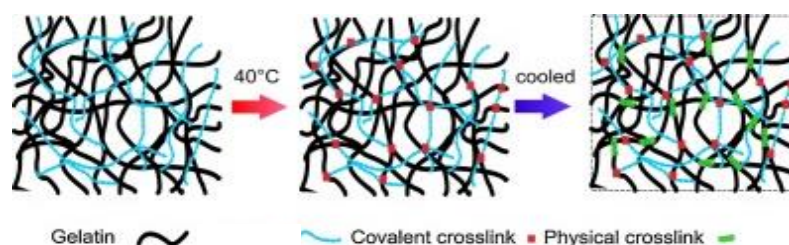


Figure 73 Image depicting the gelation process. Reproduced with permission from reference [108].

A gelatin hydrogel can be formed by physical crosslinking in water above a certain concentration at temperatures of 30 to 35 °C. During this process, gelatin molecules aggregate and undergo a conformational change from a random coil to a triple helix²³⁶. Crosslinks must be present to avoid dissolution of the polymer chains into the aqueous phase. In chemically crosslinked gels, covalent bonds are present between the different polymer chains. Cross linking is used to improve the thermal and mechanical stability of gelatin-based hydrogels. Chemical cross linking is the most widely used technique to improve

the thermal, mechanical and water sensitive properties of gelatin devices intended for long term use. The type and degree of crosslinking influences many of the network properties like swelling and elasticity. Many gelatin-based hydrogels have been synthesised using glutaraldehyde as a cross linker. It is by far the most widely used due to its low cost and excellent efficiency of the stabilisation of collagenous materials²³⁶. However, due to toxicity concerns, friendlier cross linkers have also been investigated (in this study, genipin and citric acid are selected). The field of gelatin-based hydrogels has been suffering from the lack of methodology to prepare stable nanocomposites and surmounting these obstacles is a crucial objective for this work.

Characterisation of the Hydrogel blends

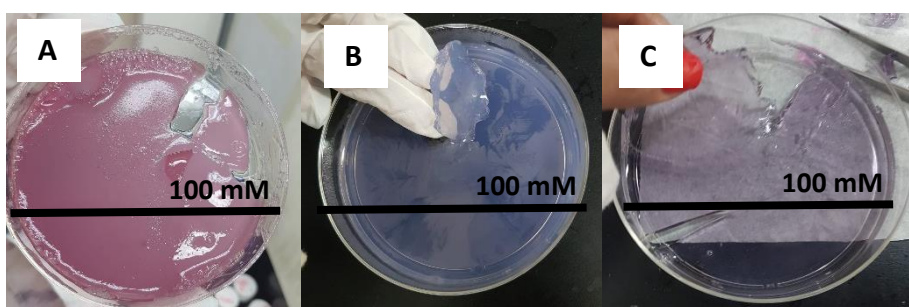


Figure 74 Photographs of the different polymer/gelatin hydrogel blends synthesised; A) PVA, B) PVP and C) PEG.

In this study, the limitations of unmodified hydrogels have been addressed by forming composite gels with different polymers which can improve mechanical stability and harness new properties in the resulting hydrogel. Polymer blending is one of the most useful ways to obtain new materials rapidly and economically rather than the development of new polymers. Blends of synthetic and natural polymers represent a relatively new class of materials and have attracted much attention, especially as biomaterials.

For the gel to experience any SERS effect, nanoparticles must be present. These can easily be dispersed in solution-phase systems. Nanoparticle suspensions alone are unstable and the interparticle structure changes from time to time. A way to combat this is by immobilising the gold NPs in the gel matrix. Hydrogels are a promising bulk material for gold NPs because of their superior water uptake capabilities. The strategy of directly embedding plasmonic

nanostructures in the hydrogel matrix would show potential as SERS substrates, making SERS measurements more reliable for many analytical applications. Furthermore, the incorporation of gold NPs in hydrogels offers stability to the NPs, allowing the NPs to be held down. The 3D network structure of a hydrogel enables it to combine with metallic NPs and helps accelerate assembly, control the morphology, and prevent agglomeration of the gold NPs. Thus, it is desirable to synthesise hydrogel composites with excellent sensitivity, stability and reproducibility as SERS substrates. Gold has been reportedly incorporated into hydrogels for tissue engineering applications as well as having antimicrobial properties for the treatment of infection.

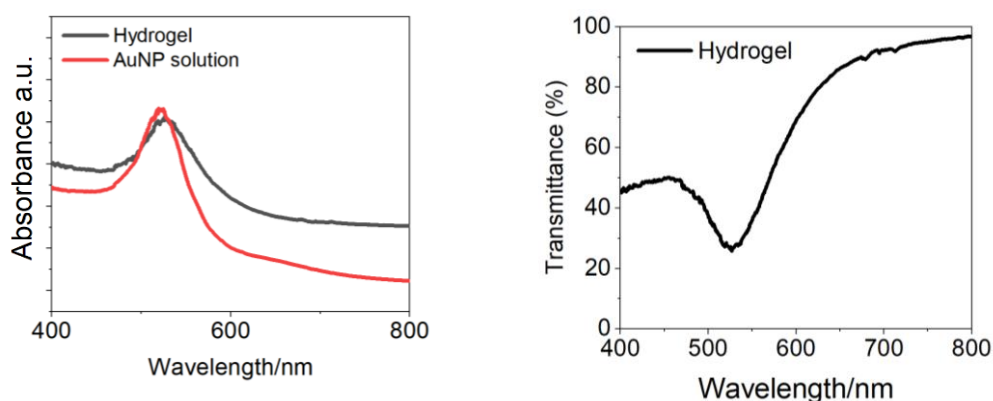


Figure 75 (Left) UV-Vis spectra of the gold NP solution and the gold incorporated gelatine hydrogel, and (right) the optical transmission graph of the hydrogel. These are typical data from the PVA/gelatine blend.

Images of the hydrogel formed can be seen in Figure 74. By simple observation, the colour is the first indicator of the gold NPs in the matrix as the gel takes on the colour of the NP solutions. However, the visible transparency of the different gels varies. The UV-Vis demonstrates the successful incorporation of the gold NPs as the SPR band of the gel matches that of the Au NP solution. A typical spectrum for all the hydrogels is presented in Figure 75. The SPR band of the hydrogel is slightly broader which is to be expected as the phase changes. As the refractive index near the nanoparticle surface increases, the nanoparticle extinction spectrum shifts to longer wavelengths. Practically, this means that the SPR band will redshift when the particles are transferred from water (in colloidal solution) to the gel. As the hydrogel has a large water content this shift is hardly noticeable. Nonetheless, the characteristic peak of spherical gold NPs at 531 nm makes it clear that the gold NPs have been incorporated

into the hydrogel network. Fresh NPs were prepared for each hydrogel synthesis with different amounts added to the gel solution, hence the colour variations. The transmittance can be calculated from the absorption data to further evaluate the optical properties of the hydrogels. Transmittance of the gels exceed 70% for wavelengths above 600 nm. At the position of the SPR band at 531 nm the transmittance reaches its minimum as expected. This shows that the hydrogels possess high optical transparency even with the addition of the highly coloured gold nanoparticles.

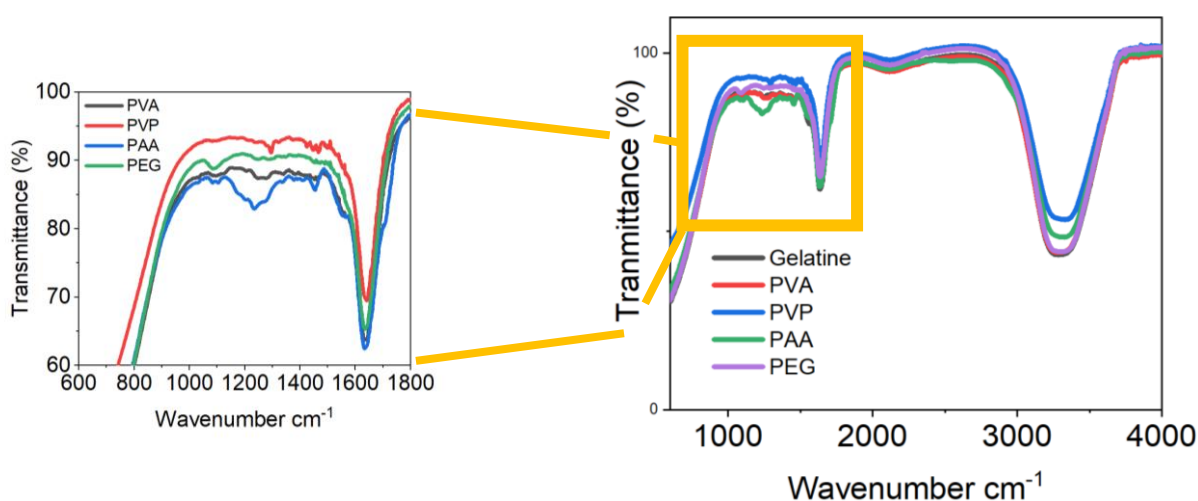


Figure 76 The IR spectra of the different polymer/gelatin hydrogel blends and the gelatin gel by itself with a zoom in into the fingerprint region of the spectra.

The type of polymer selected, and the degree of cross linking can be engineered to control the desired mechanical properties of the hydrogel to make them suitable for specific applications. Hydrogels formed by chemical cross-linking show greater stability, increased durability and higher mechanical properties (tensile, shear, bending) compared with physically crosslinked hydrogels. The mechanisms rely on the crosslinking of functional groups of the polymers with crosslinker agents. The IR was recorded of the different composite hydrogels and is presented in Figure 76. The IR shows strong absorption bands at around 3200 and 1634 cm^{-1} on account of the O-H stretch and scissoring modes of water in concurrence with literature. Most of the hydrogel is comprised of water and therefore the most intense bands are observed at these values. Some of the polymers themselves (PVA and PEG) also contain the -OH functional group which further intensifies these bands. The region below 1500 cm^{-1} shows some features that appear consistent with

the type of copolymer used. The intensities of the bands are very weak due to the proportion of hydrogel containing the polymer being low. However, activity in the fingerprint region does indicate the incorporation of the polymer into the hydrogel network confirming the composite materials being formed. Small bands present at 1325 and 1083 cm^{-1} are attributed to the O-H stretch with CH wagging and C=O stretch in the PVA/gelatine blend. The small shoulder band present at 1020-1090 cm^{-1} is due to the asymmetric C-O stretching of the repeating -O-CH₂-CH₂-O unit of the PEG polymer¹¹⁹. Absorption bands assigned to the vibrations of the -C-N- links and the CH₂ groups are identified in the 1400-1000 cm^{-1} region for the PAA/gelatine blend hydrogel as well as C-O-H out of plane bending in the range 900-992 cm^{-1} . PVP presents small bands at 1432 and 1283 cm^{-1} ascribed to the C=C and C-N vibrational modes²³⁷. It should be noted that poly(4-vinylpyridine-methyl methacrylate) had solubility difficulty and the resultant hydrogel was not correctly formed so these were discarded.

The polymers were chosen based on reviewing literature with the aim of finding the most excellent composite material fulfilling the criteria for this study taking into consideration its physical and chemical properties. PVA is a water-soluble polymer of great interest in the pharmaceutical and biomedical fields owing to its biocompatibility, nontoxicity and hydrophilic nature. PVA films have good mechanical strength and thermal and pH stability. It has been found that PEG shows great promise as a plasticising agent and is a suitable material for biological applications because it does not elicit an immune response. PEG is frequently used to prepare hydrogels in drug delivery and regenerative medicine. PAM gels are often used to study cell mechanical interactions because of their convenient usage, biocompatibility, and reproducibility of stiffness. These polymers can blend with gelatine (a water-soluble polymer) to form a hydrogel.

Visual observations

By simply touching, stretching, and arbitrarily cutting the gel, its rheological properties could be determined, Table 3. Some gels exhibited higher levels of flexibility, adhesion, and mechanical strength than others. Qualitative analysis

was performed on the gels to test these properties as a preliminary method of determining their usefulness as flexible SERS substrates. Although good adhesion is a desirable property, if the gel is too sticky, this makes it difficult to handle and transport as it attaches to whatever surface it encounters very quickly. This also reduces its elasticity as the tendency to break increases with stronger adhesion and in turn reduces its mechanical properties. These are important considerations whilst investigating suitable SERS substrates and should be appropriately evaluated and prioritised.

Polymer used in gelatine blend	General comments/observations
PVA	Easy to cut Holds shape
PEG	Thick and sticky Easy to handle
PVP	Thick and strong Holds shape
PAA	Sticky Does not hold shape- breaks easily

Table 3 Table describing the characteristics of the different hydrogel blends.

Swelling

Swelling behaviour is an intrinsic property of hydrogels, where the hydrogels enlarge due to solvent penetration into the void space between the polymeric chain networks, Figure 77. The swelling properties were investigated in both polar and non-polar solvents. The water loss affects the mechanical properties of the hydrogel, turning it rigid and brittle. The water loss reduces the quality of the interface between the gel and the analyte of interest, which would impact the quality of SERS performance. The volume fractions of the polymer components are much smaller to that of the solvent, in this case, water. When the gels are allowed to remain in contact with a solvent the gel exhibits osmotic

swelling or deswelling kinetics that give rise to a significant change in the gel volume. The swelling behaviour of hydrogels depends on the gel properties which are designable via synthesis conditions as well as on the properties of all parts present in solution. When environmental stimuli (pH, temperature, electric field and light) change, it takes time for the hydrogel to respond. Therefore, it is important to study the transient properties during the responses. Due to the PAM/gelatine blend not maintaining its form, it was removed from the remainder of experiments.

T hours in water	Swelling (%) of PVA	Swelling (%) of PEG	Swelling (%) of PVP	T hours in EtOH	Swelling (%) of PVA	Swelling (%) of PEG	Swelling (%) of PVP
2	184.4	137.6	95.1	2	-50.8	-23.3	-33.3
4	191.4	149.5	141.8	4	-43.6	-20.2	-36.9
24	267.2	161.6	223.5	28	-55.6	-43.1	-55.1

Table 4 Table showing the swelling measurements of the different hydrogel blends both in water and EtOH.

The general trend is that with all the polymer/gelatine composite hydrogels the materials swells in water and contracts (dries out) in ethanol. The swelling and deswelling performance are time dependent with the biggest change in volume being measured after leaving the gel in the solvent for at least 24 hours. The rate of swelling in water is greater than the rate of deswelling in ethanol.

PVA hydrogels are known for a high degree of swelling in water which is consistent with the findings reported here²³⁸. The swelling properties are said to be highly influenced by the stoichiometric relationship between the polymer and the gelatine as well as the pH of the swelling medium. The extent of swelling is induced by any factors that alters the electrostatic repulsion including pH, ionic strength, and the type of counter ion. When interactions between the hydrogel and the solvent create a mixed phase in which the two are mixed well, the maximal value of hydrophilicity occurs resulting in swelling. When any hydrogel encounters the solvent molecules, the solvent tries to attack the hydrogel

surface and penetrate within the network structure. If the cation concentration rises, then there is an increase in the osmotic pressure in the gel system which finally causes shrinkage in it. When the hydrogel is in its separated phase, maximum hydrophobicity takes place, and the shrinkage of hydrogel occurs.

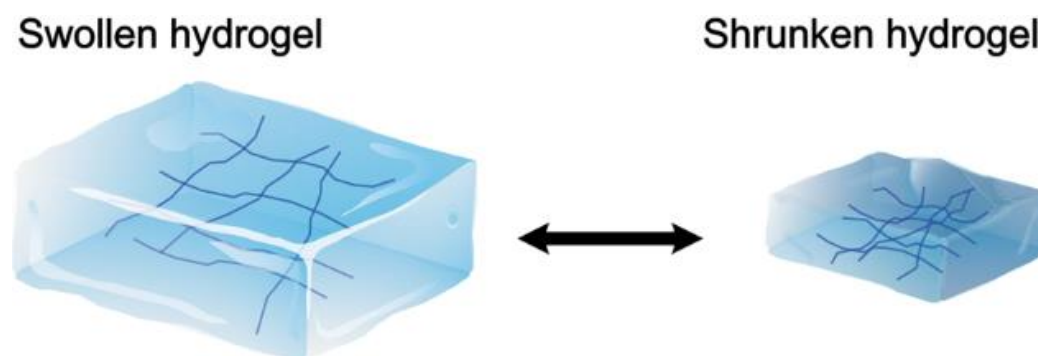


Figure 77 Schematic showing a hydrogel in its swollen and shrunken stages. Reproduced with permission from reference [238].

The swelling properties of these hydrogels abruptly change from water to ethanol which only differs slightly in its pH value which may indicate the intelligent nature of the polymer blend hydrogels. The use of ethanol does not affect the ionic strength directly because it is uncharged. This data also confirms that these polymeric materials can retain a significant fraction of water within their structure without dissolving in the medium with PVA showing the highest rate of both swelling and deswelling in the different solvents. The PEG hydrogel showed a lesser extent in volume change, corroborating with publications that the swelling degree is relatively low, which has limited its applications. PVP hydrogels alone have low swelling capabilities but blending with other polymers can result in increased properties which can be seen here.

Gelatine, in low or moderate ionic strength media, increases its degree of swelling as the charge density of the network rises. Hydrogels containing net positive charges swell to a greater extent than those carrying net negative charges, but this is difficult to establish in this instance. Gel collapse was noticeable in ethanol, due to the polymer being insoluble in ethanol. The hydrogel chains do not interact with ethanol resulting in deswelling in agreement with literature where an increase in mass fraction of ethanol leads to a decrease in the degree of swelling until the gel collapses. This property is reversible, but the dried hydrogels swell very slowly, with their swelling to equilibrium state

ranging from several hours to days due to the slow absorption of water into glassy hydrogels by diffusion. In the absence of any knowledge about the degree of ionisation of the gelatine and polymer molecules as a function of pH it is not possible to discuss the swelling properties in further detail.

The swelling data reported here for the polymer/gelatine composites has not been stated before. Swelling behaviour of polymeric blend hydrogels have found to be dependent on the polymerisation degree of the polymers²³⁹. The presence of gold in the hydrogel matrix may also affect the degree of swelling as it has been reported that Au gelatine composites swell less than unfilled crosslinked gelatine, suggesting that the gold NPs may act as a barrier for the diffusion of solvent molecules into the gel network. The swelling characteristic of the hydrogels is important as reinforcing their mechanical strength after swelling is challenging. Whilst both solvents were used in SERS experiments, the time required for SERS experiments is only a few minutes, where the phase of the gel did not alter significantly. This demonstrates that the hydrogels synthesised here can be used in solvents where there exists both solubility and insolubility of the hydrogel in the solvent, but whether the swelling affects the SERS performance is a crucial matter to consider and has not been studied before. Temperature studies should be carried out to further assess the swelling nature of the gels. Fast-swelling hydrogels are critical for many other applications like drug delivery, potential articular cartilage replacements and wound dressings²⁴⁰.

SERS

Label free SERS on hydrogels using gold NPs has not been accomplished before, to the author's knowledge. To initially demonstrate the SERS functionality of the hydrogels, Raman spectra of just the PVA/gelatine gel and the PVA/gelatine/AuNP nanocomposite gel were measured as controls to eliminate any signals that may arise from the substrate itself. These were typical of the spectra obtained for the different hydrogel blends. The spectra are depicted in Figure 78. The gelatine blend without any gold NPs exhibited no Raman bands and once gold was integrated into the gel matrix, very few broad and noisy bands can be observed but these are not distinctive peaks and can

easily be eradicated during qualitative analysis. Initial inspection of the analyte SERS shows that the gels pick up the signals of interest and these are coming from the target molecule with little interference from the substrate. Even though the signal-to-noise ratio (SNR) is low, narrower, more intense bands are present in the SERS derived from the different molecules attached to the surface of the hydrogel at concentration of 1 mM validating the use of the hydrogels as SERS-active, flexible substrates. The spectra attained highlight the specificity of the gels at recognising the individual Raman fingerprint that each of the molecules hold. To increase the SNR for better resolution, more gold was added into the gel scaffold, but this resulted in concentrated Raman signals when performing measurements, therefore the amount of gold used for the hydrogel synthesis was kept constant.

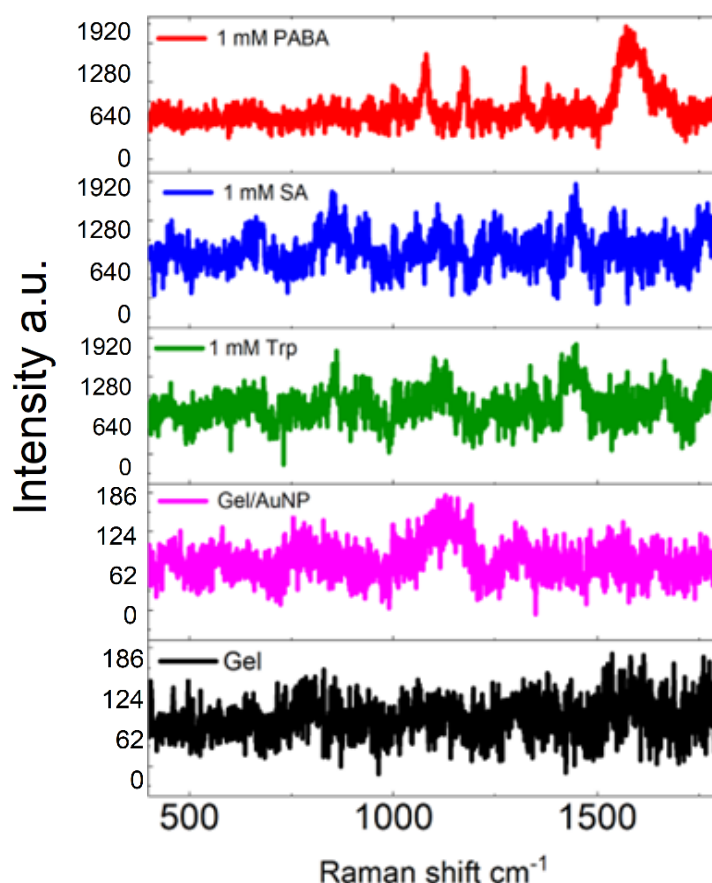


Figure 78 Normal Raman of a typical hydrogel and the SERS spectrum of the gold NPs incorporated in the hydrogel, and the SERS spectra of 1 mM tryptophan, SA and PABA on the nanocomposite hydrogels.

Different molecules with different gels

SERS was performed on the hydrogels following the method represented in Figure 79. The hydrogel was cut into smaller parts and submerged into the solution of analyte for a few hours before Raman acquisition. 10 mM of 2-naphthane thiol (NAT) was chosen as a probe molecule. It is a sulphur containing compound with a distinct Raman spectrum and has been reported to form SAMs on gold surfaces. Despite being prepared in ethanol; the SERS spectra reveal that the dominant peaks arise from the analyte, Figure 83. The PEG hydrogel blend gives a very noisy spectrum with no defined peaks, but with the other polymer hydrogel blends distinct peaks from the NAT are apparent. Bands at 763 and 1378 cm^{-1} are clearly identifiable attributed to the C-H wagging and ring stretching vibrations. The chemical nature of NAT and the surface chemistry of the gold nanoparticles should be contemplated. There is a high affinity between the thiol groups in the NAT structure and gold NPs. The present of these peaks in the SERS shows that whilst the gold NPs are immobilised on the surface, they are still interacting with the NAT molecules that have been successfully adsorbed on the hydrogel surface. Additional characteristic peaks at 1065 and 1452 cm^{-1} ascribed to the C-H bend and the ring stretch can also be observed. In the PVA/gelatine hydrogel the small band at 514 cm^{-1} owing to the ring twist mode of the NAT is evident.

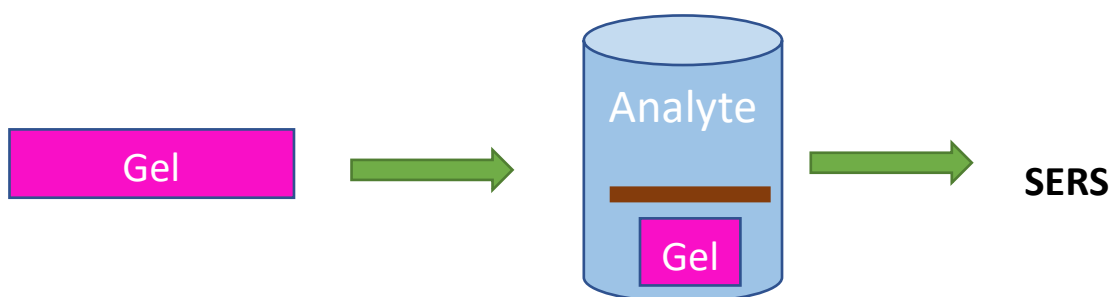


Figure 79 Schematic to show the data collection of the hydrogels. The gel was immersed into the analyte solution for a few hours before it was taken out and SERS was acquired.

The hydrogels in the analyte solutions did undergo deswelling where water loss could be observed by the naked eye. However, this did not seem to affect the SERS performance, but the mechanical properties were altered leaving the gel brittle and less flexible. By drying out the hydrogel and reducing the volume, the

SERS was easier to acquire due to less surface area of the hydrogel. By collapsing the gel, the amount of gold on the surface available for SERS would increase, and therefore increasing the possibility of finding a hotspot. Removing the hydrogel from the analyte solution and allowing it to dry reduces solvent interference as it evaporates from the surface. This may be why EtOH peaks cannot be seen in these spectra. Nonetheless, this would increase the likelihood of signal saturation which would affect the quality of the SERS. The hydrogel would return to its equilibrium structure once swelling occurs again in aqueous media. However, once it is dried, handling the gel becomes harder and so to overcome this issue, drop-casting was performed on the gel to see whether this would maintain the shape of the gel as well as be SERS responsive.

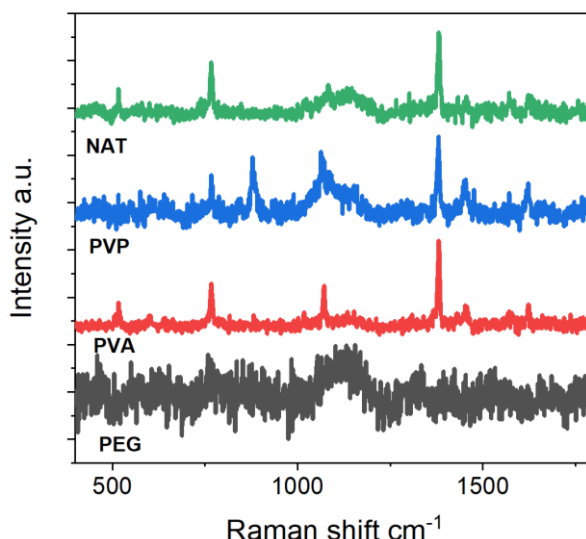


Figure 80 Normal Raman of powder NAT and SERS spectra of the different hydrogels with 10 mM NAT. The spectra were normalised for clarity.

10 mM tryptophan was then chosen as a probe molecule due to its biological significance. The PVP hydrogel blend showed a noisy spectrum with no distinguishable features. The band at 873 cm^{-1} is evident in both PEG and PVA hydrogels attributed to the pyrrole ring vibration mode. This band has been intensified differently for the different hydrogels demonstrating the complex mechanisms involved in SERS. The relative orientation of the molecule with respect to the local field may cause the Raman bands to be enhanced differently depending on the symmetry of their Raman polarizability tensor. Normalising the spectra for ease of comparison and the relative

intensities of the different bands are given in Table 5.

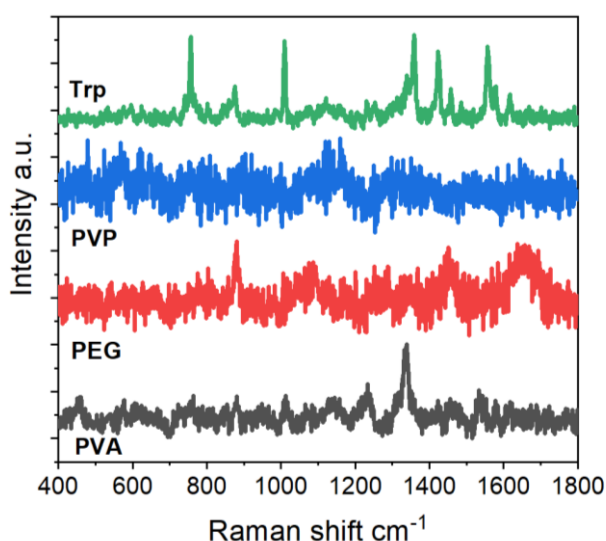


Figure 81 Normal Raman of solid tryptophan and SERS spectra of different hydrogels with 10 mM tryptophan. The spectra were normalised for clarity.

Raman shift/ cm ⁻¹	Assignment	Relative intensity (a.u.) – normal Raman	Relative intensity (a.u.) – PVA SERS	Relative intensity (a.u.) – PEG SERS
873	NH deformation	0.34	0.17	0.60
1013	NH deformation	0.42	0.62	0.27
1340	Aliphatic CH2 deformation	0.54	0.75	0.43

Table 5 Table showing the normalised relative intensities of different bands in the SERS spectra of the hydrogels with 10 mM tryptophan.

It is common for different Raman modes to experience dissimilar SERS enhancements due to the nature of the effect and that the hydrogels are not identical. The vibrational bands found in Raman spectra are often enhanced unequally, while new bands may appear due to the chemical enhancement mechanism¹³¹. The comparison of detectability of different compounds should be performed on identical substrates in order to minimise several factors

affecting it. The change in the molecular structure of the hydrogel accompanies the change in SERS due to changes in the Raman cross section, possibly coming from the charge transfer effect. The PVA hydrogel SERS spectrum demonstrates the most features with bands appearing at similar position to that of the powder form. This makes band assignment less challenging and proves that drop-casting the analyte onto the surface of the gel allows for good SERS detection. Drop-casting did not result in the hydrogel swelling, a small change in hydrogel volume did not hinder its SERS capabilities. This is the first-time gold NPs have been used in hydrogels for label-free SERS application.

Cross-linking agents

As PVA-gelatine hydrogel composite gave the best SERS activity for a diverse range of molecules as well as possessing mechanical strength and flexibility, it was studied further for better optimisation. Cross linkers are one of the key parameters to consider when discussing hydrogels. To overcome the challenges with the low mechanical properties of gelatine, establishing crosslinks are necessary as well as blending with other polymers to improve the final performance of the hydrogel. The elasticity of the hydrogel is controlled by the extent of crosslinking in the network. As the number of cross links increases, the polymer becomes more rigid and cannot stretch as much. Cross linking helps with the decrease in the viscosity of polymers as well as resulting in insolubility as the chains are tied together by strong covalent bonds²⁴¹. Chemically cross-linked hydrogels do not dissolve in solvents but can absorb them. Crosslinking with glutaraldehyde, formaldehyde, carbodiimides and acyl azides as well as physically using UV or gamma irradiation are all categories of proven ways to crosslink. However, physical cross-linking treatments tends to achieve a very limited extent of cross linking.

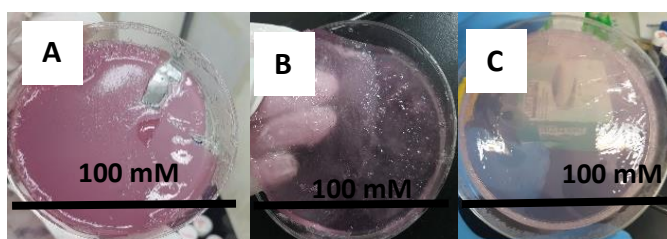


Figure 82 Photographs of PVA/gelatine hydrogel cross-linked with A) glutaraldehyde, B) genipin and C) citric acid.

Glutaraldehyde (GA) is by far the most widely used cross linking molecule due to its low cost and excellent efficiency in the stabilisation of collagenous materials, which enables achieving strength and water resistance of the obtained structure, reducing its cytotoxicity when used at very low concentration. Chemical treatments have the potential to leave toxic residue in the gels which will release upon biodegradation. Genipin is a potent yet nontoxic cross linker of proteins. It has been used in the preparation of cross-linked gelatine films and hydrogels and employed in nerve guiding conduits, wound dressing and cartilage scaffolds²⁴². The cytotoxicity of genipin is around 10,000 times lower than that of glutaraldehyde, and so genipin is extremely valuable in the development of biocompatible materials. It has been found that citric acid can be used as a cross linking agent to generate low cost 2D polymeric scaffolds²⁴³. It has excellent properties such as high cytocompatibility, solubility and available at low cost. Citric acid (CA) has been used to modify gelatine-based materials, enhancing the biopolymer's functional properties. Three different PVA/gelatine hydrogel blends were synthesised utilising glutaraldehyde, genipin and citric acid to test their mechanical and chemical properties as functional, flexible SERS substrates.

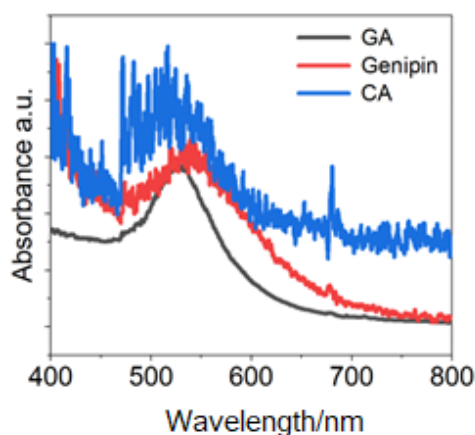


Figure 83 UV-Vis spectra of the PVA/gelatine nanocomposite hydrogel with the different cross-linking agents.

The gels were all synthesised using different concentrations of cross linker and transparent, strong and flexible hydrogels were produced with a good level of firmness and stretch. The ratio of gelatine and PVA were kept the same in all experiments. The colour indicates the incorporation of the gold in the 3D gel

network. The best hydrogels in terms of mechanical strength and stability are shown in Figure 82, after optimising the quantities of each component in the hydrogel. All the crosslinkers were successful at inducing gelation of the PVA gelatine blends, forming a solid, partly transparent 3D free-standing network. Air bubbles formed towards the end of the gel occur due to the pouring of the gel mixture into the mould and can easily be removed by more careful setting of the gel. They all possessed similar mechanical properties and the thickness of each gel could be controlled by the volume of gel in the mould. The UV-Vis, Figure 83, depicts the SPR band for all three hydrogels. The data has been normalised for ease of comparison. All the SPR bands are around 535 nm which matches the SPR from the gold NP solution. The slight deviations from this arises from the gels being in a different phase, thus the interaction with light changing slightly. The signal to noise (SNR) is something to notice as with both genipin and citric acid these become obvious. The spectral SNR affects the optimal resonance wavelength and resolution, and this may be due to the instrument used. The sensitivity of the instrument affects the SNR, and with the relative change in the index of refraction of the fluid medium, this may have enhanced the SNR for the citric acid and genipin hydrogels. As the interest lies in the position of the SPR band, it is not too significant. All three crosslinking agents did not affect the nanoparticle incorporation into the gel.

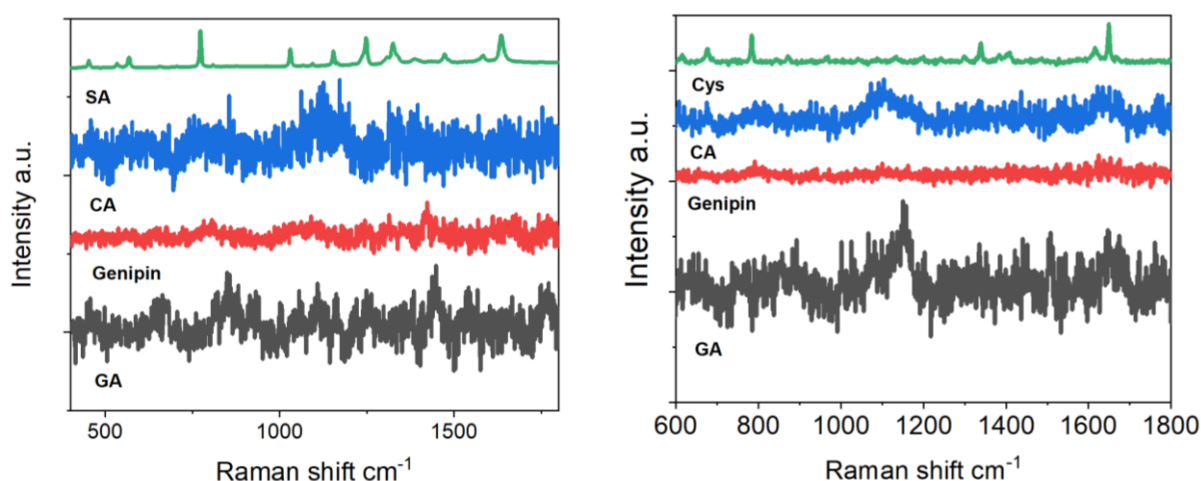


Figure 84 (Left) Normal Raman of solid SA and SERS of the PVA/gelatin nanocomposite gel with 1 mM SA with the different cross-linking agents, and (right) the same, with 10 mM Cys. The spectra were normalised for clarity.

SERS was performed on the hydrogels to assess the Raman capabilities and whether the cross linker could affect the SERS performance of the PVA/gelatin

blends. 1 mM salicylic acid (SA) was drop cast onto the surface of the hydrogel and SERS was immediately acquired. The SNR ratio of the SERS is quite high for all the spectra, but some peaks can be seen with the glutaraldehyde. The hydrogels absorb water but the SA in ethanol may have hindered the adsorption process on the hydrophilic gels. The bands at 1471 cm^{-1} , 1247 cm^{-1} and 1066 cm^{-1} can be attributed to the SA, even though these are at low intensity. The large measurable background provides an extra challenge in ascertaining clear Raman peaks. The timing between casting the analyte onto the gel and acquiring the spectrum might be significant as it allows for the solvent to evaporate before the SERS is collected. This suggests that for non-aqueous samples, allowing time to dry is an important step to consider as this can improve the quality of the results. While the hydrogel is still wet by nature, the drying of the solvent molecules on the surface allows for better resolution of the microscopic image to determine the position of the analyte molecules whilst carrying out the analysis. The ethanol from the analyte solution and the water on the hydrogel surface can form hydrogen bonds on the surface which may be the dominant interaction occurring, and manipulating the surface of the gel, preventing SERS to be observed. This data alone is not enough to conclude the use of the hydrogels.

More analytes were tested on the hydrogels for further assessment on their applicability as SERS substrates. 1 mM cysteine (Cys) was chosen as an aqueous probe molecule. The use of aqueous solutions will cause the hydrogels to swell which may affect the SERS experiments. The SNR remains low for Cys, with similar SNRs for the hydrogels for both analytes. However, the SERS profiles for both analytes are unique showing that the hydrogels are sensitive to the change in probe molecule. The genipin does not reveal a SERS spectrum, and no distinguishable bands can be identified with the citric acid, but the glutaraldehyde does show a few broad bands upon close inspection. The Cys molecule was difficult to determine with just the gold NPs alone, so on the hydrogel which features many more components it is unsurprising that a clear spectrum could not be obtained. It is worthy to note that the SERS spectra on the hydrogels will differ greatly from the ordinary Raman of the free-standing cysteine powder due to changes in conformation and the SERS selection rules

that dictate what bands are enhanced. This is the first time, to the knowledge of the author, that label-free SERS has been performed like this on hydrogels. Therefore, there is a lack of mechanistic details in literature about how the substrate may encourage specific conformations that may alter the observed SERS. However, this Raman can be used to further characterise the hydrogels as the broad shoulder presenting itself at 1097 cm^{-1} is ascribed to the PVA corroborating that the polymer has been introduced to the gel network. The absence of other distinct PVA peaks implies that the surface has been covered uniformly with the analyte molecules. The lack of SERS response is not unsurprising for biomolecules in this label-free methodology. The observation of some spectral bands is evidence that the gels are SERS active, but optimisation is required.

Increasing gold concentration

The lack of certain SERS may be indicative of a low concentration of gold on the surface which will make it less likely for gold-analyte interactions to occur, thus decreasing the chances of analytes positioned at hotspots. To combat this, the gold NP solution used in the hydrogel was maintained and equal measures of both gold and analyte were mixed before coating onto the hydrogel as portrayed in Figure 85.

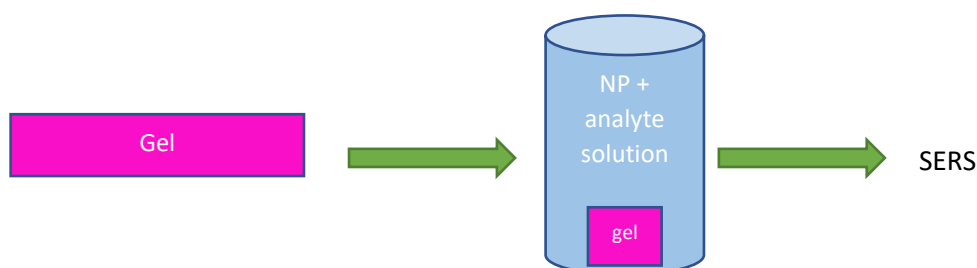


Figure 85 Schematic showing the method for incorporating more gold into the SERS system by immersing the gel into a solution containing 1:1 ratio of gold NPs and analyte before Raman acquisition.

With this method, the SERS profiles, Figure 86, show many more features than with the previous approach. 1 mM SA was initially tested to compare the effect of the addition of gold NP solution. The genipin hydrogel seems to still be noisy with a lack of distinct bands, but for both citric acid and glutaraldehyde the spectra exhibit more activity. The differences in both these spectra may also be

indicative of the different ways the SA interacts and its orientation on the hydrogels, and that whilst the polymer components remain identical the cross-linking agent may influence the gel's structure which in turn can affect its SERS function. The appearance of additional bands is not uncommon for SERS as well as the shifting of the peaks. The chemical enhancement of SERS that controls the frequency shifts has been explored, but the related mechanism is poorly understood. The glutaraldehyde hydrogel shows a strong band at 1471 cm^{-1} attributed to the C=C stretching vibration of the benzene ring. Whilst there is a lot of motion in the $1200\text{--}1600\text{ cm}^{-1}$ range, not owing to the SA entirely, the strong distinct band at 1386 cm^{-1} is related to the O-H in plane bending. The citric acid gel shows a strong, distinctive band at 1635 cm^{-1} corresponding to the C=O vibrations of carboxylic groups.

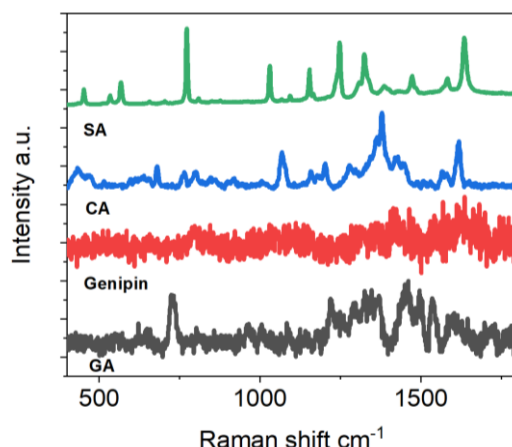


Figure 86 Normal Raman of solid SA and the SERS spectra of 1 mM SA on the PVA/gelatine hydrogels with the different cross-linking agents using new protocol as demonstrated in Figure 89. The spectra were normalised for clarity.

The microstructure of the gels may differ, which affects the AuNPs adsorbed on the substrate surface. The state of the adsorbed AuNPs on the substrate surface influences the SERS effect to some extent. The degree of porosity has influence on the interparticle distance of the gold NPs as well as having a substantial effect on the mechanical properties, with the stiffness of the network decreasing as porosity increases. As reported, increasing the concentration of crosslinker decreases the water absorbency of the hydrogel composite. It has been stated that different cross-linking agents can reduce or increase the pore size of gelatine which are in the range of 5 to 20 nm which tend to decrease with increasing monomer and cross linker concentration. Hydrogels with smaller

pore size would decrease water uptake capacity. A smaller pore size would result in low permeability, making the travel of water through the gel much slower. As SERS is a surface-sensitive technique, the absorbance of the analyte into the bulk would greatly decrease its effect so a smaller pore size in the hydrogel would be required. The porous structure of the hydrogels is unknown, but the concentration of cross linker does affect the porosity, swelling characteristics and mechanical strength of hydrogels. In published literature, the type of crosslinking method, even though the hydrogel compositions are the same, strongly influences the ability of the material to absorb fluids. Chemically cross-linking hydrogels results in a more regular and denser surface. To assess the microstructure, SEM is required, however, performing SEM on hydrogels would not work unless they have been completely dehydrated which is impractical for this study as it degrades the material's shape and flexibility.

As the citric acid and glutaraldehyde crosslinked PVA hydrogels demonstrated the best SERS ability, they were further studied with 10 mM arginine (Arg), Figure 87. The citric acid hydrogel is showing more defined spectral bands than the hydrogel with glutaraldehyde but the profiles for both are matching each other, demonstrating the specificity of the hydrogels. The peaks at 1479, 934 and 839 cm^{-1} are attributed to the NH and CH deformation vibrational modes. The small intensity band at 615 cm^{-1} can be ascribed to the COO^- deformation²²⁴. These are the most probable assignments based on the literature.

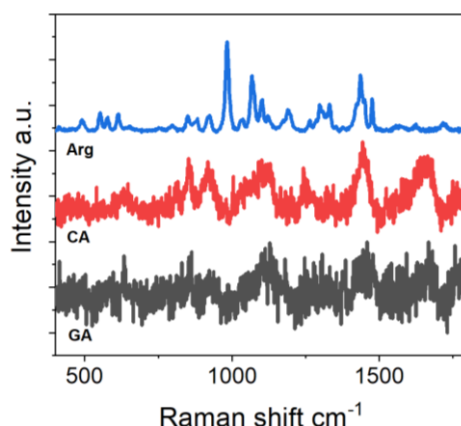


Figure 87 Normal Raman of solid Arg and SERS spectra of PVA/gelatine hydrogels with 10 mM Arg with the different cross-linking agents; citric acid (CA), and glutaraldehyde (GA). The spectra were normalised for clarity.

Summary

The cross-linking agent seems to influence the SERS response of the hydrogel blends. The results indicate that the SERS from both glutaraldehyde and citric acid are comparable. Glutaraldehyde is easily available, inexpensive, and its aqueous solution can effectively cross link collagenous tissue in a relatively short period. However, it is toxic if biodegraded, hence the increasing demand for a crosslinking agent to form stable and biocompatible crosslinked products, without added cytotoxicity problems. The glutaraldehyde utilised in these experiments was to be kept minimal, a low concentration (0.125%) in an attempt at reducing its toxicity. Nonetheless, the exposure limit for glutaraldehyde is 0.2 ppm which is much lower than the concentration employed in this study. Genipin, although enhancing the mechanical strength of the gel, it did not exhibit SERS activity and its high cost makes it unaffordable for certain applications. Citric acid has emerged as a nontoxic crosslinking agent for the preparation of hydrogels, being named 'the green cross-linker'. It can actively participate in hydrogen bonding interactions with other polymer networks and improve their properties owing to its three carboxylic acid groups and hydroxyl group. Cross-linking is achieved through the attachment of the COOH functional group to the hydroxyl group of the gelatine and PVA by esterification reactions based on anhydride intermediate formation. A citric acid cross-linking reaction usually requires elevated temperature of 120 -190 °C, but here, the reaction was completed at 70 °C, making the conditions greener than those that have been reported to date.

Multiplexing

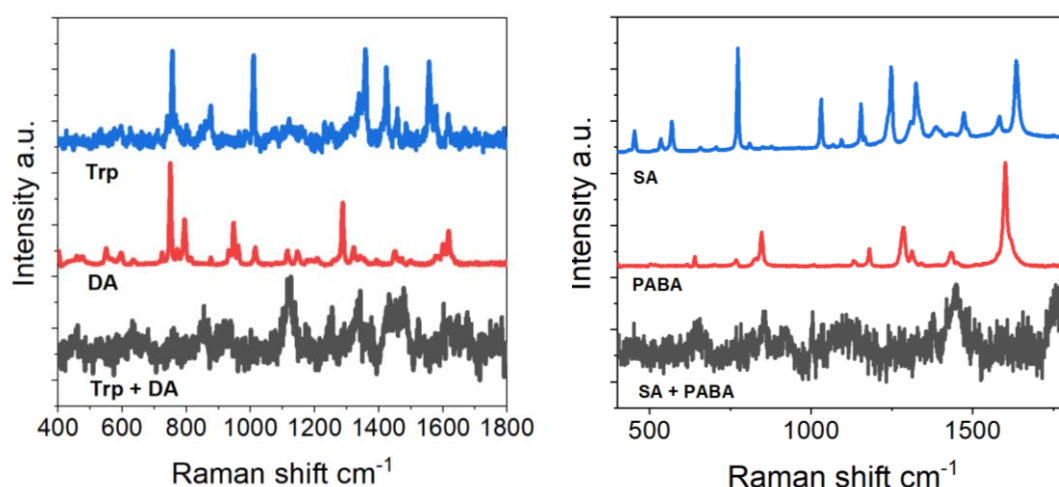


Figure 88 (Left) Normal Raman of solid tryptophan (Trp) and dopamine (DA) and the SERS spectrum of PVA/gelatine nanocomposite gel with 10 mM tryptophan and 10 mM DA combined, and (right) normal Raman of solid SA and PABA and the SERS spectrum of the hydrogel with 1 mM SA and 10 mM PABA combined. The spectra were normalised for clarity.

Specificity and sensitivity are important aspects when considering the SERS potential of a biomaterial. The citric acid hydrogel composite was tested with a couple of analytes to assess its duplex capacity. The optical properties of the SERS substrate dictate its sensitivity. Sensitivity refers to the limit of detection, whereas the specificity is the ability to recognise specific molecules on the substrate. The gel was immersed into a solution containing 1:1 ratio of both analytes. The results are displayed in Figure 88. Dopamine (DA) is a neurotransmitter involved in several functions and is a biomarker for Parkinson's disease (PD), with dopamine loss causing motor deficiency in PD patients. 10 mM of tryptophan (Trp) and dopamine were combined for the first multiplex study. The spectra are normalised for ease of comparison. The SERS spectrum is dominated by tryptophan signals, most notably at 882 and 1334 cm^{-1} . The Raman modes surrounding 1600-1700 cm^{-1} are noisy but the weak band at 1617 cm^{-1} may be attributed to the ring deformation of DA. There is also Raman activity around the 1455 cm^{-1} position which can be ascribed the CH scissoring which may be overlapping the weak 1463 cm^{-1} band of tryptophan. The intense band at 1123 cm^{-1} is attributed to both the CH and NH twisting vibration of DA and tryptophan.

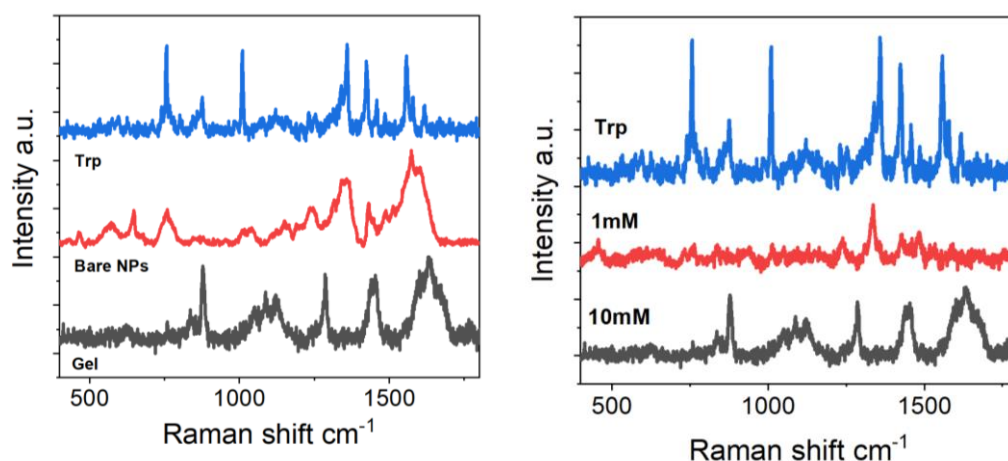


Figure 89 (Left) Normal Raman of solid tryptophan and the SERS spectra of just gold NPs and the hydrogel with 10 mM tryptophan and (right) normal Raman of solid tryptophan and the SERS spectra of the hydrogel with 1 mM and 10 mM concentration of tryptophan. The spectra were normalised for clarity.

To expand the duplex proficiency of the hydrogel, 10 mM PABA and 1 mM SA were tested to assess whether different solvents and concentrations affect the SERS output. The SNR is quite high, but a few bands can be ascertained in the SERS spectrum. The band at 848 cm⁻¹ is attributed to the PABA, assigned the OH bending mode. There is a narrow peak present at 1066 cm⁻¹ referencing the C-C stretch of the SA. However, the background encompasses most of the spectrum, adding difficulty to identify the presence of certain peaks. As the PABA is in greater concentration it would be expected that the resulting SERS would be overshadowed by PABA peaks, evidenced by the broad bands appearing at 700 and 1434 cm⁻¹. The SA which in a lower concentration cannot be as easily detected and as the location of the SA molecules would be distributed randomly on the hydrogel surface, it is statistically more complex to position the SA in a hot spot for maximum enhancement. Even though the SERS is not well resolved, it may provide information on how the duplex system works and how the analytes compete along with the solvent (EtOH) for site adsorption as well as how they may interact with each other. The Raman peak locations are sensitive to the vibrating bond's local environment; position and intensity shifts occur when an analyte favours a specific orientation to the metal surface. This is yet to be understood in the context of hydrogel substrates. The surface chemistry at the substrate and the charge of the analytes influences the existence of ions which can alter the peak location of the analyte in relation to

the solvent and background. Hence, the bands here are appearing broader and slightly shifted. This could also suggest an overlap from vibrational modes present in both SA and PABA.

To discern the quality of the hydrogel, the SERS was compared to that of just the bare NPs on a solid, rigid substrate with 10 mM tryptophan. Clear bands are present in both SERS spectra, Figure 88, and whilst there are clear differences, follows the same pattern in the range 1400 cm^{-1} to 1800 cm^{-1} . The differences in the spectra may be indicative of how the tryptophan molecule is attaching itself to the substrate, providing useful information that can be used to estimate the interactions between the gold and the amino acid. The bands at 1609 and 1573 cm^{-1} are attributed to the asymmetric stretch of the COO^- group and the bending vibration of the ring, respectively. The bands appear to be more shifted in the hydrogel than with the gold colloidal solution. When the tryptophan molecules are adsorbed on the surface, the symmetry of the system can change, leading to differences in mode selections. The intense band at 1432 cm^{-1} due to the CN and CC ring vibrations is evident in both spectra. Strong bands at 1362 and 759 cm^{-1} in the SERS for the bare NPs are assigned the CC stretching vibrations and the stretching vibrations of the ring and carboxyl group. Distinct bands at 1129 and 873 cm^{-1} are observed in the SERS of the hydrogel due to the liberation of NH_3^+ and the bending vibrations of benzene and pyrrole rings. This data shows that 10 mM concentration of tryptophan can be successfully identified on a SERS- active hydrogel, with analogous intensities to those of bare NPs on a glass slide confirming that the biomaterial is a valuable, flexible alternative for label-free SERS detection.

Figure 88 also reveals the SERS for both 10 mM and 1 mM of tryptophan on the citric acid hydrogel. Peak areas and heights can be correlated to concentration for quantitative analysis, but these spectra have similar intensities showing that the intensity does not decrease greatly when the concentration of the analyte has been reduced. The SERS enhancement are independent of the analyte concentration in low-concentrations systems, but with a higher concentration adsorption saturation may occur. The bands are very different in the two spectra, indicating that there are structural changes occurring at the surface owing to the chemical enhancement mechanism. Even with the same analyte,

the spectrum will not always match that of the ordinary Raman, nor that of the SERS. This highlights that the surface of the hydrogel should be studied extensively as it can have a major effect on the SERS. A lower concentration means a higher volume of water which will impact the swelling behaviour of the hydrogel which could stimulate different SERS responses. At 1 mM tryptophan, unique bands owing to the analyte can still be observed and distinguished. The stretching of the benzene and pyrrole ring gives rise to a strong band at 1338 cm^{-1} . Weaker intensity peaks at 760, 1011 and 1410 cm^{-1} can be seen and are attributed to the ring breathing modes, the H bending of the rings and the COO^- symmetrical stretch. Further concentration studies should be carried out to analyse the relationship between the concentration and SERS intensity.

The hydrogels were synthesised following a reproducible protocol. Once the experimental conditions were optimised, reproducibility was measured, with the hydrogels possessing identical properties in terms of structure, mechanical strength and chemical stability. The shelf-life was also investigated. Storing at room temperature would maintain the hydrogel up to a certain point, but mould may start growing on the hydrogel as well as the gel drying out in air. Storing it at a refrigerated temperature would lengthen the shelf-life of the hydrogel to several months.

3.4 Conclusions

Flexible substrates are desired for SERS in several applications. Whilst filter paper and PDMS showed promise, their SERS capability was limited by overpowering signals arising from the material itself and controlling the gold NP concentration on the surface was difficult to achieve.

Several hydrogels were prepared and investigated for their mechanical properties and SERS efficacy. Many of the hydrogel composite materials showed great potential as flexible substrates. Optimal hydrogel materials should:

- Be synthesised efficiently under mild conditions.
- Possess structural and mechanical properties appropriate for the intended application.

- Be biocompatible.
- Be reproducible.
- Have a good SERS efficacy.
- Have a long-lasting shelf life.

It was found that PVA/gelatine blends were the best in terms of the above criteria. A reproducible protocol for synthesis and method of obtaining the SERS was established. The method is facile, quick and does not entail many processes, meaning it is scalable and many can be synthesised in a day, if necessary. The effect of the cross-linking agent was examined, with the 'green' citric acid showing enormous potential as an alternative to the toxic glutaraldehyde and expensive genipin. However, the effect of citric acid cross-linking on the physiochemical and mechanical properties of hydrogels still requires further scientific elucidation.

The hydrogels were tested with a range of analytes with some analytes exhibiting a better SERS result than others. The SNR was an issue for most SERS making the separation of the analyte signals from the background challenging. Nonetheless, the obtained SERS output was comparable to bare NPs, underlining the suitability of the hydrogel nanocomposites as SERS substrates. Duplex detection did not give conclusive results, but the presence of certain peaks ascribing to both probe molecules is a preliminary test, requiring optimisation. Concentrations as low as 1 mM were determined successfully. This is the first-time, to the author's knowledge, that label-free SERS has been performed on hydrogels. Whilst other groups have looked at the incorporation of gold into hydrogels, they have served a different purpose and have used other macromolecules for their primary gel component. The application of the gelatine-based hydrogels developed in this chapter is not limited to optical methods and with additional research, other properties may be discovered.

Whilst SERS answers qualitative questions, scepticism surrounding the quantitative analysis regarding SERS is heavily questioned. That is why the SERS effect covered in this chapter has not been quantified using any EF equation. The data presented here is novel and without other research to compare it to, adding a numeric value to the data is futile. The emphasis is on

the determination of identifiable peaks directly from the SERS spectrum of a range of bio-analytes on substrates that have not been investigated before.

The temperature at which gelation occurs also offers a parameter that determines the microstructural features of the hydrogel. There are many factors that can be investigated to further advance the understanding of the hydrogel behaviours providing opportunity for additional research into these nanocomposite materials. The properties not only make them suitable for flexible SERS substrates, but the applicability can be extended to other uses in the biomedical field. These hydrogels provide a foundation for supplementary scientific exploration.

Chapter Four

Label-free SERS on Biological Samples



Chapter IV: Label-free SERS on Biological Samples

4.1 Introduction and Aims

SERS has been increasingly utilized as a label-free detection and quantification method for biologically relevant molecules and has been intensively reported in recent years as an alternative diagnostic method⁸⁹. A few label-free SERS approaches are available, and the results are promising for future applications. It has the advantages of rapidness, reproducibility and appropriate high sensitivity. Clinical Raman and SERS is a relatively new field and there is emerging evidence suggesting that biofluids from patient with diseases display characteristic spectral features that could be employed for point of care diagnosis. SERS has been reported to both identify and quantify diverse biomolecules based on the intrinsic vibrations within a molecule¹³¹. The rapid progress in this field has poised SERS technology to play a key role for biomolecular detection to enable next generation diagnostics.

Some SERS studies have explored the label-free detection of proteins. However, many of the techniques implicate the use of a SERS label approach, Figure 90. While direct detection may seem straightforward, complications have been attributed to low Raman cross-section of certain analytes as well as interferences. Quantitative SERS is notoriously difficult, with challenges arising from the subtle differences in nanostructures that affect the observed Raman enhancements²⁴⁴. SERS based label-free identification of proteins that have no conjugated chromophores is a cause of concern due to irreproducible SERS substrates or different orientation of proteins on a metal surface. Many barriers exist that make it difficult to obtain strong SERS signals from label-free proteins. Therefore, the application of powerful chemometrics or innovative separation procedures is well established in conjunction with SERS⁷⁵.

The sensitive and specific detection of proteins, mostly related to biomarkers for clinical detection schemes, is of great importance. The analysis of these can offer relevant information of the health status of patients. By means of SERS the structure and the orientation of the proteins on the metallic surface, the chemical environment of proteins and the protein interactions can be

monitored¹⁵². There has been significant progress in this field with reports that SERS can both identify and quantify diverse biomolecules based on the intrinsic vibrations within a molecule. Most biological methods have the disadvantages of being very time exhaustive, consuming large amounts of materials and resulting in low product yield. SERS- based methods have advantages over popular fluorescence-based methods in terms of photo-stability and spectral multiplexing as well as a higher sensitivity²⁴⁵.

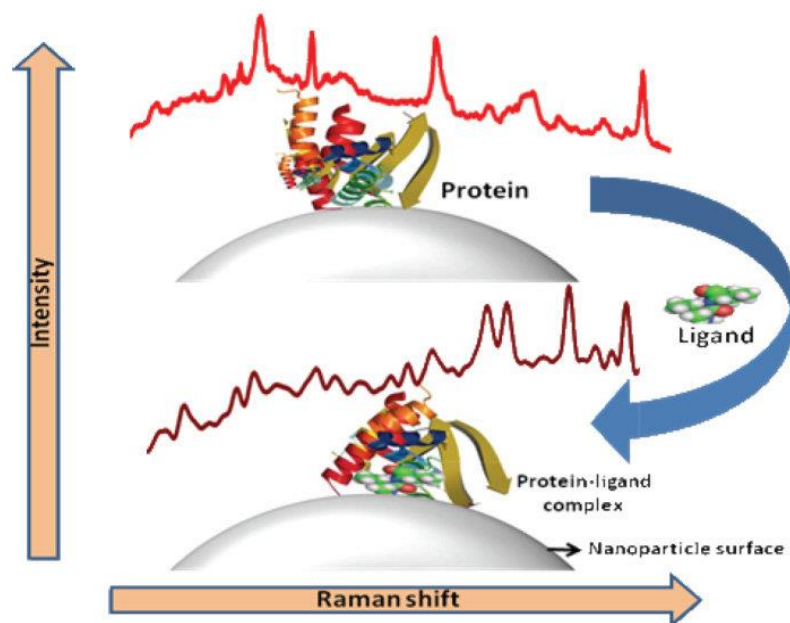


Figure 90 Image showing the direct and label approach for SERS of proteins. Reproduced with permission from reference [224].

It is still difficult to detect small molecules dissolved in complex mixtures with the SERS technique without pre-treatment of samples. Yet SERS has become a useful spectroscopic method in the detection and analysis of biomolecules. To reiterate, a biomarker is either produced by the diseased organ or by the body in response to a disease. Distinguishing biomarkers is valuable in diagnostic tests and other objective measures of an individual's health status. There is great need in the medical fields to investigate real-time expression of biomarkers to better understand their role in disease progression. Numerous factors can make wound care a difficult process. Specific biomarkers characterise the non-healing of wounds. Both local and systematic factors contribute to delayed healing. Chronic wounds represent a major healthcare burden in many countries including financial stress and impact on morbidity as a result of undiagnosed or untreated wounds. Currently, wounds are assessed

based on physical symptoms and signs. Present methods used for predicating wound healing depend on meticulous and consistent clinical observation over several weeks. However, these need to be further supported for effective wound management. It is necessary to understand and identify wound biomarkers involved in their pathological conditions that triggers a wound to a non-healing situation. The possibility of detecting the clinically relevant biomarkers would be of great help in assisting clinicians' assessment of the status of the wound.

The research presented in this chapter aims to study the label-free SERS detection of proteins and applying it to real-life wound samples from patients. The quantification and qualitative analysis of certain proteins using SERS-based methods require less time and fewer reagents than the common process utilising ELISA kits. The focus of these results is on the qualitative outcomes as the determination of these proteins using SERS is yet to be established. Quantification of the results can be performed subsequently when enough data has been collected to validate the initial findings. The proteins studied have biological importance in wound healing. The gold colloids alone as well as the SERS-active hydrogels are investigated as substrates and repeated experiments are conducted to validate the reproducibility. The protocol of data collection is established. Different concentration of proteins as well as multiplexing are researched to evaluate the efficiency of the substrates. Attempts are made at identifying potential trends and patterns in the data relating the biomarkers with indication of the wound status. Statistical analysis is performed on the data for better clarity of results. This is the first-time label-free SERS has been implemented for the study of clinical wound samples. The objective is to examine the ability of SERS to detect concentrations of wound biomarkers in aqueous solutions as well as effluent using both a colloidal suspension of citrate capped gold NPs and active hydrogels as SERS substrates without labels or incubation time.

4.2 Experimental

The research was supported by the Agency for Science Technology and Research (A*STAR) under its Industry Alignment Fund- Prep-positioning

Programme (IAF-PP), grant number H17/01/a0/oH9 & H17/01/a0/oG9, Wound Care Innovations for the Tropics (WCIT) Programme. The author acknowledges the efforts of the study team at St Luke's Hospital who collected samples and data and managed the research under approved IRB-02 2019-08-28. The author acknowledges the efforts of the WCIT Programme Office team who has supported the management of this research under approved A*STAR IRB 2020 -044. All ethical forms were approved under A*STAR policies in Singapore.

4.2.1 Reagents and Materials

The following were purchased as indicated and used without further treatment: Recombinant human TNF- α protein, > 98% , (TNF- α), recombinant human MMP-9 protein, > 95%, recombinant human IL1- α protein, > 95%, recombinant human IL-6 protein, > 95%, recombinant human IL-18 protein, > 95% were all purchased from Abcam. Bovine serum albumin (BSA) was purchased from Sigma Aldrich Ltd.

4.2.2 Methods

The citrate-capped gold NPs produced in chapter II and the SERS active PVA-gelatine hydrogel blend discussed in chapter III were employed as SERS substrates. These were used as prepared.

Several proteins were looked at that were biologically relevant to this study. These have been established in literature as biomarkers significant in wound management. Specific concentrations were prepared by dissolving the protein in 1% BSA solution and were stored in the refrigerator at $\sim 4^{\circ}\text{C}$. For multiplexing 1:1 ratio of two proteins were mixed using the vortex for 30 seconds. Then a 1:1 mixture of the resulting solution and gold NPs were used before SERS acquisition.

The wound samples were collected from 30 different patients over 4 weeks at 1-week intervals. Some samples were missing due to the patient not attending their session. These were stored at -20°C and taken out to defrost at time of measurement. Not all the Raman spectra is presented in this thesis. There is a focus on a few patients to display typical spectra that were compiled. The

patient data that has been selected for this thesis is based on the corresponding photographic measurements that were obtained.

EF calculations

The EFs were calculated using the same equation as chapter III, the analytical EF using the Raman band intensity and the concentration of the analyte for the normal Raman and the SERS measurements.

4.2.3 Characterisation

Raman

SERS measurements of samples were performed using a Renishaw InVia Raman upright microscope (Renishaw InVia, UK) with a 633 nm laser. This Raman system was integrated with a Leica microscope and the laser light was coupled through an objective lens (20 x, 0.75 numerical aperture), which was used to excite the sample and also to collect the scattered Raman signal. The prominent Rayleigh scattering was blocked using a notch filter and the beam spot on the sample was $\sim 1 \mu\text{m}$. 10 spectra per sample were acquired over 10 different spot areas. Each spectrum was integrated for 10 seconds, in the range of $400\text{-}1800 \text{ cm}^{-1}$. After collecting the SERS spectra, post processing was done using Wire 3.4 software associated with the instrument. The background subtraction was done by a cubic spine interpolation. The instrument was calibrated with signal from standard silicon at 520 cm^{-1} .

For the gold colloidal solution, the simple approach of 1:1 mixing and drop casting a small quantity onto a glass slide was employed. Data was then collected immediately by applying a slipcover on the wet droplet.

The hydrogel used in all the experiments was the PVA/gelatine composite hydrogel with citrate-capped gold NPs embedded into the matrix. This was the gel which showed the best properties in Chapter II. Two approaches were used for the SERS of the hydrogel. One involved drop-casting the wound samples/ proteins on the hydrogel directly, and the other was cutting the hydrogel into smaller pieces before immersing them into a vial containing either the protein or wound sample. Data was acquired immediately.

As with all the Raman data presented in this thesis, the duplex graphs are shown without the intensities as normalised spectra for ease of comparison and peak identification. The primary concern is that specific protein peaks can be detected using SERS as a preliminary study.

Data analysis

Statistical analysis was attempted using the data from the wound samples and proteins. Principal Component Analysis (PCA) was first performed on measured Raman spectra, using Origin. The file used was PCASpec.opx, which was installed onto the Origin workspace. This tool was used to create loading plots and score plots of the data.

4.3 Results and Discussion

4.3.1 Proteins

The SERS of several proteins were gathered and studied. Proteins exist in many structures from its primary to its quaternary structure. This is already at increased intricacy from the small molecules looked at in earlier chapters. Powder forms were not used as reference material, but the normal Raman was taken from the aqueous solution of the protein. Because of the selection rules of SERS, there are significant differences between the SERS spectra of macromolecules and those of small molecules. Previous studies have reported that SERS spectra of adsorbed macromolecules may not closely resemble their normal Raman spectra, because only the residues near the metal surface will be enhanced. Having this basis of data would help with the identification of spectra from more complex samples. Probing the proteins by themselves would produce reference data for the latter part of the study. Cytokines are a group of proteins that act as regulators of immune and inflammatory responses. They include interleukins, TNFs, interferons and chemokines. Standard reference spectra were produced by examining the different proteins at the same concentration for ease of qualitative comparison. 1 mg/mL concentration of the proteins were synthesised in 1% BSA. Several samples of varying concentrations were produced by altering the volume of BSA.

The interleukins relevant to this study were IL-6, IL-18 and IL-1 α . There has been reports suggesting that the levels of these are raised in non-healing wounds¹⁴³. The rapid induction of IL-18 during wound healing suggests a role within the early phase of repair. TNF- α and MMP9 are both other biomarkers of significance. Wound levels of MMPs can be a good prognosticator of wound behaviour. The lower the level, the higher the chance of improved wound healing. TNF- α is a cytokine, constituting 157 amino acids, well known for its involvement in the genesis of inflammation and autoimmunity. The levels of TNF- α are significantly higher in non-healing wounds. When healing occurs the level then falls. Hence, monitoring the levels of these proteins are key indicators in the prognosis of the wound. Much attention has been drawn to understanding the strategies, functions and structure of the different interleukins. Interleukins represent invaluable biomarkers in versatile diseases.

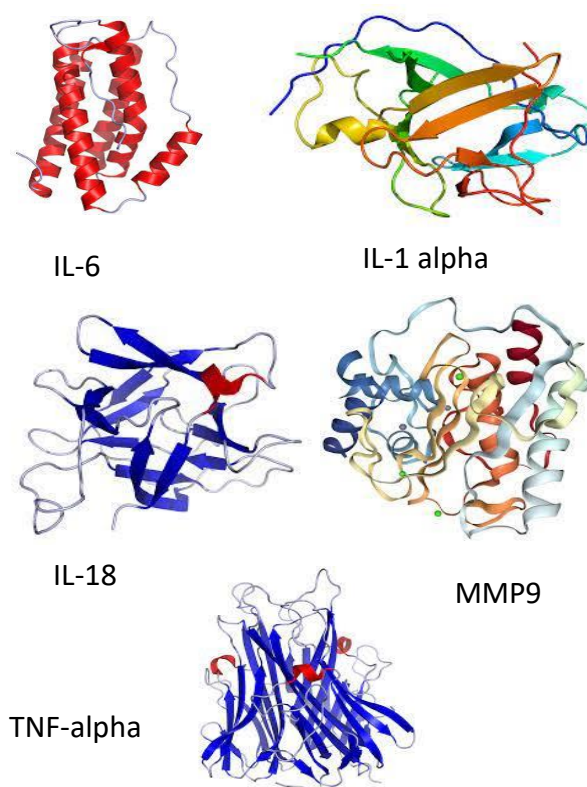


Figure 91 Molecular diagrams of the different protein biomarkers.

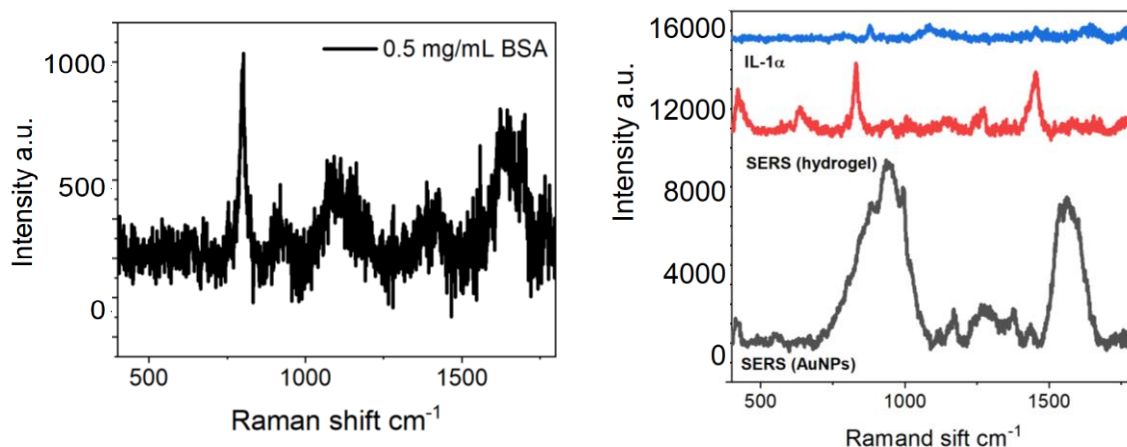


Figure 92 (Left) Normal Raman of aq. BSA and (right) Normal Raman of aq. 5 mg/mL IL-1 α and the SERS spectra of 1 mg/mL IL-1 α on the gold NPs and the hydrogel. The background was removed and the baseline was offset for clarity.

The SERS was carried out on both gold colloids and the hydrogel with the results presented in Figure 92. The normal Raman of BSA is shown as a control. The BSA solution does have its own inherent Raman signals, but it is crucial to note that the concentration is 50 times higher than what was used in the protein experiments. The most notable peak is at 797 cm^{-1} which is also observed in the hydrogel SERS of the protein. However, the other signals do not match the BSA profile confirming that these are in fact, from the analyte investigated. Ordinary Raman was collected from the substrates alone to further disregard any contaminant signals. As proteins are made up of the same amino acids, but arranged differently, similar peaks would be expected. The data is displayed as SERS performed on the bare metallic NPs and on the hydrogel, at the same analyte concentration, with background correction. Differences in the data can be attributed to the way the protein positions itself on the surface. It is uncommon for the SERS spectra of the same protein from different research groups to alter significantly due to the selective enhancement of amino acids near a metal surface or the denaturation of proteins resulting from interactions between proteins and metal surfaces. The biggest variation of the two substrates to mention is the phase with the colloidal solution being in a liquid state whereas the hydrogel is a partial free-standing 3D network. The protein will mix with the gold solution before deposition whereas the protein is layered on to a surface with immobilized gold particles and this can greatly

influence the analyte-gold interactions and thus, the SERS observed. Normal Raman on the proteins produces no signals so it can be said that all the peaks are enhanced in this instance. Quantifying the enhancement is impossible for this reason, but relative comparisons between the intensities can be made that can be quantified for general analysis of the data. Different concentrations of the proteins were probed to determine a link between concentration and peak intensities to establish some sort of calibration curve. From this point forward, any reference made to hydrogel is referring explicitly to the PVA/ gelatine nanocomposite hydrogel cross-linked with citric acid.

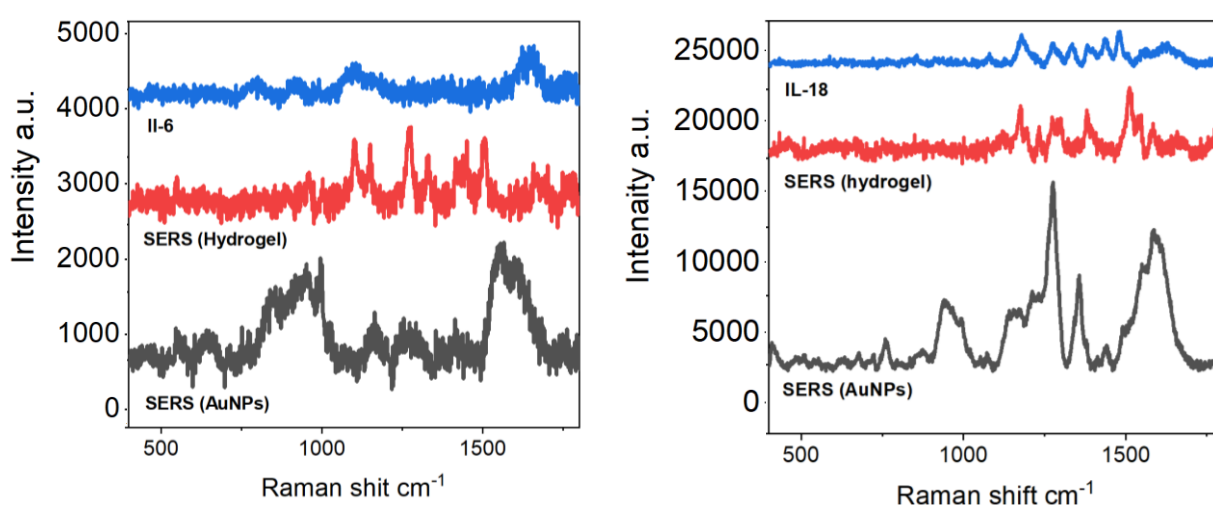


Figure 93 Normal Raman of 10 mg/mL aq. solution of (Left) IL-6 and (right) IL-18, followed by the SERS spectra of the hydrogels and the gold NPs with 1mg/mL of the respective proteins. The background was removed and the baseline was offset for clarity.

The primary observation from the spectra is the similarity between the proteins at this concentration, and there are many features present in the graphs, shown in Figure 93. Even though the proteins are expected to have overlapping Raman vibrations, the data here shows that there are contrasting differences between them that may be useful in further analysis. The actual value of the concentration is not significant, so long as several concentrations are studied to identify patterns in the data. Initial examination of the spectra reveals that, whilst the protein exhibits a very weak normal Raman spectrum, bands appear in both SERS spectra. Yet there are differences in the enhanced bands for the bare AuNPs and the hydrogels. The SERS with the gold colloids reveals more features in the 500-1000 cm^{-1} range where bands from 1000-1500 cm^{-1} are the dominant ones on the hydrogels for IL-18 and IL-6, with IL-18 showing the most

defined spectra out of all the interleukins. IL-1 α demonstrates spectral bands throughout the data range and certain signals from both SERS spectra can be identified. These spectra will be looked at separately before general comparisons are made between all of them. The band assignments were made following the well-established criteria for the assignment of protein bands.

For interleukin 6, both SERS have a strong peak at around 1000 cm^{-1} which can be due to the phenyl group stretching mode, the ring breathing vibration. Interestingly, the hydrogel shows more distinguishable bands. The strong band at 1268 cm^{-1} can be assigned the amide III with a α -helix conformation, involving C-N stretching, N-H in plane bending vibration of the peptide bond and contributions from C-C stretching modes. The bands at 1350 and 1451 cm^{-1} can be attributed to the C-H deformation and the CH_2 and CH_3 bending vibrations, respectively²⁴⁶. The SERS of IL-6 with just the bare AuNPs reveals a broad band at 1548 cm^{-1} ascribed to the amide II vibrations.

The greatest enhancement for interleukin 18 arises from the SERS with the gold NPs. Both SERS show a band at 1549 and 1551 cm^{-1} due to the amide II vibrations and tryptophan. The strong band at 1275 cm^{-1} can be attributed to amide III, and the strong band at 1356 cm^{-1} may be a combination of CH_3 stretching, bending and rocking vibrations. The small intensity bands at 1076 and 1440 cm^{-1} are assigned the C-C and C-O stretching vibrations and the bending modes of CH_2 and CH_3 . On the hydrogel, the Raman activity from 1200 to 1350 cm^{-1} can be attributed to CN and CC stretching vibrations in proteins^{38,229,247,248}.

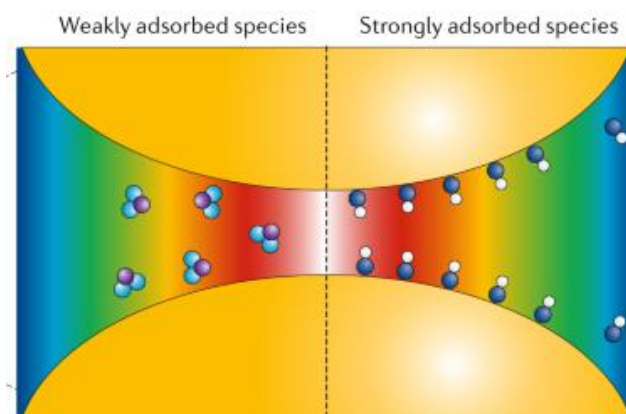


Figure 94 diagram showing how molecules can be weakly and strongly adsorbed onto the gold NPs. Reproduced with permission from reference [210].

The hydrogel SERS spectrum for IL-1 α has an intense band at 830 cm⁻¹ which can be attributed to tyrosine. The two adjacent bands with medium enhancement at around 1260 cm⁻¹ can be attributed to amide III. The peak at 1451 cm⁻¹ is a C-H bending vibration. The SERS of the protein with the bare NPs has a greater SNR which can obscure the observed bands, but distinct bands can still be assigned to certain amino acids. The bands at 878 cm⁻¹ and 1370 cm⁻¹ can be ascribed to tyrosine and heme group respectively, as well as a small peak at 1450 cm⁻¹ which is present in all three spectra due to C-H bending¹⁵³.

Comparing all three interleukins, the SERS of the proteins with the bare gold NPs follow a similar spectral profile with broad shoulders before 1000 cm⁻¹ and after 1500 cm⁻¹. The resolution of the spectra can imply how well the interleukin adsorbs to the gold NPs. The different interleukins serve different functions in the human body and are composed of different amino acids as well as having a variety of structures. This could indicate that IL-18 binds more strongly with the gold NPs in a way to maximise the enhancement, resulting in clearer peaks as illustrated in Figure 94. The proteins do not discriminate on the hydrogel with similar intensities being observed for all three. The unique spectra collected suggest a good sensitivity of the hydrogel as a SERS substrate. The label-free strategy has given vibrational information about the proteins themselves as well as hinting at conformational and orientational changes amongst them. Some studies of proteins furnished SERS of amino acid side residues only, whereas some groups have obtained SERS signals from both amide groups and side residues. Hence, it is tricky to compare the data attained here to that published in literature. No previous study on the SERS of proteins has enabled routine detection of label-free proteins with high sensitivity in aqueous solution using gold NPs. The procedure presented here combines simplicity, rapidness and specificity, showing great potential in practical label-free protein detection. The tentative assignment to the components of the amide III and amide II bands indicates the interaction of the gold NPs with the peptide backbone as well as

signalling a more intact, folded protein chain, where the likelihood of specific side chain-NP interactions is reduced.

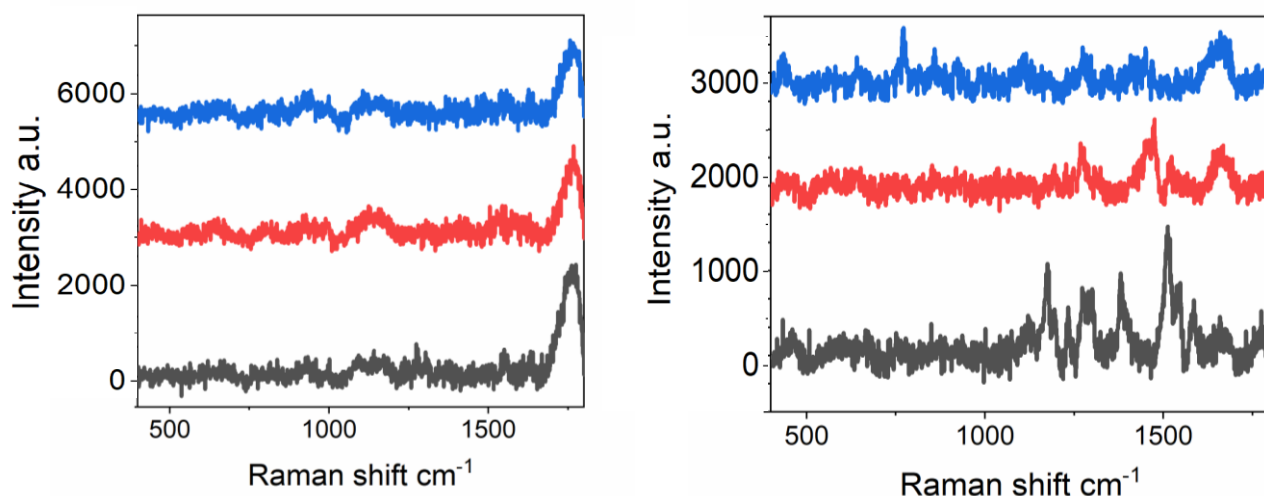


Figure 95 Repeated measurements of SERS spectra on the same substrate but at different locations with 1mg/ mL of IL-6 on (Left) Gold NPS and (right) hydrogel. The background was removed and the baseline was offset for clarity.

Reproducibility is a hot topic for SERS, especially for proteins with no chromophores because of the different orientation of analytes on the metal surface. To assess the reproducibility in this work, repeated spectra were acquired for the same concentration at different time points, in different position, maintaining the same experimental conditions. The results are presented in Figure 95 and are typical for all three interleukins. The gold nanospheres show similar spectra that are very alike, with almost identical profiles. However, the bands themselves are hard to interpret because of the low intensity. The locations of the hotspots are unknown and whilst no great enhancement is measured, the reproducibility of the SERS signal is a good result. The hydrogels showcase greater variation in the SERS with different modes enhanced for the same sample, although the spectral shape from 1100-1500 cm^{-1} is similar as well as the presence of the small shoulder at 1630 cm^{-1} albeit at different intensities. These visible changes in the spectra suggest that the protein interacts with the 3D hydrogel surface in a manner that is not uniform. The distribution of the protein may, be in a way such that different conformations are present on one sample. It can also indicate that whilst certain vibrational modes are being enhanced at different points on the hydrogel, that other signals can be detected which confirms the presence of the protein. The

strong band at 757 cm^{-1} for one of the measurements is attributed to the symmetric breathing mode of tryptophan. The signal may be present in the other spectra but could be masked by the fluorescence which can be seen, under close inspection for the band at 890 cm^{-1} . The bands present in all the spectra can tentatively be assigned to distinctive protein vibrations. The position of the encapsulated gold on the hydrogel surface is unknown and so at any given position, predicting the outcome of the protein-hydrogel interaction, and the subsequent SERS output, is challenging.

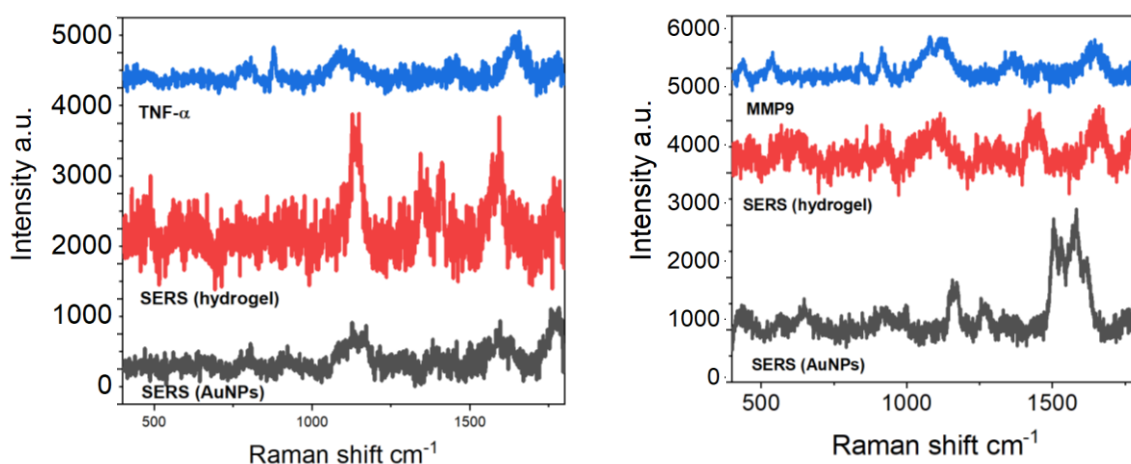


Figure 96 (Left) Normal Raman of 5 mg/mL TNF- α and SERS spectra of 0.1 mg/mL TNF- α on the bare gold NPs and the hydrogel, and (right) the normal Raman of 5 mg/mL MMP9 and the SERS spectra of 0.1 mg/mL MMP9 on bare gold NPs and the hydrogel. The background was removed and the baseline was offset for clarity.

The SERS of TNF- α and MMP9 were carried out with the results are illustrated in Figure 96 and the proposed band assignments are attempted based on literature values. For TNF- α , the SERS spectra of the hydrogel demonstrates more characteristic peaks compared to that from the gold colloids. The small peak at 914 cm^{-1} is attributed to the C-C stretch of proline ring. The band at 1228 cm^{-1} is due to amide III and the stretching vibrations of both tryptophan and tyrosine (Tyr). The bands around $1420\text{--}1460\text{ cm}^{-1}$ can be attributed to symmetric CO_2^- stretching of aspartic acid and the CH_2 bending and scissoring modes of glutamine. The bands present around 1600 cm^{-1} can be ascribed to the C-C stretching and C=C stretching and vibration modes of phenylalanine (Phe). For MMP9 there is a strong band at 1620 cm^{-1} attributed to tryptophan, Tyr and Phe. The bands observed at 829 and 1030 cm^{-1} are attributed to Tyr and Phe, respectively. The spectral activity from $1230\text{--}1280\text{ cm}^{-1}$ can be

assigned to Amide III²⁴⁹. Amide I, II and III are the main vibrational modes for proteins differing in the H bonding interaction in the peptide bonds.

In contrast with TNF- α the MMP9 shows a better-quality SERS spectrum on the gold nanoparticles than the hydrogels. The hydrogel SERS follows the spectrum from the aqueous protein with no great enhancement observed. Again, this can be used to hypothesise the structure and orientation of the protein on the gold surface. Not only is SERS useful in the direct detection of proteins, but the rich spectral information has also enabled the measurements of the biophysical aspects of the protein. It could also mean that the MMP9 protein has a stronger affinity to the solution-based substrates than the hydrogels. Multiple conformations of the protein are present, and it has been reported that the ring breathing mode of hydrophobic residues, such as tryptophan, can become more hydrophobic depending on the chemical environment of the SERS system. The proteins are adsorbed on the nanoparticle surface through amino acids but can undergo significant conformational changes that alter their secondary structure, with the consistent observation of a more unfolded, disordered protein structure on the surface of gold NPs, see Figure 97. Even though it goes beyond the scope of this study, the ability of SERS to elucidate specific protein interactions without the need for labelling has made it an attractive tool for the study of protein-ligand interactions.

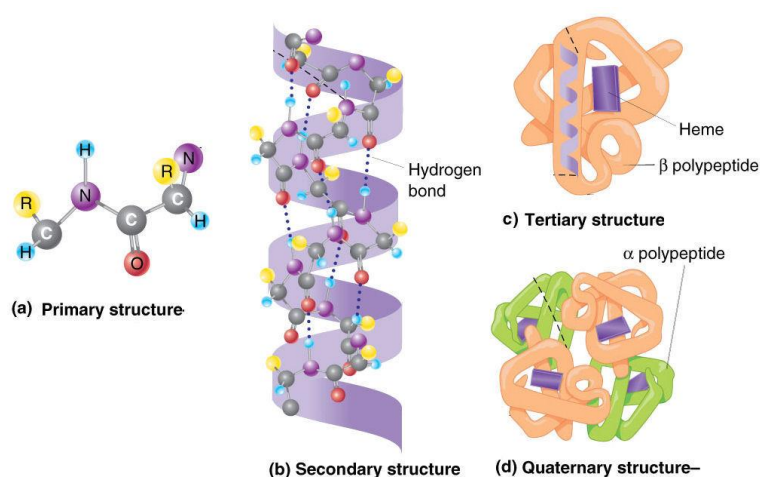


Figure 97 Diagram showing the different kinds of structures of a protein. Reproduced with permission from reference [248].

Concentration studies and calibration

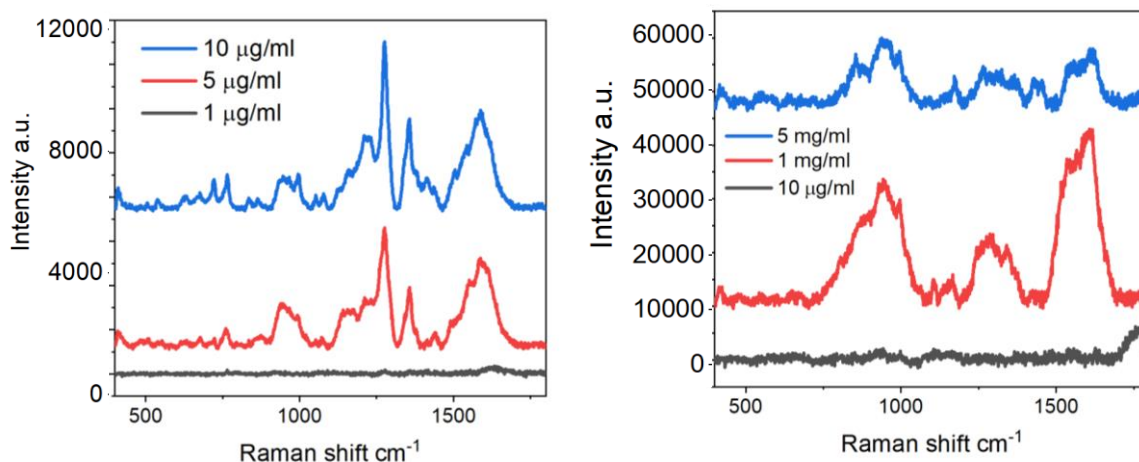


Figure 98 (Left) The SERS spectra of different concentration of IL-18 on gold NPs and (right) the SERS spectra of different concentrations of IL-6 on gold NPs. The background was removed and the baseline was offset for clarity.

Different concentrations of the proteins were analysed. To establish an understanding between the SERS intensity and the concentration, at least three different concentrations were analysed with results from some of the proteins displayed in Figure 98. The gold colloid solutions were used as the substrates for these measurements. Even at lower concentration peaks attributed to the protein can be seen. The spectral profiles match for the different concentrations. However, certain bands are enhanced differently as well as the appearance of additional bands at different concentrations. For IL-18 the enhancement increases greatly from 1 $\mu\text{g/mL}$ to 5 $\mu\text{g/mL}$, and then there is a slight increase from 5 to 10 $\mu\text{g/mL}$. For IL-6 the enhancement increases greatly from 10 $\mu\text{g/mL}$ to 1 mg/mL . The concentration increase is not at regular intervals nor the same for both proteins. There does not appear to be a linear relationship between the intensity recorded and the concentration; the highest SERS enhancement for IL-6 is not measured for the highest concentration. However, there is a lower SNR in the spectrum at 1 mg/mL and this could mask the actual intensity of the signals whereby the bands are overpowered by a strong background making the spectra look more enhanced. The fluorescence interference raises the baseline levels of the spectra. Whilst a solution to this may be to use a longer laser wavelength, it was found that no SERS intensities were observed at the longer wavelength of 735 nm when used in this study. The baseline correction

utilised is automated but even so, it is a challenge to find baseline correction parameters that fit a wider variety of different sample types. The spectra for the highest concentration for both interleukins are clearer, with distinctive bands that could be useful for protein identification. This suggests that taking the intensity data at face value is not a true indication of the enhancement.

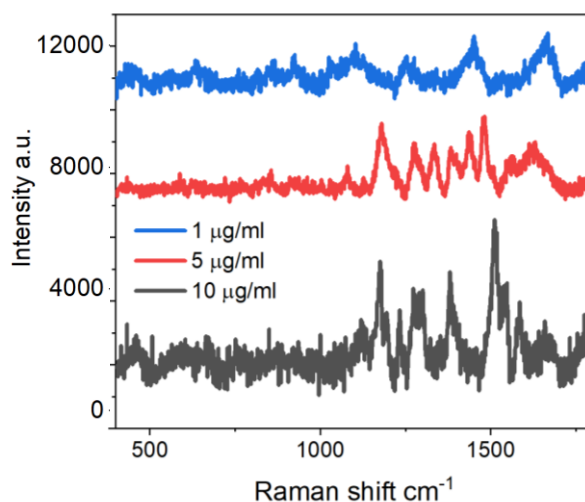


Figure 99 SERS spectra of different concentration of IL-18 on hydrogel. The background was removed and the baseline was offset for clarity.

The hydrogels were also tested as SERS substrates for the different protein concentrations. Figure 99 displays the SERS spectra obtained for interleukin-18. There is a large disparity between the SERS on the aqueous substrates and the solid supports as anticipated because of the very nature of SERS, where two very diverse substrates cannot be compared as the effect present in both will vary. The SERS shows greater enhancement at higher concentrations with bands diminishing and becoming broader at lower concentrations. There is not such an evident intensity enhancement from the lower concentrations to the higher concentrations, but the SNR does get lower as the concentration decreases. The different concentrations exhibit SERS activity in the 1200-1350 cm^{-1} range which can be attributed to amide III with more intense bands at higher concentrations. This implies that the interaction is through the peptide linkage and, as the concentration decreases, the bonding mechanism may change. At lower concentration, the statistical probability of the analyte being at hotspot reduces greatly accounting for the low measured intensity for typical colloidal systems. For the hydrogel case, the fact that a moderate spectrum

can be observed with relative intensities akin to the higher concentrations shows that the protein is captured well on the hydrogel surface.



Figure 100 Diagram to show gold NP-protein complexes. Adapted from reference [248]

Certain peaks determined to be unique to the proteins were examined and their intensities were plotted against the concentration. To validate these findings, multiple peaks from the SERS spectra were evaluated as shown in Figure 101. While a linear correlation seems to be the most probable trend, it is not always the case due to several factors that can affect the resultant SERS effect, and the mechanisms involved. The SERS intensity has been reported to be directly proportional to surface coverage for low concentrations, but at higher coverage, this relationship becomes inverse. At higher concentration, the saturation effect is often reported. At very low concentrations the SERS amplification has been known to be missing, where no enhancement can be seen. Not enough data points are available in this study to fully evaluate the findings. But certain remarks about the outcomes can be introduced. Not all the peaks follow the same trend, which is not uncommon in SERS, as certain bands may become detectable at lower concentrations due to the surface selection rules and their intensity may alter, due to changes in the polarizability, from a higher concentration to a lower concentration and vice versa.

Proteins are complex structures and the basic principles from small molecules do not necessarily apply here, Figure 101. However, generally there is an upward trend for IL-18 where the concentrations measured were relatively low, and the results for IL-6 are a bit more ambiguous. Nonetheless, even though a relationship cannot be deduced, the outline for both peaks match. The trendline shown is generally positive showing that the intensity increases with the concentration, but the error is meaningful. The error bars indicate that the values are not statistically significant emphasising the randomness of SERS

when conducting multiple experiments of the same sample. It also highlights how one peak in isolation is not a reliable indicator for identification of the molecule and that several should be considered simultaneously. For IL-6, the pattern of the data points follows the same trend, and this may suggest that maximum coverage has occurred at the concentration of 1 mg/mL where the protein takes up all the space on the nanoparticle surface so no additional enhancement will be present despite increasing the concentration. It may also be likely that a single protein molecule can bind to two different nanoparticles at the same time which would affect the surface coverage obscuring the parallel between Raman intensity and analyte concentration. The two interleukins have very different structures and so their interactions with the gold NPs may diverge considerably. The charge transfer mechanism is short-ranged and is strongly dependent on the geometry, bonding, and the molecular energy levels. These are challenging to map out for such large macromolecules. More concentrations

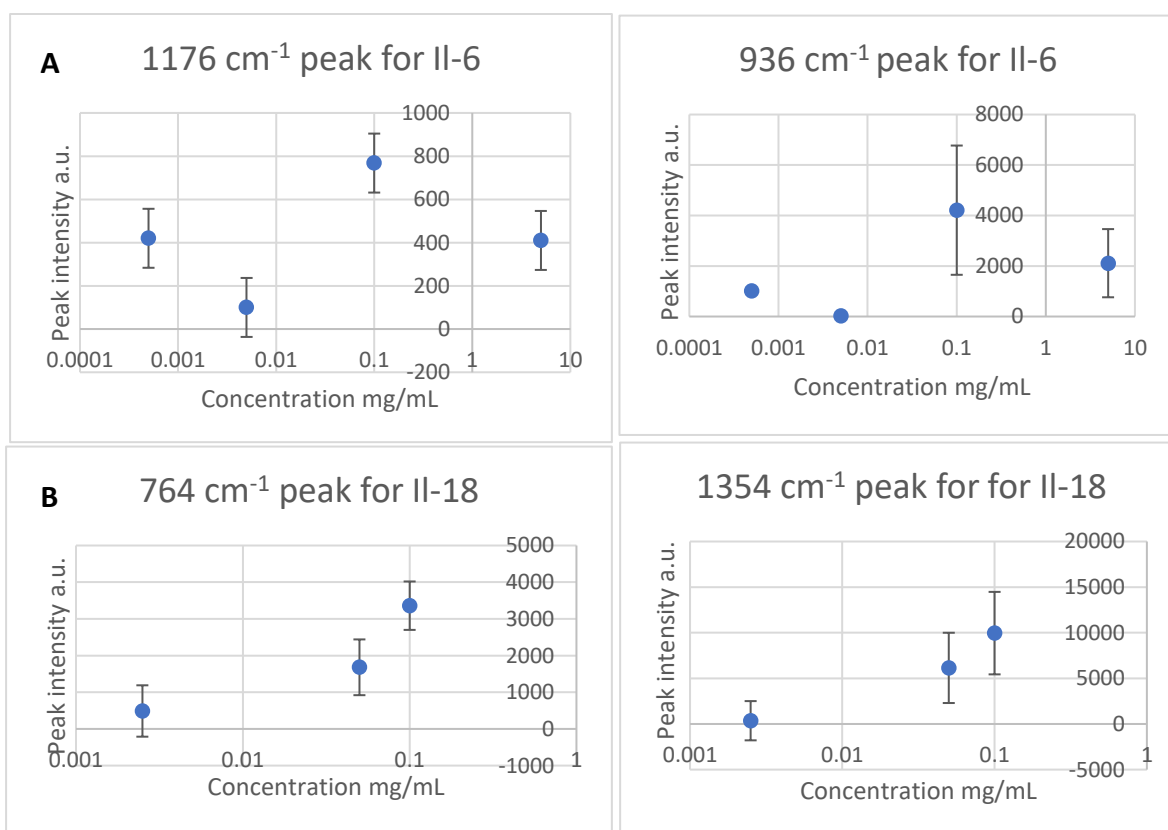


Figure 101 Graphs showing intensity vs concentration for two different peak positions for A) IL-6 and B) IL-18 with error bars. The data was averaged over 10 spectra collected for each concentration at different positions of the laser spot on the same sample.

need be studied to give a more accurate idea of the relationship, before an attempt to form a calibration graph is made.

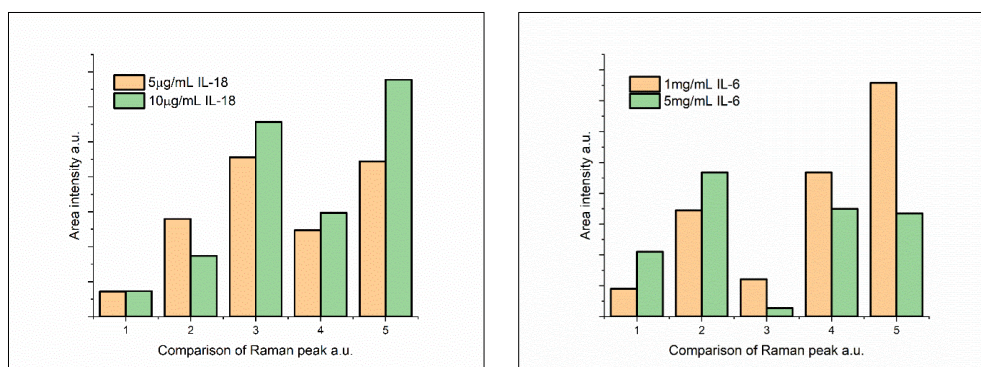


Figure 102 Peak intensity for two different concentrations at several peak positions for A) IL-18 and B) IL-6.

The chemical enhancement effect is the least studied and most difficult to quantify experimentally due to its small contribution to the overall enhancement, yet the formation of metal-molecular complexes can modify the dipole effectively opposing or amplifying its amplitude. These effects may be at play here with the proteins interacting with the gold nanoparticles. The probing of proteins by SERS using gold NP solution in the absence of immobilizing agents or aggregating salts have been reported not to affect the tertiary structure of the protein so it might be plausible that the findings in this work represent the native protein structures and can provide further information about the chemistry occurring in the SERS system, although the data is not conclusive.

Considerable fluctuations of the SERS intensity are observed and this deviation from the expected relationship is assumed to be due to the changes in the adsorption geometry of the proteins on the gold NPs which becomes important as the amount of analyte increases. The lack of definitive correlation means that determination of an unknown concentration of these proteins would not be possible. Controlling the hotspot formation and the positioning of the laser onto a specific area is a serious problem using gold colloidal solution. Several peaks were chosen from both IL-6 and IL-18 and their intensities are plotted at two different concentrations. Figure 102 confirms the absence of correlation between the intensity and concentration. Even if certain peaks are being enhanced positively, this is not replicated with other points in the SERS spectra.

This emphasises how not all bands are enhanced equally, and the selection rules governing SERS are complex.

Due to the distance dependency of SERS, the gold NPs need to be in close contact with the protein. But it has been shown that contact between the protein and plasmonic nanoparticles leads to denaturation and loss of function in gold which may explain the discrepancies in the data. Many studies have concluded that proteins are denatured on the NP surface with native resonance Raman spectra not matching the SERS spectra. This loss of activity has been suggested to occur through unfavourable adsorption orientation relative or lateral interactions between molecules of the adsorbed protein⁷⁹. Contact between a protein with a metal surface induces significant conformational changes and how this behaviour may be influenced by the concentration has yet to be examined. However, this does mean that the true extent of the EM mechanism cannot be exploited.

Even though the quantification of proteins based on their concentration has been rendered impossible i.e., calibration curves cannot be devised to measure unknown concentrations of the proteins, comparisons of overall SERS intensity can be made. EFs of the signals can be calculated by looking at the bands of the normal Raman. The strongest band on the normal Raman was used for these calculations with the results presented in Table 6. Despite no direct correlation, SERS can detect proteins at several separate concentrations with similar bands being amplified demonstrating the sensitivity of the gold NPs as effective SERS substrates. The EFs are shown for the different proteins at different concentrations to give a more complete view on the efficacy of the gold NPs, Table 6. When compared to the ordinary Raman, the SERS intensities are greatly amplified and, as the concentration measured decreases, the EF increases proportionately which is expected. The ordinary Raman generally shows low activity due to the poor Raman cross sections of the proteins. The proteins at the same concentrations (IL-18 and IL-1 α) show similar EFs at the same order of magnitude demonstrating consistency in the SERS substrates. This ensures reliability in the SERS data for the gold NPs. The ability to detect at such low concentrations, even at pg concentration proves the practicality of

the substrates. These substrates have the potential to be used for identification purposes and greater optimisation may lead to future quantification capabilities.

Protein	Peak/cm ⁻¹	Concentration / mg mL ⁻¹	EF
IL-18	1277	0.01	5.74E+10
IL-6	1557	1	2.06E+06
IL- 1 α	992	0.01	3.02E+10
MMP9	997	0.001	1.89E+11
TNF- α	1128	0.000000005	3.19E+17

Table 6 Table showing the EF calculations for the different proteins at specified concentrations.

Normally, IL-6 is not detected in the blood or is present at low levels. That means that any sensor is not looking for low levels, but the existence of the interleukin at elevated levels, which is a symptom of inflammatory condition. Therefore, the successful detection of IL-6 in the body can be extremely useful for prognosis. Determining a limit of detection would be very useful for the practical applications of these gold NPs. TNF- α has a recommended range from non-detectable to 8.1 μ g/ml with elevated levels linked to a variety of diseases. The efficient detection of these proteins at various concentrations paves the way for greater optimisation for the translation of these positive results into real-life functions.

Multiplexing

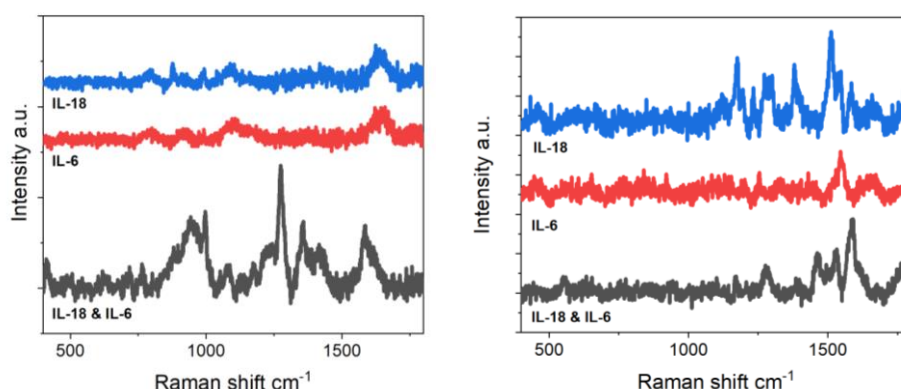


Figure 103 Normal Raman of the proteins IL-18 and IL-6 and the SERS spectrum of 1 mg/mL IL-6 and 1 mg/mL IL-18 on (Left) gold NPs and (right) hydrogel.

Proteins do show similar vibrational bands in their Raman spectrum, however, the proteins studied here did show a unique spectrum that could be used for identification. To assess the accuracy and efficacy of the SERS substrates, a couple of proteins were mixed at the same concentration before Raman acquisition. It is valuable to know whether two very complex macromolecules can be independently and confidently verified using label-free SERS.

Equal concentrations of the proteins were mixed before the addition of gold, followed by the immediate SERS acquisition. The results, as displayed in Figure 103, show the SERS spectrum of the duplex sample with the normal Raman of the proteins. These were carried out on the gold NP colloidal solution and the SERS-active hydrogel. For the case of the hydrogel, the duplex SERS spectrum was compared with the SERS spectra of the proteins on the gel.

The gold nano-spheres exhibit a SERS spectrum with many features that can be attributed to both proteins in the sample. As both IL-6 and IL-18 share many spectral bands, the independent assignment of the bands is difficult. The small bands at 747, 747 and 757 cm^{-1} can all be attributed to the symmetrical breathing of tryptophan. The narrow, high intensity bands at 1004 and 1257 cm^{-1} can be ascribed to the phenyl ring and amide III from IL-6 and IL-18, respectively. These have been deduced by looking at the SERS spectra of the proteins, however, these are still tentative. All the bands present from 1420 to 1485 cm^{-1} are assigned the CH_2 and CH_3 bending modes and deformations. The dominating signals appear to be coming from the IL-18 which has a stronger SERS response but certain signals that appear in the IL-6 spectrum are identifiable. The hydrogel spectra also share the same challenge, with signals overlapping from both proteins. As with both proteins, the SERS of the duplex shows most of the activity from 1200 cm^{-1} , with the band at 1255 cm^{-1} coming from the amide III bond, the 1522 cm^{-1} band can be assigned the $\text{C}=\text{C}$ carotenoid vibration and the bands present at 1447-1460 cm^{-1} due to the CH vibrational modes. By qualitatively comparing the spectra, it may be possible to discriminate between the proteins, but this is still very challenging due to the similarities in the spectra.

Further duplexing was carried out between two proteins that demonstrated more distinctive SERS spectra to see if bands belonging to the different proteins could be distinguished with the results shown in Figure 104. This time, for ease of qualitative comparison, the SERS is compared to the SERS of the proteins rather than the normal Raman of the neat samples. MMP9 shows the highest intensity spectrum, and the duplex spectrum follows the profile somewhat of the TNF- α but the band present at $\sim 1000\text{ cm}^{-1}$ can be attributed to the MMP9. The bands at 1356 and 1433 cm^{-1} can be an indication to the presence of both proteins and are attributed to the CH_2 and CH_3 bending vibrations and the C=O stretching vibration, respectively.

On the hydrogel, there is sufficient SERS activity with bands from IL-6 dominating the spectrum. As the TNF- α alone did not display a strong SERS response, it is difficult to assign the bands to it even though the presence of additional bands in the duplex SERS may be indicative of TNF- α in the sample. The band observed at 1560 cm^{-1} in the SERS of TNF- α assigned to the amide II vibration may be shifted in the SERS of the duplex which could signal a change in orientation and interaction of the proteins on the hydrogel surface. It should also be noted that the duplex SERS spectra are all unique highlighting the sensitivity of the SERS technique and the ability of the substrates to enhance the Raman bands of different proteins. With machine learning methods, the label-free SERS spectra can be used to isolate and classify multiple proteins in one sample. Duplex measurements may also provide additional structural

information about the proteins as the complexity of the chemistry increases with increasing number of macromolecules present in the sample.

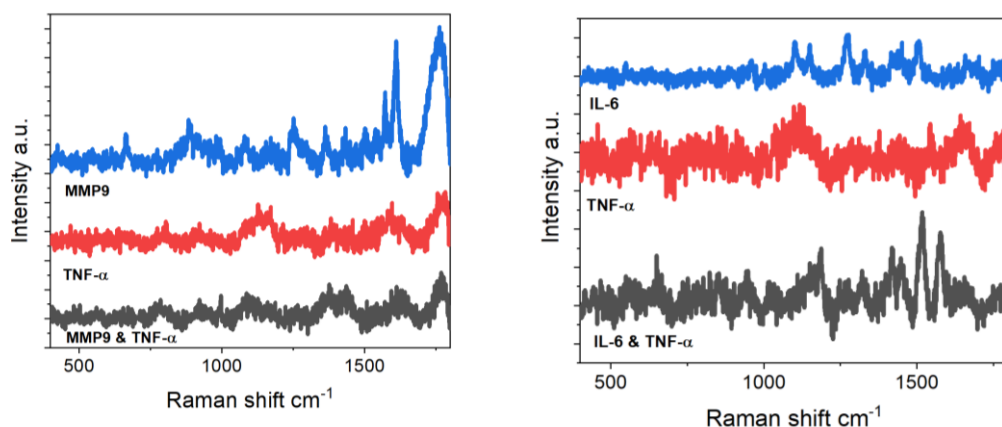


Figure 104 Normal Raman of MMP9 and TNF- α and the SERS spectrum of 1 mg/mL of MMP9 and 1 mg/mL of TNF- α on (Left) gold NPs and (right) hydrogel.

4.3.2 Wound Samples

When it comes to SERS technology in clinical tests, there is always a controlled group observed. It is important to note that in this work, the data cannot be compared with healthy individuals as a control. In other studies, looking at applications of SERS in biomedical fields, biomarkers can be compared for example, a cancer patient vs. a cancer-free patient. The same cannot be extended to looking at patients with chronic wounds as the interest lies in the biochemical composition of the wound itself. This makes the analysis and results much more difficult to interpret.

Serum and effluent are both ideal biological samples for measuring host proteins because they demonstrate the current state of recuperating¹⁴⁷. Wound effluent is considered highly revealing on the justification that it directly reflects the wound site's microenvironment which displays the current mechanism of repair.

The gold NPs Raman spectrum was taken initially to ensure no signals arose from them, as well as the wound samples themselves. The normal Raman of the wound samples gave no signals. All 30 patients' data was looked at, noting

that some samples were not available at certain points, and these were then repeated for both the gold nanoparticles and the hydrogels.

Figure 105 shows the SERS spectra of a single patient over 4 weeks, on both the bare gold NPs and the hydrogels. A few patients' data is shown to give a sense of the results obtained. From simple observation, the spectra changes over time but is similar in its profile and shape. This means that the composition of the wound sample detected by SERS does not change drastically over the four weeks which is to be expected, but the monitoring of slight changes may be significant. The broad band at 650 cm^{-1} attributed to the C-C wagging of tyrosine and cysteine, and this appears in all the spectra but with diminishing intensity. This band is also present in the SERS spectrum of IL-18. There is also a small, weak band evident at 999 cm^{-1} that can be attributed to the stretching vibration of phenylalanine present in most of the proteins. The intensities of these peaks are plotted against the week number and there is a general negative correlation for both. Interestingly, the trend is similar for both peaks with a slower rate of decrease between weeks 2 and 3. These bands can represent the biomarker concentrations. It is well known that phenylalanine (Phe) blood concentration is increased in patients with HIV infection, cancer and other diseases. Whilst there is no direct data linking Phe to wound healing, it may be a biomarker of interest.

Not all bands present in the SERS can be assigned to a specific amino acid or molecular vibration and so, not every peak intensity will give the same correlation. It is also possible that the intensities can fluctuate between the weeks for reasons not directly concerning the current study. By observing the spectra, it can also be seen that for weeks 3 and 4 the rather broad band at $\sim 1550\text{ cm}^{-1}$ becomes more resolved. The absolute intensity is not definitive as it does not consider the large background or fluorescence that may be affecting the SERS and, thus, some of the values may be very high even when there is no clear band present. Nonetheless, these preliminary observations do suggest that that SERS can be used on wound samples. To further assess whether these peaks hold any significance, and can be interpolated in a different case,

another patients' data is also reported in Figure 108. The overall outline of the SERS spectra matches with patient 1, but different peaks have been enhanced.

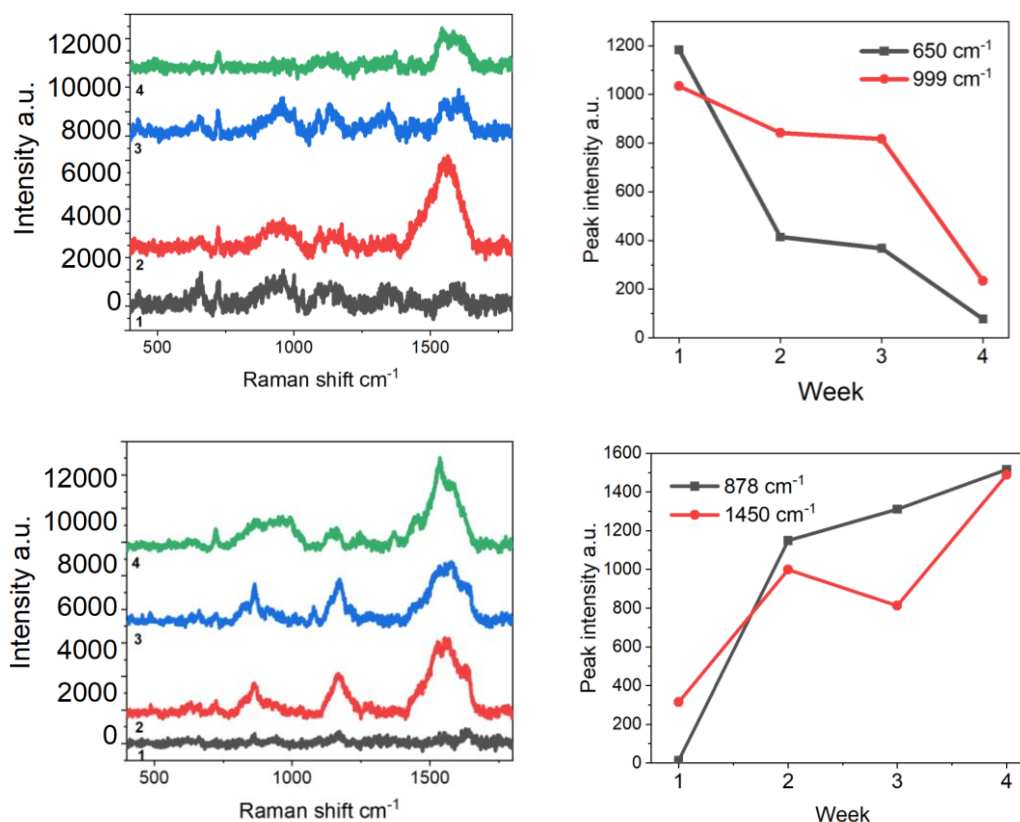


Figure 105 SERS spectra of wound samples for patient 1 (top) and patient 2 (bottom) over 4 weeks on gold NPs. The background was removed and the baseline was offset for clarity. (Right) Graphs showing the intensity of certain peaks over the 4 weeks. These are averaged over 20 spectra taken from different laser spot positions of the same sample.

Whilst the chemical composition may not change greatly in the wounds, it is possible that certain proteins and amino acid residues are more prominent in wounds from other individuals and thus, the SERS outcome will vary from person to person. It is important to treat each patient's sample as individual rather than a collective, and compare the SERS only from the same patient, although general comments can be made on all the data. The bands that were present in the first patient are not clearly identifiable in the second. This suggests that those signals may be suppressed as others are enhanced more, or simply the way the wound sample attaches onto the gold NP surface, which dictates the final SERS observation. All these measurements were repeated, and the results showed that, even with a new batch of gold NPs, the

consequential SERS spectra is reproducible and unique for each sample, despite the complexity of the wound biofluids. Yet, there are certain peaks present in the SERS that can be detected in each sample over the weeks. The band present at 878 cm^{-1} ascribed to tryptophan, evident in the SERS of MMP9 shows intensity that gradually increases as time goes on, and the band at 1450 cm^{-1} is assigned to the C-H bending vibrations that is also evident in the SERS of IL-1 α . There is a general positive correlation between the peak intensity and the time, with the rate of change varying between the weeks. MMP9 and IL-1 α levels are usually elevated in non-healing wounds, both acute and chronic. MMP enzymes are highly expressed during wound healing while its activity leads to a delay in wound healing.

Discerning the peaks in the SERS to be from a certain protein is challenging and so these statements are very superficial without more data to confirm these findings. Four weeks is not a long enough period to reach conclusive results as there is a lack of data points to assess any meaningful trends, and usually these experiments would extend over 12 weeks but that was not possible in this study due to time constraints. The important information to take from these is any noticeable changes overall and identifying general trends. Visual inspection of the data can give qualitative indications of biological changes in the wound fluid.

Hydrogels

To validate the results, the same two patients had their samples tested on the hydrogels and the same peaks were analysed to verify any similarities between the SERS on the bare gold NPs and the hydrogels, Figure 105. The exact position of the peaks may have shifted due to the change in substrate material. There is a continuity of the SERS spectra for each patient, but it does evolve as the time changes. The similarity in the spectra for both patients verify the likeness in the samples, as the biological components present remains the same and their Raman vibrations are related. Yet, by simple examination, the two patients display different SERS on the hydrogel demonstrating its ability to discriminate between patients to produce unique spectra. The monitoring of the intensity results in similar trends as with the gold colloids, with a general negative and positive correlation, respectively. The peak $\sim 1450\text{ cm}^{-1}$ exhibits a

pattern like the gold NPs, whilst the rest show different rates of change, the overall inclination remains the same for both colloidal solution and 3D hydrogel substrates.

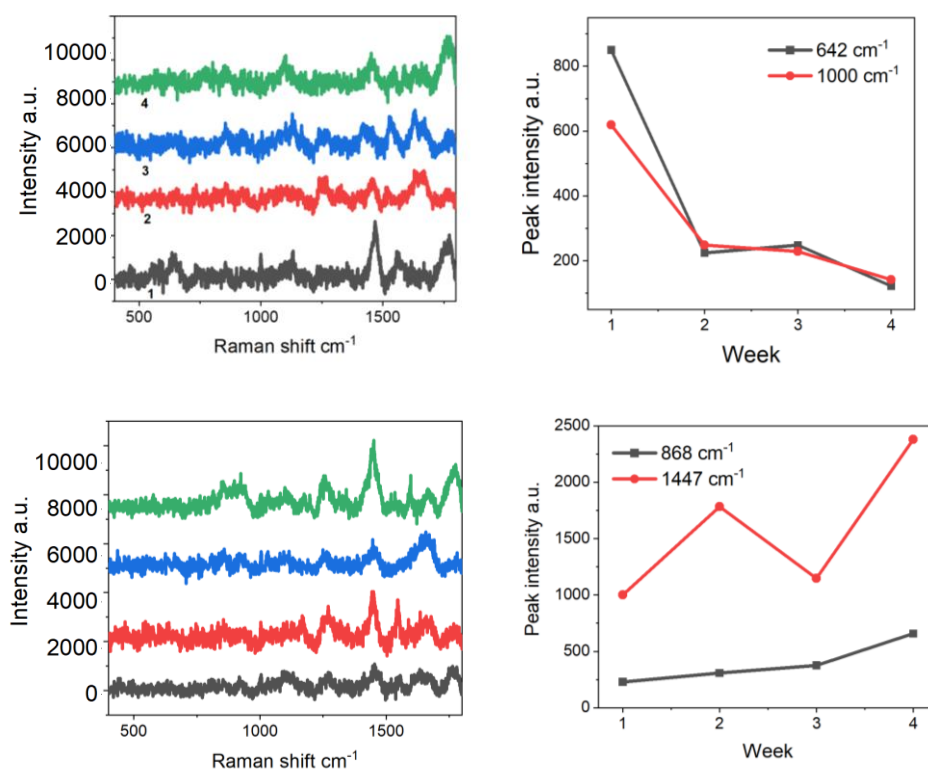


Figure 106 SERS spectra for (top) patient 1 and (bottom) patient 2 over 4 weeks on hydrogels. The background was removed and the baseline was offset for clarity. (Right) peak intensities changing over time for each patient. These are averaged over 20 spectra taken from different laser spot positions of the same sample.

The hydrogel results were collected after the gel was submerged in the wound serum overnight. To see whether the method could be developed, the wound effluent was applied to the gel in a swab style. This was to test if the analyte signals could be picked up on the hydrogel surface very quickly, dip coating the gel within seconds as illustrated in Figure 107. Patient 3's samples were studied with the results depicted in Figure 108. Both sets of spectra exhibit differences with the first two weeks showing similar spectral profiles. Due to the randomness of data collection, these differences can simply be due to ineffective locating of the hotspots on the hydrogel surface. This could be

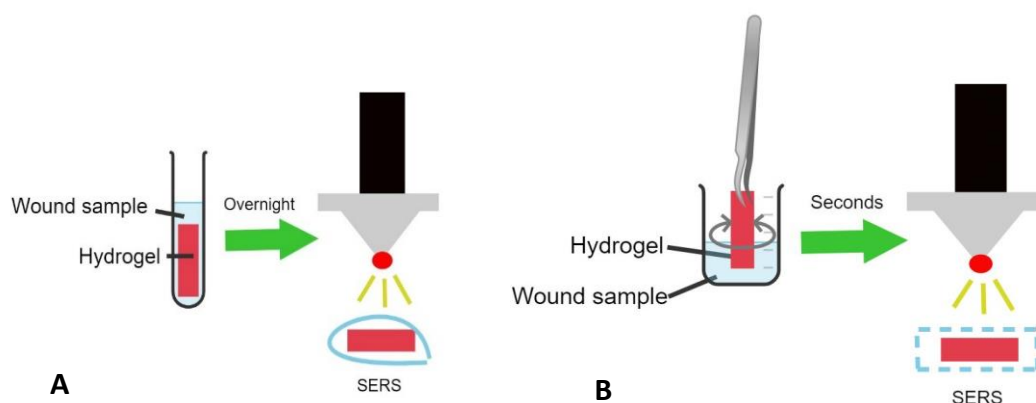


Figure 107 Schematic illustrating the different methods for hydrogel data collection when A) the hydrogel is left overnight and B) the hydrogel is quickly dip coated in the wound samples.

improved by taking more spectra across the sample, or it may indicate that the gel did not make sufficient contact with the sample for effective SERS performance. Nonetheless the hydrogels did produce spectra with moderate intensities. Both sets of spectra show bands at $\sim 1444\text{ cm}^{-1}$ which are caused by C-H vibrations of the proteins. The swab test, Figure 112 showed a signal at 854 cm^{-1} , attributed to the ring breathing vibration of Tyr with the intensities remaining constant throughout the weeks. This is also identified in the overnight test. The swab test shows a narrow band at 1560 cm^{-1} assigned to tryptophan and this intensity increases throughout the weeks. Images were not available for this patient so comparisons cannot be made.

It is not surprising that altering the method gives different results as differences in the SERS effect can be subjected by only slight changes in experimental conditions. It is important that the samples are mixed well before Raman acquisition as this could seriously affect the analytes on the surface. Since these studies were conducted under ambient temperature and pressure conditions, the state of the wound sample is constantly changing on the substrate surface namely, thermal movement, migration, configuration changes, so it no surprise that, sometimes drastic changes are observed in the spectrum. To overcome this, conducting the measurements in ultra-high vacuum and at ultra-low temperature may elucidate the enhancement more comprehensively, but this is impractical. These results are promising as it shows that even with rapid contact with the target analyte, the hydrogel picks up enough molecules for sufficient probing.

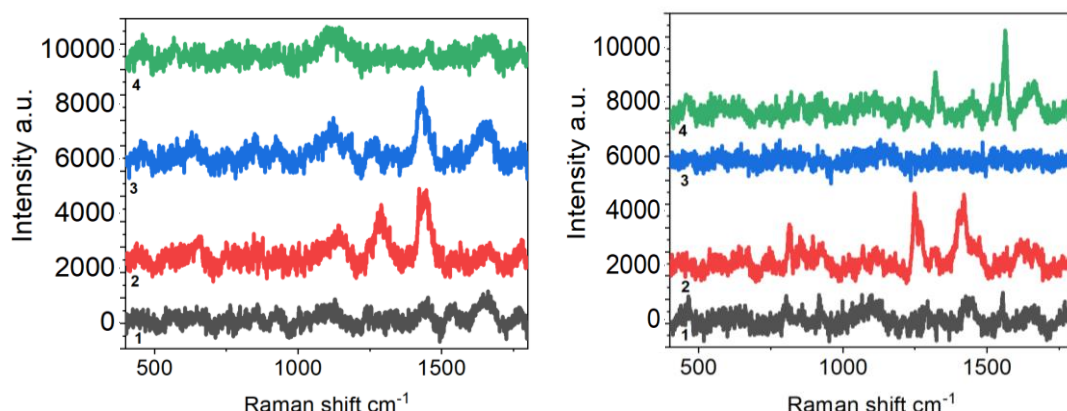


Figure 108 SERS spectra for patient 3 on hydrogels after different contact time with the samples A) overnight and B) few seconds. The background was removed and the baseline was offset for clarity.

Photographs

Currently, physicians screen the status of wounds by digital photographs and weekly measurements of the dimensions to evaluate whether the wound is healing or non-healing. Other existing techniques track healing through measures of pH, oxygen or moisture⁷. This current wound care can cause stress and inconvenience to patients. The patient data presented in this study is accompanied with digital photographs and sizes, presented in Table 7.

The wounds for both patients appear to be getting smaller, and thus would indicate that it is healing. The peaks identified with SERS at approximately 650 and 1000 cm^{-1} for patient 1 may be attributed to TNF- α and MMP9 in turn, as these peaks are found in the SERS of the proteins, after careful studying of the spectra. Both cytokines impair wound healing and so, a decrease in the level of these would imply a healing wound¹⁴⁶. This result agrees with the information and photographs provided where the wound reduces greatly in size over the 4 weeks. The SERS for patient 2 demonstrated an ambiguous but positive correlation hinting at increased levels of MMP9 and IL-1 α , which points towards a non-healing wound. This contradicts the images which show the wound decreasing in size suggesting its healing nature. However, this wound is much bigger, and the healing disposition may not be as straight-forward as simple measurements. The accuracy of the photographs should be considered as well as the reliability of this method for wound assessment. A report found that the accurate evaluation of wounds based on digital images is possible; however, it

requires training of participants and is facilitated using an assessment tool and certain types of wounds are better at being evaluated⁷. Studies have only compared photographs with bedside judgements, where the outcome shows that wound images are reliable and valid. However, photographs have not been shown to provide clinicians with information about changes in wound healing overtime and whether the tools currently accessible are responsive to changes in the wound status.





Week	Image	Size
1		Length:4.1cm Width: 1.0cm Area:2.8cm ²
2		Length: 4.2cm Width: 0.9cm Area: 2.1cm ²
3		Length:2.7cm Width:0.4cm Area: 1.0cm ²
4		Length:3.7cm Width:0.4cm Area:0.7cm ²

Table 7 Table showing the photographs and the measurements of the wound over 4 weeks for patient 1.

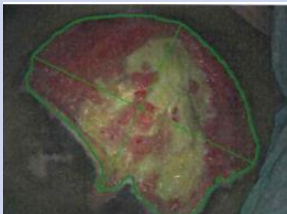

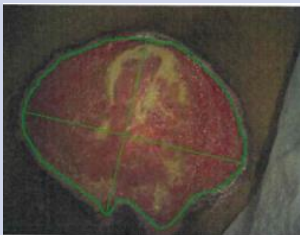
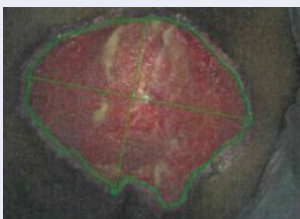
Week	Image	Size
1		Length:16.3cm Width: 12.6cm Area:148.7cm ²
2		Length: 14.5cm Width: 11.8cm Area: 123.9cm ²
3		Length:13.6cm Width:11.0cm Area: 113.1cm ²
4		Length:12.0cm Width:9.8cm Area:79.5cm ²

Table 8 Table showing the photographs and the measurements of the wound over 4 weeks for patient 2.

Summary

The results presented thus far, have all been qualitative with some attempt at experimental quantification. Both gold colloidal solution and gelatin/PVA hydrogel blend give spectra that can be interpreted with relative ease by visual inspection. The data acquired from the hydrogel corroborates the findings from the gold nanoparticles as well as some reproducibility in the spectral signals which is notably very difficult to obtain. The presence of certain biomarkers

may also be influenced on factors such as sex, age and other pharmaceutical treatment which need to be considered. Other groups have looked at purifying the contents of the sample without using external labels which may be an avenue of advancing the research presented here. However, wound and serum cytokine levels are very inconsistent and thus difficult to use as valid biomarkers of poor healing. In label-free samples, it is usually impossible to find a new band differentiating two sets of samples and so such classification is not definitive, and it is hard to say if this could ever be possible. Nonetheless, SERS is one of the most sensitive detection technologies and holds significant advantages over routine methods.

Multivariate data analysis

Despite the advantages of label-free SERS for biomarker analysis, quantitative analysis cannot be obtained without rigorous qualitative analysis, because the peak position and relative peak intensity may vary for the normal Raman and SERS spectra and under different measuring environments at different concentrations.

The translation of Raman signals to high level chemical and biological information of interest usually requires a statistical model that takes in the Raman data and outputs the meaningful information such as biological compositions²⁵⁰. These models are built on a certain number of known samples that can then be used to predict unknown samples in future to obtain the valuable information directly.

Principal component analysis (PCA) and partial least-squares regression are multivariate data dimensionality reduction methods that are valuable in biological SERS, as signals are often convoluted by other molecules in complex biological media or by the intrinsic complexity of macromolecules such as proteins. PCA is a statistical analysis method used to classify major patterns in data sets. Its main concern is to reduce the dimensionality of datasets comprising a large number of variables, while retaining characteristics of the original data-set that contribute most to its variance¹⁵⁵. It is effective in categorising SERS spectra that visually are otherwise scarcely distinguishable. Although many bands exist that can be employed to separate one protein to

another in a direct visual way. It is not possible to differentiate all the proteins in the samples because they show a lot of similarity, and the changes are very subtle and hard to detect. Classifying Raman spectra in biological applications is challenging due to a multitude of reasons.

Each spectrum exhibits heterogenous peak compositions due to the molecular composition on the wound surface being varied. Therefore, PCA was applied to the wound data to identify major trends in the SERS spectra. The information content of each spectrum is described by a limited number of variables, known as principal components (PCs). Looking at the wound data for patient one, the data can be satisfactorily described by 4 components. The first two PCs account for nearly 92% of variance in the data, demonstrating that most of the variance in the data can be explained by only two PCs. 96% of the variance is described by the first two PCs for patient 2, with very similar weightings of the PCs to patient 1. This means that a good approximation of the variance present

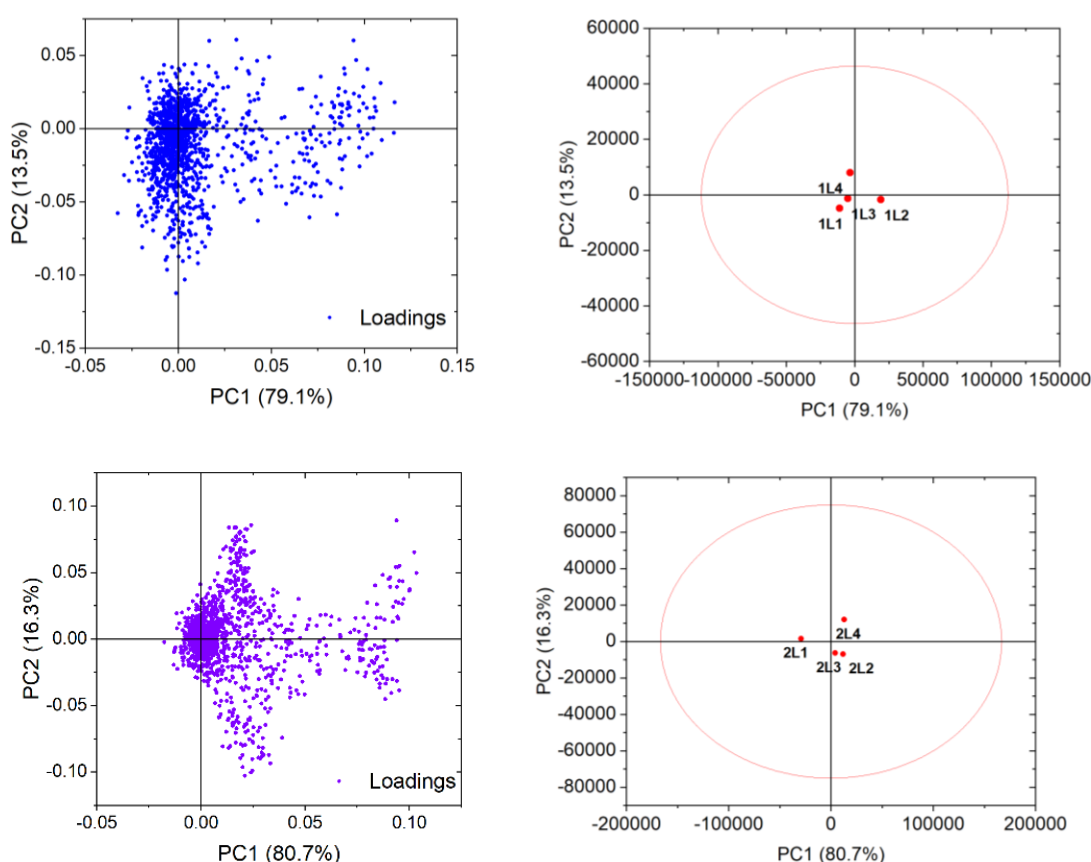


Figure 109 (Left) Loading plot and (right) Score plot with a 95% confidence ellipses for (top) patient 1 and (bottom) patient 2.

in the original spectral data is provided by only 2 PCs for both patients, and the PCA scatter plots are presented in Figure 109. These graphs agree that there is little differentiation in the SERS spectra of the wound samples regardless of the patient. Score plots are useful in assessing the data structure and detecting clusters, outliers and trends. The loadings for each patient are different and the PCs demonstrate that there is a larger variation in the data for patient 2. Patient 1 shows a greater contribution in the x-direction, yet the absolute values are close to 0 indicating the variable has a weak influence on the component. However, the values are greater than for PC2 implying there is a stronger correlation of the data with PC1. Each loading here represents the Raman shift of the wavenumber in the range 400-1800 cm^{-1} . The main discriminant appears to be PC1 for both patients. The sign indicates whether a variable and a PC are positively or negatively correlated. For patient 1, there is a positive correlation with PC1 and a general negative correlation with PC2. Nonetheless the loadings are quite spread out, making it difficult to distinguish clusters in the data with no clear outliers in the data. There is a larger distribution along the x-axis with a narrower distribution along the y-direction for PC2. This may allude to an overlap of the signals exhibiting a similarity in the spectra across the weeks which is consistent with the visual inspection of the SERS.

Patient 2 shows similar correlations with the PCs but there is a greater distribution along PC2 in both directions with a smaller cluster at the origin, yet the absolute value of the loadings remains small indicating that the variables do not have a strong effect on the PCs but there is a stronger correlation for PC2. The points do not spread out too far from the origin of the plot which agrees that the spectra for the patients across the 4 weeks are very similar to each other. The profile of the loadings is different from patient 1 hinting that there may be more defined clusters present. There might be a bigger differentiation between the SERS spectra over the four weeks which suggests a greater progression or regression in the wound status. PCA is unable to explicitly quantify the biochemical changes in the wound samples. This data could be improved by labelling the loading at each week to observe any clustering over time. However, PCA does not reveal physically or chemically interpretable

information of the sample but provides abstract information representing entire features broadly distributed in the data.

Alongside the loading plots are the score plots for each patient labelled with the week the sample was obtained. The score plots give a better idea of how the spectra affect each component. These points are close together indicating the similarities in the spectra. Graphically they are close to the origin demonstrating no significant differentiation in the spectra. Both sets of data fit into the 95% confidence ellipse.

Looking at the score plot for patient 1, the spectra for weeks 2 and 3 are more closely correlated with PC1 whereas the spectra for weeks 1 and 4 are more closely correlated with PC2. The variables contributing similar information are grouped together, meaning that they are correlated. The distance to the origin also conveys information. The spectra for week 4 are furthest from the origin so has the most distinguishable data from the others, which implies that there is the largest differentiation in the Raman signals which could indicate healing or non-healing in the wound. Also, 1L1 and 1L4 are positioned on opposite sides of the plot suggesting a negative correlation, which would mean that the signal intensity between these two spectra is inversely related so when the signals for week 1 increases, the signals for week 4 decreases which can also imply changes in the spectra concerning wound status.

The spectra for weeks 2 and 3 regarding patient 2 are close to the origin insinuating very little differentiation in the spectra, that is to say, not a lot of spectral change in this time frame. The spectrum for week 1 is closely correlated with PC1 whereas the spectrum for week 4 is more strongly correlated with PC2. This points to differentiation in the spectra from the 1st week to the 4th week which corroborates with the qualitative observation made of the spectra. There is a greater separation in weeks 1 and 4 spectra for patient 2 than patient 1, indicating a bigger differentiation in the spectra alluding to a more rapid healing or non-healing, the former which would agree with the photographic evidence of the wound when comparing the ratios of the wound size at the different time intervals. Nonetheless, it is important to note that solid conclusions cannot be drawn because of the limitations in the data. As

previously stated, 4 weeks is not long enough to attain sufficient patterns in the wound samples.

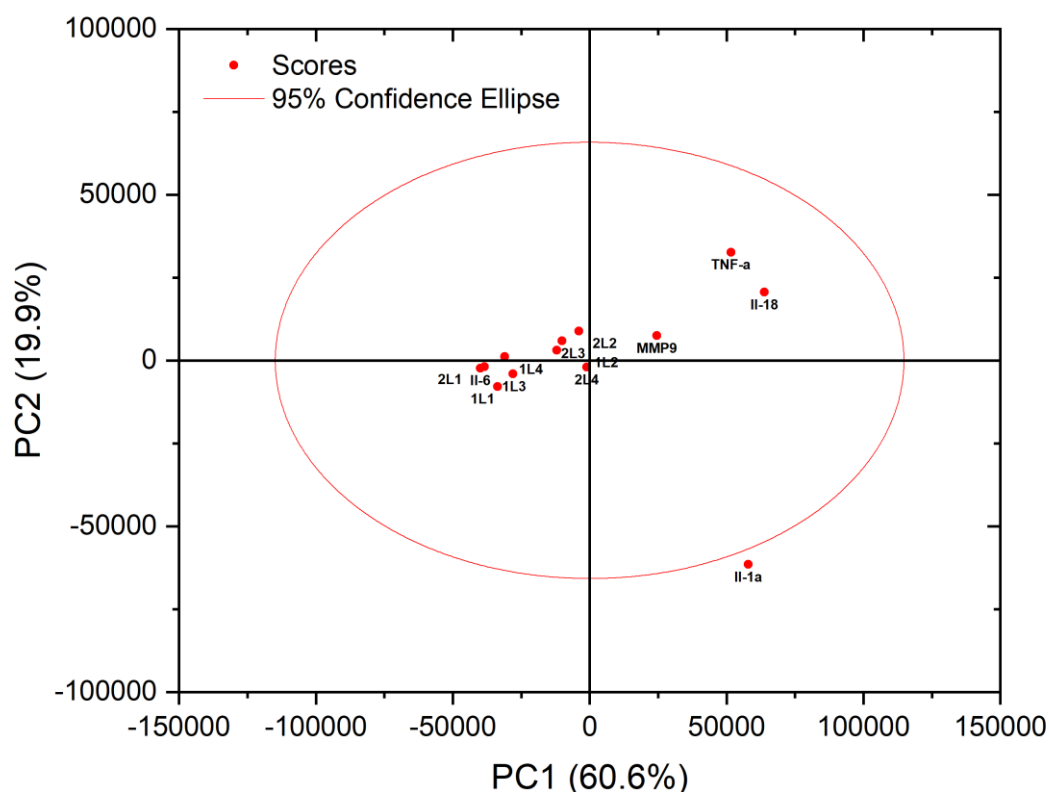


Figure 110 The score plot for the spectral data for both patients and the proteins with a 95% confidence ellipse.

An attempt to characterise both patients' wound samples and the SERS spectra of the proteins using PCA was made. The score plot in Figure 110 shows the results. Here, three PCs are needed to describe over 90% of the variation but the first 2 PCs are adequate to serve this purpose. The position of the scores show that the protein SERS spectra are more distinguishable than the wound samples. The distinction between the different spectra and patients supports the notion that SERS has the potential to be employed in differentiating healing and non-healing wounds based on the biochemical changes with reference to their biomarker values. The biggest contribution to the variation seems to come from IL-1 α followed by IL-18 and TNF- α which show correlations with both PCs. The proteins on the positive side of the score plot can be associated with having spectral features with high intensity in the

1200-1350 cm^{-1} range attributed to amide III stretching typical in proteins. The IL-1 α has the most unique, dissimilar spectrum with high intensity around 850 cm^{-1} attributed to the ring breathing vibration of tyrosine. This is on the other side of the plot highlighting the separation of IL-1 α to the other proteins and the wound samples. The patient data is grouped with IL-6 meaning that they are positively correlated demonstrating similarities in their spectra as well as proposing healing behaviour as higher levels of IL-6 aids wound healing. Patient 1 has more of an inverse relationship with MMP9, IL-18 and TNF- α , whereas patient 2 has more of an inverse relationship with IL-1 α . These are usually all raised in non-healing wounds so this correlation may suggest the wounds are healing. The ellipse in the data is used to determine outliers. It is to be expected that 95% of the data on average is within the ellipse, but IL-1 α falls outside of this. This indicates a discrepancy in the spectrum, but also the most discerning SERS out of all the measurements.

To understand this further, the loadings of PC1 and PC2 are presented in Figure 111. Examining these allows for an association to be made between the spectral features and the score plot trend. Spectral interpretations can be made but these are limited by the subtraction nature of the loadings. PC1 shows positive loadings with a higher absolute value where PC2 has both positive and negative loadings. The PCA loadings for PC1 include broad bands at 1549 cm^{-1} and 1607 cm^{-1} (amide III vibrations and the aromatic ring vibrations of Phe and Tyr), 1205 cm^{-1} (ring deformation of Tyr and Phe) and 880 cm^{-1} (bending ring vibration of tryptophan). These bands are all quite wide which indicate overlapping, but they are distinctive enough for approximate assignments. Scoring highly on a single component means that the original data is overwhelmingly explained by a single component. In this instance, most of the variation is explained by PC1 and there is largely positive correlations between the data. By comparing the original spectrum, the loadings largely resemble MMP9 indicating that these loadings are largely, positively associated with MMP9. The profile also shows similarity to IL-1 α and IL-18. The loadings for PC2 are positively associated with phenylalanine (1003 cm^{-1}), CH_2 and CH_3 bending vibrations (1342 cm^{-1}) and amide II vibrations (1549 cm^{-1}), and negatively associated with the ring deformation of Phe and Tyr (1205 cm^{-1}) and

amide I with α -helix conformation (1655 cm^{-1}). The negative loadings can be associated with the TNF- α spectrum where the positive loadings can be related to IL-6. These association observations suggest that these proteins are present in the wound samples, but the individual amino acids may be easier to classify. The loadings also reveal that there are slight changes in the data and that these Raman spectral features can be considered as markers of wound healing. To reiterate, the absence of a control group of patients makes the data more challenging to comprehend and so, only very general inferences are made.

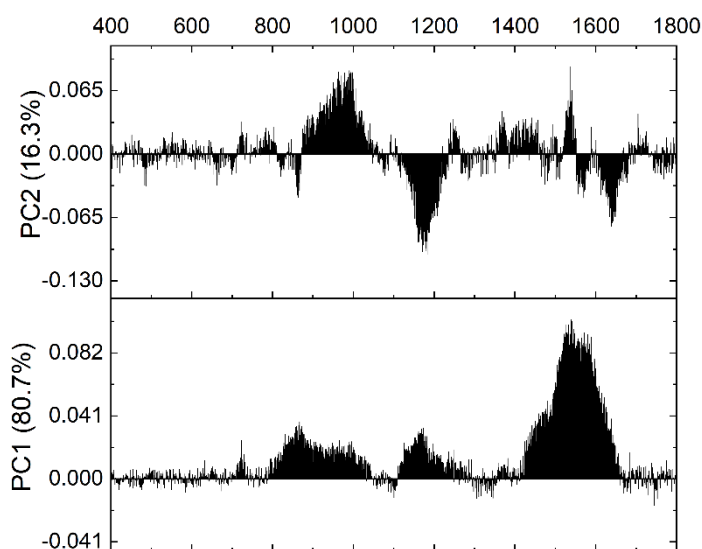


Figure 111 PC1 and PC2 loadings for the spectral data from both patients and proteins.

Summary

Overall, the aim of PCA is to uncover the identity of PCs and use them to explain the data as succinctly as possible. It has been found to be useful in a range of analytical techniques. It allows for the identification of maximal chemical information from the spectra even without prior knowledge of the chemical properties of the sample. The mathematical equations describing PCA are beyond the scope of this thesis. Many research groups have debated the PC loadings with the most common response being that PCs are not easily interpreted. There is a limit to the interpretability of PCs. Analytes that exhibit correlated behaviour will be overlapped in principal component space. Other tools that have been developed for the extraction of information and meaning from PCA can be adopted for a clearer explanation of the data.

4.4 Conclusions

While SERS remains a powerful analytical tool, the advances of its capabilities are contingent in the substrates used. The substrate determines the sensitivity, compatibility with the probed molecule, and the reproducibility of the measurement. The hydrogels demonstrate strong SERS efficacy as well as offering many benefits over traditional solution-based systems. Label-free SERS detection of large biological molecules, such as proteins and human samples at biologically relevant concentrations have been demonstrated. This work provides proof of concept of functional, easy to prepare, reproducible NPs and hydrogels as favourable SERS substrates. The proteins were prepared in serum albumin (BSA) to imitate actual biological condition. Further concentration studies can be conducted to consolidate the findings in this chapter.

Understanding the mechanisms that impair wound healing has led to potential predictive biomarkers with their role determined in the wound healing cascade of events. The SERS on the wound samples has shown the capability of monitoring the spectral changes over a time period. SERS provides an alternative to current analysis techniques by offering quick and easy detection as well as being non-destructive. By using PCA, loadings were produced that gave some indication of the trends in the data. However, the biggest drawback is the lack of data points to give more of a complete picture of the changes in the wound over time. A continuation of this study over a longer time frame will be helpful in validating the preliminary results obtained. The results are not conclusive as there is some disagreement with the SERS predictions and the photographic measurements and thus, employing another technique may be needed to provide more evidence for more confident evaluation of the outcomes.

SERS offers a convenient, non-invasive solution to conventional processes that could improve clinical decisions. Classic, established methods like ELISA and liquid chromatography mass spectrometry (LC-MS) have the capability to detect multiple biomarkers with high sensitivity and specificity, but these are not feasible for point of care (POC) analysis due to expense, both time and

financial. The substrates presented in this chapter are cost effective and sustainable which provides incentive to adopt the technology, having the potential to predict the healing status of wounds and monitor healing trajectory. The hydrogels have shown to produce decent enhancements for a rapid contact time with the analyte, in a swab manner. This is the first time, to the author's knowledge that such a study has been conducted and thus, the results presented in this chapter are novel and have the potential to add to the arsenal of much needed clinical decision-making tools.

Further multivariate statistical analysis can be employed to rigorously demonstrate the diagnostic ability of the approach. PCA can be favourable when the spectra of basic constituents of samples are unavailable. It has been reported to show excellent performance in classifying proteins, DNA and lipids. The detection of fine biochemical changes in spectra will help develop SERS to monitor wound healing. It is important to note that the interest lies with the spectral changes over time per patient and not the differences between the patients which may cause obscurity in the findings.

The data described in this chapter is very preliminary yet does offer proof-of-concept of applying PCA to wound samples. Collaboration with groups specialising in statistical analysis for Raman data will lead to clearer insight into the data. PCA is a well-suited method for spectral analysis because the individual channels of a spectrum are all inextricably linked by the underlying phenomena imposing a rich correlation across the signals. Modifying PCA with a supervised technique like partial least squares (PLS) can assist with overcoming the main disadvantage of PCA. As it is an unsupervised method, the resulting components do not necessarily reveal patterns that are directly related to classification. The directions of maximum variance in the data do not necessarily correspond to the directions of maximum class discrimination. PLS slightly improves this situation, but its performance depends on the number of components used in the subsequent analysis. This is the first time that PCA has been applied to the study of label-free SERS of wound effluent and with a longer time frame of sample collection and more sophisticated analytical methods, more profound and substantial conclusions can be reached.

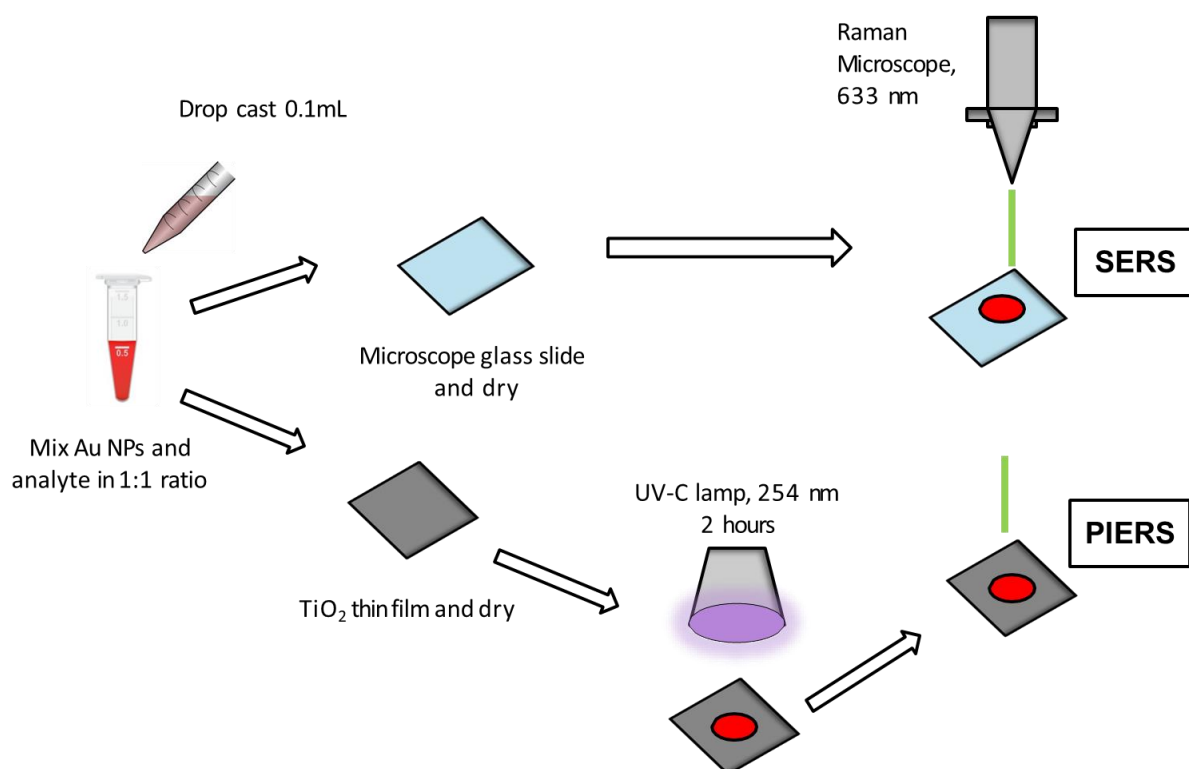
Future improvement for SERS substrates will likely involve more spatial control of hot spots. Incorporation of biocompatible interfaces can improve the native state retention making the SERS more accurate and reliable. Other label-mediated methods like ELISA can be used to cross-validate the SERS method and to provide validation to the results presented in this chapter. Creating substrates in which the metal surface can be modified to protect the protein structure from direct contact with the metal surface to minimise any undesirable affects is an area for future research. The hydrogels also offer multifunctionality, exemplified in Figure 112. They have the potential to be utilised as wound dressings for patients, which can double up as a sensor for the routine monitoring of wound biomarkers, offering a prospective opportunity to explore for future work.



Figure 112 Diagram showing how a hydrogel can be multi-functional. Reproduced with permission from reference [122].

Chapter Five

PIERS



Chapter V: PIERS

5.1 Introduction and aims

Whilst SERS has been extensively researched for over three decades, a new technology has evolved which provides additional Raman enhancement termed photo-induced enhanced Raman spectroscopy (PIERS). This exciting, novel process is still yet to be fully understood and so any research based on it can be critical in building fundamental knowledge of the PIERS effect. The PIERS technique introduces light irradiation, activating the substrate surface for operation. The magnification of the PIERS signal can be increased to over a dozen times over SERS. This improves the sensitivity which is of great importance in bioanalysis. Within the limited realms of PIERS research, little has been done to study the PIERS effect, if any, on biological molecules. Investigating PIERS as an additional sensing technology is appropriate and a natural extension to the work already carried out in this thesis by studying the enhancements for surfaces that show PIERS as complimentary to SERS for biomarker molecules.

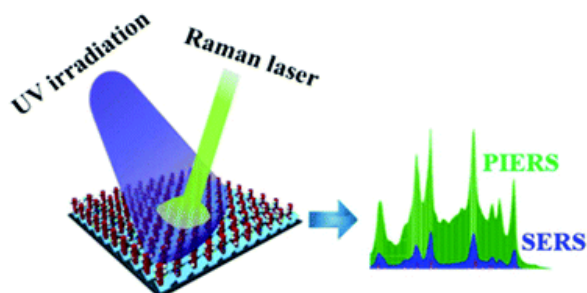


Figure 113 Diagram illustrating the PIERS effect. The addition of the UV irradiation improves the signals greatly over the SERS spectrum. Reproduced with permission from reference [164].

The photo excitation of TiO_2 has been reported to give rise to a strong Raman enhancement beyond the traditional SERS effect. Combining plasmonic nanoparticles with photo-activated substrates, the rapid and reliable development of PIERS sensors can be developed. Extensive investigations have demonstrated that additional Raman scattering enhancements arise from semiconductor hybrid nanostructures, in which charge transfer occurs efficiently

among them. The chemical enhancements mechanism is believed to contribute to the observed large enhancement signals in these cases. Additionally, surface plasmons on heterogeneous surfaces can induce hot electron migration among the semiconductor and metallic particles upon UV irradiation, resulting in simultaneous enhancement induced by multiple mechanisms^{164,251}. The PIERS effect is seen after UV light irradiation, with intensities of Raman signals reported to be ~3 times of that without irradiation.

A more detailed theory of PIERS has been discussed in chapter I. Briefly, mobile electrons can migrate from the conduction band of the TiO₂ to the plasmonic nanoparticle, where a charge transfer occurs from the metal to the adsorbed molecules. No effort has yet been made to map out the energy levels involved in establishing the mechanism, and in one study the most likely mechanism involves the increase of the intrinsic polarizability of an adsorbed molecule upon charge transfer¹⁵⁸. The exact mechanistic details are beyond the scope of this work.

PIERS is a time dependent phenomenon, with signals reducing to a normal SERS effect, attributed to the surface healing upon exposure of the photo-active substrate to air, and so it is of importance that the measurements are taken in a quick and consistent manner. For practical SERS detection, a recyclable SERS substrate is highly desirable as it reduces the cost and prevents additional contamination. Integrating the PIERS effect with a portable Raman instrument would make it fully possible to construct a tool for trace detection of organic analytes. Despite the recent progress in the PIERS field, this technique has not yet been widely applied to biomolecular detection. To date, there are only a few papers on the preparation of PIERS substrates and the practical detection applications.

In this chapter, PIERS and SERS is performed on different TiO₂ substrates as well as characterizing the TiO₂ synthesised with AACVD. Several analytes were chosen as probe molecules to determine the effectiveness of the PIERS technology and its suitability in different applications. The phases of TiO₂ as well as composite materials were looked at, and the wettability was investigated. There is a lack of literature illustrating the influence of the different

parameters of TiO₂ that may affect its SERS and PIERS capability. This study provides more insight into the considerable factors affecting the PIERS effect. Characterisation was only done to clarify certain properties of the thin films that related to SERS and PIERS. It is the first time that the PIERS effect is applied to research biomolecules.

5.2 Experimental

5.2.1 Reagents and Materials

All chemicals utilized for the synthesis of the thin films were used without any further treatment. Titanium (IV) ethoxide, reagent grade, 97% and toluene, HPLC grade, 99.8%, were purchased from Sigma Aldrich Ltd. Further details can be found below. Pilkington Activ™ glass was procured from Pilkington. Gold NPs were borrowed from collaborators in initial tests as well as using the ones reported in chapter II for more exhaustive experiments. These were all the same size, following similar seed-mediated growth methods. The gold NPs were kept consistent with each test run.

5.2.2 Synthesis

Chemical vapour deposition (CVD) was used to synthesise the titanium dioxide thin films. Titanium dioxide was the basis of the thin films, but composite and variations were also looked at. A range of films were researched. Any thin film material that exhibited photocatalytic properties could theoretically be used as a potential PIERS substrate.

APCVD

The TiO₂ thin films were prepared using APCVD (500, N₂ at 1L/min, 4 minutes) on Pilkington barrier glass. The exact protocol will not be shared here.

AACVD

Pilkington barrier glass was used as the substrate material and deposition was carried on the atmospheric side of the glass to prevent leaching of ionic

impurities from the glass. These were cleaned using tepol, isopropyl alcohol (IPA) and acetone and were fully oven dried prior to use. This process was repeated to ensure that all surface dirt was removed from the glass. A piece of metal was loaded into the reaction chamber suspended 8 mm above the glass to ensure laminar flow created by a baffle. The reagents were used as supplied. Titanium (IV) ethoxide was used as a titanium source. The precursor was dissolved in 20 mL of toluene in a 100 mL round bottom flask. The gas inlet allowed the carrier gas, nitrogen, to pass into the solution and transported the aerosol into the heated reactor at a rate of 1 L/min. The flow rate was controlled by a flow gauge. An ultrasonic humidifier was used to generate the aerosol. The experiments were carried out under atmospheric pressure²⁵².

5.2.3 Characterisation

X-ray diffraction (XRD)

Powder X-ray diffraction (XRD) patterns were recorded using a Bruker D8 Discover X-ray diffractometer using monochromatic Cu K α 1 and Cu K α 2 radiation of wavelengths 1.54056 and 1.54439 Å respectively, emitted in an intensity ratio of 2:1 with a voltage of 40 kV and a current of 40 mA. The incident beam angle was 1° and data was collected between 10° and 66° 2 θ with a step size of 0.05° at 1.0 s/step. The system was calibrated using a silicon reference.

Raman

A Renishaw 1000 spectrometer equipped with a 633 nm laser was used for Raman spectroscopy studies. The diameter of the light spot area was 1 μ m and the spectral resolution and the incident power were 1 cm⁻¹ and 9 mW respectively. The spectra were recorded with an accumulation time of 10 s. For PIERS measurements, the samples were irradiated by UV (254 nm) light for approx. 2 hours before immediately carrying out Raman measurements.

All chemical solutions were well mixed before SERS measurements were carried out. This was either done by magnetically stirring or sonicating the sample followed by vortexing for 30 seconds.

SEM

SEM images were obtained from either a JEOL 6103 field emission gun (FEG) or JEOL JSM6700F scanning electron microscope, without any conductive coating on the sample.

XPS

X-ray photoelectron spectroscopy was conducted on a Thermo Scientific K-alpha spectrometer with monochromated Al K α radiation, a dual beam charge compensation system and constant pass energy of 50 eV (spot size 400 μ m). Survey scans were collected in the binding energy range 0–1200 eV. High-resolution peaks were used for the principal peaks of titanium, oxygen, silicone and fluorine depending on the sample. Data was calibrated against C1s (285.0 eV). Data was fitted using CASA XPS software.

Water contact angle

Water contact angles were measured using a FTA 1000 drop shape analyser. A volume of 5.00 μ L was dispensed at a dispense rate of 2 μ L/s. Images and videos were recorded using FTA_32 software. The samples were irradiated with 254 nm light for two hours prior to measurement.

Film thickness

Room temperature Hall Effect measurements were carried out on an Ecopia HMS-3000 using a current of 1 mA and 0.58 T magnetic field, utilising film thickness values obtained from a Filmetrics f20 spectral reflectance system in air against as as-supplied FTO standard.

5.3 Results and discussion

TiO₂ is an important material as it contributes to the chemical enhancement of regular SERS which provides up to 10² increase in the Raman scattering, when the molecules is adsorbed strongly on the surface of the metal, leading to changes in its polarizability. To induce SERS, the gold and analyte was drop

cast on the surface. The enhancement is known to depend strongly on the surface of the TiO_2 thin films. A typical SEM image is presented in Figure 114 of the AACVD TiO_2 thin film, which most of the PIERS experiments were conducted on. The back scatter image is also shown which displays the distribution of the gold NPs on the TiO_2 . The titanium dioxide has a homogenous structure with compact pyramidal and oval shapes particles densely packed with many grain boundaries. This increases the surface area increasing the number of gold NPs that can coat the surface, yielding a higher electromagnetic enhancement of the Raman signal.

The image shows that the gold NPs are randomly distributed over the surface of the TiO_2 thin film and therefore, the randomisation of Raman enhancement. Certain areas have a higher cluster of gold NPs but it is not uniform over the surface demonstrating the challenges for reproducible signals on PIERS substrates when employing the drop cast method. The inhomogeneous distribution of electromagnetic and chemical enhancement effects associated with the uncontrollable surface imperfections gives rise to several complexities in SERS. Even though increasing the volume of gold should, theoretically lead to a higher concentration of gold, there is no way of discerning the dissemination of gold NPs on the surface, and thus a heterogeneous electromagnetic energy distribution. The element of randomness is introduced in the position of the NPs on the surface. It is possible the particles will not be in ideal SERS arrangements resulting in areas where the analyte molecules are masked. The aggregated gold leads to a coupled EM effect leading to higher enhancements while isolated nanoparticles result in fewer hotspots. The best way to overcome this is to make sure to perform as many Raman runs over the sample and to average the result.

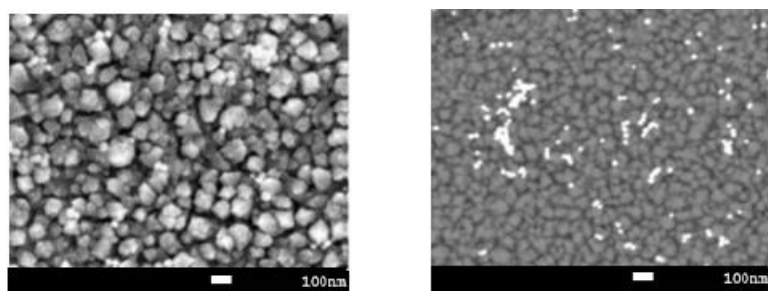


Figure 114 SEM images of (Left) TiO_2 surface and (right) backscatter to show the gold NP distribution on the surface of the TiO_2 thin film.

5.3.1 PIERS measurements

1 mM 4-mercaptobenzoic acid (4-MBA) was chosen as the initial target molecule due to its relatively simple Raman spectrum and low fluorescence quantum yield. It has several binding sites and adsorbs strongly to the gold through the S atom. For accurate and reliable comparison, the SERS measurements were carried out under the same conditions as PIERS but without the UV irradiation, Figure 115. The two distinct bands at 1595 and 1090 cm^{-1} are assigned to the characteristic aromatic ring vibrations, in good agreement with established literature²⁵³. By simple observation there is not a great increase in the intensity from the SERS and the PIERS. The 4-MBA molecules have high affinity towards the gold NPs and therefore show high SERS. The SERS on TiO_2 is similar to the SERS performed of 4-MBA on just a glass slide. The PIERS effect is not apparent in this instance, and this could be due to the time taken for the experiments to be completed. When performing several scans across the sample, even when trying to be as rapid as possible, the PIERS effect becomes reduced. This could lead to not observing any significant enhancement compared to the SERS. Some groups have also reported no enhancement over SERS, which could be ascribed to the position of the analyte molecule with respect to the metal-semiconductor interface, the distribution of AuNPs and the effective surface vacancy states within hotspot regions¹⁷⁰. Just as the chemical enhancement in SERS, the enhancement mechanisms of PIERS are still under debate¹⁷⁰. Several models have been put forward, but these depend on the specific system under study. Titanium dioxide

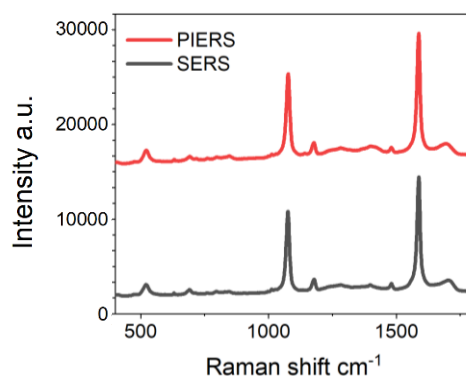


Figure 115 PIERS and SERS spectra of 1 mM 4-MBA on gold NPs. The background was removed and the baseline was offset for clarity.

is the most researched semiconductor for PIERS, so the creation of oxygen vacancies is relevant when explaining the phenomenon. Thus, like SERS both the CM and EM are produced at the same time for PIERS.

When comparing the actual values for the intensities the PIERS has a higher nominal intensity than the SERS, Table 9. The bands have not been enhanced equally; the 1090 cm^{-1} band has enhanced by 45% whereas the 1595 cm^{-1} band has only been enhanced by 15%. This, once again, emphasises that different vibrational modes are increased differently, owing to the surface selection rules dictated by the orientation of the molecule on the surface of the gold. The enhancement varies for different Raman bands and analyte molecules. Even for the same substrate, the Raman signal enhancement further depends on the surface facets and properties. These numbers do not illustrate a prominent improvement of the PIERS effect compared to the regular SERS but do show that there is a slight boost which can be attributed to the UV irradiation.

Peak position/ cm^{-1}	SERS intensity / a.u.	PIERS intensity a.u.
1595	46371	53744
1090	21256	30926

Table 9 Table showing the peak intensities of two significant 4-MBA peaks in their SERS and PIERS spectra.

5.3.2 Concentration studies

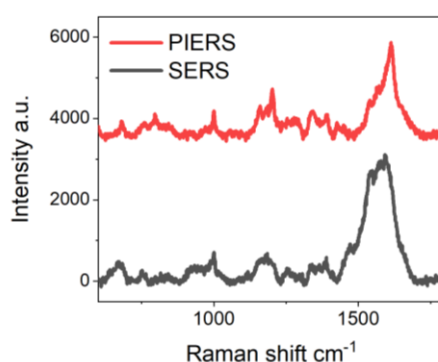


Figure 116 PIERS and SERS spectra of 1 mM glucose on gold NPs. The background was removed and the baseline was offset for clarity.

To expand the range of analytes, glucose (Gluc) was monitored at several concentrations comparing the SERS with PIERS. Diabetes requires frequent monitoring of blood glucose level, and so glucose presents a biomarker in terms of diagnosis, management and prediction of long-term vascular complications in the clinical care of diabetic patients²⁵⁴. There is an urgent requirement for the development of non-invasive sensing techniques for glucose, especially detection at low concentration. SERS based detection of glucose has been reported by various research groups. Glucose has a very small Raman cross section and a very low affinity with metal nanoparticles, therefore its detection using SERS is difficult, and often involves indirect methods. 1 mM of aqueous glucose was mixed in a 1:1 ratio of gold NPs and subsequently the SERS and PIERS (after UV irradiation) spectra were acquired.

The SERS and PIERS, shown in Figure 116, follow the same spectral profile which demonstrates that the peaks are from the analyte itself. The PIERS spectrum appears to be more resolved with more discernible bands identifiable. The normal Raman was collected from the powder form of glucose. As mentioned before, the vibrational frequencies and relative Raman cross sections of SERS spectra are generally different from those measured in neat samples. Therefore, additional bands may become observable in SERS while existing bands may be attenuated beyond the detection limit. The bands present at around 1000, 1158, and 1342 cm^{-1} are seen for both SERS and PIERS and are attributed to the COC stretching, the CO stretching and the CH_2 wagging of the glucose consistent with the standard Raman. The 900-1200 cm^{-1} is often referred to as the fingerprint region, dominated by exo and endo cyclic C-O and C-C stretches and has been reported that this region is difficult to interpret²⁵⁵. While the Raman spectrum of glucose is rich, there are certain Raman modes that are considered as the fingerprint signals of blood glucose. The ones that are present in the data obtained here are at 1365 and 1456 cm^{-1} although these have shifted slightly, which is common. Changes in the polarizability of molecule-metal complexes have been found to contribute to the frequency shifts. As both spectra were collected on TiO_2 , a metal substrate, known to influence the chemical enhancement mechanism of SERS, it is unsurprising that shifts of the vibrational modes are evident. The charge transfer

(CT) process has been shown to selectively increase non-totally symmetric intensities, which is a resonance Raman-like process. Factors controlling frequency shift are not limited to the solvent effect and the CT but involve the isotope effect and intermolecular interactions. The change in orientation of the glucose molecules can cause the shifting and disappearance of some Raman bands stressing the impact the substrate geometry has on the scattering processes²⁵⁶. With the addition of UV irradiation, there may be further CT resonance Raman enhancement due to the photo-assisted electron transfer from the substrate to the glucose molecules, but there is no evidence to assume this in this study. Further investigation of this phenomenon is required to understand the role that the TiO₂ (CM effects) might have on the resultant SERS and PIERS mechanisms. Nonetheless the presence of these peaks shows that 1 mM concentration of glucose can be detected by both SERS and PIERS. Like the 4-MBA, the enhancement from PIERS, although slightly higher than its SERS counterpart, is not above an order of magnitude greater.

Glucose is also known to have a poor affinity towards gold NPs so the ability of label-free SERS and PIERS is a positive outcome. Whilst the intensity of a certain peak cannot be used to determine the concentration, the presence of both SERS and PIERS bands, show that the TiO₂ thin film is a sensitive substrate for the use in these technologies. Due to the heightened intricacy of these spectra, compared with simple molecules with simple Raman spectra, it is difficult to determine the extent of the PIERS effect, and whether the UV irradiation can lead to a change in the surface selection rules. Prior reports into PIERS do not involve extending its use in the identification of more complex molecules, so this research is paving the way for additional exploration in this field. It may be that, whilst the TiO₂ thin film is photo-active, and the electrons transfer to the Fermi level of the AuNPs, the electron transfer from the AuNPs to the adsorbed glucose molecule may not be as available due to the low adsorption coefficient of the glucose onto the gold, and this step is what increases the intrinsic polarizability of the molecule giving rise to the PIERS enhancements.

5.3.3 Different TiO₂ thin films

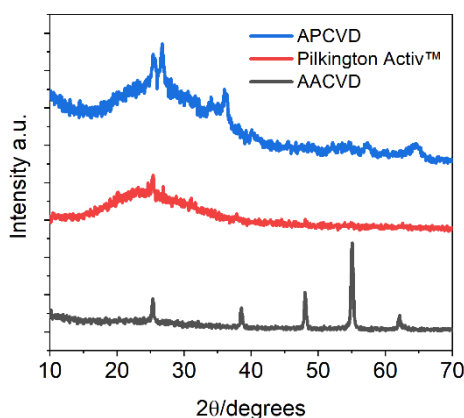


Figure 117 XRD patterns for the different TiO₂ thin films.

Several synthetic approaches exist to form TiO₂. In this study the focus was on thin films, primarily composed of anatase. Three different TiO₂ films were examined to observe how different parameters affect the character and properties of the TiO₂, which in turn may change the PIERS and SERS behaviour. AACVD and APCVD synthesised TiO₂ thin films and Pilkington Active™, a commercially available self-cleaning glass were used in this study. Pilkington Activ™ uses a microscopic coating of TiO₂ for dual action in self-cleaning.

XRD was used to determine the phase(s) of TiO₂ and confirmed the majority phase of TiO₂ in all the sample to be anatase - the kinetic product to be expected at the reaction temperature of synthesis. The sharp peak at $2\theta = 23$, corresponds to the $\{1\ 0\ 1\}$ facet indicating the presence of anatase. The TiO₂ thin film formed by AACVD showed the $\{2\ 0\ 0\}$ and $\{2\ 0\ 1\}$ planes but the higher intensity of the $2\theta = 55$ shows a change in preferential orientation of the phase²⁵⁷. The AACVD has the most prominent anatase peaks with the least amount of noise. Anatase TiO₂ thin films have shown to be good photocatalysts, superiors than their rutile phase counterparts. This has been attributed to anatase having a higher surface adsorption capacity to hydroxyl groups and a lower charge recombination rate to rutile. The Pilkington Activ™ also showed a very low intensity peak at $2\theta = 23$ and 38 showing that albeit a very thin layer, the TiO₂ on the Activ™ glass is anatase. The intensity from XRD patterns is

indicative of the film thickness as well as the crystallinity of the sample. The XRD gives an idea about the bulk material and thus, an amorphous pattern is expected for very thin films on glass substrates.

The largest enhancement reported for PIERS has been AuNPs on rutile, with hybrid heterostructures of rutile/anatase showing amplified Raman signals¹⁷⁰. There have not been many studies focused on anatase, and those that have, have been of hybrid structures. The different phases possess a different refractive index, surface energy, band structure, and other properties, making them react differently under UV irradiation.

The thin film made from APCVD showed anatase peaks but the occurrence of additional bands reveal that it is not purely titanium dioxide. It is hard to determine from the XRD alone what the other component may be, but the presence of 2 θ peaks at 26 and 34 alludes to tin oxide²⁵⁸. Tin oxide is an attractive metal oxide because of its unique optical and electrical properties making it an excellent material in several applications as well as creating multifunctional thin films. It is a n-type semiconductor with a rutile structure. The XRD pattern suggests a tin doped titanium dioxide composite thin film. The slightly noisy diffractogram agrees with literature where films containing SnO₂ nanoparticles are less crystalline than pure titanium dioxide films. TiO₂ doped with Sn have been reported to shows considerable photocatalytic activity under visible light irradiation and therefore should be a good PIERS substrate.

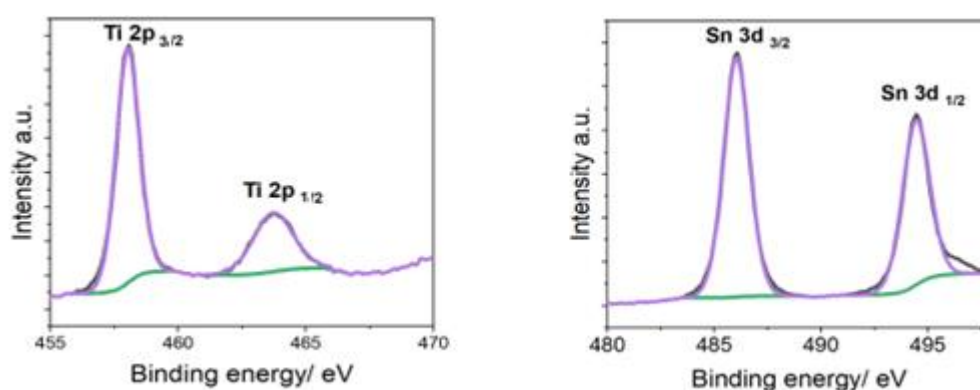


Figure 118 XPS data for (Left) Ti 2p, typical for all films and (right) Sn 3d found in the APCVD film.

To assess the surface composition of the TiO₂ thin films, XPS was performed on all the samples. A Shirley background was used to correct for inelastic losses and the line has been fitted using two almost pure Gaussian peaks. Ti,

O and Si were found as expected in all three samples. They all displayed similarities in their spectra verifying that TiO_2 was present in the samples. The presence of Sn was confirmed in the APCVD thin film. The binding energy for both components at 486.6 eV indicated the presence of SnO or SnO_2 since their binding energies are similar and is in agreement with published data for SnO_2 thin films²⁵⁹. This suggests that the oxidation of tin in the TiO_2 thin film can be either Sn^{4+} or Sn^{2+} , but other researchers looking into tin doped TiO_2 thin films have found the tin to be the same oxidation state as the Ti. It is important to note that not all the titania thin films are pure TiO_2 and the addition of tin may have interesting effects on the PIERS behaviour although it is not the focus of this work.

Film thickness

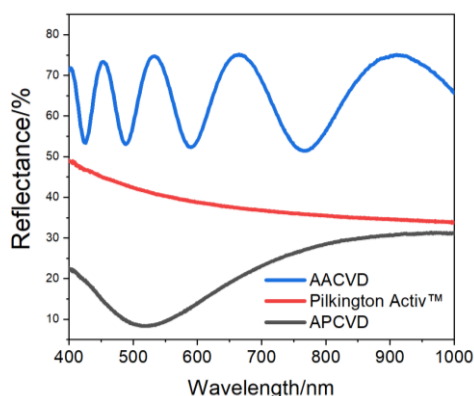


Figure 119 Hall effect measurements on the different titania thin films.

AACVD	446 nm
APCVD	140 nm
Pilkington	24 nm
Activ™	

Table 10 Table showing the average calculated film thickness of the different films.

The film thickness was quantified using the Hall effect measurements with the data displayed in Figure 119 and Table 10. The electrical properties determined by the Hall effect are dependent on the film composition and thickness. The values obtained are rough approximations and the thickness of the metal film can vary across the glass which can be visually deduced by the naked eye. The film thickness does correlate with the XRD pattern observed. The nominal value is not significant here, but rather the respective order of thickness with Pilkington Activ™ expected to have the thinnest coating. The film thickness has been reported to increase with synthesis temperature. AACVD is similar to APCVD but uses an aerosol to transport the precursors. Growth rates are often much lower than in APCVD, and the carrier solvent becomes involved in the chemistry. The reaction time also affects the final film with the deposition in the

APCVD process occurring much faster, usually no longer than a few seconds, compared with AACVD which is deposited over a long time and thereby able to produce a thicker layer of film. The increase of film thickness has shown to increase the amount of mass matter, increasing the adsorption process in photocatalysis verified by several studies, one claiming that the anatase films reach a higher photocatalytic activity for thick films²⁶⁰. A link between film thickness and its effective photocatalysis with its PIERS ability has yet to be established.

PIERS measurements

The PIERS effect was studied with a range of biological molecules as analytes. The experimental conditions were kept as consistent as possible. 1 mM glucose was tested, and the results are shown in Figure 120. The PIERS spectra appear to have a low SNR with some distinguishable glucose bands in the AACVD and Pilkington Activ™ films. The bands present at 1000, 1363 and 1449 cm^{-1} are all attributed to the glucose. Discussions on glucose have already been presented in this chapter, but to supplement that, the type of TiO_2 can significantly change the resulting spectra obtained. Interestingly, there is no evidence on the Raman spectra of the TiO_2 itself, and the noisy spectrum appears this way due to the baseline correction. No clear signals could be detected on the film prepared by APCVD. As PIERS relies heavily on the charge-transfer (CT) process, the analyte being probed is of significance. The UV light induces electron transfer from the TiO_2 to the AuNPs to amplify the Raman scattering. The photogenerated electrons on the gold NP surface provides additional CT from the gold to the detected molecules, leading to a larger enhancement. The glucose here is adsorbed on the gold NPs which should enable the SERS enhancement from both of its contributing mechanisms, however, it is known that glucose does not attach well to gold, and this could seriously hinder its successful detection in both SERS and PIERS cases.

1 mM tryptophan was also investigated with clearer results. All three of the substrates showed tryptophan bands at 759, 1019, 1354 and 1560 cm^{-1} assigned to the indole ring bend, Ph ring breathing, CH_2 wag and C-C stretching vibration modes of the molecule. All three spectra follow the same profile confirming that the signals do come from the target and are consistent with the SERS results of tryptophan reported by many other research groups. The intensities seem to correlate with the thickness of the films with the TiO_2 thin film prepared via the AACVD route exhibiting the highest PIERS. The AACVD thin film show the highest intensities for the different analytes. The intensity, however, is not significantly greater for any of the films for multiple analytes. This emphasises the sensitive nature of PIERS and the multiple parameters that effect the result. This challenges its power to function as a practical alternative to SERS.

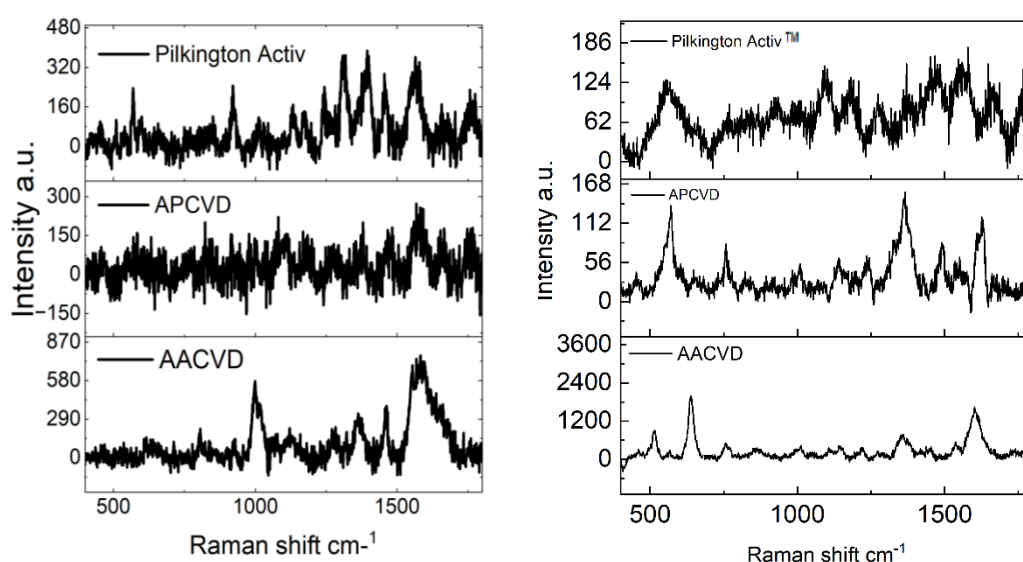


Figure 120 The PIERS spectra of 1 mM glucose (left) and tryptophan (right) on different TiO_2 thin films.

Presumably, the film thickness and increased PIERS activity may be due to the superior photocatalytic activity of the film, but the commercially available Pilkington ActivTM is an established photocatalyst with several studies proving its self-cleaning functions²⁶¹. However, research groups have synthesised TiO_2 materials exhibiting greater photocatalysis properties than Pilkington ActivTM²⁶². As photocatalytic studies were not conducted in this work it is difficult to assert a direct link between photocatalytic capability and PIERS behaviour. The detection of tryptophan on the TiO_2 -based substrates confirms that the

interaction between the gold and the tryptophan is much stronger than the gold with the glucose. With citrate-reduced gold NPs, tryptophan molecules mainly adsorb via the protonated amine group while maintaining a perpendicular geometry of the indole ring to the surface. Thus, it is important to note that PIERS is only a useful technology if the requirements of a good SERS result are being met for example, NP-analyte interactions. However, this is the first time that PIERS technique has been applied to biomolecules with a degree of success proving its potential for this application.

Wettability

Another factor to examine is the wettability of the thin films, before and after UV irradiation. All the thin films were slightly hydrophilic in their natural state, in other words, the water droplet spreads on the surface. Upon UV irradiation a greater decrease in contact angle was observed, with the thin films becoming near to super-hydrophilic. Pilkington Activ™ showed the lowest water contact angle post-UV, with the APCVD and AACVD synthesised films not too far behind. The wettability is important when considering SERS and PIERS as the distribution of the gold and analyte on the sample is determined by the deposition technique. As the drop-cast method was employed in this work, to keep it consistent throughout the entire study, the way the water spreads on the TiO₂ surfaces can affect the consequential Raman spectra acquired. As both the gold NPs and the biomolecules were dissolved in water, the water contact angle measurement is a good extrapolation of the sample performance, and these can be seen in Figure 121.

The images show that while the contact angle is low and the surface is hydrophilic, the droplet is not centrosymmetric and forms a non-spherical shape on the surface, a unique feature that is unanticipated for TiO₂. This makes the exact angle harder to estimate, but also the delivery of the sample drop is not symmetrical on the TiO₂ surfaces referring to differences in the surface tension of the thin films. The inhomogeneity of the thin films can alter the free surface energy at the solid surface. Non-uniformity of thin films was assumed in the TiO₂ produced through AACVD and APCVD. From the XRD and XPS it was established that the APCVD film was doped with tin, and this may play a role in

the shape of the droplet. However, the Pilkington Activ™ glass is not expected to display this behaviour as the coating of TiO₂ is constant throughout. Ostensibly, this impacts the drying process, and results in non-uniform evaporation. The ‘coffee-ring’ phenomenon will not be active here and may mean that it has been reversed with the molecule deposition at the droplet centre rather than the edge²⁶³. This would affect the positions of the hot spots on the surface sample making it difficult to estimate the locations, leading to greater variation in the PIERS data. Furthermore, the UV lamp produces a substantial amount of heat, and it could be possible that the films’ surface changed characteristics upon an increase in surface temperature. Marangoni instabilities can occur when a liquid interface is subjected to a temperature gradient. The Marangoni concentration mechanism occurs when heat and mass begin to flow due to temperature and/or composition gradients. A small temperature difference between the atmosphere and the substrate can prevent a liquid from wetting the surface²⁶⁴. Impurities in the film can alter the wetting patterns of the water. This behaviour is quite complex and will not be deliberated in any more detail in this work but elicits interesting scientific questions regarding the wetting properties of the thin films.

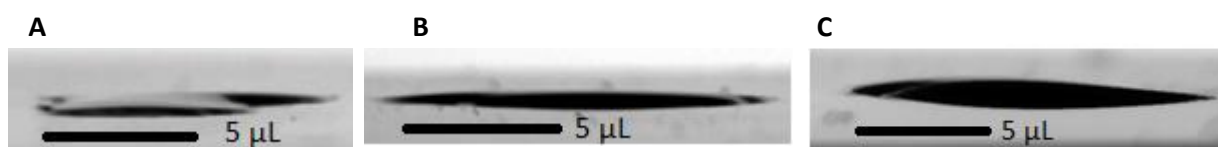


Figure 121 Water contact angle images for A) Pilkington Activ™ B) APCVD and C) AACVD TiO₂ thin films displaying the non-centrosymmetric droplets on the surface.

There may be a correlation with film thickness but that would have to be determined by further research. From the images, the AACVD synthesised TiO₂ film shows the most amount of symmetry in the water droplet and may be why it displayed the highest PIERS outcome, and Pilkington Activ™ with the least symmetric droplet. This effect may be the reason why the PIERS signals were not enhanced as much as they could have been. Other studies regarding the droplet and drying process have found that there is a significant difference with the middle and edge of the droplet, but practically only microscopic regions of the droplet were measured, so the droplet shape itself may have little effect. This certainly provokes further research into this area.

The PIERS was compared to the SERS for 1 mM arginine (Arg), another small biological molecule on the AACVD thin film. The PIERS spectral profile, Figure 122, matches well with the ordinary Raman of the powder from 1200-1500 cm^{-1} . The SERS shows a small intensity band at 918 cm^{-1} that can be ascribed to Arg. The PIERS and SERS still show similar enhancements of signals but when looking at the intensity values for the 1317 cm^{-1} band attributed to the COO^- symmetrical stretch, the PIERS enhancement is 7 times greater than the SERS. There is inhomogeneity in the enhancements between the different peaks in the spectra when comparing both. However, just because the intensity of the peaks is greater does not mean it yields better data. The information provided in the SERS gives more spectral evidence related to the Arg molecule. The reason for not quantifying this as an enhancement factor (EF) value is the ordinary Raman for these biomolecules in this concentration cannot be collected, and therefore accurate predictions for the EF cannot be made. The spectra result may be different than the Raman of the bulk material. While similar peaks can be present in both, significant differences, including peaks at different height, shape, peak shifting, and new peaks may be observed. This is evident in the spectra gathered from 1 mM Alanine (Ala). The PIERS spectrum has many more features with distinct bands compared to the SERS. The different spectral profiles for the two analytes demonstrate the sensitivity of the substrates, being able to detect unique fingerprint signals from the analytes directly.

L-Alanine has three different ionic forms depending on the pH of the solution and the negatively charged citrate-capped gold NPs will interact with the analyte to maximise the coulomb interfaces. The bands at 923, 1113 and 1464 cm^{-1} are all observed assigned the C-N stretch, C-C asymmetric bend and C-C asymmetric rocking vibrations of the alanine molecule. The PIERS intensities approximately double the enhancement of the SERS. This examination may be molecule specific as some peaks are enhanced due to the way the molecules lie on the surface. The locally induced defect may change the orientation of the molecule due to the defect's charge, thereby affecting some vibrations over others. Therefore, only specific peaks for each molecule are used for measurements and comparisons. Thus, whilst the PIERS is not living up to its scientific promotion, it still is proving to have an edge over traditional SERS,

despite the considerations already mentioned in this chapter. Label free PIERS has not been conducted on these materials to the author's knowledge highlighting the novelty of this approach to this application. Nonetheless, PIERS itself often results from complex vibronically coupled systems which have yet to be fully explained.

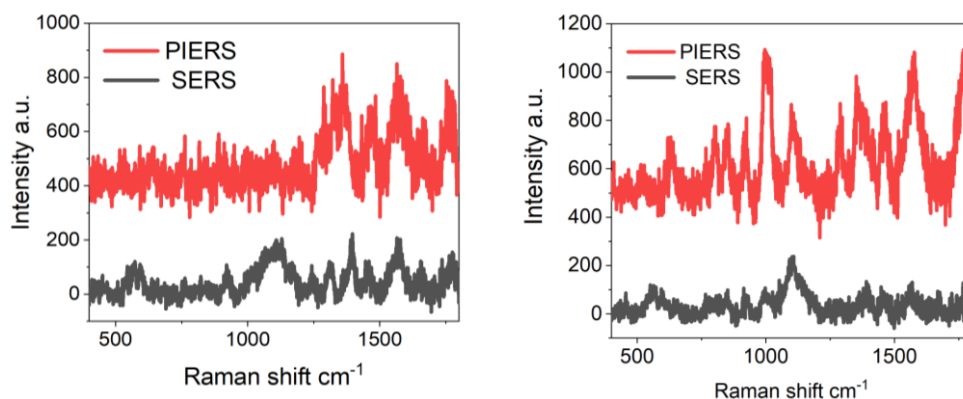


Figure 122 (Left) PIERS and SERS spectra of 1 mM Arg on gold NPs and AACVD TiO₂ thin film and (right) the same set of spectra for 1 mM Ala. The background was removed and the baselines was offset for clarity.

5.4 Considerations

The Raman intensity initially increases with irradiation time, reaching a maximum value at 24 minutes. In this study, the films were irradiated for a minimum of 2 hours, and this may explain why the enhancements were not fully realised. In addition, the relaxation time after the removal of the UV has been recorded to be about 30-40 mins where the Raman intensity returned to their original level²⁶⁵. These times may also be different with AuNPs on anatase as these have not been reported before. The relaxation time for AuNPs on rutile is about 15 minutes in another paper, and so this time constraint may greatly hinder the ability to acquire sufficient PIERS data. The relaxation time is related to the composition and characteristics of the thin film and is not easily defined, as it is influenced by the light intensity, the irradiation time, the irradiation sequence, analyte molecule and environment²⁶⁶. Hence, all these parameters need to be considered when looking at PIERS.

Numerous works to date have largely focused on silver nanoparticles decorated on TiO₂ thin films which have yielded the strongest PIERS results, with very

little investigations on other plasmonic nanomaterials. Gold NPs were used in this study, and this may impact the spectra collected. The way the TiO_2 interacts with gold and silver nanoparticles may differ. In both AgNP and AuNP cases, the injected charges will shift the Fermi level of the nanoparticle to more negative potentials and it has been reported that the exact value of the new Fermi level is dependent on the size of the nanoparticle. With PIERS, the 'system' itself plays a big role so the semiconductor substrate and choice of NPs are important as the energy levels in regard to the analyte of interest may be more, or less aligned (vis-à-vis the HOMO and the LUMO of the metal semiconductor and the analyte).

Many studies have concluded that most of the physical and photocatalytic properties of thin films depend enormously on the preparation technique. Whilst strong conclusions cannot be drawn, it can be said that AACVD may be the best synthetic route to produce PIERS-active substrates. Several advantages over APCVD have already been established such as its reliance on soluble precursors over volatile ones, varying the solvent leading to a control in the morphology and is relatively inexpensive. There have been reports linking photocatalytic activity with PIERS EF, where a strong correlation was concluded between the atomic oxygen vacancy lifetimes and the photocatalytic activity. The band gap may also affect the PIERS activity of the thin films but the influence of the band gap on the photocatalytic activity is not clear. The APCVD film which shows signs of tin doping, would have a narrower band gap than only TiO_2 , being active under visible light, where it is possible that higher activity is induced via visible light irradiation instead of UV light irradiation.

5.5 Conclusions

The results presented in this chapter are difficult to interpret as several factors can influence the PIERS behaviour of the substrates. However, this current work does demonstrate that PIERS could be a useful tool for the identification of small biomolecules, but there is a need for optimisation to realise its full potential. PIERS has shown some enhancement for several different small molecules, both biological and non-biological. The photo-degradation free enhanced Raman signals with its biocompatibility could lead to a wide range of

applications in the biosciences. The limit of detection of nanomolar concentration was reached in the study of glucose. Different TiO₂ thin films were looked at with anatase prepared by AACVD demonstrating the best PIERS effects. As PIERS is a surface specific technique, film thickness may not play a significant role but there is a lack of literature on this, so even though it may not be a dominant effect it may still be involved in the final PIERS results. As all the films contained the anatase phase, this could be indicative that the phase plays an important role in PIERS as significantly lower enhancements have been observed for anatase compared with rutile. Generally, the PIERS result was greater than the SERS outcome, agreeing that UV irradiation adds an additional enhancement mechanism.

The different measurements show that PIERS is analyte dependent which is due to the difference in coupling between the molecules HOMO/LUMO and the Fermi level of the nanoparticle, the band gap of the semiconductor, the type of defect produced and the energy band for the defect. This suggests that the choice of molecule may alter the PIERS behaviour of the substrate. However, there have been reports that although different molecules have different PIERS enhancements the PIERS effect itself is not affected by the type of molecule. In theory, any Raman active molecule should be able to show a PIERS effect. The results in this chapter support this statement as the PIERS function was present in all measurements at varying capacity specifically, the spectra were different to the SERS.

Future work will address the discrepancies found in this study and help advance research into areas that were initiated here such as film thickness, wetting behaviour and different synthetic routes. The PIERS technique is still in its early stages and much effort is needed to investigate the influence of UV irradiation on the Raman scattering from these materials accounting for differences in morphology, crystalline phase, crystal size and composition. This is the first time PIERS has been extensively applied to biological molecules, and with additional work, there is a possibility that PIERS could be potentially adopted in a clinical setting.

Chapter Six

Conclusions and Future Work



Chapter VI: Conclusions and Future Work

The work described in this thesis has demonstrated the synthesis, characterisation and functional testing of SERS and PIERS substrates. All the measurements were conducted without the use of external labels, probing the analyte directly to give a unique Raman fingerprint. Novel materials were produced that offer great enhancement despite challenges in the approach which hindered quantification of the data. A vast range of biomarkers were studied to provide proof-of-concept of the versatility of the substrates. The ability to detect multiple analytes was mildly successful and a protocol for reproducible synthesis was established for the most efficient substrates. Whilst the conclusions are not as strong, the novelty of the research should be emphasised. The lack of literature makes it more difficult to prove or disprove certain findings, but most of the data supports the themes in this work as proof-of-concept.

The development of flexible hydrogels followed an easy to use, low-cost and sustainable method making it appealing for the application in biomedical fields for POC analysis. However, this can be extended to look at other pertinent industries where identification of target molecules is required.

The hypotheses that this thesis set out to address have been realised to some extent, and the preliminary results offer proof of concept for much of the novel work carried out, propelling further research into areas touched on in this thesis. The quantification of the SERS effect was not deemed relevant at this stage of experimentation since the focus was on the initial qualitative indications of positive detection of a host of biomolecules using label free SERS. This demonstrates the functional nature of the materials, both the colloidal gold and the flexible substrates, fabricated in this study.

6.1 Results overview

6.1.1 Chapter II

Different gold nanoparticles were synthesised employing a seed mediated growth method. Several shapes and sizes were investigated as well as capping agents to determine the most efficient gold NPs for SERS. Citrate-capped gold nanoparticles exhibited strong SERS as well as stability and duplex capabilities. Modification of the gold NPs using self-assembled monolayers (SAMs) was investigated to improve the affinity of the gold to the biological molecules. However, strong solvent effects were observed in the SERS masking any analyte signals. Therefore, the modification did not help with increasing the intensity of SERS and bare gold NPs were reported to be the optimal colloidal substrates for further testing. Several biomarkers of biological status were successfully identified with the gold NPs within a mM concentration. For some of these biomarkers, this was the first time a label-free SERS approach was exploited for their detection.

6.1.2 Chapter III

Flexible substrate materials were investigated for their SERS functionality as well as appropriateness for adoption in the biomedical field as sensor materials. Filter paper and PDMS exhibited some SERS enhancements, but bands from the materials itself dominated the spectra making interpretation of the data difficult. Several gelatine-based hydrogels were fabricated with a variety of polymers to increase the mechanical strength. PVA/gelatine hydrogel blend incorporated with gold NPs made in chapter III was reported to be the most suitable substrate due to its transparency, adhesive properties, mechanical strength and SERS performance. Citric acid was determined to be an effective 'green' cross-linker adding to the desirable qualities of the hydrogel. Functional testing showed SERS response from a range of biomarkers and even duplex testing. Methods for synthesis and data collection were recognised and improved as additional tests were carried out.

6.1.3 Chapter IV

Biologically relevant proteins were studied, and their label-free SERS was acquired. Concentration studies did not reveal a correlation between the amount of analyte and the intensity, but this could be attributed to the mechanisms involved in the formation of protein-NP complexes. Different bands were enhanced differently demonstrating the unpredictable nature of SERS, highlighting the challenges that come with it. However, enhancement factor calculations proved that low concentrations of the proteins could be detected using gold NPs. Studies were carried out using wound samples from real patients. Unique spectra were obtained proving the sensitivity and specificity of the substrates. Minor changes in the spectra could be attributed to changes in the biomarker but these were unclear. Quantification of the results remains a challenge, but initial findings establish some trends correlating biomarkers with wound healing. PCA was applied to ascertain a better understanding of the data and some patterns were identified and justified. The loadings look convincing and with more data, greater adequacy in the results can be achieved.

6.1.4 Chapter V

PIERS substrates were looked at for their ability to detect biomolecules. TiO_2 thin film produced by AACVD exhibited excellent PIERS outcomes with a limit of detection as low as nM range for glucose. Different TiO_2 thin films were investigated to assess the parameters that may influence the final PIERS result. This proof-of-concept study demonstrated that film thickness and crystallinity may affect the PIERS enhancement. The wetting behaviour also plays an important role in the distribution of the analyte droplet on the surface which was reflected in the PIERS data. Non-centrosymmetric droplets were observed which could lead to a reduced enhancement and important considerations were addressed. Whilst reaching convincing outcomes was difficult, thin films prepared by way of AACVD appeared to result in the best PIERS enhancement. PIERS of biomarkers were carried out and reproducible signals were generated with additional enhancement over the SERS, albeit not to an extent reported in existing literature.

6.2 Summary

Overall, this thesis demonstrates that reproducible, citrate capped gold nanoparticles synthesised via a seed mediated growth mechanism have a long shelf life, and excellent SERS functionality with a diverse detection range extending from biological macromolecules to simple dyes as well as expressing duplex capabilities. The integration of these plasmonic nanoparticles into flexible materials like hydrogels can render new properties making gelatine-based hydrogel blends SERS-active. These hydrogels offer mechanical stability, biocompatibility and are synthesised in a facile method using a green crosslinker. They exhibit SERS capabilities, detecting a range of molecules at different concentrations. Both the gold nanoparticles and the nanocomposite hydrogels can produce spectra from complex proteins and wound samples. Titanium dioxide thin films possess PIERS efficacy, but this thesis reveals many avenues for further research for a better understanding of the effect and the sensitivity of the system to minor changes in experimental conditions. PIERS can be employed to detect a range of biomolecules proving itself to be a complimentary tool to SERS for bioanalysis. The results in this thesis provide proof-of-concept to many novel experiments with initial findings reported to be encouraging in the label free SERS field for, but not limited to, biomedical applications.

6.3 Future areas of research

Based on the reproducible seed-mediated growth protocol for the synthesis of gold colloidal nano-spheres, further modifications for better substrate design can be made to fine tune the methodology. The effect of solvent on SERS can be studied to improve the understanding of the mechanistic details and the influence non-aqueous solvents have on the SERS performance, to expand its applicability outside of a laboratory.

The gelatine-based hydrogels offer a fantastic, flexible alternative to current, rigid substrates but further development to fully optimise the hydrogels for

maximum performance has yet to be realised. There is also potential for the gels to be used as both SERS-active materials and a wound dressing. Advance research into the mechanical properties as well as swelling behaviour should be looked at to assess the practicality of the hydrogels. Concentration studies will reveal the limit of detection and the true sensitivity of the hydrogels. A longer study using clinical samples is critical in evaluating the data obtained and acquiring trends that will help with the monitoring of biomarkers.

Complementary studies utilising established approaches like lateral flow devices (LFDs) and ELISA to provide corroborative data can be investigated, as well as combining the methods with SERS for a more reliable, accurate detection tool. The use of machine learning for the processing of complex spectra for more meaningful interpretation will help in providing more conclusive results, Figure 123. Sample pre-treatment may help significantly improve the accuracy of quantitative analysis. This will help diminish the detrimental interference of the non-specific adsorption of the complex matrix. This can be done by implementing statistical methods like PLS and linear discriminant analysis (LDA) alongside PCA to establish more definitive trends that can be applied to unknown sample. This would benefit from more data since, the more data acquired, the clearer the analysis. The SERS function of the hydrogels can be fostered for use in other areas for label-free detection such as warfare agents, environmental pollution and food health and safety.

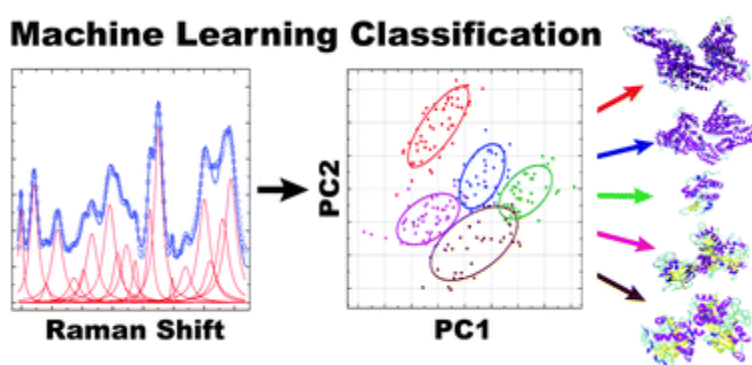


Figure 123 Diagram illustrating how Raman spectra can be converted to a plot used for the classification of complex molecules using PCA. Reproduced with permission from reference [155].

PIERS has shown to have higher intensity signals over SERS for some analytes. Probing additional molecules will help to give more insight into the feasibility of its implementation in several applications. As it is still quite novel

effect, many parameters for future work can be researched including, but not limited to, the phase structure, the wettability, the semiconductor, the effect of doping and the method of Raman acquisition. All this additional exploration will develop better understanding of the mechanisms and factors involved in the PIERS phenomenon. Furthermore, combining the PIERS technology with flexible materials is an area that has not been tapped into yet and may offer a new class of materials with great promise as sensitive substrates for different research communities.

References

- (1) Cialla-May, D.; Zheng, X. S.; Weber, K.; Popp, J. Recent Progress in Surface-Enhanced Raman Spectroscopy for Biological and Biomedical Applications: From Cells to Clinics. *Chemical Society Reviews*. Royal Society of Chemistry July 7, 2017, pp 3945–3961. <https://doi.org/10.1039/c7cs00172j>.
- (2) Jia, M.; Li, S.; Zang, L.; Lu, X.; Zhang, H. Analysis of Biomolecules Based on the Surface Enhanced Raman Spectroscopy. *Nanomaterials* **2018**, 8 (9), 730. <https://doi.org/10.3390/nano8090730>.
- (3) Sinha, G.; Depero, L. E.; Alessandri, I. Recyclable SERS Substrates Based on Au-Coated ZnO Nanorods. *ACS Appl. Mater. Interfaces* **2011**, 3 (7), 2557–2563. <https://doi.org/10.1021/am200396n>.
- (4) Lenzi, E.; Jimenez de Aberasturi, D.; Liz-Marza, L. M. Surface-Enhanced Raman Scattering Tags for Three-Dimensional Bioimaging and Biomarker Detection. **2019**. <https://doi.org/10.1021/acssensors.9b00321>.
- (5) Robson, M. C. Wound Infection: A Failure of Wound Healing Caused by an Imbalance of Bacteria. *Surg. Clin. North Am.* **1997**, 77 (3), 637–650. [https://doi.org/10.1016/S0039-6109\(05\)70572-7](https://doi.org/10.1016/S0039-6109(05)70572-7).
- (6) Dargaville, T. R.; Farrugia, B. L.; Broadbent, J. A.; Pace, S.; Upton, Z.; Voelcker, N. H. Sensors and Imaging for Wound Healing: A Review. *Biosensors and Bioelectronics*. 2013. <https://doi.org/10.1016/j.bios.2012.09.029>.
- (7) Thompson, N.; Gordey, L.; Bowles, H.; Parslow, N.; Houghton, P. Reliability and Validity of the Revised Photographic Wound Assessment Tool on Digital Images Taken of Various Types of Chronic Wounds. *Adv. Ski. Wound Care* **2013**, 26 (8), 360–373. <https://doi.org/10.1097/01.ASW.0000431329.50869.6F>.
- (8) Jia, M.; Li, S.; Zang, L.; Lu, X.; Zhang, H. Analysis of Biomolecules Based on the Surface Enhanced Raman Spectroscopy. *Nanomater. (Basel,*

- Switzerland) **2018**, 8 (9). <https://doi.org/10.3390/nano8090730>.
- (9) Das, R. S.; Agrawal, Y. K. Raman Spectroscopy: Recent Advancements, Techniques and Applications. *Vib. Spectrosc.* **2011**, 57, 163–176. <https://doi.org/10.1016/j.vibspec.2011.08.003>.
 - (10) Sackmann, M.; Materny, A. Surface Enhanced Raman Scattering (SERS)-a Quantitative Analytical Tool? †. *J. RAMAN Spectrosc. J. Raman Spectrosc* **2006**, 37, 305–310. <https://doi.org/10.1002/jrs.1443>.
 - (11) Holzinger, M.; Le Goff, A.; Cosnier, S. Nanomaterials for Biosensing Applications: A Review. *Front. Chem.* **2014**. <https://doi.org/10.3389/fchem.2014.00063>.
 - (12) (PDF) Development of Spectroscopic Methods for Dynamic Cellular Level Study of Biochemical Kinetics and Disease Progression. https://www.researchgate.net/publication/317093156_Development_of_Spectroscopic_Methods_for_Dynamic_Cellular_Level_Study_of_Biochemical_Kinetics_and_Disease_Progression (accessed 2022-06-17).
 - (13) E. C. Le Ru, *; E. Blackie; M. Meyer, and; Etchegoin†, P. G. Surface Enhanced Raman Scattering Enhancement Factors: A Comprehensive Study. **2007**. <https://doi.org/10.1021/JP0687908>.
 - (14) Mosier-Boss, P. A. Review of SERS Substrates for Chemical Sensing. *Nanomaterials* **2017**, 7 (6). <https://doi.org/10.3390/nano7060142>.
 - (15) Qian, X.-M.; Nie, S. M. Single-Molecule and Single-Nanoparticle SERS: From Fundamental Mechanisms to Biomedical Applications. <https://doi.org/10.1039/b708839f>.
 - (16) Dasary, S. S. R.; Singh, K.; Senapati, D.; Yu, H.; Ray, P. C. Gold Nanoparticle Based Label-Free SERS Probe for Ultrasensitive and Selective Detection of Trinitrotoluene. <https://doi.org/10.1021/ja905134d>.
 - (17) Bhachu, D. S.; Sathasivam, S.; Sankar, G.; Scanlon, D. O.; Cibilin, G.; Carmalt, C. J.; Parkin, I. P.; Watson, G. W.; Bawaked, S. M.; Obaid, A. Y.; Al-Thabaiti, S.; Basahel, S. N. Solution Processing Route to Multifunctional Titania Thin Films: Highly Conductive and Photocatalytically

Active Nb:TiO₂. *Adv. Funct. Mater.* **2014**.

<https://doi.org/10.1002/adfm.201400338>.

- (18) Stefan Kruszewski, S.; Kruszewski, S. Enhancement Mechanisms in the SERS Phenomenon. <https://doi.org/10.1117/12.301353> **1998**, 3320 (1), 281–293. <https://doi.org/10.1117/12.301353>.
- (19) Gersten, J.; Nitzan, A. Electromagnetic Theory of Enhanced Raman Scattering by Molecules Adsorbed on Rough Surfaces. *J. Chem. Phys.* **1980**, 73 (7), 3023–3037. <https://doi.org/10.1063/1.440560>.
- (20) Stiles, P. L.; Dieringer, J. A.; Shah, N. C.; Van Duyne, R. P. Surface-Enhanced Raman Spectroscopy. *Annu. Rev. Anal. Chem.* **2008**, 1 (1), 601–626. <https://doi.org/10.1146/annurev.anchem.1.031207.112814>.
- (21) Saikin, S. K.; Chu, Y.; Rappoport, D.; Crozier, K. B.; Aspuru-Guzik, A. *Separation of Electromagnetic and Chemical Contributions to Surface-Enhanced Raman Spectra on Nanoengineered Plasmonic Substrates*. <https://arxiv.org/pdf/1009.1673.pdf> (accessed 2019-06-03).
- (22) Zhang, L.; Zhao, Q.; Jiang, Z.; Shen, J.; Wu, W.; Liu, X.; Fan, Q.; Huang, W. Recent Progress of SERS Nanoprobe for PH Detecting and Its Application in Biological Imaging. *Biosens. 2021, Vol. 11, Page 282* **2021**, 11 (8), 282. <https://doi.org/10.3390/BIOS11080282>.
- (23) Ng, C.; Cadusch, J. J.; Dligatch, S.; Roberts, A.; Davis, T. J.; Mulvaney, P.; Gómez, D. E. Hot Carrier Extraction with Plasmonic Broadband Absorbers. *ACS Nano* **2016**, 10 (4), 4704–4711. <https://doi.org/10.1021/acsnano.6b01108>.
- (24) Pinkhasova, P.; Yang, L.; Zhang, Y.; Sukhishvili, S.; Du, H. Differential SERS Activity of Gold and Silver Nanostructures Enabled by Adsorbed Poly(Vinylpyrrolidone). **2012**, 28. <https://doi.org/10.1021/la2047992>.
- (25) Moskovits, M. *Surface-Enhanced Spectroscopy*; 1985. <https://journals.aps.org/rmp/pdf/10.1103/RevModPhys.57.783> (accessed 2019-06-03).
- (26) Kwee Lee, H.; Hong Lee, Y.; Sher Lin Koh, C.; Chuong Phan-Quang, G.;

- Han, X.; Leng Lay, C.; Howard Yi Fan Sim, ab; Kao, Y.-C.; An ac, Q.; Yi Ling, X. Designing Surface-Enhanced Raman Scattering (SERS) Platforms beyond Hotspot Engineering: Emerging Opportunities in Analyte Manipulations and Hybrid Materials. *Chem. Soc. Rev* **2019**, *48*, 731. <https://doi.org/10.1039/c7cs00786h>.
- (27) Ding, S.-Y.; You, E.-M.; Tian, Z.-Q.; Moskovits, M. Electromagnetic Theories of Surface-Enhanced Raman Spectroscopy. *This J. is Cite this Chem. Soc. Rev* **2017**, *46*, 4042. <https://doi.org/10.1039/c7cs00238f>.
- (28) Kleinman, S. L.; Frontiera, R. R.; Henry, A.-I.; Dieringer, J. A.; Van Duyne, R. P. Creating, Characterizing, and Controlling Chemistry with SERS Hot Spots. *Phys. Chem. Chem. Phys.* **2013**, *15* (1), 21–36. <https://doi.org/10.1039/C2CP42598J>.
- (29) Kumar, S.; Lodhi, D. K.; Goel, P.; Neeti; Mishra, P.; Singh, J. P. A Facile Method for Fabrication of Buckled PDMS Silver Nanorod Arrays as Active 3D SERS Cages for Bacterial Sensing. *Chem. Commun.* **2015**, *51* (62), 12411–12414. <https://doi.org/10.1039/c5cc03604f>.
- (30) Wang, K.; Li, S.; Petersen, M.; Wang, S.; Lu, X. Detection and Characterization of Antibiotic-Resistant Bacteria Using Surface-Enhanced Raman Spectroscopy. *Nanomaterials* **2018**, *8* (10). <https://doi.org/10.3390/NANO8100762>.
- (31) Satya Bharati Moram, S.; Byram, C.; Nanadath Shibu, S.; Madhuri Chilukamarri, B.; Rao Soma, V. Ag/Au Nanoparticle-Loaded Paper-Based Versatile Surface-Enhanced Raman Spectroscopy Substrates for Multiple Explosives Detection. **2018**, *3*, 8201. <https://doi.org/10.1021/acsomega.8b01318>.
- (32) Pérez-Jiménez, A. I.; Lyu, D.; Lu, Z.; Liu, G.; Ren, B. Surface-Enhanced Raman Spectroscopy: Benefits, Trade-Offs and Future Developments. *Chem. Sci.* **2020**, *11* (18), 4563–4577. <https://doi.org/10.1039/D0SC00809E>.
- (33) Page, K.; Palgrave, R. G.; Parkin, I. P.; Wilson, M.; Savin, S. L. P.; Chadwick, A. V. Titania and Silver–Titania Composite Films on Glass—

Potent Antimicrobial Coatings. *J. Mater. Chem.* **2007**.
<https://doi.org/10.1039/B611740F>.

- (34) Israelsen, N. D.; Hanson, C.; Vargis, E. Nanoparticle Properties and Synthesis Effects on Surface-Enhanced Raman Scattering Enhancement Factor: An Introduction. **2015**. <https://doi.org/10.1155/2015/124582>.
- (35) Kahl, M.; Voges, E.; Kostrewa, S.; Viets, C.; Hill, W. Periodically Structured Metallic Substrates for SERS. *Sensors Actuators B Chem.* **1998**, 51 (1–3), 285–291. [https://doi.org/10.1016/S0925-4005\(98\)00219-6](https://doi.org/10.1016/S0925-4005(98)00219-6).
- (36) Fisk, H.; Westley, C.; Turner, N. J.; Goodacre, R. Achieving Optimal SERS through Enhanced Experimental Design. *J. Raman Spectrosc.* **2016**, 47 (1), 59–66. <https://doi.org/10.1002/JRS.4855>.
- (37) Tian, F.; Bonnier, F.; Casey, A.; Shanahan, A. E.; Byrne, H. J. Surface Enhanced Raman Scattering with Gold Nanoparticles: Effect of Particle Shape. **2014**. <https://doi.org/10.1039/c4ay02112f>.
- (38) Schlücker, S.; Wiley InterScience (Online service). *Surface Enhanced Raman Spectroscopy: Analytical, Biophysical and Life Science Applications*; Wiley-VCH, 2011.
- (39) Haynes, C. L.; Mcfarland, A. D.; Van Duyne, R. P. *RAMAN SPECTROSCOPY*. <https://doi.org/10.1021/ac053456d>.
- (40) Tahghighi, M.; Janner, D.; Ignés-Mullol, J. Optimizing Gold Nanoparticle Size and Shape for the Fabrication of SERS Substrates by Means of the Langmuir-Blodgett Technique. <https://doi.org/10.3390/nano10112264>.
- (41) Farag, A. A. M.; Yahia, I. S. Structural, Absorption and Optical Dispersion Characteristics of Rhodamine B Thin Films Prepared by Drop Casting Technique. *Opt. Commun.* **2010**, 283 (21), 4310–4317.
<https://doi.org/10.1016/J.OPTCOM.2010.06.081>.
- (42) Wang, Y.; Gao, Z.; Han, Z.; Liu, Y.; Yang, H.; Akkin, T.; Hogan, C. J.; Bischof, J. C. Aggregation Affects Optical Properties and Photothermal Heating of Gold Nanospheres. *Sci. Reports* | **123AD**, 11, 898.

<https://doi.org/10.1038/s41598-020-79393-w>.

- (43) Rahman, M. R.; Saleh, F. S.; Okajima, T.; Ohsaka, T. PH Dependence of the Size and Crystallographic Orientation of the Gold Nanoparticles Prepared by Seed-Mediated Growth. **2011**, 27.
<https://doi.org/10.1021/la200150h>.
- (44) Cheng, H. W.; Skeete, Z. R.; Crew, E. R.; Shan, S.; Luo, J.; Zhong, C. J. Synthesis of Gold Nanoparticles. *Compr. Anal. Chem.* **2014**, 66, 37–79.
<https://doi.org/10.1016/B978-0-444-63285-2.00002-X>.
- (45) Cialla, D.; März, A.; Böhme, R.; Theil, F.; Weber, K.; Schmitt, M.; Popp, J. Surface-Enhanced Raman Spectroscopy (SERS): Progress and Trends. *Anal. Bioanal. Chem.* **2012**, 403 (1), 27–54.
<https://doi.org/10.1007/S00216-011-5631-X>.
- (46) Lv, W.; Gu, C.; Zeng, S.; Han, J.; Jiang, T.; Zhou, J. One-Pot Synthesis of Multi-Branch Gold Nanoparticles and Investigation of Their SERS Performance. *Biosensors* **2018**, 8 (4), 113.
<https://doi.org/10.3390/bios8040113>.
- (47) Agunloye, E.; Panariello, L.; Gavriilidis, A.; Mazzei, L. A Model for the Formation of Gold Nanoparticles in the Citrate Synthesis Method. *Chem. Eng. Sci.* **2018**, 191, 318–331. <https://doi.org/10.1016/j.ces.2018.06.046>.
- (48) Yang, Y.; Jiang, X.; Chao, J.; Song, C.; Liu, B.; Zhu, D.; Sun, Y.; Yang, B.; Zhang, Q.; Chen, Y.; Wang, L. Synthesis of Magnetic Core-Branched Au Shell Nanostructures and Their Application in Cancer-Related MiRNA Detection via SERS. *Sci. China Mater.* **2017**, 60 (11), 1129–1144.
<https://doi.org/10.1007/s40843-017-9022-1>.
- (49) Javed, R.; Zia, M.; Naz, S.; Aisida, S. O.; Ul Ain, N.; Ao, Q. Role of Capping Agents in the Application of Nanoparticles in Biomedicine and Environmental Remediation: Recent Trends and Future Prospects. *J Nanobiotechnol* **2020**, 18, 172. <https://doi.org/10.1186/s12951-020-00704-4>.
- (50) Garcia-Leis, A.; Vicente Garcia-Ramos, J.; Sanchez-Cortes, S. Silver

- Nanostars with High SERS Performance. *J. Phys. Chem. C* **2013**, 117–7791. <https://doi.org/10.1021/jp401737y>.
- (51) Sadhu, P. K.; Rajput, A.; Seth, A. K.; Dash, D. K.; Shah, N. V.; Kumari, M.; Patel, S. A Combined Approach of Gold Nanoparticles with Cannabinoids for the Treatment of Cancer – a Review. *Int. J. Pharm. Res.* **2020**, 12, 393–405. <https://doi.org/10.31838/IJPR/2020.SP1.077>.
- (52) Hu, J.; Wang, Z.; Li, J. Gold Nanoparticles With Special Shapes: Controlled Synthesis, Surface-Enhanced Raman Scattering, and The Application in Biodetection. *Sensors* **2007**, 7, 3299–3311.
- (53) K. Lance Kelly; Eduardo Coronado; Lin Lin Zhao, and; Schatz*, G. C. The Optical Properties of Metal Nanoparticles: The Influence of Size, Shape, and Dielectric Environment. **2002**. <https://doi.org/10.1021/JP026731Y>.
- (54) Cui, Y.; Ren, B.; Yao, J.-L.; Gu, R.-A.; Tian, Z.-Q. Synthesis of Ag_cCore Au_sShell Bimetallic Nanoparticles for Immunoassay Based on Surface-Enhanced Raman Spectroscopy. *J. Phys. Chem. B* **2006**, 110 (9), 4002–4006. <https://doi.org/10.1021/jp056203x>.
- (55) Reguera, J.; Langer, J.; Jiménez De Aberasturi, D.; Liz-Marzán, L. M. Anisotropic Metal Nanoparticles for Surface Enhanced Raman Scattering. *Chemical Society Reviews*. Royal Society of Chemistry July 7, 2017, pp 3866–3885. <https://doi.org/10.1039/c7cs00158d>.
- (56) Suzuki, S.; Yoshimura, M. Chemical Stability of Graphene Coated Silver Substrates for Surface-Enhanced Raman Scattering OPEN. <https://doi.org/10.1038/s41598-017-14782-2>.
- (57) Ji, W.; Zhao, B.; Ozaki, Y. Semiconductor Materials in Analytical Applications of Surface-Enhanced Raman Scattering. *J. Raman Spectrosc.* **2016**, 47 (1), 51–58. <https://doi.org/10.1002/JRS.4854>.
- (58) Liu, X.; Ma, J.; Jiang, P.; Shen, J.; Wang, R.; Wang, Y.; Tu, G. Large-Scale Flexible Surface-Enhanced Raman Scattering (SERS) Sensors with High Stability and Signal Homogeneity. *Cite This ACS Appl. Mater.*

Interfaces **2020**, *12*, 45341. <https://doi.org/10.1021/acsami.0c13691>.

- (59) Jiang, Y.; Wang, J.; Malfatti, L.; Carboni, D.; Senes, N.; Innocenzi, P. Highly Durable Graphene-Mediated Surface Enhanced Raman Scattering (G-SERS) Nanocomposites for Molecular Detection. *Appl. Surf. Sci.* **2018**, *450*, 451–460. <https://doi.org/10.1016/j.apsusc.2018.04.218>.
- (60) Shi, G.; Wang, M.; Zhu, Y.; Shen, L.; Wang, Y.; Ma, W.; Chen, Y.; Li, R. A Flexible and Stable Surface-Enhanced Raman Scattering (SERS) Substrate Based on Au Nanoparticles/Graphene Oxide/Cicada Wing Array. *Opt. Commun.* **2018**, *412*, 28–36. <https://doi.org/10.1016/J.OPTCOM.2017.11.075>.
- (61) Zhu, C.; Hu, X.; Wang, X. Silver Nanocubes/Graphene Oxide Hybrid Film on a Hydrophobic Surface for Effective Molecule Concentration and Sensitive SERS Detection. *Appl. Surf. Sci.* **2019**, *470*, 423–429. <https://doi.org/10.1016/j.apsusc.2018.11.169>.
- (62) Jiang, L.; You, T.; Yin, P.; Shang, Y.; Zhang, D.; Guo, L.; Yang, S. Surface-Enhanced Raman Scattering Spectra of Adsorbates on Cu₂O Nanospheres: Charge-Transfer and Electromagnetic Enhancement. *Nanoscale* **2013**, *5* (7), 2784–2789. <https://doi.org/10.1039/c3nr33502j>.
- (63) Mills, A.; Hill, G.; Stewart, M.; Graham, D.; Smith, W. E.; Hodgen, S.; Halfpenny, P. J.; Faulds, K.; Robertson, P. *Characterization of Novel Ag on TiO₂ Films for Surface-Enhanced Raman Scattering*; 2004; Vol. 58. <https://journals.sagepub.com/doi/pdf/10.1366/0003702041655520> (accessed 2019-01-31).
- (64) Yang, L.; Gong, M.; Jiang, X.; Yin, D.; Qin, X.; Zhao, B.; Ruan, W. Investigation on SERS of Different Phase Structure TiO₂ Nanoparticles. *J. Raman Spectrosc.* **2015**, *46* (3), 287–292. <https://doi.org/10.1002/jrs.4645>.
- (65) Jiang, L.; Liang, X.; You, T.; Yin, P.; Wang, H.; Guo, L.; Yang, S. A Sensitive SERS Substrate Based on Au/TiO₂/Au Nanosheets. *Spectrochim. Acta Part A Mol. Biomol. Spectrosc.* **2015**, *142*, 50–54. <https://doi.org/10.1016/J.SAA.2015.01.040>.

- (66) Prakash, O.; Kumar, S.; Singh, P.; Deckert, V.; Chatterjee, S.; Ghosh, A. K.; Singh, R. K. Surface-Enhanced Raman Scattering Characteristics of CuO: Mn/Ag Heterojunction Probed by Methyl Orange: Effect of Mn 2+ Doping. **2016**. <https://doi.org/10.1002/jrs.4904>.
- (67) Klutse, C. K.; Mayer, A.; Wittkamper, J.; Cullum, B. M. Surface-Enhanced Raman Scattering. *J. Nanotechnol.* **2012**, 2012. <https://doi.org/10.1155/2012/319038>.
- (68) Prokopec, V.; Cejkova, J.; Matějka, P.; Hasal, P. Preparation of SERS-Active Substrates with Large Surface Area for Raman Spectral Mapping and Testing of Their Surface Nanostructure. *Surf. Interface Anal.* **2008**, 40 (3–4), 601–607. <https://doi.org/10.1002/sia.2774>.
- (69) Lyandres, O.; Yuen, J. M.; Shah, N. C.; VanDuyne, R. P.; Walsh, J. T.; Glucksberg, M. R.; Glucksberg, M. R. Progress toward an in Vivo Surface-Enhanced Raman Spectroscopy Glucose Sensor. *Diabetes Technol. Ther.* **2008**, 10 (4), 257–265. <https://doi.org/10.1089/dia.2007.0288>.
- (70) Zhu, Z.; Meng, H.; Liu, W.; Liu, X.; Gong, J.; Qiu, X.; Jiang, L.; Wang, D.; Tang, Z. Superstructures and SERS Properties of Gold Nanocrystals with Different Shapes. *Angew. Chemie Int. Ed.* **2011**, 50 (7), 1593–1596. <https://doi.org/10.1002/anie.201005493>.
- (71) Chen, J.; Jiang, J.; Gao, X.; Liu, G.; Shen, G.; Yu, R. A New Aptameric Biosensor for Cocaine Based on Surface-Enhanced Raman Scattering Spectroscopy. *Chem. - A Eur. J.* **2008**, 14 (27), 8374–8382. <https://doi.org/10.1002/chem.200701307>.
- (72) Weisbecker, C. S.; Merritt, M. V.; Whitesides, G. M. *Molecular Self-Assembly of Aliphatic Thiols on Gold Colloids*; 1996. <https://pubs.acs.org/sharingguidelines> (accessed 2020-04-15).
- (73) Vericat, C.; Vela, M. E.; Benitez, G.; Carro, P.; Salvarezza, R. C. Self-Assembled Monolayers of Thiols and Dithiols on Gold: New Challenges for a Well-Known System. **2010**. <https://doi.org/10.1039/b907301a>.

- (74) Badia, A.; Singh, S.; Demers, L.; Cuccia, L.; Brown, G. R.; Lennox, R. B. *FULL PAPER Self-Assembled Monolayers on Gold Nanoparticles***.
- (75) Jaworska, A.; Fornasaro, S.; Sergo, V.; Bonifacio, A.; Jaworska, A.; Fornasaro, S.; Sergo, V.; Bonifacio, A. Potential of Surface Enhanced Raman Spectroscopy (SERS) in Therapeutic Drug Monitoring (TDM). A Critical Review. *Biosensors* **2016**, 6 (3), 47.
<https://doi.org/10.3390/bios6030047>.
- (76) Chen, L.; Li, G. Functions of 1-Dodecanethiol in the Synthesis and Post-Treatment of Copper Sulfide Nanoparticles Relevant to Their Photocatalytic Applications. **2018**.
<https://doi.org/10.1021/acsanm.8b00893>.
- (77) Schmitt, J.; Mächtle, P.; Eck, D.; Möhwald, H.; Helm, C. A. Preparation and Optical Properties of Colloidal Gold Monolayers. *Langmuir* **1999**, 15 (9), 3256–3266. <https://doi.org/10.1021/la981078k>.
- (78) E. C. Le Ru, *; E. Blackie; M. Meyer, and; Etchegoin†, P. G. Surface Enhanced Raman Scattering Enhancement Factors: A Comprehensive Study. **2007**. <https://doi.org/10.1021/JP0687908>.
- (79) Haynes, C. L.; Yonzon, C. R.; Zhang, X.; Van Duyne, R. P. Surface-Enhanced Raman Sensors: Early History and the Development of Sensors for Quantitative Biowarfare Agent and Glucose Detection. *J. Raman Spectrosc.* **2005**, 36 (6–7), 471–484.
<https://doi.org/10.1002/jrs.1376>.
- (80) Shiohara, A.; Langer, J.; Polavarapu, L.; Liz-Marzán, L. M. Solution Processed Polydimethylsiloxane/Gold Nanostar Flexible Substrates for Plasmonic Sensing. *Nanoscale* **2014**, 6 (16), 9817–9823.
<https://doi.org/10.1039/c4nr02648a>.
- (81) Garcia-Rico, E.; Alvarez-Puebla, R. A.; Guerrini, L. Direct Surface-Enhanced Raman Scattering (SERS) Spectroscopy of Nucleic Acids: From Fundamental Studies to Real-Life Applications. *Chemical Society Reviews*. Royal Society of Chemistry July 7, 2018, pp 4909–4923.
<https://doi.org/10.1039/c7cs00809k>.

- (82) He, R. X.; Liang, R.; Peng, P.; Norman Zhou, Y. Effect of the Size of Silver Nanoparticles on SERS Signal Enhancement. *J. Nanoparticle Res.* **2017**, *19* (8). <https://doi.org/10.1007/s11051-017-3953-0>.
- (83) Wang, J.; Lin, D.; Lin, J.; Yu, Y.; Huang, Z.; Chen, Y.; Lin, J.; Feng, S.; Li, B.; Liu, N.; Chen, R. Label-Free Detection of Serum Proteins Using Surface-Enhanced Raman Spectroscopy for Colorectal Cancer Screening. *J. Biomed. Opt.* **2014**, *19* (8), 087003. <https://doi.org/10.1117/1.jbo.19.8.087003>.
- (84) Blanton, L. E.; Hines, S. A.; Guyot-Sionnest, M. A.; Landin, P.; Miller, L.; Pistol, M. S.; Pryor, M.-E.; Samuelson, C. E.; Empedocles, L.; Bawendi, S. A.; Vlckova, M. G.; Gu, B.; Moskovits, X. J.; Nie, M.; Emory, S. R.; Kneipp, S. R.; Ramirez-Aguilar, K.; Rowlen, K. A.; Langmuir, K. L. Direct Observation of Size-Dependent Optical Enhancement in Single Metal Nanoparticles. *Appl. Phys. Lett* **1996**, *383* (3), 8009–8010. <https://doi.org/10.1021/ja9815677>.
- (85) Vankeirsbilck, T.; Vercauteren, A.; Baeyens, W.; Van der Weken, G.; Verpoort, F.; Vergote, G.; Remon, J. . Applications of Raman Spectroscopy in Pharmaceutical Analysis. *TrAC Trends Anal. Chem.* **2002**, *21* (12), 869–877. [https://doi.org/10.1016/S0165-9936\(02\)01208-6](https://doi.org/10.1016/S0165-9936(02)01208-6).
- (86) Qiao, X.; Su, B.; Liu, C.; Song, Q.; Luo, D.; Mo, G.; Wang, T. Selective Surface Enhanced Raman Scattering for Quantitative Detection of Lung Cancer Biomarkers in Superparticle@MOF Structure. *Adv. Mater.* **2018**, *30* (5), 1–8. <https://doi.org/10.1002/adma.201702275>.
- (87) Li, Z.; Huang, X.; Lu, G. Recent Developments of Flexible and Transparent SERS Substrates. *J. Mater. Chem. C* **2020**, 3956, 3956. <https://doi.org/10.1039/d0tc00002g>.
- (88) Chen, Z.; Tabakman, S. M.; Goodwin, A. P.; Kattah, M. G.; Daranciang, D.; Wang, X.; Zhang, G.; Li, X.; Liu, Z.; Utz, P. J.; Jiang, K.; Fan, S.; Dai, H. Protein Microarrays with Carbon Nanotubes as Multicolor Raman Labels. *Nat. Biotechnol.* **2008**, *26* (11), 1285–1292. <https://doi.org/10.1038/nbt.1501>.

- (89) Lee, J.-H.; Cho, H.-Y.; Choi, H.; Lee, J.-Y.; Choi, J.-W.; Lee, J.-H.; Cho, H.-Y.; Choi, H. K.; Lee, J.-Y.; Choi, J.-W. Application of Gold Nanoparticle to Plasmonic Biosensors. *Int. J. Mol. Sci.* **2018**, *19* (7), 2021. <https://doi.org/10.3390/ijms19072021>.
- (90) Kumar, S.; Kumar, P.; Das, A.; Pathak, C. S. Surface-Enhanced Raman Scattering: Introduction and Applications. *Recent Adv. Nanophotonics - Fundam. Appl.* **2020**. <https://doi.org/10.5772/INTECHOPEN.92614>.
- (91) Langer, J.; de Aberasturi, D. J.; Aizpurua, J.; Alvarez-Puebla, R. A.; Augu  , B.; Baumberg, J. J.; Bazan, G. C.; Bell, S. E. J.; Boisen, A.; Brolo, A. G.; Choo, J.; Cialla-May, D.; Deckert, V.; Fabris, L.; Faulds, K.; Javier Garc  a de Abajo, F.; Goodacre, R.; Graham, D.; Haes, A. J.; Haynes, C. L.; Huck, C.; Itoh, T.; K  ll, M.; Kneipp, J.; Kotov, N. A.; Kuang, H.; Le Ru, E. C.; Lee, H. K.; Li, J. F.; Ling, X. Y.; Maier, S. A.; Mayerh  fer, T.; Moskovits, M.; Murakoshi, K.; Nam, J. M.; Nie, S.; Ozaki, Y.; Pastoriza-Santos, I.; Perez-Juste, J.; Popp, J.; Pucci, A.; Reich, S.; Ren, B.; Schatz, G. C.; Shegai, T.; Schl  cker, S.; Tay, L. L.; George Thomas, K.; Tian, Z. Q.; van Duyne, R. P.; Vo-Dinh, T.; Wang, Y.; Willets, K. A.; Xu, C.; Xu, H.; Xu, Y.; Yamamoto, Y. S.; Zhao, B.; Liz-Marz  n, L. M. Present and Future of Surface-Enhanced Raman Scattering. *ACS Nano* **2020**, *14* (1), 28–117. <https://doi.org/10.1021/ACSNANO.9B04224>.
- (92) Le Ru, E. C.; Etchegoin, P. G. (Pablo G. *Principles of Surface-Enhanced Raman Spectroscopy: And Related Plasmonic Effects*; Elsevier, 2009.
- (93) Ru, E. C. Le; Meyer, M.; Blackie, E.; Etchegoin, P. G. Advanced Aspects of Electromagnetic SERS Enhancement Factors at a Hot Spot. **2008**, No. March, 1127–1134. <https://doi.org/10.1002/jrs>.
- (94) Pilot, R.; Signorini, R.; Durante, C.; Orian, L.; Bhamidipati, M.; Fabris, L. A Review on Surface-Enhanced Raman Scattering. *Biosensors* **2019**, *9* (2). <https://doi.org/10.3390/BIOS9020057>.
- (95) Le Ru, E. C.; Etchegoin, P. G. Rigorous Justification of the $|E|^4$ Enhancement Factor in Surface Enhanced Raman Spectroscopy. *Chem. Phys. Lett.* **2006**, *423* (1–3), 63–66.

<https://doi.org/10.1016/J.CPLETT.2006.03.042>.

- (96) Cialla, D.; März, A.; Böhme, R.; Theil, F.; Weber, K.; Schmitt, M.; Popp, J. Surface-Enhanced Raman Spectroscopy (SERS): Progress and Trends. <https://doi.org/10.1007/s00216-011-5631-x>.
- (97) Meyer, M. W.; McKee, K. J.; Nguyen, V. H. T.; Smith, E. A. Surface Enhanced Raman Scattering Enhancement Factors: A Comprehensive Study. *J. Phys. Chem. C* **2012**. <https://doi.org/10.1021/jp308882w>.
- (98) Le Ru, E. C.; Blackie, E.; Meyer, M.; Etchegoin, P. G. Surface Enhanced Raman Scattering Enhancement Factors: A Comprehensive Study. **2007**. <https://doi.org/10.1021/jp0687908>.
- (99) Cialla, D.; März, A.; Böhme, R.; Theil, F.; Weber, K.; Schmitt, M.; Popp, J. Surface-Enhanced Raman Spectroscopy (SERS): Progress and Trends. <https://doi.org/10.1007/s00216-011-5631-x>.
- (100) Kumar, S.; Goel, P.; Singh, J. P. Flexible and Robust SERS Active Substrates for Conformal Rapid Detection of Pesticide Residues from Fruits. *Sensors Actuators B Chem.* **2017**, *241*, 577–583. <https://doi.org/10.1016/j.snb.2016.10.106>.
- (101) Langer, J.; Novikov, S. M.; Liz-Marzán, L. M.; Kurniawan, A.; Wang, J.; Ogundare, S. A.; Van Zyl, W. E.; Nguyen, B. H.; Nguyen, V. H.; Tran, H. N. Advances in Natural Sciences: Nanoscience and Nanotechnology REVIEW • OPEN ACCESS To Cite This Article: Bich Ha Nguyen et Al. *Adv. Nat. Sci Nanosci. Nanotechnol* **2016**, *7*, 33001. <https://doi.org/10.1088/2043-6262/7/3/033001>.
- (102) Lee, C. H.; Tian, L.; Singamaneni, S. Paper-Based SERS Swab for Rapid Trace Detection on Real-World Surfaces. *ACS Appl. Mater. Interfaces* **2010**, *2* (12), 3429–3435. <https://doi.org/10.1021/am1009875>.
- (103) Lu, G.; Li, H.; Zhang, H. Gold-Nanoparticle-Embedded Polydimethylsiloxane Elastomers for Highly Sensitive Raman Detection. *Small* **2012**, *8* (9), 1336–1340. <https://doi.org/10.1002/smll.201102258>.
- (104) Jaipan, P.; Nguyen, A.; Narayan, R. J. Biomaterials for 3D Cell Biology

Prospective Article. <https://doi.org/10.1557/mrc.2017.92>.

- (105) Guo, J.; Zhong, Z.; Li, Y.; Liu, Y.; Wang, R.; Ju, H. “Three-in-One” SERS Adhesive Tape for Rapid Sampling, Release, and Detection of Wound Infectious Pathogens. *ACS Appl. Mater. Interfaces* **2019**, *11*, 36399–36408. <https://doi.org/10.1021/acsami.9b12823>.
- (106) Zhou, X.; Li, H.; Yu, G.; Chen, Y.; Wang, Y.; Zeng, Z.; Chi, L. A Highly-Efficient, Stable, and Flexible Kapton Tape-Based SERS Chip †. *Mater. Chem. Front* **2021**, *5*, 6471. <https://doi.org/10.1039/d1qm00547b>.
- (107) Perumal, J.; Lim, H. Q.; Attia, A. B. E.; Raziq, R.; Leavesley, D. I.; Upton, Z.; Dinish, U. S.; Olivo, M. Novel Cellulose Fibre-Based Flexible Plasmonic Membrane for Point-of-Care SERS Biomarker Detection in Chronic Wound Healing. *Int. J. Nanomedicine* **2021**, *16*, 5869–5878. <https://doi.org/10.2147/IJN.S303130>.
- (108) Hu, S. W.; Qiao, S.; Pan, J. Bin; Kang, B.; Xu, J. J.; Chen, H. Y. A Paper-Based SERS Test Strip for Quantitative Detection of Mucin-1 in Whole Blood. *Talanta* **2018**, *179*, 9–14. <https://doi.org/10.1016/j.talanta.2017.10.038>.
- (109) Zhou, R.; Wu, Z.; Sun, Z.; Su, X. Sensitive Surface Enhanced Raman Scattering Substrates Based on Filter Paper Loaded with Au Porous Nanospheres. *Nanosci. Nanotechnol. Lett.* **2015**, *7* (10), 801–805. <https://doi.org/10.1166/nnl.2015.2033>.
- (110) Wang, J.; Wong, J. X. H.; Kwok, H.; Li, X.; Yu, H.-Z. Facile Preparation of Nanostructured, Superhydrophobic Filter Paper for Efficient Water/Oil Separation. *PLoS One* **2016**, *11* (3), e0151439. <https://doi.org/10.1371/journal.pone.0151439>.
- (111) Wu, M.; Li, P.; Zhu, Q.; Wu, M.; Li, H.; Lu, F. Functional Paper-Based SERS Substrate for Rapid and Sensitive Detection of Sudan Dyes in Herbal Medicine. *Spectrochim. Acta - Part A Mol. Biomol. Spectrosc.* **2018**, *196*, 110–116. <https://doi.org/10.1016/j.saa.2018.02.014>.
- (112) Singh, J. P.; Chu, H.; Abell, J.; Tripp, R. A.; Zhao, Y. Flexible and

Mechanical Strain Resistant Large Area SERS Active Substrates.

<https://doi.org/10.1039/c2nr00020b>.

- (113) Zhou, J.; Ren, K.; Zhao, Y.; Dai, W.; Wu, H. Convenient Formation of Nanoparticle Aggregates on Microfluidic Chips for Highly Sensitive SERS Detection of Biomolecules. *Anal. Bioanal. Chem.* **2012**, *402* (4), 1601–1609. <https://doi.org/10.1007/s00216-011-5585-z>.
- (114) Kumar, S.; Goel, P.; Singh, J. P. Flexible and Robust SERS Active Substrates for Conformal Rapid Detection of Pesticide Residues from Fruits. *Sensors Actuators, B Chem.* **2017**, *241*, 577–583. <https://doi.org/10.1016/j.snb.2016.10.106>.
- (115) Novara, C.; Dalla Marta, S.; Virga, A.; Lamberti, A.; Angelini, A.; Chiadò, A.; Rivolo, P.; Geobaldo, F.; Sergo, V.; Bonifacio, A.; Giorgis, F. SERS-Active Ag Nanoparticles on Porous Silicon and PDMS Substrates: A Comparative Study of Uniformity and Raman Efficiency. *J. Phys. Chem. C* **2016**, *120* (30), 16946–16953. <https://doi.org/10.1021/acs.jpcc.6b03852>.
- (116) Hydrogels for Biomedical Applications: Cellulose, Chitosan, and Protein/Peptide Derivatives. *Gels* **2017**, *3* (3), 27. <https://doi.org/10.3390/gels3030027>.
- (117) Thürmer, M. B.; Diehl, C. E.; Brum, F. J. B.; Dos Santos, L. A. Preparation and Characterization of Hydrogels with Potential for Use as Biomaterials. *Mater. Res.* **2014**, *17*, 109–113. <https://doi.org/10.1590/1516-1439.223613>.
- (118) Wang, T.; Turhan, M.; Gunasekaran, S. Selected Properties of PH-Sensitive, Biodegradable Chitosan-Poly(Vinyl Alcohol) Hydrogel. *Polym. Int.* **2004**, *53* (7), 911–918. <https://doi.org/10.1002/pi.1461>.
- (119) Liang, J.; Guo, Z.; Timmerman, A.; Grijpma, D.; Poot, A. Enhanced Mechanical and Cell Adhesive Properties of Photo-Crosslinked PEG Hydrogels by Incorporation of Gelatin in the Networks. *Biomed. Mater.* **2019**, *14* (2). <https://doi.org/10.1088/1748-605X/aaf31b>.
- (120) Nagahama, H.; Maeda, H.; Kashiki, T.; Jayakumar, R.; Furuike, T.;

- Tamura, H. Preparation and Characterization of Novel Chitosan/Gelatin Membranes Using Chitosan Hydrogel. *Carbohydr. Polym.* **2009**, *76* (2), 255–260. <https://doi.org/10.1016/j.carbpol.2008.10.015>.
- (121) You, Y. H.; Nagaraja, A. T.; Biswas, A.; Hwang, J. H.; Cote, G. L.; McShane, M. J. SERS-Active Smart Hydrogels with Modular Microdomains: From PH to Glucose Sensing. *IEEE Sens. J.* **2017**, *17* (4), 941–950. <https://doi.org/10.1109/JSEN.2016.2636020>.
- (122) Kim, D. J.; Park, S. G.; Kim, D. H.; Kim, S. H. SERS-Active-Charged Microgels for Size- and Charge-Selective Molecular Analysis of Complex Biological Samples. *Small* **2018**, *14* (40), 1–10. <https://doi.org/10.1002/smll.201802520>.
- (123) Pilot, R.; Signorini, R.; Durante, C.; Orian, L.; Bhamidipati, M.; Fabris, L. A Review on Surface-Enhanced Raman Scattering. *Biosensors*. MDPI AG June 1, 2019. <https://doi.org/10.3390/bios9020057>.
- (124) Nimse, S. B.; Sonawane, M. D.; Song, K. S.; Kim, T. Biomarker Detection Technologies and Future Directions. *Analyst* **2016**, *141* (3), 740–755. <https://doi.org/10.1039/c5an01790d>.
- (125) Lindley, L. E.; Stojadinovic, O.; Pastar, I.; Tomic-Canic, M. Biology and Biomarkers for Wound Healing. <https://doi.org/10.1097/PRS.0000000000002682>.
- (126) Chisanga, M.; Muhamadali, H.; Ellis, D. I.; Goodacre, R. Enhancing Disease Diagnosis: Biomedical Applications of Surface-Enhanced Raman Scattering. *Appl. Sci.* **2019**, *9* (6). <https://doi.org/10.3390/app9061163>.
- (127) Wang, G.; Wang, Y.; Chen, L.; Choo, J. Nanomaterial-Assisted Aptamers for Optical Sensing. *Biosensors and Bioelectronics*. April 15, 2010, pp 1859–1868. <https://doi.org/10.1016/j.bios.2009.11.012>.
- (128) Managò, S.; Mirabelli, P.; Napolitano, M.; Zito, G.; De Luca, A. C. Raman Detection and Identification of Normal and Leukemic Hematopoietic Cells. *J. Biophotonics* **2018**, *11* (5), e201700265. <https://doi.org/10.1002/JBIO.201700265>.

- (129) Adomaviči, S.; Martynas Velička, |; Šablinskas, V. Detection of Aspirin Traces in Blood by Means of Surface-Enhanced Raman Scattering Spectroscopy. **2020**. <https://doi.org/10.1002/jrs.5853>.
- (130) Bruzas, I.; Lum, W.; Gorunmez, Z.; Sagle, L. Advances in Surface-Enhanced Raman Spectroscopy (SERS) Substrates for Lipid and Protein Characterization: Sensing and Beyond. *Analyst* **2018**, *143* (17), 3990–4008. <https://doi.org/10.1039/C8AN00606G>.
- (131) Zong, C.; Xu, M.; Xu, L.-J.; Wei, T.; Ma, X.; Zheng, X.-S.; Hu, R.; Ren, B. Surface-Enhanced Raman Spectroscopy for Bioanalysis: Reliability and Challenges. **2018**. <https://doi.org/10.1021/acs.chemrev.7b00668>.
- (132) Köker, T.; Tang, N.; Tian, C.; Zhang, W.; Wang, X.; Martel, R.; Pinaud, F. Cellular Imaging by Targeted Assembly of Hot-Spot SERS and Photoacoustic Nanoprobes Using Split-Fluorescent Protein Scaffolds. <https://doi.org/10.1038/s41467-018-03046-w>.
- (133) Agoston, R.; Izake, E. L.; Sivanesan, A.; Lott, W. B.; Sillence, M.; Steel, R. Rapid Isolation and Detection of Erythropoietin in Blood Plasma by Magnetic Core Gold Nanoparticles and Portable Raman Spectroscopy. *Nanomedicine Nanotechnology, Biol. Med.* **2016**, *12* (3), 633–641. <https://doi.org/10.1016/j.nano.2015.11.003>.
- (134) Sanles-Sobrido, M.; Rodríguez-Lorenzo, L.; Lorenzo-Abalde, S.; González-Fernández, Á.; Correa-Duarte, M. A.; Alvarez-Puebla, R. A.; Liz-Marzán, L. M. Label-Free SERS Detection of Relevant Bioanalytes on Silver-Coated Carbon Nanotubes: The Case of Cocaine. *Nanoscale* **2009**, *1* (1), 153–158. <https://doi.org/10.1039/b9nr00059c>.
- (135) Pandey, R.; Dingari, N. C.; Spegazzini, N.; Dasari, R. R.; Horowitz, G. L.; Barman, I. Emerging Trends in Optical Sensing of Glycemic Markers for Diabetes Monitoring. *Trends Analyt. Chem.* **2015**, *64*, 100–108. <https://doi.org/10.1016/j.trac.2014.09.005>.
- (136) Sooraj, K. P.; Ranjan, M.; Rao, R.; Mukherjee, S. SERS Based Detection of Glucose with Lower Concentration than Blood Glucose Level Using Plasmonic Nanoparticle Arrays. *Appl. Surf. Sci.* **2018**, *447*, 576–581.

<https://doi.org/10.1016/J.APSUSC.2018.04.020>.

- (137) Lai, H.; Xu, F.; Zhang, Y.; Wang, L. Recent Progress on Graphene-Based Substrates for Surface-Enhanced Raman Scattering Applications. *Journal of Materials Chemistry B*. Royal Society of Chemistry 2018, pp 4008–4028. <https://doi.org/10.1039/c8tb00902c>.
- (138) Casella, M.; Lucotti, A.; Tommasini, M.; Bedoni, M.; Forvi, E.; Gramatica, F.; Zerbi, G. Raman and SERS Recognition of β -Carotene and Haemoglobin Fingerprints in Human Whole Blood. *Spectrochim. Acta - Part A Mol. Biomol. Spectrosc.* **2011**, 79 (5), 915–919. <https://doi.org/10.1016/j.saa.2011.03.048>.
- (139) Chen, L.; Chao, J.; Qu, X.; Zhang, H.; Zhu, D.; Su, S.; Aldalbahi, A.; Wang, L.; Pei, H. Probing Cellular Molecules with PolyA-Based Engineered Aptamer Nanobeacon. *ACS Appl. Mater. Interfaces* **2017**, 9 (9), 8014–8020. <https://doi.org/10.1021/acsami.6b16764>.
- (140) Bin Phyo, J.; Woo, A.; Jae Yu, H.; Lim, K.; Hwan Cho, B.; Sang Jung, H.; Lee, M.-Y. Label-Free SERS Analysis of Urine Using a 3D-Stacked AgNW-Glass Fiber Filter Sensor for the Diagnosis of Pancreatic Cancer and Prostate Cancer. *Cite This Anal. Chem* **2021**, 93, 3785. <https://doi.org/10.1021/acs.analchem.0c04200>.
- (141) Lyons, T. J.; Basu, A. Biomarkers in Diabetes: Hemoglobin A1c, Vascular and Tissue Markers. *Transl. Res.* **2012**, 159 (4), 303–312. <https://doi.org/10.1016/j.trsl.2012.01.009>.
- (142) Kalashnikova, I.; Das, S.; Seal, S. Nanomaterials for Wound Healing: Scope and Advancement. *Nanomedicine*. 2015. <https://doi.org/10.2217/nnm.15.82>.
- (143) Patel, S.; Maheshwari, A.; Chandra, A. Biomarkers for Wound Healing and Their Evaluation. *J. Wound Care* **2016**, 25 (1), 46–55. <https://doi.org/10.12968/jowc.2016.25.1.46>.
- (144) Patel, S.; student, P.; Pharm in Pharmaceutical Biotechnology, M.; Maheshwari, A.; Student, P.; Chandra, A.; Professor, A. *Education J O U*

4 6 Biomarkers for Wound Healing and Their Evaluation Biomarkers, Wound, Abnormal Wound Healing, Cytokines, Protease. <http://scribd>. (accessed 2019-07-26).

- (145) Parani, M.; Lokhande, G.; Singh, A.; Gaharwar, A. K. Engineered Nanomaterials for Infection Control and Healing Acute and Chronic Wounds. *ACS Appl. Mater. Interfaces* **2016**.
<https://doi.org/10.1021/acsami.6b00291>.
- (146) Battaglia, T. M.; Masson, J.-F.; Sierks, M. R.; Beaudoin, S. P.; Rogers, J.; Foster, K. N.; Holloway, | G Allen; Booksh, K. S. Quantification of Cytokines Involved in Wound Healing Using Surface Plasmon Resonance. **2005**. <https://doi.org/10.1021/ac050568w>.
- (147) Ghebremedhin, M.; Yesupriya, S.; Crane, N. J. Surface Enhanced Raman Spectroscopy as a Point-of-Care Diagnostic for Infection in Wound Effluent. *Opt. Diagnostics Sens. XVI Towar. Point-of-Care Diagnostics* **2016**, 9715 (March 2016), 97150B. <https://doi.org/10.1117/12.2212667>.
- (148) Lugoda, P.; Hughes-Riley, T.; Oliveira, C.; Morris, R.; Dias, T. Developing Novel Temperature Sensing Garments for Health Monitoring Applications. **2018**. <https://doi.org/10.3390/fib6030046>.
- (149) Lee, H. K.; Lee, Y. H.; Koh, C. S. L.; Phan-Quang, G. C.; Han, X.; Lay, C. L.; Sim, H. Y. F.; Kao, Y. C.; An, Q.; Ling, X. Y. Designing Surface-Enhanced Raman Scattering (SERS) Platforms beyond Hotspot Engineering: Emerging Opportunities in Analyte Manipulations and Hybrid Materials. *Chem. Soc. Rev.* **2019**, 48 (3), 731–756.
<https://doi.org/10.1039/c7cs00786h>.
- (150) Zheng, X. S.; Jahn, I. J.; Weber, K.; Cialla-May, D.; Popp, J. Label-Free SERS in Biological and Biomedical Applications: Recent Progress, Current Challenges and Opportunities. *Spectrochim. Acta - Part A Mol. Biomol. Spectrosc.* **2018**, 197, 56–77.
<https://doi.org/10.1016/J.SAA.2018.01.063>.
- (151) Mahajan, S.; Cole, R. M.; Speed, J. D.; Pelfrey, S. H.; Russell, A. E.;

- Bartlett, P. N.; Barnett, S. M.; Baumberg, J. J. Understanding the Surface-Enhanced Raman Spectroscopy "Background" †.
<https://doi.org/10.1021/jp907197b>.
- (152) Han, X. X.; Zhao, B.; Ozaki, Y. Surface-Enhanced Raman Scattering for Protein Detection. <https://doi.org/10.1007/s00216-009-2702-3>.
- (153) Barucci, A.; D'Andrea, C.; Farnesi, E.; Banchelli, M.; Amicucci, C.; De Angelis, M.; Hwang, B.; Matteini, P. Label-Free SERS Detection of Proteins Based on Machine Learning Classification of Chemo-Structural Determinants. *Analyst* **2021**, *146* (2), 674–682.
<https://doi.org/10.1039/d0an02137g>.
- (154) Yu, Y.; Lin, Y.; Xu, C.; Lin, K.; Ye, Q.; Wang, X.; Xie, S.; Chen, R.; Lin, A. J. Label-Free Detection of Nasopharyngeal and Liver Cancer Using Surface-Enhanced Raman Spectroscopy and Partial Least Squares Combined with Support Vector Machine. **2018**.
<https://doi.org/10.1364/BOE.9.006053>.
- (155) Renwick Beattie, J.; Esmonde-White, F. W. L. Exploration of Principal Component Analysis: Deriving Principal Component Analysis Visually Using Spectra. <https://doi.org/10.1177/0003702820987847>.
- (156) Fatima, A.; Cyril, G.; Vincent, V.; Stéphane, J.; Olivier, P. Towards Normalization Selection of Raman Data in the Context of Protein Glycation: Application of Validity Indices to PCA Processed Spectra †.
Cite this Anal. **2020**, *145*, 2945. <https://doi.org/10.1039/c9an02155h>.
- (157) Chen, G.; Lin, X.; Lin, D.; Ge, X.; Feng, S.; Pan, J.; Lin, J.; Huang, Z.; Huang, X.; Chen, R. Identification of Different Tumor States in Nasopharyngeal Cancer Using Surface-Enhanced Raman Spectroscopy Combined with Lasso-PLS-DA Algorithm. **2016**.
<https://doi.org/10.1039/c5ra24438b>.
- (158) Glass, D.; Cortés, E.; Ben-Jaber, S.; Brick, T.; Quesada-Cabrera, R.; Peveler, W. J.; Zhu, Y.; Blackman, C. S.; Howle, C. R.; Parkin, I. P.; Maier, S. A. Photo-Induced Enhanced Raman Spectroscopy (PIERS): Sensing Atomic-Defects, Explosives and Biomolecules. In *Chemical*,

Biological, Radiological, Nuclear, and Explosives (CBRNE) Sensing XX;
Guicheteau, J. A., Howle, C. R., Eds.; SPIE, 2019; Vol. 11010, p 13.
<https://doi.org/10.1117/12.2518948>.

- (159) Ye, J.; Arul, R.; Nieuwoudt, M. K.; Dong, J.; Gao, W.; Simpson, M. C. Understanding the Chemical Mechanism behind Photo-Induced Enhanced Raman Spectroscopy.
- (160) Zhang, M.; Sun, H.; Chen, X.; Yang, J.; Shi, L.; Chen, T.; Bao, Z.; Liu, J.; Wu, Y. Highly Efficient Photoinduced Enhanced Raman Spectroscopy (PIERS) from Plasmonic Nanoparticles Decorated 3D Semiconductor Arrays for Ultrasensitive, Portable, and Recyclable Detection of Organic Pollutants. **2019**. <https://doi.org/10.1021/acssensors.9b00562>.
- (161) Glass, D.; Quesada-Cabrera, R.; Bardey, S.; Promdet, P.; Sapienza, R.; Keller, V.; Maier, S. A.; Caps, V.; Parkin, I. P.; Cortés, E. Probing the Role of Atomic Defects in Photocatalytic Systems through Photoinduced Enhanced Raman Scattering. **2021**. <https://doi.org/10.1021/acseenergylett.1c01772>.
- (162) Ben-Jaber, S.; Peveler, W. J.; Quesada-Cabrera, R.; Cortés, E.; Sotelo-Vazquez, C.; Abdul-Karim, N.; Maier, S. A.; Parkin, I. P. Photo-Induced Enhanced Raman Spectroscopy for Universal Ultra-Trace Detection of Explosives, Pollutants and Biomolecules. *Nat. Commun.* **2016**. <https://doi.org/10.1038/ncomms12189>.
- (163) Man, T.; Lai, W.; Xiao, M.; Wang, X.; Chandrasekaran, A. R.; Pei, H.; Li, L. A Versatile Biomolecular Detection Platform Based on Photo-Induced Enhanced Raman Spectroscopy. *Biosens. Bioelectron.* **2020**, *147*, 111742. <https://doi.org/10.1016/j.bios.2019.111742>.
- (164) Zhang, M.; Chen, T.; Liu, Y.; Zhu, J.; Liu, J.; Wu, Y. Three-Dimensional TiO₂ ÅAg Nanopore Arrays for Powerful Photoinduced Enhanced Raman Spectroscopy (PIERS) and Versatile Detection of Toxic Organics. <https://doi.org/10.1002/cnma.201800389>.
- (165) Glass, D.; Cortés, E.; Ben-Jaber, S.; Brick, T.; Quesada-Cabrera, R.; Peveler, W. J.; Zhu, Y.; Blackman, C. S.; Howle, C. R.; Parkin, I. P.;

- Maier, S. A. Photo-Induced Enhanced Raman Spectroscopy (PIERS): Sensing Atomic-Defects, Explosives and Biomolecules. In *Chemical, Biological, Radiological, Nuclear, and Explosives (CBRNE) Sensing XX*; Guicheteau, J. A., Howle, C. R., Eds.; SPIE, 2019; Vol. 11010, p 13. <https://doi.org/10.1117/12.2518948>.
- (166) Ye, J.; Arul, R.; Nieuwoudt, M. K.; Dong, J.; Gao, W.; Simpson, M. C. *Understanding the Chemical Mechanism behind Photo-Induced Enhanced Raman Spectroscopy*.
- (167) Glass, D.; Cortés, E.; Peveler, W. J.; Howle, C. R.; Quesada-Cabrera, R.; Parkin, I. P.; Maier, S. A. Enhancing Hybrid Metal-Semiconductor Systems beyond SERS with PIERS (Photo-Induced Enhanced Raman Scattering) for Trace Analyte Detection. **2020**, *1141602* (April 2020), 2. <https://doi.org/10.1117/12.2557517>.
- (168) Cong, S.; Wang, Z.; Gong, W.; Chen, Z.; Lu, W.; Lombardi, J. R.; Zhao, Z. Electrochromic Semiconductors as Colorimetric SERS Substrates with High Reproducibility and Renewability. *Nat. Commun.* **2019**, *10* (1), 1–10. <https://doi.org/10.1038/s41467-019-08656-6>.
- (169) Marchand, P.; Hassan, I. A.; Parkin, I. P.; Carmalt, C. J. Aerosol-Assisted Delivery of Precursors for Chemical Vapour Deposition: Expanding the Scope of CVD for Materials Fabrication. *Dalt. Trans.* **2013**. <https://doi.org/10.1039/c3dt50607j>.
- (170) Zhao, J.; Wang, Z.; Lan, J.; Khan, I.; Ye, X.; Wan, J.; Fei, Y.; Huang, S.; Li, S.; Kang, J. Recent Advances and Perspectives in Photo-Induced Enhanced Raman Spectroscopy. **2021**, *13*, 8707. <https://doi.org/10.1039/d1nr01255j>.
- (171) Man, T.; Lai, W.; Xiao, M.; Wang, X.; Chandrasekaran, A. R.; Pei, H.; Li, L. A Versatile Biomolecular Detection Platform Based on Photo-Induced Enhanced Raman Spectroscopy. *Biosens. Bioelectron.* **2020**, *147* (September 2019). <https://doi.org/10.1016/j.bios.2019.111742>.
- (172) Lee, W.; Nanou, A.; Rikkert, L.; Coumans, F. A. W.; Otto, C.; Terstappen, L. W. M. M.; Offerhaus, H. L. Label-Free Prostate Cancer Detection by

- Characterization of Extracellular Vesicles Using Raman Spectroscopy. *Anal. Chem* **2018**, *90*, 4. <https://doi.org/10.1021/acs.analchem.8b01831>.
- (173) Yang, Y.; Matsubara, S.; Nogami, M.; Shi, J. Controlling the Aggregation Behavior of Gold Nanoparticles. *Mater. Sci. Eng. B Solid-State Mater. Adv. Technol.* **2007**, *140* (3), 172–176. <https://doi.org/10.1016/j.mseb.2007.03.021>.
- (174) Zhang, X.; Servos, M. R.; Liu, J. Instantaneous and Quantitative Functionalization of Gold Nanoparticles with Thiolated DNA Using a PH-Assisted and Surfactant-Free Route. *J. Am. Chem. Soc.* **2012**, *134* (17), 7266–7269. <https://doi.org/10.1021/ja3014055>.
- (175) Potara, M.; Maniu, D.; Astilean, S. The Synthesis of Biocompatible and SERS-Active Gold Nanoparticles Using Chitosan. *Nanotechnology* **2009**, *20* (31). <https://doi.org/10.1088/0957-4484/20/31/315602>.
- (176) Le Ru, E. C.; Etchegoin, P. G. (Pablo G. *Principles of Surface-Enhanced Raman Spectroscopy: And Related Plasmonic Effects*; Elsevier, 2009.
- (177) Alvarez-Puebla, R. A.; Arceo, E.; Goulet, P. J. G.; Garrido, J. J.; Aroca, R. F. Role of Nanoparticle Surface Charge in Surface-Enhanced Raman Scattering. **2005**. <https://doi.org/10.1021/jp045015o>.
- (178) Sangwan, S.; Seth, R. Synthesis, Characterization and Stability of Gold Nanoparticles (AuNPs) in Different Buffer Systems. **1956**. <https://doi.org/10.1007/s10876-020-01956-8>.
- (179) Jenkins, J. A.; Wax, T. J.; Zhao, J. Seed-Mediated Synthesis of Gold Nanoparticles of Controlled Sizes To Demonstrate the Impact of Size on Optical Properties. **2017**. <https://doi.org/10.1021/acs.jchemed.6b00941>.
- (180) Sun, C. H.; Wang, M. L.; Feng, Q.; Liu, W.; Xu, C. X. Surface-Enhanced Raman Scattering (SERS) Study on Rhodamine B Adsorbed on Different Substrates. *Russ. J. Phys. Chem. A* **2015**, *89* (2), 291–296. <https://doi.org/10.1134/S0036024415020338>.
- (181) Lin, S.; Hasi, W. L. J.; Lin, X.; Han, S. Q. G. W.; Lou, X. T.; Yang, F.; Lin, D. Y.; Lu, Z. W. Rapid and Sensitive SERS Method for Determination of

- Rhodamine B in Chili Powder with Paper-Based Substrates. *Anal. Methods* **2015**, 7 (12), 5289–5294. <https://doi.org/10.1039/c5ay00028a>.
- (182) Lai, Y. H.; Koo, S.; Oh, S. H.; Driskell, E. A.; Driskell, J. D. Rapid Screening of Antibody-Antigen Binding Using Dynamic Light Scattering (DLS) and Gold Nanoparticles. **2015**. <https://doi.org/10.1039/c5ay00674k>.
- (183) *DLS and zeta potential – What they are and what they are not? | Elsevier Enhanced Reader*.
<https://reader.elsevier.com/reader/sd/pii/S0168365916303832?token=272840C0E3C760CA893BA1DDBA49DD55711866ABFCD00D0F7CB513AA131576C0A5484CE10BD3BFF57E67F6BEF6BAC745&originRegion=eu-west-1&originCreation=20220210162609> (accessed 2022-02-10).
- (184) Smith, D. K.; Korgel, B. A. The Importance of the CTAB Surfactant on the Colloidal Seed-Mediated Synthesis of Gold Nanorods. *P. J. Phys. Chem. B* **2007**, 111 (6), 644–649. <https://doi.org/10.1021/la703625a>.
- (185) Alvarez-Puebla, R. A.; Arceo, E.; Goulet, P. J. G.; Garrido, J. J.; Aroca, R. F. Role of Nanoparticle Surface Charge in Surface-Enhanced Raman Scattering. *J. Phys. Chem. B* **2005**, 109 (9), 3787–3792.
<https://doi.org/10.1021/jp045015o>.
- (186) Stankus, D. P.; Lohse, S. E.; Hutchison, J. E.; Nason, J. A. Interactions between Natural Organic Matter and Gold Nanoparticles Stabilized with Different Organic Capping Agents. *Environ. Sci. Technol.* **2011**, 45 (8), 3238–3244. <https://doi.org/10.1021/es102603p>.
- (187) Hussain, M. H.; Fitrah, N.; Bakar, A.; Mustapa, A. N.; Low, K.-F.; Othman, N. H.; Adam, F. Synthesis of Various Size Gold Nanoparticles by Chemical Reduction Method with Different Solvent Polarity.
<https://doi.org/10.1186/s11671-020-03370-5>.
- (188) Peter N. Njoki; I-Im S. Lim; Derrick Mott; Hye-Young Park, †; Bilal Khan; Suprav Mishra; Ravishanker Sujakumar; Jin Luo, and; Zhong*, C.-J. Size Correlation of Optical and Spectroscopic Properties for Gold Nanoparticles. **2007**. <https://doi.org/10.1021/JP074902Z>.

- (189) Hong, S.; Li, X. Optimal Size of Gold Nanoparticles for Surface-Enhanced Raman Spectroscopy under Different Conditions. *J. Nanomater.* **2013**, 2013, 1–9. <https://doi.org/10.1155/2013/790323>.
- (190) Quester, K.; Avalos-Borja, M.; Rafael Vilchis-Nestor, A.; Antonio Camacho-López, M.; Castro-Longoria, E. SERS Properties of Different Sized and Shaped Gold Nanoparticles Biosynthesized under Different Environmental Conditions by *Neurospora Crassa* Extract. **2013**. <https://doi.org/10.1371/journal.pone.0077486>.
- (191) Sabur, A.; Havel, M.; Gogotsi, Y. SERS Intensity Optimization by Controlling the Size and Shape of Faceted Gold Nanoparticles. *J. RAMAN Spectrosc. J. Raman Spectrosc* **2008**, 39, 61–67. <https://doi.org/10.1002/jrs.1814>.
- (192) Osinkina, L.; Lohmüller, T.; Jäckel, F.; Feldmann, J. Synthesis of Gold Nanostar Arrays as Reliable, Large-Scale, Homogeneous Substrates for Surface-Enhanced Raman Scattering Imaging and Spectroscopy. *J. Phys. Chem. C* **2013**, 117 (43), 22198–22202. <https://doi.org/10.1021/jp312149d>.
- (193) Weitz, D. A.; Lin, M. Y.; Sandroff, C. J. Colloidal Aggregation Revisited: New Insights Based on Fractal Structure and Surface-Enhanced Raman Scattering. *Surf. Sci.* **1985**, 158 (1–3), 147–164. [https://doi.org/10.1016/0039-6028\(85\)90292-4](https://doi.org/10.1016/0039-6028(85)90292-4).
- (194) Suh, J. S.; Moskovits, M.) Varsanyi, G. Vibrational Spectra of Benzene Derivatives-. *J. I. Spectrochim. Acta, Part A* **1986**, 108 (2), 7.
- (195) Park, H.; Boklee, S.; Kim, K.; Kim, M. S. Surface-Enhanced Raman Scattering of p-Aminobenzolc Acid at Ag Electrode. *J. Phys. Chem* **1990**, 94, 7576–7580.
- (196) He, S.; Chua, J.; Khay, E.; Tan, M.; Chen, J.; Kah, Y. Optimizing the SERS Enhancement of a Facile Gold Nanostar Immobilized Paper-Based SERS Substrate †. **2017**. <https://doi.org/10.1039/c6ra28450g>.
- (197) Hu, H.; Larson, R. G. Marangoni Effect Reverses Coffee-Ring

- Depositions. **2006**. <https://doi.org/10.1021/jp0609232>.
- (198) Karakoçak, B. B.; Raliya, R.; Davis, J. T.; Chavalmane, S.; Wang, W. N.; Ravi, N.; Biswas, P. Biocompatibility of Gold Nanoparticles in Retinal Pigment Epithelial Cell Line. *Toxicol. Vitr.* **2016**, 37, 61–69. <https://doi.org/10.1016/J.TIV.2016.08.013>.
- (199) Chen, F.; Wang, Y.; Ma, J.; Yang, G. A Biocompatible Synthesis of Gold Nanoparticles by Tris(Hydroxymethyl)Aminomethane. *Nanoscale Res. Lett.* **2014**, 9 (1), 220. <https://doi.org/10.1186/1556-276X-9-220>.
- (200) Guo, J.; Armstrong, M. J.; O'driscoll, C. M.; Holmes Bc, J. D.; Rahme, K. Positively Charged, Surfactant-Free Gold Nanoparticles for Nucleic Acid Delivery †. **2015**. <https://doi.org/10.1039/c4ra16294c>.
- (201) Sully, R. E.; Moore, C. J.; Garelick, H.; Loizidou, E.; Podoleanu, A. G.; Gubala, V. Nanomedicines and Microneedles: A Guide to Their Analysis and Application. **2021**. <https://doi.org/10.1039/d1ay00954k>.
- (202) Phan, H. T.; Haes, A. J. Impacts of PH and Intermolecular Interactions on Surface-Enhanced Raman Scattering Chemical Enhancements. *J. Phys. Chem. C* **2018**, 122, 122–14846. <https://doi.org/10.1021/acs.jpcc.8b04019>.
- (203) Cyrankiewicz, M.; Wybranowski, T.; Kruszewski, S. Study of SERS Efficiency of Metallic Colloidal Systems. *J. Phys. Conf. Ser.* **2007**, 79 (1), 012013. <https://doi.org/10.1088/1742-6596/79/1/012013>.
- (204) Ngo, Y. H.; Li, D.; Simon, G. P.; Garnier, G. Gold Nanoparticle–Paper as a Three-Dimensional Surface Enhanced Raman Scattering Substrate. **2012**. <https://doi.org/10.1021/la3012734>.
- (205) Mu, Z.; Zhao, X.; Xie, Z.; Zhao, Y.; Zhong, Q.; Bo, L.; Gu, Z. In Situ Synthesis of Gold Nanoparticles (AuNPs) in Butterfly Wings for Surface Enhanced Raman Spectroscopy (SERS) †. <https://doi.org/10.1039/c3tb00500c>.
- (206) Zhang, D.; Liang, P.; Yu, Z.; Huang, J.; Ni, D.; Shu, H.; Dong, Q. min. The Effect of Solvent Environment toward Optimization of SERS Sensors for

- Pesticides Detection from Chemical Enhancement Aspects. *Sensors Actuators, B Chem.* **2018**, 256, 721–728.
<https://doi.org/10.1016/J.SNB.2017.09.209>.
- (207) Zhu, G.; Zhu, X.; Fan, Q.; Wan, X. Raman Spectra of Amino Acids and Their Aqueous Solutions. *Spectrochim. Acta - Part A Mol. Biomol. Spectrosc.* **2011**, 78 (3), 1187–1195.
<https://doi.org/10.1016/J.SAA.2010.12.079>.
- (208) Takeuchi, H. *Raman Structural Markers of Tryptophan and Histidine Side Chains in Proteins*; 2003; Vol. 72.
- (209) Dendramis, A. L.; Schwinn, E. W.; Sperline, R. P. A Surface-Enhanced Raman Scattering Study of CTAB Adsorption on Copper. *Surf. Sci.* **1983**, 134 (3), 675–688. [https://doi.org/10.1016/0039-6028\(83\)90065-1](https://doi.org/10.1016/0039-6028(83)90065-1).
- (210) Peek, A. L.; Rebbeck, T.; Puts, N. A.; Watson, J.; Aguila, M. E. R.; Leaver, A. M. Brain GABA and Glutamate Levels across Pain Conditions: A Systematic Literature Review and Meta-Analysis of 1H-MRS Studies Using the MRS-Q Quality Assessment Tool. *Neuroimage* **2020**, 210. <https://doi.org/10.1016/J.NEUROIMAGE.2020.116532>.
- (211) Lussier, elix; Bruí, T.; Bourque, J.; Charles Ducrot, bc; Louis-, bc; Trudeau bc, E.; Masson, J.-F. Dynamic SERS Nanosensor for Neurotransmitter Sensing near Neurons Faraday Discussions. **2017**, 205, 387. <https://doi.org/10.1039/c7fd00131b>.
- (212) Nezhad, F. S.; Anton, A.; Michou, E.; Jung, J.; Parkes, L. M.; Williams, S. R.; Williams, S. R.; Building, S. Quantification of GABA, Glutamate and Glutamine in a Single Measurement at 3 T Using GABA-Edited MEGA-PRESS. **2017**. <https://doi.org/10.1002/nbm.3847>.
- (213) Schlücker, S. SERS Microscopy: Nanoparticle Probes and Biomedical Applications. *ChemPhysChem*. Wiley-VCH Verlag July 13, 2009, pp 1344–1354. <https://doi.org/10.1002/cphc.200900119>.
- (214) Humbert, B.; Alnot, M.; Quilès, F. Infrared and Raman Spectroscopical Studies of Salicylic and Salicylate Derivatives in Aqueous Solution.

Spectrochim. Acta - Part A Mol. Biomol. Spectrosc. **1998**, 54 (3), 465–476. [https://doi.org/10.1016/S1386-1425\(97\)00239-4](https://doi.org/10.1016/S1386-1425(97)00239-4).

- (215) *Principles of Surface-Enhanced Raman Spectroscopy: and Related Plasmonic Effects* - Eric Le Ru, Pablo Etchegoin - Google Books. https://books.google.com.sg/books?id=dp9qw_sFZ9EC&printsec=frontcover&dq=SERS+and+its+selection+rules&hl=en&sa=X&ved=0ahUKEwih3_6T1efoAhWWbn0KHYmSCvoQ6AEIKDAA#v=onepage&q=selection+rule&f=false (accessed 2020-04-14).
- (216) Maia, L. F.; Rimulo, I. M. R.; De Oliveira, V. E.; Arvellos, J. A. F.; Costa, L. A. S.; Edwards, H. G. M.; De Oliveira, L. F. C. Understanding Solvent/Bixin Interactions by Raman Spectroscopy. *Artic. J. Braz. Chem. Soc* **1370**, 31 (7). <https://doi.org/10.21577/0103-5053.20200022>.
- (217) Ferkany, J. W.; Smith, L. A.; Seifert, W. E.; Caprioli, R. M.; Enna, S. J. Measurement of Gamma-Aminobutyric Acid (GABA) in Blood. *Life Sci.* **1978**, 22 (23), 2121–2128. [https://doi.org/10.1016/0024-3205\(78\)90456-3](https://doi.org/10.1016/0024-3205(78)90456-3).
- (218) Lee, W.; Kang, B.-H.; Yang, H.; Park, M.; Kwak, J. H.; Chung, T.; Jeong, Y.; Kim, B. K.; Jeong, K.-H. Spread Spectrum SERS Allows Label-Free Detection of Attomolar Neurotransmitters. <https://doi.org/10.1038/s41467-020-20413-8>.
- (219) Klutse, C. K.; Cullum, B. M. Optimization of SAM-Based Multilayer SERS Substrates for Intracellular Analyses: The Effect of Terminating Functional Groups. *Smart Biomed. Physiol. Sens. Technol. VIII* **2011**, 8025, 802502. <https://doi.org/10.1117/12.882309>.
- (220) Kennedy, B. J.; Spaeth, S.; Dickey, M.; Carron, K. T. Determination of the Distance Dependence and Experimental Effects for Modified SERS Substrates Based on Self-Assembled Monolayers Formed Using Alkanethiols. **1999**. <https://doi.org/10.1021/jp984454i>.
- (221) Laibinis, P. E.; Whitesides, G. M.; Allara, D. L.; Tao, Y.-T.; Parikh, A. N.; Nuzzo, R. G. *Comparison of the Structures and Wetting Properties of Self-Assembled Monolayers of n-Alkanethiols on the Coinage Metal*

Surfaces, Cu, Ag, Au1; 1991; Vol. 113.

<https://pubs.acs.org/sharingguidelines> (accessed 2020-03-03).

- (222) Kochana, J.; Starzec, K.; Wieczorek, M.; Knihnicki, P.; Góra, M.; Rokicińska, A.; Kościelniak, P.; Kuśtrowski, P. Study on Self-Assembled Monolayer of Functionalized Thiol on Gold Electrode Forming Capacitive Sensor for Chromium(VI) Determination. <https://doi.org/10.1007/s10008-019-04236-2>.
- (223) Ulman, A. *Formation and Structure of Self-Assembled Monolayers*; 1996. <https://pubs.acs.org/sharingguidelines>.
- (224) Aliaga, A. E.; Garrido, C.; Leyton, P.; Diaz F., G.; Gomez-Jeria, J. S.; Aguayo, T.; Clavijo, E.; Campos-Vallette, M. M.; Sanchez-Cortes, S. SERS and Theoretical Studies of Arginine. *Spectrochim. Acta Part A Mol. Biomol. Spectrosc.* **2010**, 76 (5), 458–463. <https://doi.org/10.1016/J.SAA.2010.01.007>.
- (225) Wu, Z.; Liu, Y.; Zhou, X.; Shen, A.; Hu, J. A “Turn-off” SERS-Based Detection Platform for Ultrasensitive Detection of Thrombin Based on Enzymatic Assays. *Biosens. Bioelectron.* **2013**, 44 (1), 10–15. <https://doi.org/10.1016/j.bios.2013.01.006>.
- (226) Bazylewski, P.; Divigalpitiya, R.; Fanchini, G. In Situ Raman Spectroscopy Distinguishes between Reversible and Irreversible Thiol Modifications in L-Cysteine. **2017**. <https://doi.org/10.1039/c6ra25879d>.
- (227) Levin, C. S.; Janesko, B. G.; Bardhan, R.; Scuseria, G. E.; Hartgerink, J. D.; Halas, N. J. Chain-Length-Dependent Vibrational Resonances in Alkanethiol Self-Assembled Monolayers Observed on Plasmonic Nanoparticle Substrates. *Nano Lett.* **2006**, 6 (11), 2617–2621. <https://doi.org/10.1021/nl062283k>.
- (228) Dinesh Raja, M.; Maria, C.; Kumar, A.; Arulmozhi, S.; Madhavan, J. Spectroscopic and Thermodynamic Properties of L-Ornithine Monohydrochloride ARTICLES YOU MAY BE INTERESTED IN Extraction of Breathing Pattern Using Temperature Sensor Based on Arduino Board AIP Conference Spectroscopic And Thermodynamic

Properties Of L-Ornithine Monohydrochloride. **2015**, 1665, 100004.
<https://doi.org/10.1063/1.4917843>.

- (229) Ma, H.; Liu, S.; Zheng, N.; Liu, Y.; Han, X. X.; He, C.; Lu, H.; Zhao, B. Frequency Shifts in Surface-Enhanced Raman Spectroscopy-Based Immunoassays: Mechanistic Insights and Application in Protein Carbonylation Detection. **2022**, 14, 55.
<https://doi.org/10.1021/acs.analchem.9b02640>.
- (230) León, C. P.; Kador, ‡ L.; Peng, B.; Thelakkat, M. Influence of the Solvent on the Surface-Enhanced Raman Spectra of Ruthenium(II) Bipyridyl Complexes. **2005**. <https://doi.org/10.1021/jp044946x>.
- (231) Fortuni, B.; Fujita, Y.; Ricci, M.; Inose, T.; Aubert, R.; Lu, G.; Hutchison, J. A.; Hofkens, J.; Latterini, L.; Uji-I, H. A Novel Method for in Situ Synthesis of SERS-Active Gold Nanostars on Polydimethylsiloxane Film. *Chem. Commun.* **2017**, 53 (37), 5121–5124. <https://doi.org/10.1039/c7cc01776f>.
- (232) Yao, G.; Huang, Q. DFT and SERS Study of L-Cysteine Adsorption on the Surface of Gold Nanoparticles. *J. Phys. Chem. C* **2018**, 122 (27), 15241–15251.
https://doi.org/10.1021/ACS.JPCC.8B00949/SUPPL_FILE/JP8B00949_SI_001.PDF.
- (233) Brolo, A. G.; Germain, P.; Hager, G. Investigation of the Adsorption of L-Cysteine on a Polycrystalline Silver Electrode by Surface-Enhanced Raman Scattering (SERS) and Surface-Enhanced Second Harmonic Generation (SESHG). **2002**. <https://doi.org/10.1021/jp025650z>.
- (234) Shiohara, A.; Langer, J.; Polavarapu, L.; Liz-Marzán, L. M. Solution Processed Polydimethylsiloxane/Gold Nanostar Flexible Substrates for Plasmonic Sensing. *Nanoscale* **2014**, 6 (16), 9817–9823.
<https://doi.org/10.1039/C4NR02648A>.
- (235) Hu, X.; Cheng, W.; Wang, T.; Wang, Y.; Wang, E.; Dong, S. Fabrication, Characterization, and Application in SERS of Self-Assembled Polyelectrolyte-Gold Nanorod Multilayered Films. **2005**.
<https://doi.org/10.1021/jp052706r>.

- (236) Akhtar, M. F.; Hanif, M.; Ranjha, N. M. Methods of Synthesis of Hydrogels ... A Review. *Saudi Pharmaceutical Journal*. Elsevier B.V. September 1, 2016, pp 554–559. <https://doi.org/10.1016/j.jsps.2015.03.022>.
- (237) Pal, K.; Banthia, A. K.; Majumdar, D. K. Preparation and Characterization of Polyvinyl Alcohol-Gelatin Hydrogel Membranes for Biomedical Applications. *AAPS PharmSciTech* **2007**, 8 (1). <https://doi.org/10.1208/pt080121>.
- (238) Althans, D.; Langenbach, K.; Enders, S. Influence of Different Alcohols on the Swelling Behaviour of Hydrogels. *Mol. Phys.* **2012**, 110 (11–12), 1391–1402. <https://doi.org/10.1080/00268976.2012.655339>.
- (239) Khan, S.; Nazar, •; Ranjha, M.; Khan, S.; Ranjha, N. M. Effect of Degree of Cross-Linking on Swelling and on Drug Release of Low Viscous Chitosan/Poly (Vinyl Alcohol) Hydrogels. *Polym. Bull* **2014**, 71, 2133–2158. <https://doi.org/10.1007/s00289-014-1178-2>.
- (240) Sakthivel, M.; Franklin, D. S.; Sudarsan, S.; Chitra, G.; Sridharan, T. B.; Guhanathan, S. Gold Nanoparticles Embedded Itaconic Acid Based Hydrogels. *SN Appl. Sci.* **2019**, 1 (2). <https://doi.org/10.1007/S42452-018-0156-Y>.
- (241) Parhi, R. Cross-Linked Hydrogel for Pharmaceutical Applications: A Review. *Tabriz Univ. Med. Sci.* **2017**, 7 (4), 515–530. <https://doi.org/10.15171/apb.2017.064>.
- (242) Yu, Y.; Xu, S.; Li, S.; Pan, H. Biomaterials Science MINIREVIEW Genipin-Cross-Linked Hydrogels Based on Biomaterials for Drug Delivery: A Review. **2021**. <https://doi.org/10.1039/d0bm01403f>.
- (243) Salihu, R.; Izwan, S.; Razak, A.; Zawawi, N. A.; Rafiq, M.; Kadir, A.; Ismail, N. I.; Jusoh, N.; Riduan Mohamad, M.; Hasraf, N.; Nayan, M. Citric Acid: A Green Cross-Linker of Biomaterials for Biomedical Applications. *Eur. Polym. J.* **2021**, 146, 110271. <https://doi.org/10.1016/j.eurpolymj.2021.110271>.
- (244) Li, D.-W.; Zhai, W.-L.; Li, Y.-T.; Long, Y.-T. Recent Progress in Surface

- Enhanced Raman Spectroscopy for the Detection of Environmental Pollutants. **2010**. <https://doi.org/10.1007/s00604-013-1115-3>.
- (245) Dougan, J. A.; Faulds, K. Surface Enhanced Raman Scattering for Multiplexed Detection. *Analyst* **2012**, *137* (3), 545–554. <https://doi.org/10.1039/c2an15979a>.
- (246) Wiercigroch, E.; Swit, P.; Agnieszka Brzozka, ·; Łukasz Pięta, ·; Malek, K. Dual-Enhancement and Dual-Tag Design for SERS-Based Sandwich Immunoassays: Evaluation of a Metal-Metal Effect in 3D Architecture. *Microchim. Acta* *1*, 3. <https://doi.org/10.1007/s00604-021-05125-0>.
- (247) Han, X. X.; Huang, G. G.; Zhao, B.; Ozaki, Y. Label-Free Highly Sensitive Detection of Proteins in Aqueous Solutions Using Surface-Enhanced Raman Scattering. *Anal. Chem.* **2009**, *81* (9), 3329–3333. <https://doi.org/10.1021/AC900395X>.
- (248) Hassanain, W. A.; Izake, E. L. Toward Label-Free SERS Detection of Proteins through Their Disulfide Bond Structure. *SLAS Discov.* **2020**, *25* (1), 87–94. <https://doi.org/10.1177/2472555219875102>.
- (249) Loredó-García, E.; Ortiz-Dosal, A.; Núñez-Leyva, J. M.; Cuellar Camacho, J. L.; Alegría-Torres, J. A.; García-Torres, L.; Navarro-Contreras, H. R.; Kolosovas-Machuca, E. S. TNF- α Detection Using Gold Nanoparticles as a Surface-Enhanced Raman Spectroscopy Substrate. *Nanomedicine* **2021**, *16* (1), 51–61. <https://doi.org/10.2217/NNM-2020-0307/ASSET/IMAGES/LARGE/FIGURE7.JPEG>.
- (250) Wang, J.; Koo, K. M.; Wee, E. J. H.; Wang, Y.; Trau, M. A Nanoplasmonic Label-Free Surface-Enhanced Raman Scattering Strategy for Non-Invasive Cancer Genetic Subtyping in Patient Samples. *Nanoscale* **2017**, *9* (10), 3496–3503. <https://doi.org/10.1039/c6nr09928a>.
- (251) Ben-Jaber, S.; Peveler, W. J.; Quesada-Cabrera, R.; Cortés, E.; Sotelo-Vazquez, C.; Abdul-Karim, N.; Maier, S. A.; Parkin, I. P. Photo-Induced Enhanced Raman Spectroscopy for Universal Ultra-Trace Detection of Explosives, Pollutants and Biomolecules. *Nat. Commun.* **2016**, *7* (1), 12189. <https://doi.org/10.1038/ncomms12189>.

- (252) Khan, Z. *Aerosol-Assisted Chemical Vapour Deposition (AACVD) of Fluorine Doped Titanium Dioxide and Titania/Silica Composite Thin Films MSci Project Final Report*, 2018.
- (253) Yang, L.; Gong, M.; Jiang, X.; Yin, D.; Qin, X.; Zhao, B.; Ruan, W. Investigation on SERS of Different Phase Structure TiO₂ Nanoparticles. *J. Raman Spectrosc.* **2015**, *46* (3), 287–292.
<https://doi.org/10.1002/jrs.4645>.
- (254) Shafer-Peltier, K. E.; Haynes, C. L.; Glucksberg, M. R.; Van Duyne, R. P. Toward a Glucose Biosensor Based on Surface-Enhanced Raman Scattering. **2003**. <https://doi.org/10.1021/ja028255v>.
- (255) Perez-Mayen, L.; Oliva, J.; Salas, P.; De La Rosa, E. Nanomolar Detection of Glucose Using SERS Substrates Fabricated with Albumin Coated Gold Nanoparticles †. **2016**, *8*, 11862.
<https://doi.org/10.1039/c6nr00163g>.
- (256) Khan, Z.; Ben-Zaber, S.; Panariello, L.; Li, T.; Laney, S.; Negrea, A.; To, K.; Cui, X. *Investigating and Developing New Materials for the Detection of Biomolecules Using SERS 1 Investigating and Developing New Materials for the Detection of Wound Biomarkers Using Surface Enhanced Raman Scattering (SERS) and Photo-Induced Enhanced Raman Scattering (PIERS) 1 St Year PhD Upgrade Report*.
- (257) Bawaked, S. M.; Sathasivam, S.; Bhachu, D. S.; Chadwick, N.; Obaid, A. Y.; Al-Thabaiti, S.; Basahel, S. N.; Carmalt, C. J.; Parkin, I. P. Aerosol Assisted Chemical Vapor Deposition of Conductive and Photocatalytically Active Tantalum Doped Titanium Dioxide Films. *J. Mater. Chem. A* **2014**, *2* (32), 12849–12856. <https://doi.org/10.1039/C4TA01618A>.
- (258) Powell, M. J.; Potter, D. B.; Wilson, R. L.; Darr, J. A.; Parkin, I. P.; Carmalt, C. J. Scaling Aerosol Assisted Chemical Vapour Deposition: Exploring the Relationship between Growth Rate and Film Properties. *Mater. Des.* **2017**, *129*, 116–124.
<https://doi.org/10.1016/J.MATDES.2017.05.017>.
- (259) Solís-Casados, D.; Viguera-Santiago, E.; Hernández-López, S.;

- Camacho-López, M. A. Characterization and Photocatalytic Performance of Tin Oxide. *Ind. Eng. Chem. Res.* **2009**, *48* (3), 1249–1252. <https://doi.org/10.1021/IE800604U>.
- (260) Mufti, N.; Laila, I. K. R.; Hartatiek; Fuad, A. The Effect of TiO₂ Thin Film Thickness on Self-Cleaning Glass Properties. In *Journal of Physics: Conference Series*; 2017. <https://doi.org/10.1088/1742-6596/853/1/012035>.
- (261) Fu, X.; Zhang, G.; Wu, T.; Wang, S. Multifunctional Gold-Loaded TiO₂ Thin Film: Photocatalyst and Recyclable SERS Substrate. *Can. J. Chem.* **2013**, *91* (11), 1112–1116. <https://doi.org/10.1139/cjc-2013-0234>.
- (262) Bhachu, D. S.; Sathasivam, S.; Carmalt, C. J.; Parkin, I. P. PbO-Modified TiO₂ Thin Films: A Route to Visible Light Photocatalysts. *Langmuir* **2014**. <https://doi.org/10.1021/la4038777>.
- (263) Schneider, J.; Matsuoka, M.; Takeuchi, M.; Zhang, J.; Horiuchi, Y.; Anpo, M.; Bahnemann, D. W. Understanding TiO₂ Photocatalysis : Mechanisms and Materials. *Chem. Rev.* **2014**, *114*, 9919–9986. <https://doi.org/10.1021/cr5001892>.
- (264) Herczyński, H. H.; Zenit, R.; Hooshanginejad, A.; Jung, S. Buoyancy-Marangoni Fingering of a Miscible Spreading Drop. **2022**. <https://doi.org/10.3390/sym14020425>.
- (265) Robinson, A. M.; Harroun, S. G.; Bergman, J.; Brosseau, C. L.; Huckridge, D. A.; Büttner, F.; Hagemann, J.; Wellhausen, M.; Funke, S.; Lenth, C.; Rotter, F.; Gundrum, L.; Plachetka, U.; Moormann, C.; Strube, M.; Walte, A.; Wackerbarth, H.; Ebert, R.; Avila, F.; Fernandez, D. J.; Arenas, J. F.; Otero, J. C.; Soto, J. Portable Electrochemical Surface-Enhanced Raman Spectroscopy System for Routine Spectroelectrochemical Analysis. *J. Raman Spectrosc.* **2010**, *84* (10), 1760–1764.
- (266) Ansari, S. A.; Khan, M. M.; Ansari, M. O.; Cho, M. H. Nitrogen-Doped Titanium Dioxide (N-Doped TiO₂) for Visible Light Photocatalysis. *New J. Chem.* **2016**, *40* (4), 3000–3009. <https://doi.org/10.1039/C5NJ03478G>.

